ULTRASONIC STUDY OF THE ELASTIC PROPERTIES AND PHASE TRANSITIONS IN SELECTED MIXED SULPHATE CRYSTALS

THESIS SUBMITTED TO
THE COCHIN UNIVERSITY OF SCIENCE AND TECHNOLOGY
FOR THE AWARD OF THE DEGREE OF
DOCTOR OF PHILOSOPHY

G5649

L. GODFREY

DEPARTMENT OF PHYSICS
COCHIN UNIVERSITY OF SCIENCE AND TECHNOLOGY
COCHIN - 682 022
INDIA

SEPTEMBER 1994

DEDICATED TO
MY LATE MOTHER

CERTIFICATE

Certified that the work presented in this thesis entitled " Ultrasonic Study of the Elastic Properties and Phase Transitions in Selected Mixed Sulphate Crystals " is based on the bonafied research work done by Mr. L. Godfrey under my guidance, at the Department of Physics, Cochin University of Science & Technology, and has not been included in any other thesis submitted previously for the award of any other degree.

Cochin - 682 022
September 5, 1994

Dr. Jacob Philip
Supervising Teacher

DECLARATION

Certified that the work presented in this thesis entitled " Ultrasonic Study of the Elastic Properties and Phase Transitions in Selected Mixed Sulphate Crystals " is based on the original research work done by me under the guidance of Dr. Jacob Philip, at Department of Physics, Cochin University of Science and Technology, and has not been included in any other thesis submitted previously for the award of any other degree.

Cochin - 682 022
September 5, 1994

L. Godfrey

PREFACE

Ultrasonics is one of the most widely used techniques to investigate phase transitions in solids. It is also the most established technique to determine the elastic moduli of solids. One unique advantage of the ultrasonic technique is that both static and dynamic properties can be measured simultaneously. Ultrasonic velocity measurements provide information about the equilibrium adiabatic properties of the system and the effects of temperature, pressure and external fields can be readily studied. Ultrasonic attenuation data provide direct information about the dynamic behaviour and from the dependence on temperature and frequency a great deal of information can be obtained about the mechanisms involved. Dynamic aspects of the theories of phase transitions require information gathered from ultrasonics work. Measurement of the elastic constants as a function of temperature enables one to locate transition points, determine phase diagrams and in favorable cases make statements about the order of the transition.

In ultrasonic experiments one measures sound velocity and attenuation. Measurement of velocity along different symmetry directions in crystals with waves of different polarizations enables one to determine the individual elastic constants. Different techniques have been developed for accurate measurement of velocity. Of these, the pulse interference techniques such as pulse echo overlap and pulse superposition techniques are the most accurate and precise ones. Pulse comparison techniques are generally used for attenuation measurements.

In this thesis we have investigated the elastic properties and phase transitions in selected mixed sulphate crystals - Lithium Hydrazinium Sulphate [$LiN_2H_5SO_4$], Lithium Ammonium Sulphate [$LiNH_4SO_4$] and Lithium Potassium Sulphate [$LiKSO_4$] - using ultrasonic technique. The pulse echo overlap

i

technique has been used for measuring ultrasonic velocity and its dependence on temperature along different directions with waves of longitudinal and transverse polarizations. The thesis is presented in seven chapters. A chapter wise description of the contents of the thesis is outlined below.

Chapter 1 is the introductory chapter which gives the necessary background for the work done in later chapters. Theory of elastic wave propagation in crystalline media are given and the necessary relations connecting the elastic constants and sound velocity in different directions are derived starting with Christoffel equation. The crystals in which we have made the measurements belong either to orthorhombic or hexagonal symmetry. The general theory and equations have been applied to these symmetries and necessary expressions are obtained. The necessary theory and details of investigating phase transitions using ultrasonic technique are outlined. We have selected some sulphates with very interesting phase transitions for our investigations. A general description of the physical properties and phase transitions in these sulphate crystals is also given in this chapter.

The second chapter is devoted to the instrumentation work done for carrying out the investigations. We have grown the crystals under study in our laboratory by the solution growth technique. A water bath and temperature controller have been fabricated for this purpose. Since we have adopted precise constant temperature evaporation method to get good quality crystals of large enough size for ultrasonics work, temperature of the bath had to be controlled very precisely for long durations of time. Details of the design of the bath and temperature controller are given. The Matec Model 7700 pulse modulator and receiver along with necessary subsystems have been used for accurate measurement of ultrasonic velocity using the pulse echo overlap technique. Details of the system and measurement technique are outlined in this chapter with

the help of block diagrams. We have applied the bond corrections necessary to eliminate errors due to phase changes occurring in ultrasonic echoes due to reflections at various boundaries. We have developed a computer program for automatic identification of correct overlap and bond correction. Details of this program are given. In phase transition studies it is necessary to vary the temperature of the sample and it should be controlled. We have designed and fabricated a cryostat for our low temperature work . An oven has been used whenever the sample temperature has to be raised above room temperature. Technical details of the cryostat, oven and temperature controllers used are discussed in this chapter.

Lithium Hydrazinium Sulphate (LHS) is an orthorhombic crystal. At room temperature it exhibits ferroelectric like hysteresis loop but other studies indicate no ferroelectricity in this crystal. It has highly temperature dependent one dimensional protonic conductivity along the c direction. Several structural, electrical, thermal, and spectroscopic investigations have been reported on this crystal but its elastic properties have not been probed. We have measured the elastic constants of LHS crystal for the first time. This crystal has nine independent elastic constants and we have determined all these nine from a total of 12 measurements. Bond correction and identification of correct overlap was done using our computer program. We have refined the measured elastic constants by applying misorientation correction by using another computer program developed by us. The details of above measurements and techniques are described in Chapter 3.

We have undertaken a detailed study of the temperature variation of elastic constants of LHS over a wide temperature range from cryogenic temperatures to well above room temperature using ultrasonic technique. These studies were aimed at detecting elastic anomalies corresponding to phase transitions in this crystal. Shear wave velocity measurements are usually difficult at high temperatures due to bond

breakdown. We have developed a new ultrasonic transducer bonding technique for shear wave velocity measurement for temperatures up to 480 K. Even though this crystal shows a ferroelectric like behaviour, the dielectric studies do not carry any signature of a ferroelectric phase transition. Similarly no specific heat anomalies have been found, indicative of phase transitions in this crystal. But there are anomalies in the thermal expansion coefficients above and below room temperature, and temperature variation of NMR spectrum also support a weak high temperature phase transition without giving definite transition temperature. The highly temperature dependent c-axis protonic conductivity, high dielectric constant and ferroelectric like hysteresis loops of this crystal are not well explained. We have tried to answer many of these questions by undertaking ultrasonic measurements along selected directions in the temperature range from 210 K to 450 K. The experimental details, the results obtained and a detailed discussion are given in Chapter 4.

The studies carried out by us on the elastic properties and phase transitions in Lithium Ammonium Sulphate (LAS) are presented in Chapter 5. Below and above room temperature, LAS goes through several phase transitions. On the high temperature side LAS undergoes a phase transition near 460 K and has orthorhombic structure at room temperature. It further undergoes a phase transition near 284 K. Recently a weak second order phase transition has been identified near 256 K in dielectric and Raman studies. There are uncertainties about the polar character of the phase below 284 K. The elastic properties at phase transition near 460 K have been investigated by ultrasonic and Brillouin scattering technique; but near 284 K only Brillouin data is available. The elastic data near the 256 K transition has not been reported. The absolute values of the elastic constants at room temperature, reported from one ultrasonic work and several Brillouin experiments show wide variation in values. We have carried out

accurate determination of all the nine elastic constants of LAS from 12 measurements in various symmetry directions using longitudinal and transverse ultrasonic waves. We have investigated the temperature variation of all the six diagonal elastic constants of LAS in the temperature range from 220 K to 310 K to study the phase transitions at 284 Kand 256 K. This is the first ultrasonic study in this temperature range in LAS. Detailed discussion of the results are presented and we have put forward a new model to resolve the controversial issues in the low temperature phase of LAS.

Lithium Potassium Sulphate (LPS) is a very intensively studied crystal because it presents an interesting sequence of phase transitions. At room temperature it has hexagonal structure and has five independent elastic constants. Only four of these have been reported in literature. We have measured all the five independent elastic constants of LPS accurately using ultrasonic pulse echo overlap technique. At low temperatures, phase transitions have been reported near 201, 190, and 138 K. At high temperatures it undergoes two phase transitions at about 705 and 940 K. In a Brillouin scattering study a new phase transition has been suggested near 333 K, but the anomaly failed to show up in a later Brillouin study by another group. We have measured the temperature variation of all the elastic constants of LPS using ultrasonics to probe the controversial elastic anomaly near 333 K. The results of these investigations are presented and discussed in Chapter 6.

Chapter 7 is the concluding chapter in which the overall conclusions drawn from the work presented in the previous chapters are discussed. It also projects the future scope of these types of investigations.

The following papers have been published in different journals during the course of this work.

1. L. Godfrey and Jacob Philip, *A temperature controller for crystal growth experiments of long duration,*
   J. Phys. E: Sci. Instrum. (UK), vol. 22, pp. 516-18 (1989)

2. Johney Isaac, L. Godfrey and Jacob Philip, *A low cost high precision proportional integral derivative temperature controller,*
   Indian J. Pure Appl. Phys., vol. 29, pp. 195-197 (1991)

3. L. Godfrey, J. Philip and M.T. Sebastian, *Elastic constants and high temperature elastic anomalies near 425 K in Lithium Hydrazinium Sulphate,*
   J. Appl. Phys. (USA) , vol. 75, pp. 2393-2397 (1994)

The following papers have been communicated for publication in different journals.

1. L. Godfrey and J. Philip, *A Numerical technique for bond correction in ultrasonic measurements,*
   Acoust. Lett. (UK)

2. L. Godfrey and J. Philip, *A Numerical procedure for misorientation correction in elastic constant measurement of anisotropic solids,*
   Measurement Science and Technology (UK)

3. L. Godfrey and J. Philip, *Phase transitions in Lithium Ammonium Sulphate, $LiNH_4SO_4$, below room temperature: An ultrasonic study,*
   Phys. Rev. B (USA)

4. L. Godfrey and J. Philip, *Ultrasonic measurement of the Elastic constants of LiKSO$_4$ between 300 and 370 K,* Solid State Commun. (UK)

The following papers have been presented in different conferences during the course of this work.

1. L.Godfrey, V. Anil Kumar and Jacob Philip, *A simple differential thermal analysis set-up for phase transition study,* XXI National Seminar on Crystallography – Dec. 27-29 (1989) BARC, Bombay

2. L.Godfrey and Jacob Philip, *Temperature variation of the elastic constants of LiHzS,* Solid State Physics Symposium Dec. 21-24, (1991) B.H.U, Varanasi.

3. L. Godfrey and J. Philip, *Elastic constants and Phase Transitions in Lithium Ammonium Sulphate,* Solid State Physics Symposium, Dec. 27-31 (1993) BARC, Bombay,

4. L. Godfrey and J. Philip, *Elastic nonlinearity parameters of tetragonal crystals,* XIX National Seminar on Crystallography. M.G. University, Kottayam (December 1987)

5. L. Godfrey, *Simple automation circuit for crystal growth by Bridgman method,* XIX National Seminar on Crystallography. M.G. University, Kottayam (December 1987)

6. L. Godfrey and J. Philip, *A temperature controller for long duration constant temperature experiments,* Symposium on current trends in Pure & Applied Physics, Cochin University of Science and Technology (November 1988)

7. Johny Isaac, L. Godfrey and J. Philip, *A low cost high precision PID temperature controller,* Symposium on current trends in Pure & Applied Physics, Cochin University of Science and Technology (November 1988)

8. L. Godfrey, *Ultrasonic study of the elastic constants and phase transitions in selected mixed sulphates*, Solid State Physics Symposium, (DAE) Dec. 27-31 (1994) Jaipur. (Thesis presentation, communicated)

ACKNOWLEDGMENTS

CONTENTS

CHAPTER 1

INTRODUCTION

1.1   Elastic wave propagation in crystalline solids

1.1.1 Elastic waves and elastic constants

Elastic waves are always generated by mechanical vibrations of various media. They can propagate through gases, liquids and solids and these waves are the result of collective vibrations of the atoms and molecules of the medium. The vibration characteristics of the atoms and molecules of the medium are determined by the interatomic forces. The nature of these forces are different in solids, liquids and gases and thus the wave propagation characteristics are also different. In solids both transverse and longitudinal wave propagation are possible while in liquids and gases only longitudinal type of wave propagation is possible. Liquids and gases have same properties in all directions and hence the wave propagation characteristics are isotropic. Some solids like glass have isotropic properties while others like a single crystal have anisotropic properties. Study of elastic wave propagation through crystals enables one to determine their elastic properties. Wave propagation in a medium is characterised by its velocity and attenuation. In general the waves can be generated over a wide range of frequencies and amplitudes. The dynamic properties of the medium limits the range of frequency for the propagating wave and the interatomic nonlinear interactions will limit the possible wave amplitude. For small amplitudes the interactions can be assumed to be linear.

The elastic properties of a medium is understood in terms of its response to an applied stress. Under the

application of an external force or stress the medium undergoes a deformation or gets strained. The amount of strain developed for a given stress is a characteristic of a medium and the ratio of stress to strain is the elastic constant or elastic modulus of the medium. Stress can be of two types - compressive type and shear type. Liquids and gases can be elastically compressed but not elastically sheared. Hence they have compressibility as their only elastic modulus. An isotropic solid can be compressed as well as sheared elastically hence they have fundamentally two elastic moduli identified as bulk and shear moduli. The elastic properties of a crystal is the most general case. Here in any spatial direction there can be three types of stresses; one longitudinal and two shear type perpendicular to each other. On resolving the generalised stress and strain on an orthogonal axial reference frame the stress and strain are second rank tensors and therefor require nine numbers to specify them. The stress and strain tensors may be expressed as arrays of nine numbers which represent the three components of stress and strain along the directions of the coordinate axes. The stress tensor represents a force which can be applied along any arbitrary direction of the crystal and is called a field tensor; similar is the case of strain tensor. The tensor which connects the stress and strain is the tensor of the medium and is called the matter tensor [1.1-1.2]. This tensor have definite orientation within the crystal and must conform to crystal symmetry and these are the elastic constants of the crystal. Since it links two second rank tensors, it is a tensor of the fourth rank.

Under the assumption that stress is proportional to strain with in the elastic deformation limit the generalised Hook's Law can be expressed as

$$\sigma_{ij} \propto \varepsilon_{kl} \qquad (1.01)$$

The constant of proportionality is the fourth rank

matter tensor. This tensor is the elastic stiffness c_{ijkl}. Its inverse is the elastic compliance s_{ijkl} and connects the strain to the stress. The relations between these constants and stress and strain are

$$\sigma_{ij} = \Sigma \, c_{ijkl} \, \varepsilon_{kl}$$

$$\varepsilon_{ij} = \Sigma \, s_{ijkl} \, \sigma_{kl} \qquad (1.02)$$

These stiffness or elastic compliances are determined by undertaking elastic wave propagation measurements in solids. Further, these are the constants which determine the velocity of elastic waves in any direction in an anisotropic solid. c_{ijkl} and s_{ijkl} have 81 elements relating 9 stress components to 9 strain components. In the absence of rotation in the material the stress and strain tensors obey the symmetry

$$\sigma_{ij} = \sigma_{ji}$$

$$\varepsilon_{ij} = \varepsilon_{ji} \qquad (1.03)$$

This reduces the number of independent stress and strain components from 9 to 6. The above symmetry lead to at most 36 independent elastic constants. At this point it is appropriate to introduce the more compact two suffix notation for the elastic constants, in which the tensor for the c_{ijkl} (i, j, k, l = 1, 2, 3) is replaced by the matrix c_{ij} (i, j = 1, 2, 3, 4, 5, 6) according to the following subscript equality:

Tensor notation	11	22	33	23,32	31,13	12,21
Matrix notation	1	2	3	4	5	6

The matrix notation is also called Voigt notation and is easily obtained from the relations

$$
\begin{aligned}
ij \rightarrow m &= i & \text{if } i = j \\
ij \rightarrow m &= 9 - i - j & \text{if } i \neq j
\end{aligned}
\tag{1.04}
$$

It may be noted that this two suffix notation is only used for convenience and they do not transform like a second rank tensor. To transform the constants to other axes it is necessary to go back to the original tensor notation.

Considering the elastic energy of the strained crystal, further symmetry can be found in the elastic constant matrix in the form

$$
\begin{aligned}
c_{ij} &= c_{ji} \\
s_{ij} &= s_{ji}
\end{aligned}
\tag{1.05}
$$

This establishes another 15 equalities in the elastic constants and reduces the maximum number of independent constants to 21.

It may be noted that the elastic constant tensor c_{ijkl} is equated to the second-order differential of the crystal potential energy function and for this reason they are sometimes referred to as second-order elastic constants. The next term in the Taylor series expansion of the crystal potential energy function gives rise to the third order elastic constants, which give a measure of the anharmonic form of the interatomic forces or their deviation from the harmonic form of an ideal Hook's law solid.

Further reduction of the number of independent elastic constants is possible when the symmetry of the crystals are considered and this number is different for the different crystal classes. When appropriate directions are chosen as axes, all crystals may be grouped on the basis of their macroscopic morphology into one of 32 crystal classes (symmetry point groups) which are subgroups among 7 crystal systems [1.3]. These 7 systems in the order of decreasing

symmetry are - Cubic, Hexagonal, Tetragonal, Trigonal, Orthorhombic, Monoclinic, and Triclinic. The crystal classes comprise the combinations of the point symmetry operations which result in distinct groupings consistent with the definition of the crystal system to which they belong. The point symmetry operations are those which operate on point in space in such a manner as to produce a symmetrically equivalent point, and by repetition of the operation, the original point is once again attained. Such point symmetry operations include, inversion, n-fold rotation, reflection, n-fold rotary inversion etc.

The following procedure can be used to determine the form of the elastic constant tensor in a crystal of specified symmetry. Given a symmetry operation $\mathbb{R}$ we can perform the corresponding coordinate transformation for the elastic constant tensor c_{ijkl} to obtain the transformed tensor c'_{ijkl}. Since the two coordinate systems are indistinguishable due to symmetry, we require that $c_{ijkl} = c'_{ijkl}$ for all components. This yields relations between the original tensor components. Additional relations follow by applying all symmetry operations, one after another, to each tensor component and requiring that it go into itself after the transformation. Once all relations between the tensor components are known, we can solve the whole set of equations and determine those components which must vanish and also find any relations between the nonvanishing terms.

Table 1.1 gives the non-zero elastic constants for the various crystal systems and point groups.
It can be noted at this point that an isotropic solid has only 2 independent elastic constants with the condition $C_{11} = C_{22} = C_{33}$, $C_{12} = C_{13} = C_{23}$ and $C_{44} = C_{55} = C_{66}$. Further, $C_{12} = C_{11} - 2C_{44}$. The two independent constants of the isotropic solid are some times called Lame constants [1.4] λ and μ, defined by

5

Table 1.1

The nonzero elastic constants for various crystal systems

System	Number of point groups	Point group (Schoenflies notation)	Number of c_{ij}s[*]	
Triclinic	2	C_i and C_1	21	(a)
Monoclinic	3	C_{2h}, C_s, C_2	13	(b)
Orthorhombic	3	D_{2h}, C_{2v}, D_2	9	(c)
Tetragonal	3	C_{4h}, S_4, C_4	7	(d)
Tetragonal	4	D_{4h}, D_{2d}, C_{4v}, D_4	6	(e)
Trigonal	2	C_{3i}, C_3	7	(f)
Trigonal	3	D_{3d}, C_{3v}, D_3	6	(g)
Hexagonal	7	D_{6h}, D_{3h}, C_{6v}, D_6, C_{6h}, C_{3h}, C_6	5	(h)
Cubic	5	O_h, T_d, O, T_h, T	3	(i)

[*]See the equalities given below

Table 1.1 continued.

(a) All 21 constants

(b) C_{11}, C_{12}, C_{13}, C_{15}, C_{22}, C_{23}, C_{25}, C_{33}, C_{35}, C_{44}, C_{46}, C_{55}

   and C_{66}

(c) C_{11}, C_{12}, C_{13}, C_{22}, C_{23}, C_{33}, C_{44}, C_{55} and C_{66}

(d) $C_{11} = C_{22}$, C_{12}, $C_{13} = C_{23}$, $C_{16} = -C_{26}$, C_{33}, $C_{44} = C_{55}$ and

   C_{66}

(e) $C_{11} = C_{22}$, C_{12}, $C_{13} = C_{23}$, C_{33}, $C_{44} = C_{55}$, and C_{66}

(f) $C_{11} = C_{22}$, C_{12}, $C_{13} = C_{23}$, $C_{14} = -C_{24}$, $-C_{15} = C_{25}$, C_{33} and

   $C_{44} = C_{55}$ also $C_{46} = 2C_{25}$, $C_{56} = 2C_{14}$ and $C_{66} =$

   $(1/2)(C_{11} - C_{12})$

(g) $C_{11} = C_{22}$, C_{12}, $C_{13} = C_{23}$, $C_{14} = -C_{24}$, C_{33} and $C_{44} = C_{55}$

   also $C_{56} = 2C_{14}$ and $C_{66} = (1/2)(C_{11} - C_{12})$

(h) $C_{11} = C_{22}$, C_{12}, $C_{13} = C_{23}$, C_{33} and $C_{44} = C_{55}$ also

   $C_{66} = (1/2)(C_{11} - C_{12})$

(i) $C_{11} = C_{22} = C_{33}$, $C_{12} = C_{13} = C_{23}$ and $C_{44} = C_{55} = C_{66}$

$$\lambda = C_{12}$$

$$\mu = C_{44}$$
(1.06)

μ is same as the shear modulus G, the bulk modulus B is defined by

$$B = \lambda + 2\mu/3$$
(1.07)

While B and G are of fundamental importance in theories of elastic constants using atomistic approach, the constants C_{11} and C_{44} are of importance respectively in longitudinal and shear elastic wave propagation studies in isotropic solids.

The elastic constant matrix C_{ij} for the most general case, that is for a triclinic crystal is given below

$$C_{ij} = \begin{bmatrix} C_{11} & C_{12} & C_{13} & C_{14} & C_{15} & C_{16} \\ C_{12} & C_{22} & C_{23} & C_{24} & C_{25} & C_{26} \\ C_{13} & C_{23} & C_{33} & C_{34} & C_{35} & C_{36} \\ C_{14} & C_{24} & C_{34} & C_{44} & C_{45} & C_{46} \\ C_{15} & C_{25} & C_{35} & C_{45} & C_{55} & C_{56} \\ C_{16} & C_{26} & C_{36} & C_{46} & C_{56} & C_{66} \end{bmatrix} \qquad C_{ij} = C_{ji}$$
(1.08)

1.1.2 Equations of motion and their general solution

The propagation of acoustic waves in elastically anisotropic solids is governed by a set of three linear equations known as the Christoffel equations. The characteristic equation relates the velocity v , the direction of the wave propagation and the elastic constants of the medium. It is cubic in v^2. These equations occupy an important position in the field of crystal acoustics, and their solution is required for a wide variety of purposes [1.4-1.10]. Considerable simplification to these equations comes about

8

when the wave normal lies along a crystal symmetry direction. In general the secular equations for these directions factor into a term which is linear in v^2 and one which is quadratic. Thus simple expressions for the velocities result, and in many cases these are easily reversed to obtain the elastic constants from the measured velocities.

Consider an anisotropic medium which shows the ideal Hook's law behavior and in which dissipative processes and nonlinear or dispersive phenomena can be neglected. A disturbance in such a medium is represented by the equation of motion for an element of the medium. This when expressed in the tensor format appears as

$$\rho \frac{\partial^2 u_i}{\partial t^2} = \frac{\partial \sigma_{ij}}{\partial x_i} \tag{1.09}$$

Where ρ is the density of the medium. To obtain the wave equation the right hand side of this equation is written in terms of the deformation components of u_i. For this the relation between stress and strain is made use of. This gives the wave equation in the form

$$\rho \frac{\partial^2 u_i}{\partial t^2} = C_{ijkl} \frac{\partial^2 u_k}{\partial x_j \partial x_i} \tag{1.10}$$

We expect that in an unbounded medium this equation has basic solutions given by plane waves

$$u_i = U_i \exp[i(\mathbf{k} \cdot \mathbf{r} - \omega t)] \tag{1.11}$$

Inserting this solution in the wave equation, we obtain, for the conditions on the wave amplitude U_i

9

$$(C_{ijkl} \, k_j \, k_l - \rho \, \omega^2 \, \delta_{ik}) \, U_k = 0 \qquad (1.12)$$

The three homogeneous equations for U_i from the above equation are the Christoffel equations and they have a solution only if the secular equations of their coefficients is satisfied. This requirement leads to the familiar form of a determinantal equation for the propagation velocity $v = \omega / k$. If we write the propagation vector in terms of direction cosines as $k = k(n_1, n_2, n_3)$, the secular determinant becomes

$$\left| \Gamma_{ik} - \rho \, v^2 \, \delta_{ik} \right| = 0 \qquad (1.13)$$

Where the coefficients Γ_{ik} are defined by

$$\Gamma_{ik} = C_{ijkl} \, n_j \, n_l \qquad (1.14)$$

Γ is called the christoffel matrix and its elements depends on the direction of wave propagation and the elastic constants. δ_{ik} has the usual meaning, that is

$$\delta_{ik} = 0, \text{ for } k \neq j$$
$$\delta_{ik} = 1, \text{ for } k = j \qquad (1.15)$$

The expanded form of this determinantal equation is

$$\left| \begin{array}{ccc} (\Gamma_{11} - \rho \, v^2) & \Gamma_{12} & \Gamma_{13} \\ \Gamma_{12} & (\Gamma_{22} - \rho \, v^2) & \Gamma_{23} \\ \Gamma_{13} & \Gamma_{23} & (\Gamma_{33} - \rho \, v^2) \end{array} \right| = 0$$

$$(1.16)$$

Using the contracted Voigt notation for the elastic constants, the Christoffel coefficients are, in the most general case given by

$$\Gamma_{11} = C_{11} \, n_1^2 + C_{66} \, n_2^2 + C_{55} \, n_3^2 + 2C_{56} \, n_2 \, n_3 + 2C_{15} \, n_3 \, n_1$$
$$+ \, 2C_{16} \, n_1 \, n_2$$

$$\Gamma_{22} = C_{66} \, n_1^2 + C_{22} \, n_2^2 + C_{44} \, n_3^2 + 2C_{24} \, n_2 \, n_3 + 2C_{46} \, n_3 \, n_1$$
$$+ \, 2C_{26} \, n_1 \, n_2$$

$$\Gamma_{33} = C_{55} \, n_1^2 + C_{44} \, n_2^2 + C_{33} \, n_3^2 + 2C_{34} \, n_2 \, n_3 + 2C_{35} \, n_3 \, n_1$$
$$+ \, 2C_{45} \, n_1 \, n_2$$

$$\Gamma_{23} = \Gamma_{32} = C_{56} \, n_1^2 + C_{24} \, n_2^2 + C_{34} \, n_3^2 + (C_{23} + C_{44}) \, n_2 \, n_3$$
$$+ \, (C_{36} + C_{45}) \, n_3 \, n_1 + (C_{25} + C_{46}) \, n_1 \, n_2$$

$$\Gamma_{13} = \Gamma_{31} = C_{15} \, n_1^2 + C_{46} \, n_2^2 + C_{35} \, n_3^2 + (C_{36} + C_{45}) \, n_2 n_3$$
$$+ \, (C_{13} + C_{55}) \, n_3 \, n_1 + (C_{14} + C_{56}) \, n_1 \, n_2$$

$$\Gamma_{12} = \Gamma_{21} = C_{16} \, n_1^2 + C_{26} \, n_2^2 + C_{45} \, n_3^2 + (C_{25} + C_{46}) \, n_2 n_3$$
$$+ \, (C_{14} + C_{56}) \, n_3 \, n_1 + (C_{12} + C_{66}) \, n_1 \, n_2$$

$$(1.17)$$

On evaluating the determinant and equating it to zero we get the secular equation. This is a cubic equation in v^2 and hence it has three solutions and three different velocities are associated with it. Thus in a given direction

there are three waves propagating with different velocities. The fastest of the three is the longitudinal wave or quasi longitudinal wave. The other two are the fast and slow transverse waves or quasi transverse waves. The waves are purely longitudinal or purely transverse only in the pure mode directions in the crystal and these directions are usually the symmetry directions or symmetry planes in the crystal. The three values of ρv^2 are the eigenvalues of the matrix Γ_{ik}, and the corresponding solutions for the displacement vector U_k are the eigenvectors. While eigenvalues give the three velocities the corresponding eigenvectors give the direction of particle motion or the polarisation direction of the wave.

1.2   Wave propagation in orthorhombic and hexagonal systems

1.2.1 Orthorhombic

In the above section the general expressions for elastic wave propagation in crystals have been presented. The general equations are formidably large when applied to specific crystal systems. While the full equations are necessary for the triclinic crystal much simplified equations can be obtained for higher symmetry crystals. This is due to the fact that several elastic constants are zero for the higher symmetry crystals as it was shown in Table 1.1. Further simplification occurs when symmetry directions or planes are chosen as propagation directions so that one or two of the direction cosines n_1, n_2, or n_3 are equal to zero. The simplest expressions are those for cubic crystals and are available in text books [1.11]. Since ultrasonic measurements have been performed on orthorhombic and hexagonal crystals in the work presented in this thesis, the necessary equations are derived for these crystals in the following paragraphes.

For the orthorhombic crystals of all point groups the

nonzero elastic constants are C_{11}, C_{22}, C_{33}, C_{44}, C_{55}, C_{66}, C_{12}, C_{13}, and C_{23}. All other constants in the general matrix are zero. Retaining only the terms that contain nonzero elements the coefficients of the Christoffel matrix Γ_{ik} can be written as

$$\Gamma_{11} = C_{11} \, n_1^2 + C_{66} \, n_2^2 + C_{55} \, n_3^2$$

$$\Gamma_{22} = C_{66} \, n_1^2 + C_{22} \, n_2^2 + C_{44} \, n_3^2$$

$$\Gamma_{33} = C_{55} \, n_1^2 + C_{44} \, n_2^2 + C_{33} \, n_3^2$$

$$\Gamma_{23} = \Gamma_{32} = (C_{23} + C_{44}) \, n_2 \, n_3$$

$$\Gamma_{13} = \Gamma_{31} = (C_{13} + C_{55}) \, n_3 \, n_1$$

$$\Gamma_{12} = \Gamma_{21} = (C_{12} + C_{66}) \, n_1 \, n_2$$

$$(1.18)$$

None of the off diagonal terms of Γ_{ik} are still not equal to zero which means that the characteristic equation cannot be factored and single term equations cannot be written for the velocity.

Now, consider wave propagation in the x-y plane, which means $n_3 = 0$. The Γ coefficients now becomes

$$\Gamma_{11} = C_{11} \, n_1^2 + C_{66} \, n_2^2 \qquad \Gamma_{23} = \Gamma_{32} = 0$$

$$\Gamma_{22} = C_{66} \, n_1^2 + C_{22} \, n_2^2 \qquad \Gamma_{13} = \Gamma_{31} = 0$$

$$\Gamma_{33} = C_{55} \, n_1^2 + C_{44} \, n_2^2 \qquad \Gamma_{12} = \Gamma_{21} = (C_{12} + C_{66}) \, n_1 n_2$$

$$(1.19)$$

The determinantal equation can now be written as

13

$$
\begin{vmatrix}
(\Gamma_{11} - \rho v^2) & \Gamma_{12} & 0 \\
\Gamma_{12} & (\Gamma_{22} - \rho v^2) & 0 \\
0 & 0 & (\Gamma_{33} - \rho v^2)
\end{vmatrix} = 0
$$

$$(1.20)$$

Expanding the determinant, we get

$$(\Gamma_{11} - \rho v^2)(\Gamma_{22} - \rho v^2)(\Gamma_{33} - \rho v^2) - \Gamma_{12}^2(\Gamma_{33} - \rho v^2) = 0$$

or

$$(\Gamma_{33} - \rho v^2)[\rho^2 v^4 - \rho v^2(\Gamma_{11} + \Gamma_{22}) + \Gamma_{11}\Gamma_{22} - \Gamma_{12}^2] = 0$$

$$(1.21)$$

The factor which is linear in ρv^2 yields the root

$$\rho v_0^2 = \Gamma_{33} \tag{1.22}$$

and the factor which is quadratic in ρv^2 provides the other two roots

$$2\rho v_1^2 = (\Gamma_{11} + \Gamma_{22}) + [(\Gamma_{11} + \Gamma_{22})^2 - 4(\Gamma_{11}\Gamma_{22} - \Gamma_{12}^2)]^{1/2}$$

$$(1.23)$$

and

$$2\rho v_2^2 = (\Gamma_{11} + \Gamma_{22}) - [(\Gamma_{11} + \Gamma_{22})^2 - 4(\Gamma_{11}\Gamma_{22} - \Gamma_{12}^2)]^{1/2}$$

$$(1.24)$$

v_0 is a pure shear wave with polarisation in the z direction, v_1 is a quasilongitudinal wave and v_2 is a quasishear wave.

On substituting the values of Γ for the x-y plane in above three equations, the velocities are obtained in terms of the elastic constants and the direction cosines, as

14

$$\rho v_0^2 = C_{55} \ n_1^2 + C_{44} \ n_2^2 \tag{1.25}$$

$$2\rho v_1^2 = (\ C_{11} \ n_1^2 + C_{22} \ n_2^2 + C_{66} \ ) + [(\ C_{11} \ n_1^2 + C_{22} \ n_2^2 + C_{66} \ )^2$$

$$- \ 4((\ C_{11} n_1^2 + C_{66} \ n_2^2 \ ) \ (\ C_{66} \ n_1^2 + C_{22} \ n_2^2 \ )$$

$$- \ (\ C_{12} + C_{66} \ )^2 \ n_1^2 \ n_2^2 \ ) \ ]^{1/2} \tag{1.26}$$

$$2\rho v_2^2 = (\ C_{11} \ n_1^2 + C_{22} \ n_2^2 + C_{66} \ ) - [(\ C_{11} \ n_1^2 + C_{22} \ n_2^2 + C_{66} \ )^2$$

$$- \ 4((\ C_{11} n_1^2 + C_{66} \ n_2^2 \ ) \ (\ C_{66} \ n_1^2 + C_{22} \ n_2^2 \ )$$

$$- \ (\ C_{12} + C_{66} \ )^2 \ n_1^2 \ n_2^2 \ ) \ ]^{1/2} \tag{1.27}$$

Use is made of the relation,

$$n_1^2 + n_2^2 + n_3^2 = 1 \tag{1.28}$$

which is obeyed by the normalised direction cosines.

Consider propagation in the x-z plane, which means that $n_2 = 0$, the coefficients are then obtained as,

$$\Gamma_{11} = C_{11} \ n_1^2 + C_{55} \ n_3^2 \qquad \Gamma_{23} = \Gamma_{32} = 0$$

$$\Gamma_{22} = C_{66} \ n_1^2 + C_{44} \ n_3^2 \qquad \Gamma_{13} = \Gamma_{31} = (C_{13} + C_{55}) \ n_3 n_1$$

$$\Gamma_{33} = C_{55} \ n_1^2 + C_{33} \ n_3^2 \qquad \Gamma_{12} = \Gamma_{21} = 0$$

$$\tag{1.29}$$

The characteristic equation is then given by,

$$(\ \Gamma_{22} - \rho v^2) \ [\ \rho^2 v^4 - \rho v^2 (\ \Gamma_{11} + \Gamma_{33} \ ) + \Gamma_{11} \ \Gamma_{33} - \Gamma_{13}^2 \ ] = 0 \tag{1.30}$$

The factor which is linear in ρv^2 yields the root

$$\rho v_0^2 = \Gamma_{22} \tag{1.31}$$

and the factor which is quadratic in ρv^2 provides the other two roots

$$2\rho v_1^2 = (\Gamma_{11} + \Gamma_{33}) + [(\Gamma_{11} + \Gamma_{33})^2 - 4(\Gamma_{11}\Gamma_{33} - \Gamma_{13}^2)]^{1/2} \tag{1.32}$$

and

$$2\rho v_2^2 = (\Gamma_{11} + \Gamma_{33}) - [(\Gamma_{11} + \Gamma_{33})^2 - 4(\Gamma_{11}\Gamma_{33} - \Gamma_{13}^2)]^{1/2} \tag{1.33}$$

On substituting values of Γ for the x-z plane in above three equations, the velocities are obtained in terms of the elastic constants and the direction cosines, as

$$\rho v_0^2 = C_{66}\, n_1^2 + C_{44}\, n_3^2 \tag{1.34}$$

$$2\rho v_1^2 = (C_{11}\, n_1^2 + C_{33}\, n_3^2 + C_{55}) + [(C_{11}\, n_1^2 + C_{33}\, n_3^2 + C_{55})^2$$

$$- 4((C_{11}n_1^2 + C_{55}\, n_3^2)(C_{55}\, n_1^2 + C_{33}\, n_3^2)$$

$$- (C_{13} + C_{55})^2\, n_1^2\, n_3^2)]^{1/2} \tag{1.35}$$

$$2\rho v_2^2 = (C_{11}\, n_1^2 + C_{33}\, n_3^2 + C_{55}) - [(C_{11}\, n_1^2 + C_{33}\, n_3^2 + C_{55})^2$$

$$- 4((C_{11}n_1^2 + C_{55}\, n_3^2)(C_{55}\, n_1^2 + C_{33}\, n_3^2)$$

$$- (C_{13} + C_{55})^2\, n_1^2\, n_3^2)]^{1/2} \tag{1.36}$$

Consider propagation in the y-z plane, which means that $n_1 = 0$, the coefficients are then obtained as,

$$\Gamma_{11} = C_{66} \, n_2^2 + C_{55} \, n_3^2 \qquad\qquad \Gamma_{23} = \Gamma_{32} = (\, C_{23} + C_{44} \,) \, n_2 n_3$$

$$\Gamma_{22} = C_{22} \, n_2^2 + C_{44} \, n_3^2 \qquad\qquad \Gamma_{13} = \Gamma_{31} = 0$$

$$\Gamma_{33} = C_{44} \, n_2^2 + C_{33} \, n_3^2 \qquad\qquad \Gamma_{12} = \Gamma_{21} = 0$$

$$(1.37)$$

The characteristic equation is then given by,

$$(\, \Gamma_{11} - \rho v^2) \, [\, \rho^2 v^4 - \rho v^2(\, \Gamma_{22} + \Gamma_{33} \,) + \Gamma_{22} \, \Gamma_{33} - \Gamma_{23}^2 \,] = 0$$

$$(1.38)$$

The factor which is linear in ρv^2 yields the root

$$\rho v_0^2 = \Gamma_{11} \qquad\qquad (1.39)$$

and the factor which is quadratic in ρv^2 provides the other two roots

$$2\rho v_1^2 = (\, \Gamma_{22} + \Gamma_{33} \,) + [\, (\, \Gamma_{22} + \Gamma_{33})^2 - 4(\, \Gamma_{22} \, \Gamma_{33} - \Gamma_{23}^2 \,)]^{1/2}$$

$$(1.40)$$

and

$$2\rho v_2^2 = (\, \Gamma_{22} + \Gamma_{33} \,) - [\, (\, \Gamma_{22} + \Gamma_{33})^2 - 4(\, \Gamma_{22} \, \Gamma_{33} - \Gamma_{23}^2 \,)]^{1/2}$$

$$(1.41)$$

On substituting values of Γ for the y-z plane in above three equations, the velocities are obtained in terms of the elastic constants and the direction cosines, as

$$\rho v_0^2 = C_{66} \, n_2^2 + C_{55} \, n_3^2 \qquad\qquad (1.42)$$

$$2\rho v_1^2 = (\, C_{22} \, n_2^2 + C_{33} \, n_3^2 + C_{44} \,) + [\, (\, C_{22} \, n_2^2 + C_{33} \, n_3^2 + C_{44} \,)^2$$

$$- 4((\, C_{22} n_2^2 + C_{44} \, n_3^2 \,) \, (\, C_{44} \, n_2^2 + C_{33} \, n_3^2 \,)$$

$$- (\, C_{23} + C_{44} \,)^2 \, n_2^2 \, n_3^2 \,) \,]^{1/2} \qquad\qquad (1.43)$$

17

$$2\rho v_2^2 = (\ C_{22}\ n_2^2 + C_{33}\ n_3^2 + C_{44}\ ) - [\ (\ C_{22}\ n_2^2 + C_{33}\ n_3^2 + C_{44}\ )^2$$

$$- 4((\ C_{22}n_2^2 + C_{44}\ n_3^2\ )\ (\ C_{44}\ n_2^2 + C_{33}\ n_3^2\ )$$

$$- (\ C_{23} + C_{44}\ )^2\ n_2^2\ n_3^2\ )\ ]^{1/2} \tag{1.44}$$

The above analysis for wave propagation in orthorhombic crystals have provided us three set of equations corresponding to the three orthogonal symmetry planes of the crystal. As a general observation it can be seen that when the wave propagation is in a symmetry plane there is always a pure shear mode which is polarised normal to the plane. These equations can be used to compute the velocities in any direction in these symmetry planes if the elastic constants are known.

Now consider the propagation along the symmetry axis of the crystal. These directions are the x, y, and z directions for the orthorhombic system and it corresponds to the a, b, and c directions of the crystal or they are the [100], [010] and [001] directions.

For propagation in x direction, the corresponding direction cosines are $n_1 = 1$, $n_2 = 0$ and $n_3 = 0$. In this case the coefficients reduce to,

$$
\begin{array}{ll}
\Gamma_{11} = C_{11} & \Gamma_{23} = 0 \\
\Gamma_{22} = C_{66} & \Gamma_{13} = 0 \qquad (1.45) \\
\Gamma_{33} = C_{55} & \Gamma_{12} = 0
\end{array}
$$

The off diagonal elements are all zero and the characteristic equation is

$$(\ \Gamma_{11} - \rho v^2)\ (\ \Gamma_{22} - \rho v^2\ )\ (\Gamma_{33} - \rho v^2) = 0 \tag{1.46}$$

18

which readily factors to give the solutions,

$$\rho v_0^2 = C_{11}, \ \rho v_1^2 = C_{66} \ \text{and} \ \rho v_2^2 = C_{55} \qquad (1.47)$$

These are pure mode waves, v_0 is longitudinal, v_1 is transverse with y polarisation and v_2 is transverse with z polarisation.

For propagation in y direction, the corresponding direction cosines are $n_1 = 0$, $n_2 = 1$ and $n_3 = 0$. In this case the coefficients reduce to,

$$\begin{array}{ll} \Gamma_{11} = C_{66} & \Gamma_{23} = 0 \\ \\ \Gamma_{22} = C_{22} & \Gamma_{13} = 0 \qquad (1.48) \\ \\ \Gamma_{33} = C_{44} & \Gamma_{12} = 0 \end{array}$$

The characteristic equation readily factors to give the solutions,

$$\rho v_0^2 = C_{66}, \ \rho v_1^2 = C_{22} \ \text{and} \ \rho v_2^2 = C_{44} \qquad (1.49)$$

These are also pure mode waves, v_0 is transverse with x polarisation, v_1 is longitudinal and v_2 is transverse with z polarisation.

For propagation in z direction, the corresponding direction cosines are $n_1 = 0$, $n_2 = 0$ and $n_3 = 1$. In this case the coefficients reduce to,

$$\begin{array}{ll} \Gamma_{11} = C_{55} & \Gamma_{23} = 0 \\ \\ \Gamma_{22} = C_{44} & \Gamma_{13} = 0 \qquad (1.50) \\ \\ \Gamma_{33} = C_{33} & \Gamma_{12} = 0 \end{array}$$

The characteristic equation readily factors to give the solutions,

$$\rho v_0^2 = C_{55}, \ \rho v_1^2 = C_{44} \ \text{and} \ \rho v_2^2 = C_{33} \qquad (1.51)$$

These are also pure mode waves, v_0 is transverse with x polarisation, v_1 is transverse with y polarisation and v_2 is longitudinal.

1.2.2 Hexagonal

Hexagonal crystals are having a six fold axis of symmetry. The nonzero elastic constants of hexagonal crystals are

$$C_{11} = C_{22}, \ C_{12}, \ C_{13} = C_{23}, \ C_{33} \text{ and } C_{44} = C_{55}$$

$$\text{Also,} \quad C_{66} = (1/2)(C_{11} - C_{12}) \text{ or } C_{12} = C_{11} - 2C_{66}$$

Retaining only the terms that contain nonzero elements the coefficients of the Christoffel matrix Γ_{ik} can be written as

$$\Gamma_{11} = C_{11} \ n_1^2 + C_{66} \ n_2^2 + C_{44} \ n_3^2$$

$$\Gamma_{22} = C_{66} \ n_1^2 + C_{11} \ n_2^2 + C_{44} \ n_3^2$$

$$\Gamma_{33} = C_{44} \ n_1^2 + C_{44} \ n_2^2 + C_{33} \ n_3^2$$

$$\Gamma_{23} = \Gamma_{32} = (C_{13} + C_{44}) \ n_2 n_3 \tag{1.52}$$

$$\Gamma_{13} = \Gamma_{31} = (C_{13} + C_{44}) \ n_3 n_1$$

$$\Gamma_{12} = \Gamma_{21} = (C_{11} - C_{66}) \ n_1 n_2$$

Now consider wave propagation in the x-y plane, which means $n_3 = 0$. The coefficients now become

$$\Gamma_{11} = C_{11} \ n_1^2 + C_{66} \ n_2^2 \qquad \Gamma_{23} = \Gamma_{32} = 0$$

$$\Gamma_{22} = C_{66} \ n_1^2 + C_{11} \ n_2^2 \qquad \Gamma_{13} = \Gamma_{31} = 0$$

$$\Gamma_{33} = C_{44} \ n_1^2 + C_{44} \ n_2^2 \qquad \Gamma_{12} = \Gamma_{21} = (C_{11} - C_{66}) \ n_1 n_2$$

$$\tag{1.53}$$

The characteristic equation is,

$$(\Gamma_{33} - \rho v^2) [\rho^2 v^4 - \rho v^2 (\Gamma_{11} + \Gamma_{22}) + \Gamma_{11} \Gamma_{22} - \Gamma_{12}^2] = 0$$

(1.54)

The factor which is linear in ρv^2 yields the root

$$\rho v_0^2 = \Gamma_{33}$$

(1.55)

and the factor which is quadratic in ρv^2 provides the other two roots

$$2\rho v_1^2 = (\Gamma_{11} + \Gamma_{22}) + [(\Gamma_{11} + \Gamma_{22})^2 - 4 (\Gamma_{11} \Gamma_{22} - \Gamma_{12}^2)]^{1/2}$$

(1.56)

and

$$2\rho v_2^2 = (\Gamma_{11} + \Gamma_{22}) - [(\Gamma_{11} + \Gamma_{22})^2 - 4 (\Gamma_{11} \Gamma_{22} - \Gamma_{12}^2)]^{1/2}$$

(1.57)

On substitution of the Γ values for the x-y plane in the above solution for hexagonal crystal, considerable algebraic simplification occurs and very simple solutions are obtained as,

$$\rho v_0^2 = C_{44}$$
$$\rho v_1^2 = C_{11}$$
$$\rho v_2^2 = C_{66}$$

(1.58)

The above result shows that the velocity is independent of the direction in this plane and that all modes are pure. v_0 is a shear mode polarised parallel to z axis, v_1 is a longitudinal mode and v_2 is a shear mode polarised normal to z axis. The above relations are valid for the directions x, y or any direction in the plane.

Consider propagation in the x-z plane, which means that $n_2 = 0$, the coefficients are then obtained as,

$$\Gamma_{11} = C_{11} \, n_1^2 + C_{44} \, n_3^2 \qquad\qquad \Gamma_{23} = \Gamma_{32} = 0$$

$$\Gamma_{22} = C_{66} \, n_1^2 + C_{44} \, n_3^2 \qquad\qquad \Gamma_{13} = \Gamma_{31} = (C_{13} + C_{44}) \, n_3 n_1$$

$$\Gamma_{33} = C_{44} \, n_1^2 + C_{33} \, n_3^2 \qquad\qquad \Gamma_{12} = \Gamma_{21} = 0$$

$$(1.59)$$

The characteristic equation is then given by,

$$(\Gamma_{22} - \rho v^2) \, [\, \rho^2 v^4 - \rho v^2 (\Gamma_{11} + \Gamma_{33}) + \Gamma_{11} \Gamma_{33} - \Gamma_{13}^2 \,] = 0$$

$$(1.60)$$

The linear part gives one root and the quadratic part gives the other two roots. On substituting the Γ values and simplifying the following expressions are obtained for the three velocities,

$$\rho v_0^2 = C_{66} \, n_1^2 + C_{44} \, n_3^2 \qquad\qquad\qquad (1.61)$$

$$2\rho v_1^2 = (\, C_{11} \, n_1^2 + C_{33} \, n_3^2 + C_{44} \,) + [(\, C_{11} \, n_1^2 + C_{33} \, n_3^2 + C_{44} \,)^2$$

$$- 4((\, C_{11} n_1^2 + C_{44} \, n_3^2 \,) \, (\, C_{44} \, n_1^2 + C_{33} \, n_3^2 \,)$$

$$- (\, C_{13} + C_{44} \,)^2 \, n_1^2 \, n_3^2 \,) \,]^{1/2} \qquad\qquad (1.62)$$

$$2\rho v_2^2 = (\, C_{11} \, n_1^2 + C_{33} \, n_3^2 + C_{44} \,) - [(\, C_{11} \, n_1^2 + C_{33} \, n_3^2 + C_{44} \,)^2$$

$$- 4((\, C_{11} n_1^2 + C_{44} \, n_3^2 \,) \, (\, C_{44} \, n_1^2 + C_{33} \, n_3^2 \,)$$

$$- (\, C_{13} + C_{44} \,)^2 \, n_1^2 \, n_3^2 \,) \,]^{1/2} \qquad\qquad (1.63)$$

v_0 is a pure shear mode polarised normal to the plane, v_1 is a quasilongitudinal wave and v_2 is a quasishear wave. It can be seen that these expressions are rotationally invariant for rotations about the z axis. Hence the same expressions are valid for the y-z plane or any meridian plane.

For the symmetry direction along the z axis, the above

expressions can be simplified by putting $n_1 = 0$, and $n_3 = 1$. This gives,

$$\rho v_0^2 = C_{44}$$
$$\rho v_1^2 = C_{33} \qquad\qquad (1.64)$$
$$\rho v_2^2 = C_{44}$$

v_1 is a longitudinal mode, v_0 and v_2 are shear modes polarised normal to the z-axis and they are degenerate. Since two transverse velocities are identical the z direction of the Hexagonal crystal is an acoustic axis of the crystal.

1.3   Ultrasonic velocity measurements to determine the elastic constants.

1.3.1 General remarks

In the last section we have found that the propagation velocity of acoustic waves in a crystal is related to the elastic constants, density of the crystal and the propagation direction. Thus by measuring the acoustic wave velocities along defined directions it is possible to deduct the elastic constants of the crystal. Although the velocity measurements are straight forward, obtaining the elastic constants from the experimental data can be very tedious, especially for low symmetry crystals. Only for certain simple directions, which occur more frequently for high symmetry crystals, will a sound wave be pure longitudinal or pure transverse [1.12]. In general, the eigenvectors which specify the modes of vibration are neither parallel nor perpendicular to the propagation direction. For such quasilongitudinal and quasishear modes it is not possible to relate the measured velocity directly to a single constant. For general directions the measured velocity can depend on as many as 21 elastic constants (triclinic) which obviously, leads to complications in reducing the data

23

[1.13]. It can be noted that only for cubic crystals it is possible to obtain all elastic constants from measurements of pure longitudinal or pure transverse waves. For all other symmetries, some of the elastic constants must be determined from measurements of quasilongitudinal and/or quasitransverse waves.

Further, great care is required in orienting, cutting and polishing the crystal exactly in the pure mode directions when measurements are to be performed along these directions.Any small deviation from the required direction will bring in contributions from several other constants and special misorientation correction techniques [1.14] are to be applied to correct the data.

Fortunately in ultrasonic experiments the three different modes in any given direction can be separately excited by choosing the transducers for longitudinal and transverse waves and by rotating the transverse mode transducer the polarisation can be selected in the desired direction. This facility simplifies the otherwise difficult problem of selecting the correct expression for the desired mode of propagation.

1.3.2. Elastic constant measurements on orthorhombic crystals

In the previous section we have derived the expressions for the velocity of elastic waves in various symmetry directions and symmetry planes in the orthorhombic crystal. For the measurement of elastic constants, these expressions are to be reversed. As we have seen for the orthorhombic crystals the crystallographic directions a, b, and c are pure mode directions. All the three velocities measured in each of these directions are related to single elastic constants only. Measurements in these directions will isolate all the diagonal constants, C_{11}, C_{22}, C_{33}, C_{44}, C_{55}, and C_{66} in the elastic

constant matrix. To find the off diagonal constants the quasilongitudinal waves in various symmetry planes, x-y, x-z and y-z can be used. The off diagonal constants C_{12}, C_{13} and C_{23} appear in combination with other constants when measurements are done in these symmetry planes. The necessary expressions for computing the elastic constants from the measured velocities are obtained by reversing the equations for the velocities obtained earlier in previous section. These reversed relations are summarised in Table 1.2. When the propagation direction is to be specified for cutting the crystal or to measure the direction of propagation, it is convenient to express the direction in a plane in terms of the angle from a crystallographic axis like a, b, or c, than in terms of the direction cosines. The direction cosines are then obtained as the sine and cosine functions of this angle. The convention adopted in this work for this is illustrated in figure 1.1.

1.3.3 Elastic constant measurements on hexagonal crystals

In section 1.2.2 we have derived the relations connecting the elastic constants to the propagation velocity for hexagonal crystals. We find that all the diagonal constants, $C_{11} = C_{22}$, C_{33}, $C_{44} = C_{55}$ and C_{66} can be obtained by measuring the velocities in the symmetry directions a and c. The measurement in the b direction gives the same information as in the a direction due to the rotational invariance of velocity in the a-b plane of a hexagonal crystal. The number of nonzero elastic constants of Orthorhombic and Hexagonal systems are the same. But for orthorhombic all the 9 constants are independent while for Hexagonal only 5 are independent as listed in Table 1.1. Once C_{11} and C_{66} are known the off diagonal constant C_{12} can be calculated using the relation,

a-c plane

Z

N

n_3

1

θ

O n_1 X

$n_1 = \sin \theta$

$n_3 = \cos \theta$

$\theta = \angle\ ZON$

$n_1^2 + n_3^2 = 1$

b-c plane

Z

N

n_3

1

θ

O n_2 Y

$n_2 = \cos \theta$

$n_3 = \sin \theta$

$\theta = \angle\ YON$

$n_2^2 + n_3^2 = 1$

a-b plane

Y

N

n_2

1

θ

O n_1 X

$n_1 = \cos \theta$

$n_2 = \sin \theta$

$\theta = \angle\ XON$

$n_2^2 + n_1^2 = 1$
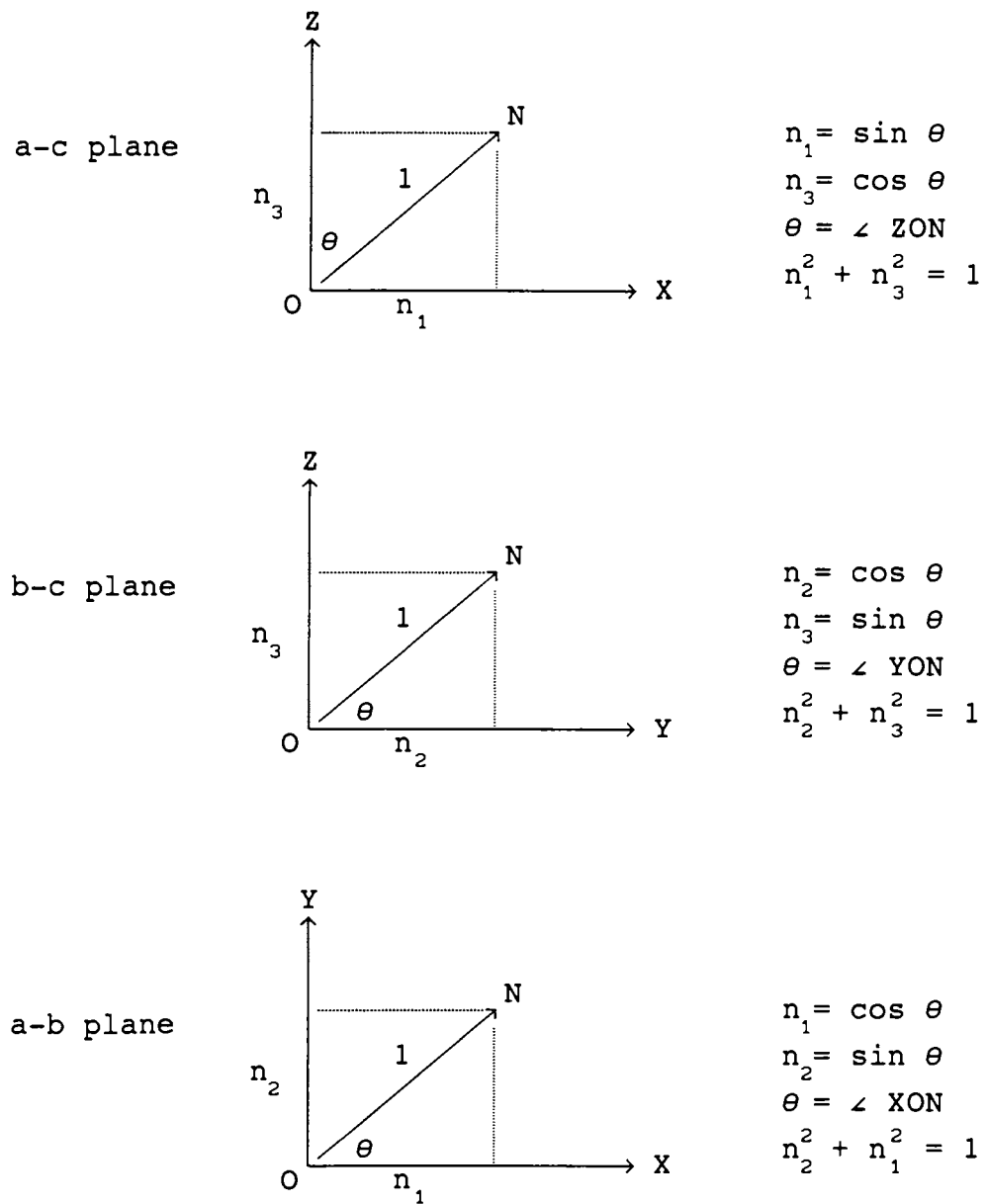
Figure 1.1

Direction cosines to rotation angle conversion

scheme in symmetry planes a-c, b-c and a-b.

Table 1.2

Sound velocity - Elastic moduli relations for the Orthorhombic system

No.	Mode	Direction of particle motion	Formula for elastic moduli
(1)	(2)	(3)	(4)

<div align="center">Propagation along a - axis</div>

1	L	a	$C_{11} = \rho v^2$
2	T	b	$C_{66} = \rho v^2$
3	T	c	$C_{55} = \rho v^2$

<div align="center">Propagation along b - axis</div>

4	L	b	$C_{22} = \rho v^2$
5	T	a	$C_{66} = \rho v^2$
6	T	c	$C_{44} = \rho v^2$

<div align="center">Propagation along c - axis</div>

7	L	c	$C_{33} = \rho v^2$
8	T	a	$C_{55} = \rho v^2$
9	T	b	$C_{44} = \rho v^2$

Table 1.2 continued

_____

(1)   (2)   (3)   (4)

_____

    Propagation   in a-b plane, angle measured from a-axis

10   QL $\perp$ c $C_{12} = f_{ab}$

11   QT $\perp$ c C_{12} = similar to f_{ab}

12   T   c $\rho v^2 = c^2 C_{55} + s^2 C_{44}$

    Propagation in b-c plane, angle measured from b-axis

13   QL $\perp$ a $C_{23} = f_{bc}$

14   QT $\perp$ a C_{23} = similar to f_{bc}

15   T   a $\rho v^2 = c^2 C_{66} + s^2 C_{55}$

    Propagation in a-c plane, angle measured from c-axis

16   QL $\perp$ b $C_{13} = f_{ac}$

17   QT $\perp$ b C_{13} = similar to f_{ac}

18   T   b $\rho v^2 = s^2 C_{66} + c^2 C_{44}$

Table 1.2 continued

The abbreviations used have the following meanings:

L - Longitudinal, T - Transverse, QL - Quasi-longitudinal, QT - Quasi-transverse, s = sine and c = cosine of angle θ from the respective axis, ρ = density , v = velocity of propagation of respective mode. a, b, c -Crystallographic axis. f_{ab}, f_{bc} and f_{ac} are defined as,

$$f_{ab} = \left[\frac{\left(c^2 C_{11} + s^2 C_{66} - \rho v^2 \right) \left(c^2 C_{66} + s^2 C_{22} - \rho v^2 \right)}{c^2 s^2} \right]^{\frac{1}{2}} - C_{66} \ ,$$

$$f_{bc} = \left[\frac{\left(c^2 C_{22} + s^2 C_{44} - \rho v^2 \right) \left(c^2 C_{44} + s^2 C_{33} - \rho v^2 \right)}{c^2 s^2} \right]^{\frac{1}{2}} - C_{44} \ ,$$

$$f_{ac} = \left[\frac{\left(s^2 C_{11} + c^2 C_{55} - \rho v^2 \right) \left(s^2 C_{55} + c^2 C_{33} - \rho v^2 \right)}{c^2 s^2} \right]^{\frac{1}{2}} - C_{55} \ .$$

29

$$C_{12} = C_{11} - 2C_{66} \qquad\qquad (1.65)$$

The only independent off diagonal constant C_{13} which is also equal to C_{23} can be obtained by velocity measurement of the quasilongitudinal wave in the a-c plane, provided the constants C_{11}, C_{33} and C_{44} are known. The form of the reversed expression obtained is similar to the orthorhombic system. All the necessary relations required for elastic constant measurement of Hexagonal crystals are listed in Table 1.3. The abbreviations used in the table carry the same meanings as that defined in Table 1.2.

1.4 Investigation of structural phase transitions using ultrasonics

1.4.1 Structural phase transitions: An overview

The change of structure during a phase transition in a solid can occur in two quite distinct ways [1.15]. In the first type the atoms of the solid *reconstruct* to a new lattice like graphite transforming to diamond or like an amorphous solid changing to a crystalline form. These reconstructive transitions are often slow recrystallization process and are not symmetry related. In the second type the regular lattice is only slightly *distorted* without disrupting the linkage of the network. This can occur as a result of small *displacements* in the lattice position of single atoms or molecular units, or due to the *ordering* of atoms or molecules among various equivalent positions. These type of transitions are symmetry related. The term structural phase transition (SPT) is sometimes used, in a narrow sense, to describe the second type only. Since two different mechanisms are there for the second type of SPT or the distortive SPT, they can be classified as

30

Table 1.3

Sound velocity - Elastic moduli relations for Hexagonal system

---

No.	Mode	Direction of particle motion	Formula for elastic moduli

---

<div align="center">Propagation along a - axis</div>

1	L	a	$C_{11} = C_{22} = \rho v^2$
2	T	b	$C_{66} = \rho v^2$
3	T	c	$C_{44} = C_{55} = \rho v^2$

<div align="center">Propagation along c - axis</div>

4	L	c	$C_{33} = \rho v^2$
5	T	a	$C_{44} = C_{55} = \rho v^2$
6	T	b	$C_{44} = C_{55} = \rho v^2$

<div align="center">Propagation in a-c plane, angle θ measured from c-axis</div>

7	QL	$\perp$ b	$C_{13} = C_{23} = f_{ac}$
8	QT	$\perp$ b	$C_{13} = C_{23} = $ similar to f_{ac}
9	T	b	$\rho v^2 = s^2 C_{66} + c^2 C_{44}$

---

where f_{ac} is defined as,

$$f_{ac} = \left[\frac{\left(s^2 C_{11} + c^2 C_{44} - \rho v^2\right)\left(s^2 C_{44} + c^2 C_{33} - \rho v^2\right)}{c^2 s^2} \right]^{\frac{1}{2}} - C_{44}$$

displacive type and order-disorder type.

The symmetry of a crystal normally undergoes a change when a SPT takes place. For a large class of systems this change consists in the loss of a part of symmetry elements by a crystal under its transformation from the higher to the lower temperature phase. In this the symmetry group of the new (less symmetrical) phase is a subgroup of the old (more symmetrical) phase.

In the study of phase transitions the order parameter is a crucial quantity. The simplest way to define the order parameter is as a variable that characterizes the magnitude of these atomic displacements or the degree of their ordering, which just represent the change in the crystal undergoing phase transition. Many diverse changes takes place in a crystal during phase transition and in general, several order parameters are to be considered to describe them. But in many cases a dominant role is played by a single order parameter. The order parameter is the starting quantity in the Landau theory of Phase transition [1.16] which has provided the most formidable and successful theoretical formulation for Phase transitions. The basic formula of the Landau theory is the expression for the thermodynamic potential considered as a function of the order parameter as outlined below.

The Landau free energy expansion can be written as

$$F = F_0 + A\ Q^2 + B\ Q^4 + \text{higher order terms} \qquad (1.66)$$

where F_0 contains all other degrees of freedom of the system, $Q = Q(T)$ is the order parameter and $A = \alpha\ (\ T - T_c\ )$. α and B can be viewed as nearly temperature independent near T_c. The order parameter $Q(T)$ is assumed to have only one dimension. Upon minimization of the free energy with respect to the order parameter, one finds a second order transition at T_c when $B > 0$ with the order parameter varying continuously as

32

$Q^2 \propto (T_c - T)$. With $B < 0$ a first order transition results with a discontinuous jump of the order parameter.

In displacive type SPT the atoms in the distorted phase are slightly displaced away from their equilibrium positions of the high temperature phase. This then led to the suggestion by Cochran [1.17] and Anderson [1.18] and earlier but largely unnoticed comments by others (Raman and Nedungadi [1.19] and Saksena [1.20]) that these phase transitions might be the result of an instability of the crystal against a particular normal mode of vibration of the high temperature phase. Since this suggestion, there have been numerous measurements of the so-called *soft modes* associated with SPT and for the displacive SPT their existence is well established. It can be seen that a mode of finite frequency exists even above T_c and tends to freeze out on approaching T_c from above. In order-disorder type SPT the ordering process of the atomic groups cannot be described in terms of small displacements from equilibrium positions. Consequently in these order-disorder systems soft mode ideas are less useful than in displacive systems.

The modes of the crystal, characterized by a dispersion relationship $\omega(q)$, of a crystal, are collective excitations and extend over the whole wave vector space q of the Brillouin zone. At a displacive transition the freezing out of the soft mode produces the lattice found on the low temperature side of the transition. For $T < T_c$, the soft mode frequency $\omega_s(q)$ has a minimum at some wave vector in q space. This minimum is most often found at the zone center $q = 0$ or at particular points of the Brillouin zone boundary q_b. Accordingly they are termed *zone center* and *zone boundary transitions.* In zone boundary transitions the unit cell gets doubled (or subject to even higher multiplication) in the low temperature phase because the point q_b gets "folded into" the zone center. These cases have been termed earlier by Gränicher and Müller [1.21] as

ferro and *antiferrodistortive* transitions. In cell multiplying zone boundary transitions if the multiplying factor n is a rational multiple of a particular Brillouin zone boundary wave vector q_b, then the transition is called *commensurate*. If, however, n is an irrational number the transitions are called *incommensurate* [1.22]. Some of the recent studies in SPT are aimed towards an understanding of this interesting class of incommensurate transitions.

In a zone center or ferrodistortive SPT the macroscopic quantities may couples linearly to the order parameter. If the spontaneous electric polarization P_s couple linearly with the order parameter then the corresponding transition is called a *Ferroelectric Transition*. On the other hand if the spontaneous strain X_s couple linearly with order parameter then the corresponding transition is called *Ferroelastic Transition*. In zone boundary transitions the macroscopic properties cannot couple linearly with the order parameter.

1.4.2 Probing SPT using ultrasonics

Ultrasonics is an accurate, convenient and a very popular tool for investigating phase transitions in solids. When a distortive phase transition is taking place in the crystal the acoustic modes of vibration in the crystal are directly or indirectly affected. This will in turn reflect as changes in the elastic constants of the crystal near the transition temperature which in turn affects the ultrasonic velocity which is being measured. In cases where the strain is linearly coupled with the order parameter, the ultrasonic measurements of velocity and attenuation can directly probe the order parameter and its static and dynamic response. Ultrasonic measurements can always be related somehow to the ordering quantity because there exists always some kind of coupling between the strain and the order parameter. A

34

complimentary tool for investigating elastic properties near phase transitions is Brillouin scattering. While ultrasonic measurements are done usually in the frequency range of 10 to 100 MHz using large sample sizes the Brillouin scattering technique probes the acoustic modes in the GHz region of frequency and requires only small sample sizes. The precision of measurement is, however, much higher for ultrasonics than for Brillouin scattering.

In the next section a brief discussion is given on how the elastic response function can be related to the relevant processes occurring at a SPT, in the frame work of Landau theory of phase transition [1.16, 1.23-1.27].

1.4.3 Theoretical analysis

In the Landau theory the free energy of the system is written in terms of the order parameter as [1.25],

$$F(Q,T) = F_0(T) + \frac{1}{2} a(T)Q^2 + \frac{1}{4} bQ^4 + \ldots \qquad (1.67)$$

with a as temperature dependent near T_0 as,

$$a = a'(T - T_0) \qquad (1.68)$$

The strain e gives an elastic energy contribution $\frac{1}{2}c_0 e^2$ with the background elastic constant c_0 taken at zero order parameter. Due to the coupling of the strain to the ordering quantity an interaction energy density F_{int} has to be added, which is phenomenologically expanded in powers of e and Q as,

$$F_{int} = geQ + heQ^2 + ie^2Q + \ldots \qquad (1.69)$$

To keep the discussion simple we consider here only one component of e and Q which is the bilinear interaction term. Actually it is the symmetry which decides which coefficients in the expansion (1.69) is different from zero. The expansion of the free energy would now appear as,

$$F(Q,T) = F_0(T) + \frac{1}{2} a(T)Q^2 + \frac{1}{4} bQ^4 + \ldots + \frac{1}{2}c_0 e^2 + geQ \quad (1.70)$$

The ordering quantity plays the role of an internal degree of freedom. It can move more or less freely under the action of forces exerted by the ultrasonic strain field and described by F_{int}. The ordering quantity responds to these forces and reacts back on the elastic system. The result is a change, in general a decrease, in the elastic stiffness. Therefore the most important information about the SPT is obtained from the temperature dependence of the elastic functions.

In the case of bilinear coupling, $F_{int} = geQ$, these forces are proportional to the strain only. There are no other forces and so

$$\frac{\partial F}{\partial Q} = ge + \left(\frac{\partial^2 F}{\partial Q^2}\right)_e \delta Q = ge + \frac{\delta Q}{\chi_Q} = 0, \quad (1.71)$$

and the order parameter can in general follow the applied varying strain: $\delta Q = -\chi_Q ge$. Its response is determined by the unnormalized order parameter susceptibility χ_Q. The moving ordering quantity δQ in turn adds a contribution to the stress σ acting within the sound wave as

$$\sigma = \frac{\partial F}{\partial e} = c_0 e + g\delta Q = (c_0 - g^2\chi_Q)e . \quad (1.72)$$

The result is a diminished elastic stiffness, which in the static limit is equal to

$$c_T = c_0 - g^2\chi_Q = c_0 \frac{T - T_0 - g^2/a'c_0}{T - T_0} \quad (1.73)$$

In the above expression $T_0 = T_0^e$ is, in the case of continuous transition, the transition temperature for zero strain

(clamped state), in the absence of strain interaction (1.69). In the free state (zero stress),

$$T^{\sigma} = T_0 + g^2/a'c_0 \qquad (1.74)$$

is the transition temperature. For discontinuous transitions T_0 denotes the lower stability limit. If this bilinear coupling prevails, the elastic stiffness probes directly the order parameter susceptibility. This is the case not only for the static or low frequency response, but also for the general dynamic response throughout the whole frequency range.

The imaginary part of χ_Q^e is the source for the critical ultrasonic attenuation. In many cases the order parameter response can be described by a relaxation process. This results in a dispersion for the real part of the elastic constant given by

$$c_T(\omega) - c_T(\omega = 0) = g^2\chi_Q^e(0) \frac{\omega^2\tau^2}{1 + \omega^2\tau^2} \qquad (1.75)$$

and an attenuation

$$\alpha(\omega) = \frac{g^2\chi_Q^e(0)\omega^2\tau}{2\rho v_s^3(1 + \omega^2\tau^2)}. \qquad (1.76)$$

For $\omega\tau \gg 1$, $c_T(\omega)$ approaches $c_T(\omega = 0) + g^2\chi_Q^e(0)$ which is, according to (1.73), the background elastic function c_0.

Summarizing the analysis of bilinear coupling of strain and order parameter, we expect an elastic instability $c_T \to 0$ can occur at T_0^{σ} and an ultrasonic attenuation increases as T tends towards T_0^{σ}. The limit $\omega\tau = 1$ is practically not reached in ultrasonic experiments at structural transitions, but Brillouin scattering can show dispersive effects.

In the above discussion we have considered only the bilinear coupling of the order parameter and strain. But there are several phase transitions in which this is not the case.

In some systems the coupling is linear in strain but quadratic in order parameter. In some other systems coupling is linear in order parameter but quadratic in strain. More complex type of nonlinear couplings also can be there. Landau theory can be extended to these cases and different types of elastic response functions can be obtained. On the other hand the experimentally obtained elastic response functions can be fitted to the theoretically predicted curves to identify the type of coupling in the system under investigation. Landau theory is a mean field theory and in its simplest form it neglects the fluctuations of the ordering quantity and close to the critical region its application is rather limited.

1.5 Phase transitions in mixed sulphate crystals

The crystals in which we have conducted investigations belong to the family of crystals with the general formula [1.28],

$$M^I M^{II} B X_4$$

where

$$M^I = \text{Li or Na}$$

$$M^{II} = \text{Na, K, Rb, } NH_4, \text{ Cs or } N_2H_5$$

$$BX_4 = BeF_4, SO_4 \text{ or } SeO_4$$
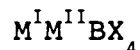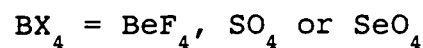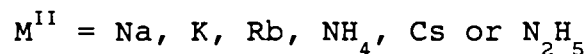
The members of this family like, $LiKSO_4$, $LiNaSO_4$, $LiNaSeO_4$ and $LiRbSO_4$ are isostructural and are all pyroelectric and belong to the hexagonal crystal system. These, in terms of the classification of Chung and Hahn [1.29], can be regarded as the *proper derivatives* of the tridymite structure (space group Pm3 (T_h^1)). Compounds with larger M^{II} ions in this family are generally orthorhombic and are said to belong to the *improper derivatives* of the tridymite structure. The

orthorhombic Lithium Ammonium Sulphate ($LiNH_4SO_4$) and Lithium Hydrazinium Sulphate ($LiN_2H_5SO_4$) are examples of the later class.

Sulphate crystals, in general, have very interesting physical properties. Many of them undergo a series of phase transitions as the temperature is varied. Some of these undergo ferroelectric transitions, while some others undergo ferroelastic transitions and some of them exhibit both these types of transitions. The object of this work has been to investigate phase transitions in these interesting materials using ultrasonic technique selecting a few representative members from this family.

From this family of mixed crystals we have selected three sulphate crystals for our investigations. They are Lithium Hydrazinium Sulphate (LHS), Lithium Ammonium Sulphate (LAS) and Lithium Potassium Sulphate (LKS). At room temperature, both LHS and LAS belong to the space group C_{2v}^9 and point group C_{2v} while LKS belong to the space group C_6^6 and point group C_6.

LKS is one of the most extensively studied member of the family. Above and below room temperature it shows an interesting sequence of phase transitions. Despite extensive studies a definite picture of the mechanisms responsible for the phase transitions is still lacking [1.30]. There have been several investigations on the elastic properties of this crystal but surprisingly the complete set of the elastic constants of this crystal are not yet reported. A controversy regarding an above room temperature phase transition is not well resolved which we chose to investigate. From a material application point of view, LKS has been identified as one of the most interesting electro-optic materials, since it has an electro optic coefficient more than three times that of quartz and can withstand temperatures up to $400^{\circ}C$ [1.31].

LAS is a fairly well investigated crystal. Below and

above room temperature LAS goes through several phase transitions. While its high temperature phase transition is well studied the investigations on the low temperature transition are few [1.32]. On the high temperature side LAS undergoes a ferroelectric phase transition near 460 K and has orthorhombic structure at room temperature. It further undergoes a ferroelastic phase transition near 284 K. Recently a weak second order phase transition has been identified near 256 K in dielectric and Raman studies [1.33]. There are uncertainties about the polar character of the phase below 284 K. The elastic properties at phase transition near 460 K have been investigated by ultrasonic and Brillouin scattering technique; but near 284 K only Brillouin data is available. The elastic data near the 256 K transition has not been reported. The absolute values of the elastic constants at room temperature, reported from one ultrasonic work [1.34] and several Brillouin experiments shows wide variation in values. Hence an accurate determination of the complete set of elastic constants of this crystal is required. The applications of LAS is in a way limited due to its highly fragile nature. Even the thermal gradient due to the frictional heat generated while polishing the crystal can crack it. LAS is a nonlinear optic material and it can find application as a second harmonic generator in laser systems.

The LHS is not a very widely investigated crystal when compared to LAS or LKS. At room temperature it exhibits [1.35] ferroelectric like hysteresis loops but other studies [1.36] indicate no ferroelectricity in this crystal. It has highly temperature dependent one dimensional protonic conductivity along the c direction. Several structural, electrical, thermal, and spectroscopic investigations have been reported on this crystal but its elastic properties have not yet been probed. There are no reports on the measurement of elastic constants of this crystal and hence a measurement

of the complete set of elastic constants is required. Eventhough this crystal shows a ferroelectric like behavior, the dielectric studies do not carry any signature of a ferroelectric phase transition. Similarly no specific heat anomalies have been found, indicative of phase transitions in this crystal. But there are anomalies in the thermal expansion coefficients above and below room temperature [1.37], and temperature variation of NMR spectrum also supports a weak high temperature phase transition without giving definite transition temperature [1.38]. Since ultrasonics is a very sensitive technique an ultrasonic investigation is appropriate here to prob for the weak phase transitions suspected in this crystal both at high and low temperatures. The highly temperature dependent c-axis protonic conductivity, high dielectric constant and ferroelectric like hysteresis loops of this crystal are not well explained, eventhough these properties make it a very ineresting sample from a scientific point of view.

References

1.1 J.F Nye: *Physical Properties of Crystals* (Oxford University Press, New York 1985)

1.2 H. J. Juretschke: *Crystal Physics* (W.A. Benjamin, Inc., Massachusetts 1974)

1.3 A. R. Verma, O. N. Srivastava: *Crystallography for Solid State Physics* (Wiley Eastern, New Delhi 1962)

1.4 B.A. Auld: *Acoustic Fields and Waves in Solids*, Vol.1, (John Wiley and Sons, New York 1973)

1.5 R. Truell, C. Elbaum, B. B. Chick: *Ultrasonic Methods in Solid State Physics* (Academic Press, New York 1969)

1.6 E. Schreiber, O. L. Anderson, N. Soga: *Elastic constants and their measurement* (Mc. Graw-Hill, New York 1973)

1.7 M.J.P. Musgrave: *Crystal Acoustics* (Holden Day, San Francisco 1970)

1.8 H. J. Mc Skimin in *Physical Acoustics,* Vol. I, Part A, ed: W. P. Mason (Academic Press, New York 1964)

1.9 F.I Fedorov: *Theory of Elastic Waves in Crystals* (Plenum Press, New York 1968)

1.10 A.G. Every: Phys. Rev. B $\underline{22}$ 1746 (1980)

1.11 C. Kittel: *Introduction to Solid State Physics*, 4th ed. (Wiley, New York 1971)

1.12 K. Brugger: J. Appl. Phys. <u>36</u>, 759 (1965)

1.13 J.R. Neighbours, G.E. Schacher: J. Appl. Phys. <u>38</u>, 5366 (1967)

1.14 P. C. Waterman: Phys. Rev. <u>113</u>, 1240 (1959)

1.15 K. A. Müller in *Topics in current physics: Structural Phase Transitions I,* eds. K. A. Müller, H. Thomas (Springer- Verlag, Heidelberg 1981)

1.16 L. D. Landau, E. M. Lifshitz: *Statistical Physics* (Pergamon, London 1959)

1.17 W. Cochran: Adv. Phys. <u>9</u> 378 (1960)

1.18 P. W. Anderson in *Fizika Dielectrikov* ed. G. I. Skanavi (Akad. Nauk. SSR, Moscow 1960)

1.19 C. V. Raman, T. M. K. Nedungadi: *Nature,* <u>145</u> 147 (1940)

1.20 B. D. Saksena: *Proc. Natn. Acad. Sci. India,* A, <u>12</u> 93 (1940)

1.21 H. Gränicher, K. A. Müller: Mater. Res. Bull. <u>6</u>, 977 (1971)

1.22 A. Janner, T. Janssen: Phys. Rev. B<u>15</u>, 643 (1977)

1.23 C. W. Garland in *Physical Acoustics,* Vol.VII eds. W. P. Mason, R. N. Thurston (Academic Press, New York 1970)

1.24 W. Rehwald: Adv. Phys. <u>22</u> 721 (1973)

1.25 B. Lüthi, W. Rehwald in *Topics in current physics: Structural Phase Transitions I,* eds. K. A. Müller, H. Thomas (Springer- Verlag, Heidelberg 1981)

1.26 V. V. Lemanove in *Proceedings of the 2nd International School on Condensed Matter Physics: Optical and Acoustic Waves in Solids - Modern Topics, Varna, 23-30,sept. 1982,* ed. M.Borissov (World Scientific, Singapore 1983)

1.27 H. Z. Cummins in *Modern Problems in Condensed Matter Sciences; Vol. 5: Light scattering near Phase Transitions,* ed. H. Z. Cummins, A. P. Levanyuk (North Holland, Amsterdam 1983)

1.28 D. P. Sharma: Pramana $\underline{13}$, 223 (1979)

1.29 S. J. Chung, T. Hahn: Mat. Res. Bull. $\underline{7}$, 1209 (1972)

1.30 A. J. Oliveira, F. A. Germano, J. Mendes Filho, F. E. A. Melo, J. E. Moreira: Phys. Rev. B$\underline{38}$, 12633 (1988)

1.31 T. R. Sliker: J. Opt. Soc. Am. $\underline{54}$ 1348 (1964)

1.32 B. Mroz, J. A. Tuszynski, H. Kiefte, M. J. Clouter: J. Phys. Condensed Matter $\underline{1}$, 783 (1989)

1.33 A. R. M. Martins, F. A. Germano, J. Mendes Filho, F. E. A. Melo, and J. E. Moreira, Phys. Rev. B $\underline{44}$, 6723 (1991)

1.34 K. S. Aleksandrov, I. P. Aleksandrova, L. I. Zherebtsova, A. I. Kruglik, A. I. Krupnyi, S. V. Melnikova, V. E. Shneider, and L. A. Shuvalov, Akad. Nauk SSR $\underline{39}$, 943 (1975) [Bull. Acad. Sci. USSR, Phys. Ser. $\underline{39}$, 44 (1975)]

1.35 R. Pepinsky, K. Vedam, Y. Okaya, S. Hoshino: Phys. Rev. 111, 1467 (1958)

1.36 V. Hugo Schmidt, J. E. Drumheller, F. L. Howell: Phys. Rev. B4, 4582 (1971)

1.37 S. Devanarayanan, K. R. K. Easwaran: Proc. Indian Acad. Sci. 64A, 173 (1966)

1.38 J. D. Cuthbert, H. E. Petch: Can. J. Phys. 41, 1629 (1963)

CHAPTER 2

EXPERIMENTAL TECHNIQUES AND INSTRUMENTATION

2.1 Ultrasonic measurement techniques

2.1.1 Survey of ultrasonic measurement techniques

For the measurement of ultrasonic velocity and attenuation a number of techniques can be used. These techniques can be broadly classified into three categories, which are,

(a) Pulse methods,

(b) Continuous wave methods,

(c) Low frequency methods.

(a) Pulse methods

In these techniques, a short pulse of sound waves is generated using a piezoelectric transducer (usually quartz) which is bonded to the crystal under investigation. The crystal for the experiment should be cut and polished to have a pair of end faces plane and parallel in the desired direction. The sound waves excited in this direction will get multiply reflected from the end faces and will produce an electric signal each time it hits the transducer. These electric echo pulses are amplified and displayed on an oscilloscope or processed otherwise. From the length of the sample, the transit time of the pulse in the sample, and the decay rate of the pulse amplitudes of the successive echoes, the velocity and attenuation can be estimated. The absolute accuracy of such methods are generally about 1%.

Using Phase sensitive methods the absolute accuracy can be increased in certain cases of pulse techniques and very high precision of 10^{-6} can be obtained in the measurement of changes in velocity. There are various kinds of phase sensitive methods: pulse superposition [2.1,2.2], phase

comparison [2.3], sing-around method [2.4,2.5], and pulse echo overlap method [2.6]. More details of these methods are available in specialized review articles [2.6-2.10].

b) Continuous wave methods

Standing waves or Continuous wave (CW) methods have also been successfully applied in various problems in physical acoustics. Similar to a Fabry-Perot interferometer one excites standing wave resonances generally also with quartz transducers. For a sample length L the number of excited resonances of frequency f is ,

$$n = \frac{2Lf}{v} \qquad (2.01)$$

whereby the sound velocity v can be determined. For 10 MHz n is of the order of 10^2. Using frequency modulation techniques one can measure changes in velocity and attenuation with high precision. A detailed discussion about this method is given in review articles [2.11,2.12].

(c) Low frequency methods

The lower limit of frequency is given by the sample dimensions. Here the number n in (2.01) is of order unity. In this case the elastic compliances (Youngs modulus Y and Shear modulus G) are determined by a CW resonance method or by measuring flexural and torsional oscillations. These techniques are described by Read et al. [2.13]. These methods are particularly suitable for piezoelectric materials which can be excited into mechanical resonances by an electric field directly without transducers [2.14]. Other nonpiezoelectric crystals can be measured in a similar way with additional dc bias field using the electrostrictive effect [2.15]. The low frequency dynamic resonance methods are also described by Schreiber et al. [2.16].

In ultrasonic experiments the frequency is usually in the range of 10 to 100 MHz. The upper limit in frequency is given

by the precision to which planeness and parallelism of the two reflecting end faces can be achieved. For coherent detection this precision has to be about 1/10 of the acoustic wavelength. For high acoustic quality materials one can go to microwave frequencies. But at GHz frequencies the Brillouin light scattering is a better technique for the measurement of elastic properties.

A serious problem with ultrasonic propagation near structural phase transitions is the bonding of transducers to the sample. Because of thermal expansion and the occurrence of spontaneous strains in the low symmetry phase the transducer sample bond may crack under such conditions [2.17].

2.1.2 The method of Pulse Echo Overlap

The Pulse Echo Overlap (PEO) method was first invented in 1958 by John E. May [2.18] and modified to essentially its present form in 1964 by E. P. Papadakis [2.6]. This modification, to a large extend, has depended on the development of Mc Skimin's Pulse Superposition Method [2.1,2.2]. The necessary factor in Mc Skimin's method, which was borrowed for the PEO method, is Mc Skimin's calculation of the correct cycle-for-cycle superposition (overlap in PEO method) of the *rf cycles* in echoes from long pulsed rf wave forms. The correct overlap, obtained by using Mc Skimin's calculation, permits travel time measurements with high absolute accuracy. The PEO method is still the most widely used technique to measure the velocity of sound in solids [2.8].

The fundamentals of PEO measurement can be understood by examining the block diagram in Fig. 2.1. The CW oscillator which is the basic clock of the system supplies the frequency which is to be set at the reciprocal of the delay time between the echoes to be measured. The CW signal goes to three places; (1) to the counter which measures the exact frequency of the
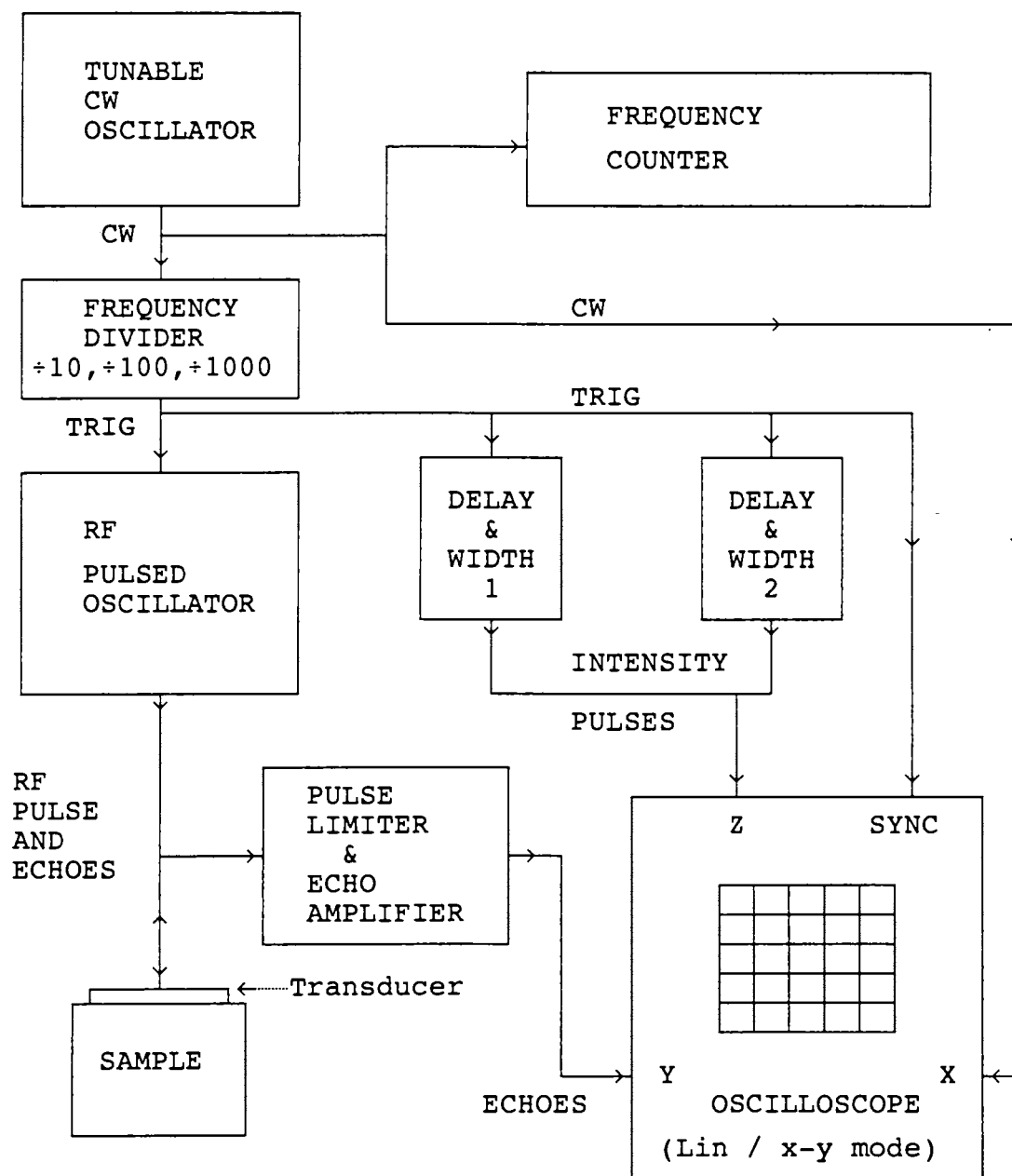
Figure 2.1

Block diagram of the Pulse Echo Overlap Method
for measuring the travel time of the waves.

CW oscillator, (2) to the x-axis of the CRO to display the overlapped echoes when the CRO is in the x-y mode, (3) to the frequency divider to provide synchronous triggers for the pulsed rf oscillator and for the delay circuits. The delay generators provide the two synchronized intensifying pulses of adjustable width and delay to permit the observation of two selected echoes by intensifying the CRO display at the two echoes of interest. The rf generator must be a pulsed oscillator (not gated type) so that the phase of the rf is synchronous with the divided trigger generated from the CW oscillator. The rf pulse energizes the piezoelectric transducer, which sends the ultrasonic signal and receives its echoes. The echoes go to the y-axis of the CRO after amplification. The diode pulse limiter protects the amplifier input from the high power rf pulses.

When the CRO is in linear sweep mode the x-axis sweep is triggered by the sync input signal which is the same as the one triggering the rf pulsed oscillator. In this mode if the time base is properly set then all the echoes, with exponentially decaying amplitudes, along with the first rf pulse can be seen on the screen. The two echoes of interest between which the time delay is going to be measured can now be selected by positioning the intensifying pulses on them by adjusting the delay and width of the intensifying pulses. The approximate time interval between the echoes can now be noted from the CRO to enable an initial frequency setting for the CW oscillator. When the CRO is switched to the x-y mode the x-axis sweep is produced by the cw oscillator and a sweep is there corresponding to every echo. The echoes appear on the screen one after the other on successive sweeps. Due to the persistence of vision the echoes appear as if one is overlapped on the other. By adjusting the intensifying pulse amplitude the two echoes of interest alone can be made visible in the overlapped condition. The overlap is exact if the CW frequency is equal to the reciprocal of the time interval

50

between the echoes. The echoes appear on the screen in an expanded form with the individual rf cycles in the echo visibly resolved and an rf cycle to cycle overlap can be achieved by fine tuning of the CW oscillator. The frequency of the CW signal can now be obtained from the frequency counter, the reciprocal of which gives the round trip travel time of the echoes in the sample. By knowing the length of the sample the velocity can be computed. In PEO method the next rf pulse is applied only after all the echoes in the sample have died out. This is ensured by switching the frequency divider to 10, 100 or 1000 division mode.

In contrast with PEO method, in pulse superposition method the rf pulses are applied at a rate which corresponds to simple multiple of echo interval, thus producing actual interference or superposition of waves in the sample. The cycle to cycle overlap is achieved in pulse superposition technique from the amplitude variations, resulting from the constructive and destructive interference of the waves as the CW frequency is varied.

Due to attenuation and other pulse distortion effects the number of rf cycles in the two selected echoes will be different and hence there is no easy way to find which cycle of the first echo should be overlapped with which cycle of the second echo. In Section 2.3 we discuss how Mc Skimin's calculation can be used to find the correct overlap along with our contributions to the basic technique.

2.1.3 Measurement of attenuation

Ultrasonic attenuation is defined by the solution

$$A = A_0 \ e^{-\alpha x} \cos(kx - \omega t) \tag{2.02}$$

for the ultrasonic wave propagating in the x-direction with a propagation constant $k = 2\pi/\lambda = 2\pi f/v$, a radian frequency $\omega = 2\pi f$, and an attenuation coefficient α. In these

51

definitions λ is the wavelength, f the frequency and v the phase velocity. The ultrasonic attenuation as defined in Eq. (2.02) must be measured as the logarithm of the ratio of the amplitude of the ultrasonic wave at two distances along its propagation path. Then α is given as

$$\alpha = \frac{\ln(A_1/A_2)}{(x_2 - x_1)} \tag{2.03}$$

in units of nepers per unit length or

$$\alpha = \frac{20 \log_{10}(A_1/A_2)}{(x_2 - x_1)} \tag{2.04}$$

in decibels per unit length for amplitudes A_1 and A_2 sensed at positions x_1 and x_2.

Various schemes have been used in pulse techniques to find the amplitudes of echoes. Comparison pulses run through an attenuation box and a delay line have been applied on alternate or chopped oscilloscope sweeps to find amplitude directly in decibels [2.19]. An ingenious arrangement has been devised by Chick et al [2.20] displaying an electrically generated decaying exponential function and the echoes on alternate sweeps of an oscilloscope. The decaying exponential is calibrated in decibels per microsecond as a matter of convenience from the electronic standpoint, although nepers per centimeter is a more natural unit in theoretical derivations. The slope of the decaying exponential can be varied by a ten-turn dial, so that the attenuation between any pair of echoes can be measured.

The attenuation can be most conveniently measured by an automatic procedure for which commercial equipment is available (Matec. Inc.(USA) Model 2470). In the automatic system, two gates with variable delay are set on the two echoes of interest to sample them. The amplitude of the first echo is held constant by AVC circuitry, and the amplitude of the second echo is sampled at its peak. A calibrated logarithmic amplifier converts the sampled amplitude to

decibels relative to the constant amplitude of the first echo. The decibel level is recorded on a built-in strip chart that has several calibrated scales and a variable baseline, so that small changes in attenuation can be measured at various total loss levels. In this equipment the attenuation can also be noted from a panel meter calibrated in dB.

2.2 The experimental setup

2.2.1 The basic experimental setup

The experimental setup used for making the ultrasonic measurements consists of mainly the PEO system, the temperature measuring and control system, the cryostat for low temperature measurements and the oven for high temperature measurements.

The PEO system was setup mostly by using equipments from MATEC. Inc.(USA). These equipments include Matec Model 7700 pulse modulator and receiver together with model 760 V rf plug-in, Model 110 high resolution frequency source, Model 122 B decade divider and dual delay generator, Model 2470 B attenuation recorder, Model 70 impedance matching network etc. The frequency counter used was HIL (India) Model 2722 and the oscilloscope was a 100 MHz one with z-axis input (HIL Model 5022). For temperature measurement and control Lakeshore Cryogenics (USA) Model DR 82C temperature controller was used. The cryostat used was specially designed and fabricated for the ultrasonic measurements at low temperatures using liquid nitrogen as the cryogen. The details of this cryostat will be discussed separately in the next section (sec. 2.2.2). A high temperature oven for Ultrasonic measurements from System Dimension (India) was used for high temperature measurements.

The block diagram of the experimental setup used is shown in Fig. 2.2. The tunable cw source (model 110) has a highly stable internal high frequency oscillator (12-50 MHz) from
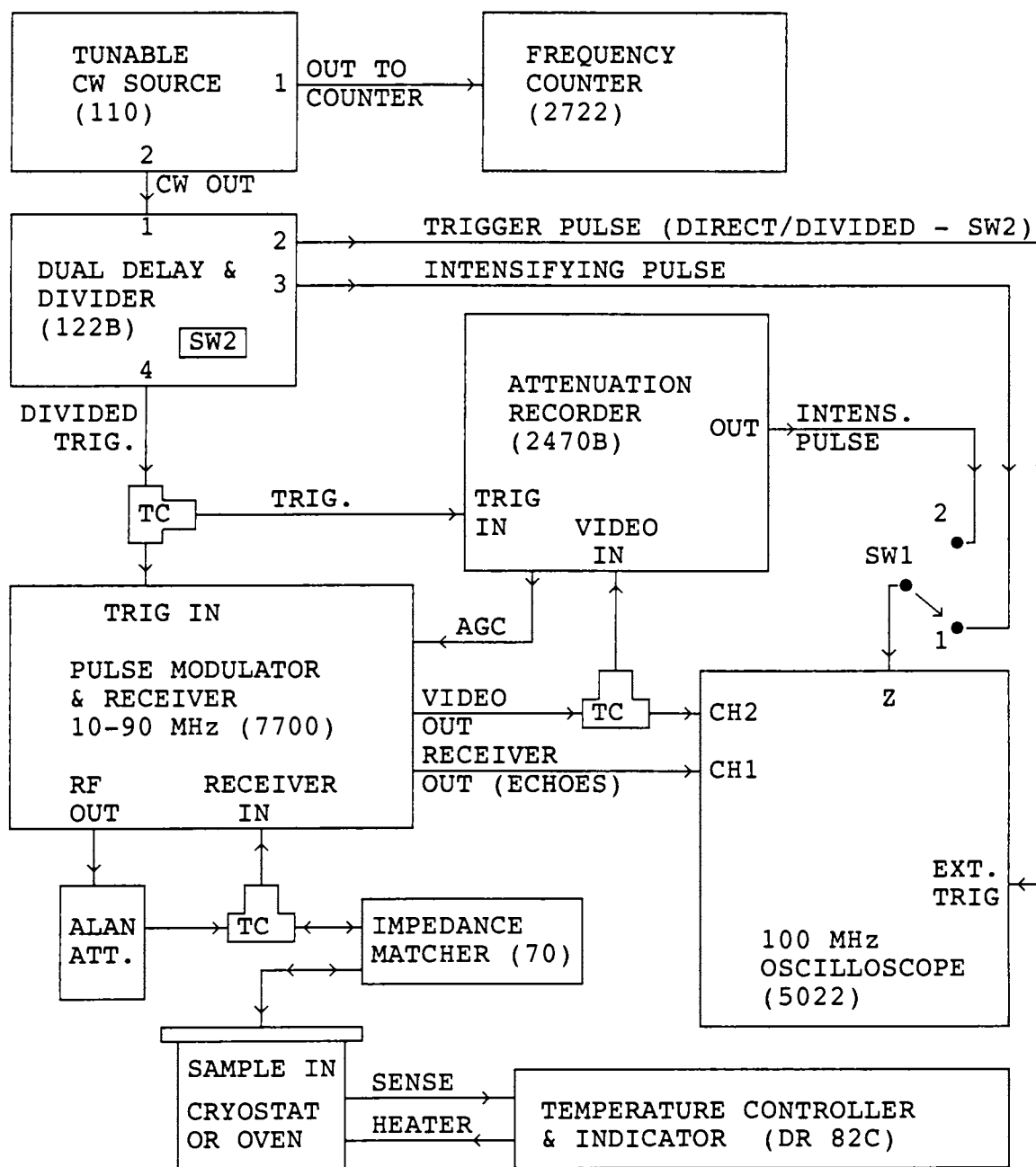
Figure 2.2

Block diagram of the Experimental setup

which the required low frequency cw signal for PEO is generated by selectable frequency division. This signal is available at terminal 2, while the high frequency is available at terminal 1 for accurate counting by the frequency counter (model 2722). The dual delay and divider unit (model 122B) has dividers selectable as 10, 100 or 1000. The division factor 100 is quite acceptable for most measurements, which means that the next rf pulse is sent to the sample only after a time interval corresponding to 100 number of echoes. The terminal 2 of this unit gives trigger pulses for the CRO. The CRO is always operated in the external sweep trigger mode. By using switch SW2 in 122B the trigger at terminal 2 can be made direct trigger or divided trigger for observing the overlapped echoes or the full echo pattern respectively. The dual delay generators in 122B can be adjusted for delay and width of the intensifying pulses for selecting the two echoes of interest for overlap. These pulses are available at terminal 3 and are connected to the z-input of the CRO through the selector switch SW1.

The divided trigger from 122B goes to the pulse modulator & receiver unit (model 7700 with rf-plug-in model 760 V). This is the most important unit in the setup. An rf pulse packet of peak power 1 KW is obtained at the output when the unit is triggered at the input. The rf frequency of the triggered power oscillator can be adjusted in the range 10 to 90 MHz. The width and amplitude of the pulse are adjustable. For good pulse shape the unit is usually operated at full amplitude and the amplitude reduction is achieved by using an rf attenuator (Alan Attenuator) at the output as shown in Fig.2.2. The unit has a sensitive tunable superhetrodyne receiver with a maximum gain of 110 dB for amplifying the echoes. The amplified echoes are available through the receiver out terminal which is connected to the CRO channel 1 input. The amplified echoes are also detected and the detected output (envelope of the echoes) is available at the video out terminal which is connected to

the attenuation recorder and CRO channel 2 input. For optimum signal to noise ratio in the amplification of weak echoes, an impedance matching network (model 70) is connected before the quartz transducer.

The working of the attenuation recorder (model 2470B) is as discussed in Section 2.1.3. The switch SW1 can be toggled to pole 2 for connecting the intensifying pulse output from the attenuation recorder to the Z-input of the CRO. By this way the two echoes of interest can be selected for attenuation measurement. One important advantage of the PEO technique is the capability to measure the velocity and attenuation at the same time.

A timing diagram of the various signals in the measurement system is given in Figure 2.3. The first and second echoes are shown as selected. In a typical setting one divided sync pulse will be produced for every 100 direct sync pulses. The diagram shown is for an overlapped situation.

2.2.2 The fabricated cryostat

For the low temperature ultrasonic measurements on crystals, we have designed and fabricated a cryostat with Liquid Nitrogen as the cryogen. The essential parts of the cryostat are shown in Figure 2.4. The metallic outer case is one meter long. The top lid is removable and is made vacuum tight by using a rubber "O" ring of 27 cm diameter. The 50 cm long liquid nitrogen inlet tube along with the liquid nitrogen reservoir are welded to the top lid of the cryostat. The liquid nitrogen reservoir has a thick copper bottom to which the sample chamber assembly is tightly bolted. The sample chamber assembly is a 24 cm long, thick copper hollow cylinder with 8.5 cm internal diameter and having a removable bottom cover. A 6 mm dia copper tube is wound on the outer side of the sample chamber assembly and ends of this tube is connected to the nitrogen reservoir such that liquid nitrogen flows

DIRECT SYNC
TRIGGER PULSE

DIVIDED SYNC
TRIGGER PULSE

R F ECHOES

VIDEO OUT

INTENSIFYING
PULSES
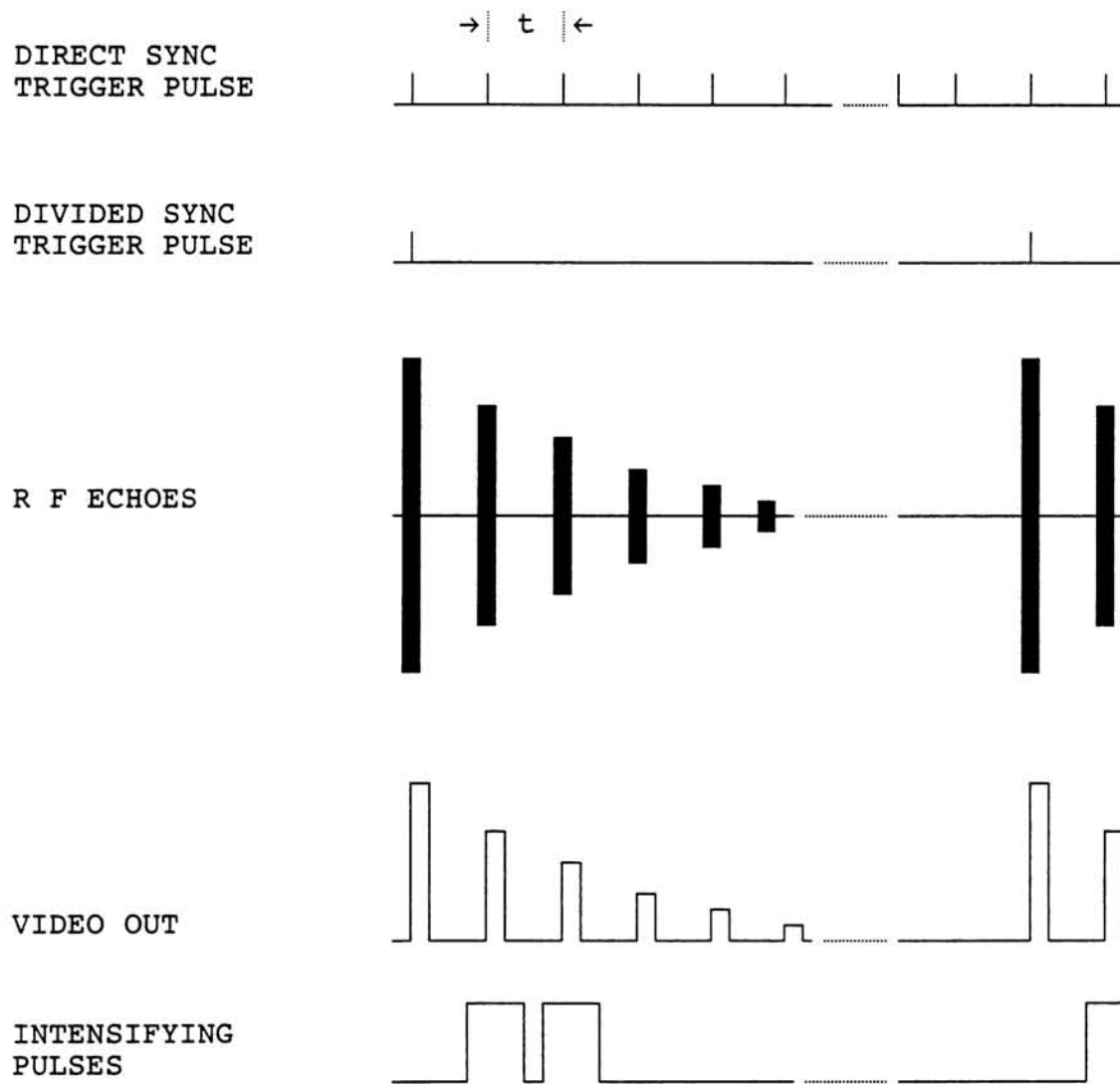
Figure 2.3

A timing diagram of the various system signals. The interval t
is the travel time in an overlapped situation.

57

through this tube under the action of gravity. Thus the sample chamber assembly works like an efficient cold finger due to the circulating liquid nitrogen. This arrangement also helps to create a uniform temperature in the sample chamber. The sample holder and heater assembly are introduced into the sample chamber after removing the bottom cover of the sample chamber assembly. The sample holder consists of four long threaded rods with plates fixed to these rods using nuts. The sample along with the ultrasonic transducer are held between the plates with the help of a spring loaded arm fixed to the top plate. The sample holder is surrounded by a 20 cm long copper hollow cylinder having removable lids on top and bottom. Thin insulated copper wire is closely wound on this copper cylinder to almost fully cover its outer surface. This copper wire winding acts as the heater element for temperature regulation. Due to the extended nature of this heater winding the sample holder is uniformly heated and the temperature gradients are minimized.

The special features of this cryostat can be summarized as follows.

(1) It has a large sample chamber and sample holder with minimum temperature gradients to accommodate large crystal samples used in ultrasonic investigations.

(2) Large thermal mass provides slow cooling and heating and prevents sudden heating and cooling which would easily crack large crystal samples.

(3) A rope and multi-pulley arrangement with good mechanical advantage is provided to easily lift and lower the lid assembly. This makes the loading and unloading of the sample easy.

(4) It has a cold finger with circulating liquid nitrogen to ensure the uniform cooling of the sample chamber.

(5) A distributed heater coil with copper wire for uniform heating and temperature regulation.

(6) An optical window to perform experiments involving light
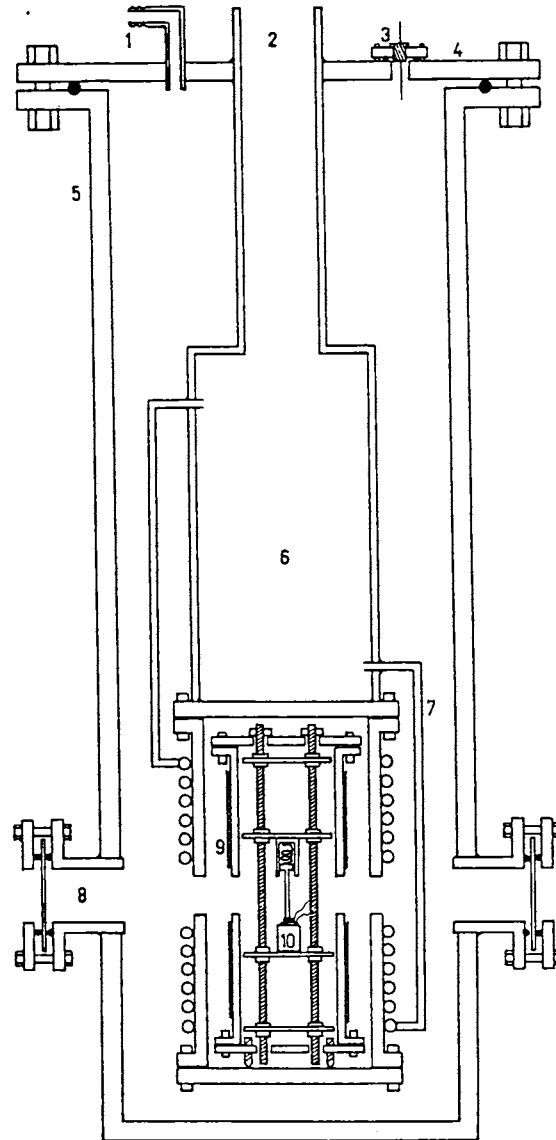
1 - To vacuum pump
2 - LN_2 inlet
3 - Electrical connectors
4 - Top lid
5 - Outer case

6 - LN_2 reservoir
7 - LN_2 circulation tube
8 - Optical window
9 - Sample chamber
10 - Sample

Figure 2.4

The cryostat for low-temperature measurements

interaction with ultrasonic waves. (This facility was not used for the present work but was included in the design as an optional facility for future applications of this cryostat). A photograph of the whole experimental setup including the cryostat is shown in Plate 2.1.

2.3 Bond correction and overlap identification

2.3.1 Basic theory

The following analysis [2.1,2.2,2.6-2.8,2.21] pertains to a burst of ultrasonic waves of principally one frequency echoing back and forth within a specimen. The specimen is bare on one end but has a transducer bonded to the other end. The transducer is half a wavelength thick at its resonant frequency, and the bond has a finite thickness. The transducer is unbacked. We will consider the effect of the bond and transducer upon the phase of the reflected wave at the bonded end of the specimen in order to derive a method of choosing the correct cycle-for-cycle matching of one echo with any subsequent echo.

Consider the sketch of the specimen, bond, and the transducer in Fig. 2.5. The phase angle γ relating the reflected wave phase to the incident wave phase is defined in that figure, as are the impedances of the specimen, bond, and transducer. The specific acoustic impedances are Z_s for the specimen, Z_1 for the bond, and Z_2 for the transducer. The impedance looking into the termination (bond and transducer) from the specimen is Z_d. Since the transducer is unbacked the impedance Z_a seen by it at it's back is that of air , which is approximately zero.

Assuming negligible attenuation in bond and transducer, the theory of lossless transmission line [2.22] can be used to obtain an expression for Z_d as
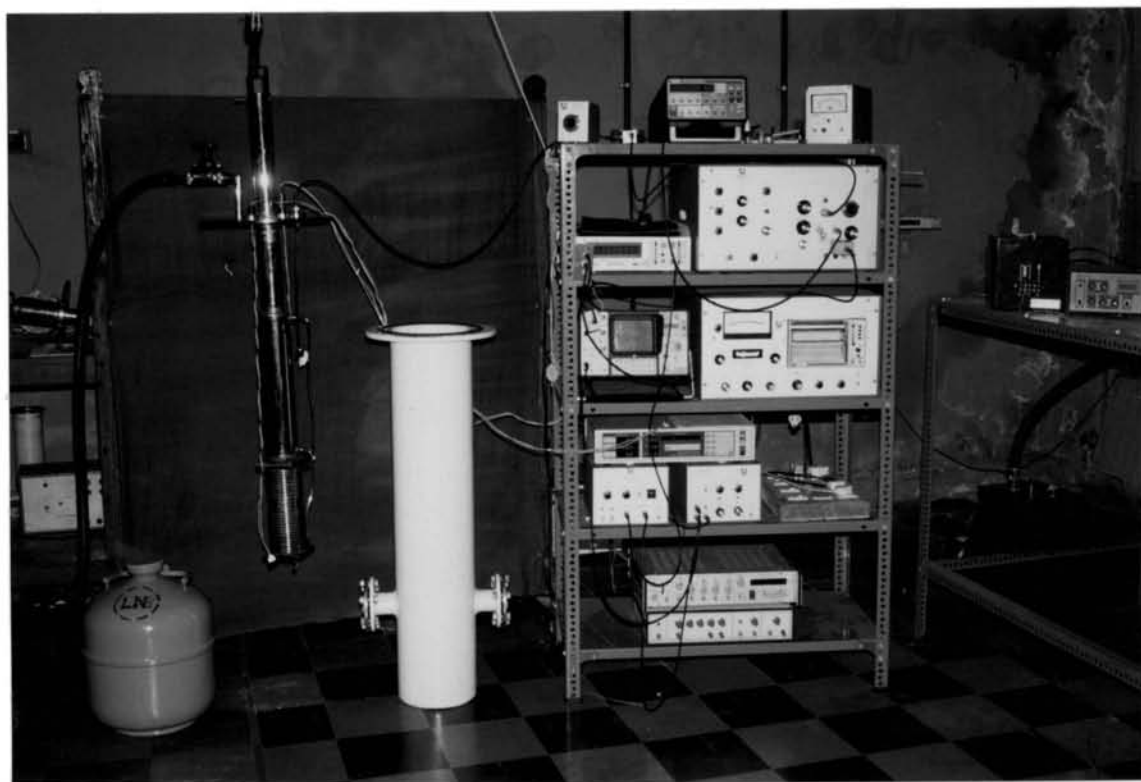
Plate 2.1
The photograph of the experimental setup

a)

SPECIMEN (Z_s)

BOND (Z_1)

TRANSDUCER (Z_2)

AIR $(Z_a \approx 0)$

b)

Transmission line equivalent circuit

c)
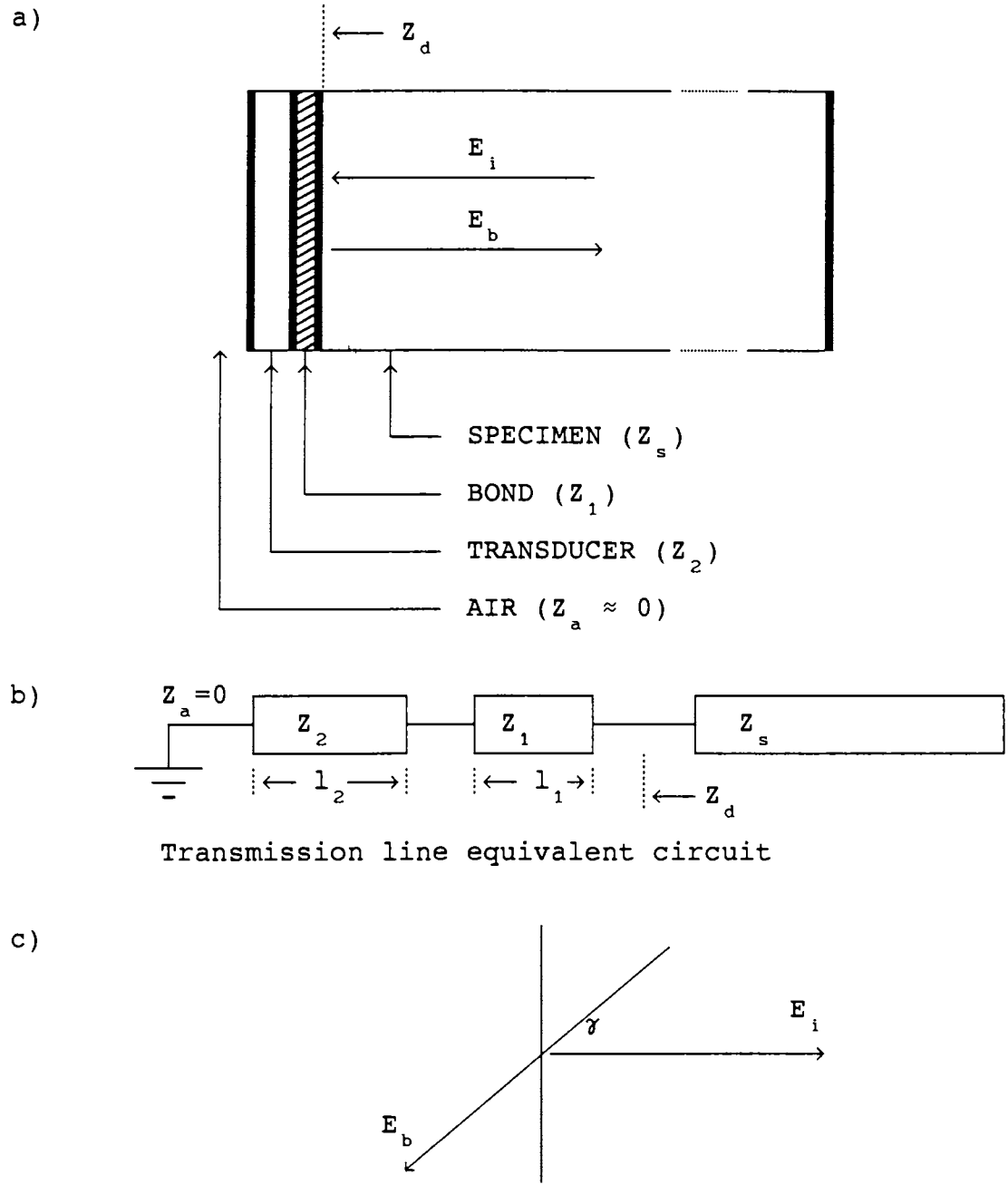
Figure 2.5

The phase angle γ generated at each reflection of the echoes
from the specimen/bond/transducer interface is shown here
diagrammatically.

62

$$Z_d \equiv jZ_e = jZ_1 \left[\frac{(Z_1/Z_2) \tan \beta_1 l_1 + \tan \beta_2 l_2}{(Z_1/Z_2) - \tan \beta_1 l_1 \tan \beta_2 l_2} \right] \qquad (2.05)$$

where β_1 and β_2 are the propagation constants in the bond and transducer, and l_1 and l_2 are the thicknesses of the bond and transducer, respectively. The propagation constants β_1 and β_2 are related to the ultrasonic frequency f impressed upon the transducer by the RF pulse generator and also to the velocities v_1 and v_2 of the wave in bond and transducer respectively. The relations are

$$\beta_1 = \frac{2\pi f}{v_1} \quad \text{and} \quad \beta_2 = \frac{2\pi f}{v_2} \qquad (2.06)$$

Z_d can now be used to define the ratio of reflected to incident pressure as

$$\frac{E_b}{E_i} = \frac{Z_d - Z_s}{Z_d + Z_s} \qquad (2.07)$$

With Z_d imaginary ($Z_d = jZ_e$), the real and imaginary parts of Eq. (2.07) can be seperated as

$$\frac{E_b}{E_i} = \frac{Z_s^2 - Z_e^2}{Z_e^2 + Z_s^2} - \frac{j2Z_e Z_s}{Z_e^2 + Z_s^2} \qquad (2.08)$$

from which the phase angle γ on reflection is given by

$$\tan \gamma = \frac{-2Z_e Z_s}{(Z_s^2 - Z_e^2)} \qquad (2.09)$$

for the vectors sketched in Fig. 2.5 (c). The impedance Z_e is as defined in Eq. (2.05).

In these formulae there is one unknown parameter, the bond thickness l_1, and one running variable, the ultrasonic frequency f. By varying f one can change β_1 and β_2 using the

relations (2.06).

The phase angle γ is the relevant measure of the effect of the transducer and bond upon the reflected wave. Mc Skimin has shown that the measured travel time t_M is made up of the true round-trip travel time t plus some increments:

$$t_M = pt - (p\gamma / 2\pi f) + (n / f)$$ (2.10)

Here p is the number of round trips in the measurement. The phase angle γ per reflection yields a fraction $\gamma/2\pi$ of a period of the RF, so a time increment $\gamma/2\pi f$ is generated per round trip. Also a mismatch of n cycles will yield a time error n/f. The object of the mathematical analysis is to develop a method to find the overlap case n = 0, and to minimize and estimate the residual γ.

It is clear from the above equations that both γ and t_M are functions of the frequency f. It is possible to utilize this dependence of t_M on frequency to eliminate n, the mismatch. To do this consider the possibility of making the measurement of t_M at a high frequency f_H and at a low frequency f_L (for example, at the resonant frequency $f_H = f_r$ and at $f_L = 0.9f_r$). Then t_H is measured time at f_H and t_L is measured time at f_L. These times are

$$t_H = pt - (p\gamma_H / 2\pi f_H) + (n / f_H)$$

$$t_L = pt - (p\gamma_L / 2\pi f_L) + (n / f_L)$$ (2.11)

where the same overlap condition (same n) has been maintained by shifting the repetition frequency slightly as the RF frequency is changed. Subtraction eliminates t, the true travel time, as

$$\Delta t_{M} \equiv t_{L} - t_{H} = \frac{1}{f_{L}} \left(n - \frac{p\gamma_{L}}{2\pi} \right) - \frac{1}{f_{H}} \left(n - \frac{p\gamma_{H}}{2\pi} \right) \quad (2.12)$$

Equation (2.12) expresses Mc Skimin's Δt criterion for finding n = 0 case. Stated verbally, Eq. (2.12) indicates that if f_{L}, f_{H}, t_{L} and t_{H} are measured, and if γ_{L} and γ_{H} are computed from l_{1}, l_{2}, v_{1}, v_{2}, Z_{1}, Z_{2}, and Z_{s} by Equations (2.05), (2.06) and (2.09), then there is only one possible value for Δt_{M} when n = 0. Conversely, if n = 0 is set in the measurement, the measured value of Δt_{M} will agree with the value calculated theoretically.

2.3.2 The correction and identification technique

To apply the Mc Skimin Δt criterion to PEO technique, one follows the following procedure:

1. With the oscilloscope on triggered sweep with divided sync, find the approximate time between echoes of interest from the graticule of the CRO, and set the cw oscillator frequency to have that time as its period.

2. Switch to the direct sync sweep trigger mode and adjust the cw oscillator frequency to bring about a plausible overlap with the leading edges of the echoes nearly aligned and every cycle of the later echo smaller than the corresponding cycle of the earlier echo because of attenuation.

3. Measure t_{L} and t_{H} of Eq. (2.11) at proper frequencies f_{L} and f_{H}, usually $0.9f_{r}$ and f_{r}.

4. Repeat step 3 for several possible adjacent overlaps, e.g., three toward lower cw repetition frequencies and as many towards higher.

5. Compute Δt_{M} of Eq. (2.12) for each of these sets of measurements.

6. Compare Δt_{M} found experimentally with theory, and

choose the correct cycle- for-cycle match. Then t_H measured at $f_H = f_r$ will be t_M in Eq. (2.10) with n = 0. This time t_M is the correct expression for the measured time before correction for bond phase shift.

The step no. 6 given above for choosing the correct overlap is not a straight forward procedure. This is because of the unknown bond thickness and consequent difficulty for computing a theoretical value of Δt_M for comparision. To overcome this difficulty a graphical technique is often used. For this it is assumed that the bond is very thin, that is less than a quarter of the acoustic wavelength (this condition is usually satisfied in experimental situation). This means that the bond phase $\beta_1 l_1$ expressed in degrees can be in the range 0 to 90 degrees. Using the equations presented above, the value of Δt_M can be computed (for n = 0 case) for increasing values of bond angle from 0 to 90 degrees. A plot of Δt vs bond angle is then made. This gives a range of possible Δt values for the given transducer, bond, and sample combination for n = 0 case. It can then be examined, which overlap-case in the measured values falls in this range and that overlap-case can be taken as the n = 0 case. Thus the correct overlap can be identified. Next step is to find the correction factor. In Eq. (2.10) we see that the correction can be calculated if the phase angle γ is known. All parameters except the bond thickness (or bond angle), are known for the computation of γ. The bond angle can now be found out from the plot as the angle corresponding to the measured value of Δt which has fallen in the possible range. Thus the correction factor in Eq. (2.10) can be estimated and the true round-trip time t in the sample can be obtained. It may be noted that a graph has to be ploted for every measurement.

66

2.3.3 The computer program developed for bond correction and overlap identification

The usually used manual computation and graphical procedure for finding the correct overlap and bond correction which have been discussed in Section 2.3.2 is very laborious especially if a number of measurements are to be made. We have developed a numerical procedure and a computer program which can process the experimental data and output the corrected velocity and elastic constant. This program is extremely useful for experimenters who are making ultrasonic measurements using pulse echo overlap technique or pulse superposition technique. The special features of our numerical procedure includes a linear regression technique for eliminating random errors in experimental observation, automatic computation of RF pulse frequency, auto finding of the correct overlap and a manual mode for selecting an overlap-case in the event when no overlap-case is found in the possible range of Δt values.

The importance of the linear regression technique which we have introduced as an improvement of the basic techinique can be understood as follows.

Consider the equations (2.11). They define the measured values of travel time t_L and t_H corresponding to frequencies f_L and f_H respectively. An examination of these equations reveal that they are equations of straight lines of the form

$$t_H = A_H + nB_H$$

$$t_L = A_L + nB_L \qquad (2.13)$$

where,

$$A_H = pt - (p\gamma_H / 2\pi f_H)$$

$$A_L = pt - (p\gamma_L / 2\pi f_L) \qquad (2.14)$$

and

$$B_H = 1/f_H$$
$$B_L = 1/f_L \qquad (2.15)$$

In an actual measurement the correct value of n is initially unknown and Eq.(2.13) can be written as

$$t_H = A_H + XB_H$$
$$t_L = A_L + XB_L \qquad (2.16)$$

where X is an arbitary overlap number and it can be defined as X = (n + m), where m is an unknown integer whose value is known when the correct overlap is identified.

In usual technique the value of Δt for successive overlap number X is obtained as the difference $(t_L - t_H)$ of the measured t_L and t_H. Here t_L and t_H are large numbers when compared to their difference Δt and hence even very small errors in the measurement of t_L or t_H can greatly influence the value of Δt. This can lead either to incorrect identification of the correct overlap or to a situation where none of the measured Δt values are in the calculated range.

In the method we have developed the Δt value is not directly obtained from the measured values of t_L and t_H for each case of overlap but it is obtained from the equation

$$\Delta t = (A_L - A_H) + X(B_L - B_H) \qquad (2.17)$$

The coefficients A_L, A_H, B_L and B_H are obtained from linear regression analysis with least squares fitting of measured t_L and t_H on successive values of overlap X. Eq. (2.16) shows that the points of t_L plotted against the overlap no. X should ideally lie on a straight line. This is also the case with t_H. In regression analysis t_L or t_H are fitted to two different straight lines against X values. Because of the fitting process the random errors in the measurement of t_L and t_H cancel out to some extent and the overall accuracy is

increased. The correlation coefficient is also computed which gives a measure of how well the the measured data fits into a straight line. Further, the deviation of each of the measured values of t_L and t_H from the fitted straight line is also computed to clearly indicate the errors involved.

Another useful feature of our straight line fitting technique is the estimation of the frequency of the RF pulse which excite the ultrasonic waves. This frequency is usually difficult to measure. A frequency counter cannot be used because of the small duty cycle plus the pulsed nature of this waveform. Eq. (2.15) shows that the required frequencies f_L and f_H can be estimated as the reciprocal of the fitting coefficients B_L and B_H respectively. Hence a separate measurement of these frequencies is not necessary in the present technique.

A description of the program developed for correct overlap identification and to apply bond correction is given below. The program was written in BASIC language and the source code of the program is listed in Appendix 2.1. The program can run on an IBM PC or compatible with GWBASIC interpreter or with compilers like Turbo Basic or Quick Basic.

The program opens with a menu of three choices: 1) To create a data file, 2) To process a data file, 3) To quit the program. If the first option, for creating data file, is selected then the program requests various parameters like sample name, bond material name, direction of propagation, length of sample in cm, whether wave is longitudinal or transverse, and if transverse the direction of polarization, number of data values, value of p, repetition rates in MHz for high and low RF frequencies for different cases of overlap, bond impedance, sample density, and any other information. These experimental data are then written on to a data file whose name can be specified. The program then returns to the opening menu where the next option to process the data can be selected.

69

If the process data file option is selected then on entry of the data file name the the file is read from the disk and processing begins. The linear regression process is first performed to find the straight line fitting coefficients and the correlation coefficients for t_L and t_H. The intersection of the straight lines corresponds to the zero Δt value. It can be shown that for the case of correct overlap the value of Δt is a small negative value which is usually one or two overlap cases away from the overlap case near to the zero Δt value. From the fitted lines the experimental Δt values are estimated for different cases of overlaps, 4 no. of $+\Delta t$ cases and 4 no. of $-\Delta t$ cases from the overlap case near the zero Δt value, and are tabulated. The low and high RF frequencies are then estimated from the slope of the lines. It is assumed in the processing that the estimated high RF frequency corresponds to the resonant frequency of the transducer. The acoustic impedance of the sample is also estimated as the product of sample density and approximate velocity which is estimated from sample length and t_H corresponding to the overlap case near the zero Δt value.

All parameters necessary to calculate the Δt value corresponding to any bond angle is now ready. It is assumed that for thin bonds the bond angle is in the range from $0°$ to $60°$. The Δt values corresponding to $0°$ and $60°$ are now estimated and one of this Δt values is the minimum Δt value in this range of bond angle. The curve of Δt vs bond angle is like an approximate parabola and it usually has a maximum in between $0°$ and $60°$ bond angles. This maximum Δt in this range of bond angle is now estimated using the Interval Halving numerical search procedure. The maximum is found in less than 20 iterations. The estimated minimum and maximum values of Δt gives the range of possible Δt values for n = 0 case or for the correct overlap. The experimental values from the straight line fitting is now searched for the case which fall in the possible range of Δt. Thus the correct overlap case is

identified. To apply the bond correction the bond angle should be known. For this Equation (2.12) is solved numerically by using Bisection Method to find the root (bond angle) corresponding to the observed Δt value in the possible range. The correct velocity is now calculated and the corresponding elastic constant is also found as the product of the square of velocity and the density of the sample. In case, due to some experimental problem, no experimental Δt values are falling in the possible range then there is an option to manually select an overlap case and calculate the velocity and elastic constant without bond correction. After printing or displaying the results the program goes back to the opening menu.

2.4 Sample preparation techniques

In this section details of sample preparation technique and the instrumentation developed for the same are described. The samples used were Lithium Hydrazinium Sulphate, Lithium Ammonium Sulphate, and Lithium Potassium Sulphate. These crystals are water soluble and hence they can be crystalized from their aqueous solutions.

2.4.1 Crystal growth from solution

Growth from solutions [2.23-2.28] is the most widely used method of growing crystals. It is always used for substances that melt incongruently, decompose below the melting point, or have several high-temperature polymorphous modifications. Even in the absence of above restrictions the crystal growth from solution is an efficient method. The equipment needed is relatively simple, the crystals exhibit a high degree of perfection, and the conditions of growth-temperature, composition of the medium and types of impurities can be widely varied. On the other hand, in contrast to other methods like growth from melt or vapor, in solution growth the

71

crystals are not grown in a one component system. The presence of other components (a solvent) materially affects the kinetics and mechanisms of growth. The migration of nutrient to the crystal faces is hindered, and thus diffusion plays an important part. The heterogeneous reactions at the crystal-solution interface are complicated by adsorption of the solvent on the growing surface and by the interaction between the particles of the crystallizing substance and the solvent (hydration in aqueous solutions). A theoretical analysis or description of the effects of the above factors on the mechanism of growth, the morphology, and the deficiencies of crystals is generally rather complicated. For this reason, empirical investigations on solution growth are to be given more weight. The skill of the crystal grower is of great importance in producing good quality crystals.

Controlled crystal growth is possible only from metastable solutions. The driving force of the process is the deviation of the system from equilibrium. This can be conveniently characterized either by the supersaturation ΔC or by the value of "supercooling", ΔT, i.e., the difference between the temperature of saturation of the solution and that of growth. The supercooling ΔT is related to the supersaturation ΔC by the expression

$$\Delta C = (\partial C_0 / \partial T) \Delta T \tag{2.18}$$

where $\partial C_0 / \partial T$ is the temperature coefficient of solubility, i.e., the change in solubility of the substance per $1°K$ change in the temperature of the solution.

The methods of growing crystals from solutions are classified into several groups according to the principle by which supersaturation is achieved.

1) Crystallization by *changing the solution temperature.* This includes methods in which the solution temperature differs in different parts of the crystallization vessel (temperature-difference methods), as well as isothermal crystallization, in which the entire volume of the solution is

72

cooled or heated.

2) Crystallization by *changing the composition* of the solution (solvent evaporation)

3) Crystallization by *chemical reaction.*

The choice of the method mainly depends on the solubility of the substance and the temperature solubility coefficient $\partial C_o/\partial T$. For many crystals both the slow cooling technique and the constant temperature solvent evaporation technique can be successfully used.

For a continuously growing crystal the substance has to be transported to the growing face from the solution. In a motionless solution the delivery of the substance is by a slow diffusion process. In a pure diffusion regime the supersaturation differs over different areas of the faces. To reduce this nonuniformity of the supersaturation and nutrition of different areas of the faces, and for faster mass transport for increased growth rate, motion of the crystal and solution relative to one another must be ensured. In low-temperature aqueous solutions, rotation of the crystal in solution or stirring is usually applied.

The samples necessary for our investigations have been grown by constant temperature solvent evaporation method with solution stirring as well as with crystal rotation.

2.4.2 The fabricated constant temperature bath

In this section the details of the bath which has been fabricated for crystal growth at constant temperature by solvent evaporation method are discussed. A special feature of this constant temperature bath is that it is protected against mains power failures by using an automatically recharged battery backup.

The bath is a glass tank on iron frame measuring about 40 cm in length, 28 cm in width and 25 cm in height. Figure 2.6 illustrate the essential details of the bath. The tank is
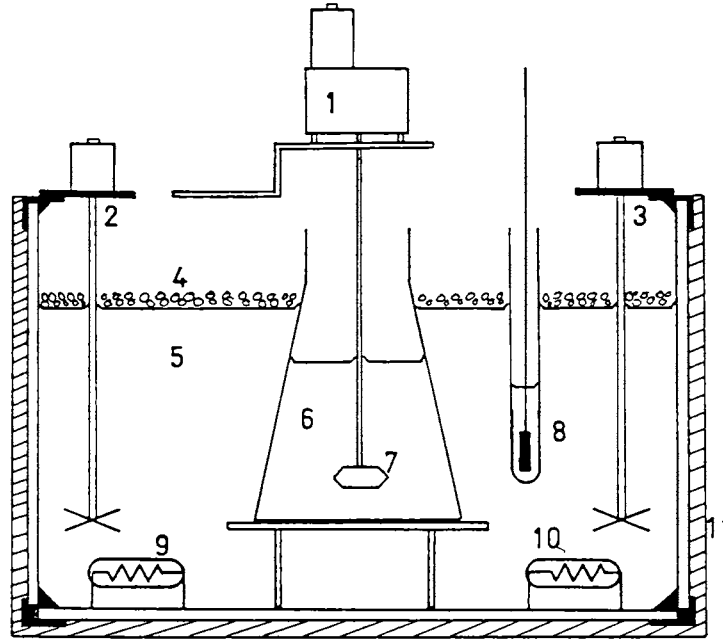
1 - Crystal rotator
2,3 - Bath stirrers
4 - Thermocol granules
5 - Bath liquid

6 - Solution
7 - Growing crystal
8 - Temperature sensor
9,10 - Bath heaters
11- Outer puf lining

Figure 2.6

The constant temperature bath for crystal growth

given a 1 cm thick heat insulating outer lining made of polyurethine foam. This is to prevent unnecessary heat loss from the bath and hence to reduce the power required to keep the tank at a regulated temperature above room temperature. For the same reason, thermocole granules are also allowed to float on the bath-water surface to reduce evaporation and consequent heat loss. There is a window with a foam shutter in front of the tank made in the foam lining for observing the growing crystal. Heater coils which are sealed inside glass tubes are fitted at the bottom of the tank. This prevents any electrical contact between bath-water and heater coils. A Diode temperature sensor enclosed in an oil filled glass tube is kept in the bath-water for temperature sensing. This arrangement of heater and sensor permits a closed loop proportional temperature control of the bath. The details of the temperature controller are discussed in the next section (sec. 2.4.3). Two stirring motors with stirrers are fitted near left and right ends of the bath for uniform temperature distribution in the bath.

The solution for crystal growth may be taken in a beaker or a wide mouth conical flask of 500 ml capacity and can be kept dipped in the bath at a suitable depth by using a bench made of perspex. The seed crystal was attached to a thin perspex strip and was hung in the solution from a rotation mechanism. The rotation mechanism consists of a DC motor which can rotate in both directions and a reduction gear arrangement for slowing down the motor speed. The motor is driven by specially designed control circuit which can periodically reverse the rotation direction and having facility for presetting the motor speed. A description of this control circuit is given in section 2.4.4. The bidirectional rotation of the growing crystal is very essential for perfection in growth. The same control circuit can also be used for controlling a stirrer in the solution and this way the solution can be periodically stirred in opposite directions.

75

2.4.3 The designed temperature controller

A temperature controller for crystal growth by constant temperature solvent evaporation technique has to meet several requirements. It is necessary to have precise control of the temperature of the bath for durations as long as several weeks or for a few months when and large single crystals of good quality are required. Any temperature fluctuation during this period is likely to introduce defects into the growing crystal. In a temperature controlled bath which is operating from AC mains, even a brief power failure can cause a damaging temperature fluctuation. One solution to this problem is to use a battery backup for the control power. But the available bath temperature control circuits [2.29,2.30] and general purpose temperature control circuits [e.g. 2.31] are not easily adaptable for battery backup.

We have designed and fabricated a proportional temperature controller that can be used ideally for crystal growth experiments of long duration. The control is protected against power failures by using a battery backup. The circuit diagram and other details of this controller have been published by us [see Ref. 2.32]. A description of the circuit and its operation is given below.

A block diagram of the temperature controller is shown in Fig. 2.7 and its circuit diagram is shown in Fig. 2.8. For sensing the temperature, a forward biased emitter-base junction of a silicon transistor (BC178) is used with its collector shorted to the base [2.33]. This forms a sensitive and linear temperature sensor as the forward voltage has a negative temperature coefficient of about -2 mV K^{-1}. The junction is forward biased with a constant current of about 200 μA. Transistor TR1 acts as a constant current source. The three terminal voltage regulator IC 7805 provides a stable output voltage of 5V, from which the reference voltage for temperature setting is derived. A multi-turn potentiometer VR1

is used to set the temperature. An Instrumentation amplifier formed with two operational amplifiers A1 and A2 acts as an error amplifier. The gain of this stage is R6/R9, with R6 = R7 and R9 = R8, and is about 50 in this circuit. A triangle-wave generator with operational amplifier A3 provides a triangle wave of amplitude 0.5 V across C3 with a positive offset with respect to the midpoint voltage at M. The period of this waveform is

$$T \approx 0.2(R14)(C3) \qquad\qquad (2.19)$$

and is about 10 ms in this circuit.

An operational amplifier comparator A4 compares the error signal with the triangle wave and provides a square wave, the pulse width of which is proportional to the error signal. The output of A4 is amplified by the current amplifier configuration formed by TR2, TR3, and TR4 which in turn drives the heater load. Any decrease in temperature from the set value will increase the error voltage, causing the pulse width to increase, resulting in more average power to the load, which in turn corrects the decreasing temperature, thereby completing the control loop. This pulse width modulation technique of proportional power control was also successfully used by the author earlier in an high-temperature control circuit [2.34]. The switching type of power output has an advantage that there is no power loss in the output transistor and the system becomes highly power efficient, a factor which is highly relevant when battery backup is used.

The circuit diagram of the power supply for the temperature controller is shown in Fig. 2.9. Operational amplifier A5 along with transistors TR5 and TR6 produce a symmetrical dual supply voltage for the controller circuit. While the power is ON, TR7 acts as a series pass voltage regulator with the reference voltage taken from the battery which is being charged through R22 and D3. During the power ON period the relay is active and the normally open (NO) relay contact is closed. As a result, power is taken from the
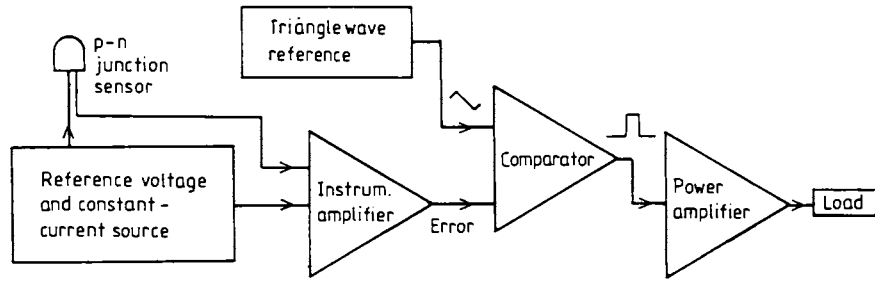
Figure 2.7

Block diagram of the Temperature controller

78
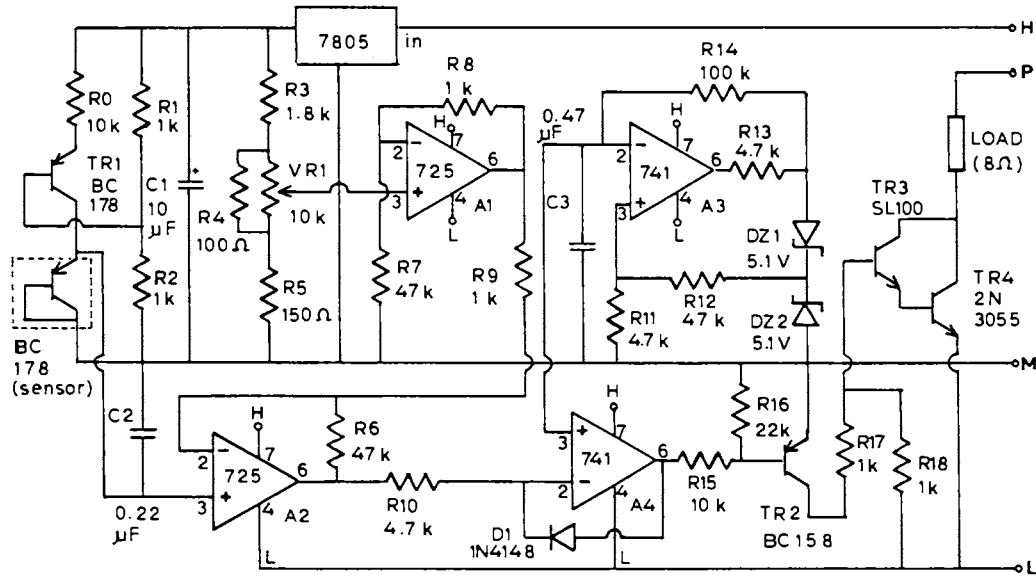
Figure 2.8

Circuit diagram of the temperature controller

79
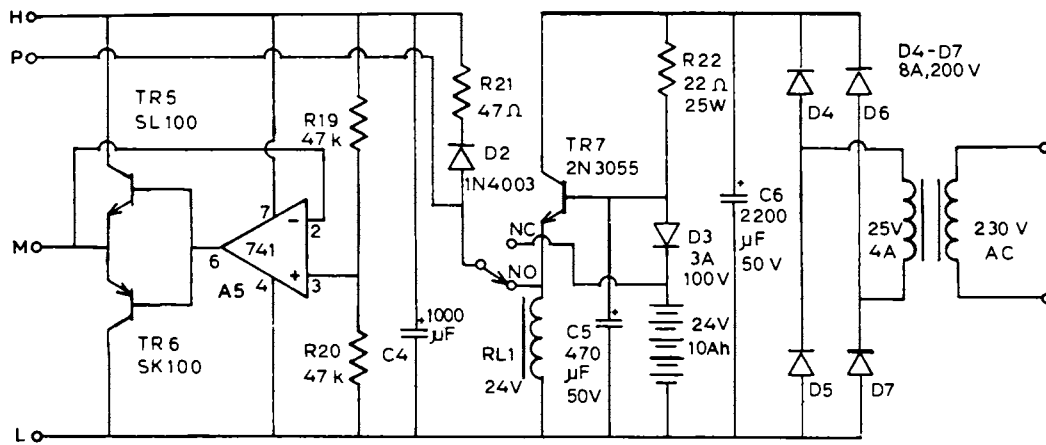
Figure 2.9

Circuit diagram of the temperature controller power supply

80

emitter terminal of TR7. During a power failure the normally closed (NC) relay contact is closed and power is taken from the battery. During the power ON period the battery is given only a trickle charging to avoid overcharging. However, the charging rate can be adjusted to the required value by selecting an appropriate value for the resistance R22. The gain of the controller may be adjusted by changing the gain of the error amplifier. The proportional band can be changed by adjusting the amplitude of the triangle wave, which is possible by changing the value of R11. The amplitude of the triangle wave in volts is approximately equal to 5.1(R11)/(R12+R11).

The present controller uses a silicon junction sensor, which has a large signal output compared with thermocouples, and this avoids problems of noise and drift at microvolt level. Also its low non-linearity permits an easy temperature calibration, in contrast with the highly nonlinear thermistors. This controller is not provided with a temperature indicating display because a dial calibration is sufficient for the present purpose. A digital panel meter can be incorporated in the circuit in case temperature indication is also needed, as we have done for a general purpose PID temperature controller [2.35].

The performance of the controller has been monitored while controlling the temperature of the bath discussed in section 2.4.2 and it was found that the temperature of the bath was steady within ± 0.1 K at 312 K over several weeks, even with mains power off for several hours.

2.4.4 The designed crystal rotation controller

In this section, a motor control circuit which was designed for controlling the crystal rotation is described. The need for crystal rotation or solution stirring in solution growth of crystal was explained in section 2.4.1. The present

circuit is versatile and has some novel features. It has provision for adjusting the speed of rotation. The period of time between rotation reversals can be adjusted. Further, there is a dead time before a rotation reversal during which no power is given to the motor. This dead time is to allow the inertia of the rotating crystal to die out before a reversal. In the absence of the dead time, a jerky movement can be produced which would strain the crystal and the suspension system. The motor control circuit has a fully solid state design and electromechanical relays are not used.

The circuit diagram of the crystal rotation motor controller is shown in Figure 2.10. The circuit essentially has two parts. One is the oscillator, counter and logic section and the other is the complementary transistor bridge type power output stage. The oscillator and counter function is performed by the CMOS type IC CD4060 (IC1). This IC has a 14 bit binary counter and an internal oscillator, the frequency f of which can be set using external components as

$$f = 1 / (2.3 R C) \tag{2.20}$$

where $R = (VR1 + R2)$ and $C = C1$ in the circuit. This frequency is divided by the internal binary counter and fixes the period between reversals of the motor. Hence the period is adjustable using VR1. The outputs of the counter from 7th to 10th stages $(Q_7$ to $Q_{10})$ are used for producing the control waveform. Examination of the 4 bit binary sequence shows that Q_{10} produces a symmetrical square wave output. Further, when Q_{10} goes to 0 or 1 state then all the three outputs Q_7 to Q_9 together goes to 0 state for a period equal to 1/16th of Q_{10} output waveform period. This short period is decoded by using one section of a Dual 4 input CMOS NOR gate CD4002 (IC2) for producing the dead time (C). The other section of the NOR gate is used to invert the Q_{10} output to produce the biphase output (A and B) for driving the power stage. It may be noted that the Q_{10} output has a period which is 2^{10} times (i.e. 1024) the period of the internal oscillator. With VR1 wiper set at the
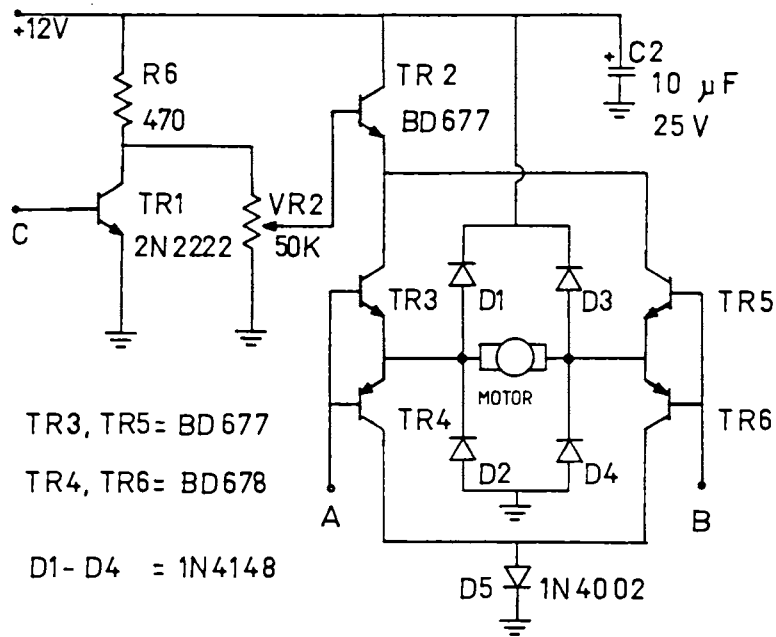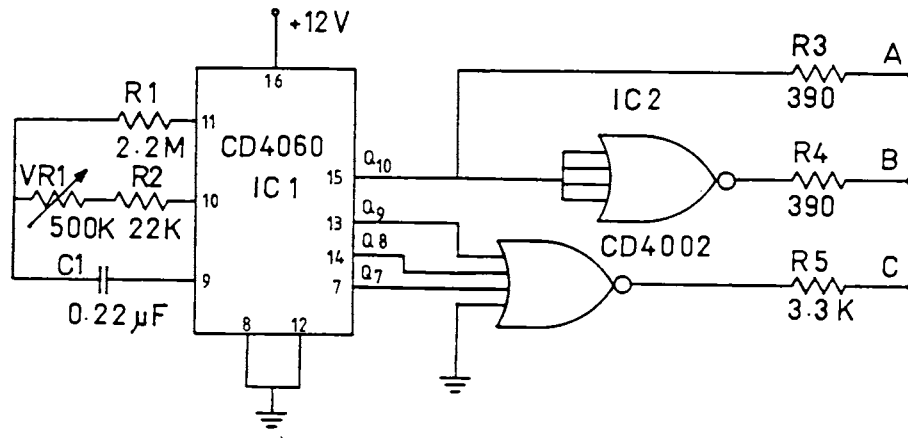
Figure 2.10

Circuit diagram of the Crystal rotation controller

midpoint the Q_{10} output has a period of about 140 seconds.

The bridge type power stage is formed by two set of complementary pairs having high gain Darlington type power transistors (TR3 to TR6). With a biphase drive (A & B) from the logic section, the motor can be driven in forward and reverse directions. Diodes D1 to D4 protects the transistors from inductive surges produced by the motor. In an emitter follower mode, TR2 works as a speed regulator with speed setting possible with VR2. TR1 is driven by the dead time logic (C), and when C is High, the power to the motor is fully cutoff. D5 ensures effective switching of the power stage transistors.

Appendix 2.1

Program for overlap identification and bond correction

(See section 2.3.3 for a description of this program)

PEO.BAS

```
10   CLS:KEY OFF:SCREEN 0 :COLOR 15:LOCATE 25,5
20   PRINT"Program by L.Godfrey -For Ultrasonic measurements-"
30   LOCATE 17,1:PRINT "1. Creats Ultrasonic Experiment Data
     files"
40   PRINT "2. Process data with bond correction"
50   PRINT "3. Quit":PRINT
60   INPUT "Select (1 - 3)";SEL
70   IF SEL<1 OR SEL>3 THEN 30
80   ON SEL GOTO 2410,110,100
90   GOTO 10
100  COLOR 7:CLS:KEY ON:END
110  CLEAR:LOCATE 17,1
120  PRINT SPACE$(50):PRINT SPACE$(50):PRINT SPACE$(50):PRINT
130  PRINT SPACE$(50):LOCATE 1,1 :PRINT "files present are.."
140  FILES "*.IN":PRINT
150  INPUT"enter the name of selected data file:[    .IN]",DTA$
160  DEFDBL A-H,L-Z
170  OPEN "I",#2,DTA$+".IN"
180  INPUT #2,DTAI$
190  INPUT #2,NA$,BM$,DR$:PRINT NA$,BM$,DR$
200  INPUT #2,W$,POL$:PRINT W$,POL$
210  INPUT #2,LS,N,P:PRINT LS,N,P:PRINT
220  DIM XD(N),YD(2,N)
230  FOR I=1 TO N
240    XD(I)=I
250    INPUT #2,YD(1,I),YD(2,I):PRINT I,YD(1,I),YD(2,I)
260    YD(1,I)=100/YD(1,I):YD(2,I)=100/YD(2,I)
270  NEXT I
280  INPUT #2,ZB,RHO,ZT :PRINT :PRINT ZB,RHO,ZT
290  INPUT #2,OTR$:PRINT OTR$
300  CLOSE
310  X1=0:X2=0:YSQ1=0
320  Y1=0:Y2=0:YSQ2=0
330  P1=0:P2=0
340  FOR I=1 TO N
350    X1=X1+XD(I)
360    Y1=Y1+YD(1,I):Y2=Y2+YD(2,I)
370    YSQ1=YSQ1+YD(1,I)*YD(1,I):YSQ2=YSQ2+YD(2,I)*YD(2,I)
380    X2=X2+XD(I)*XD(I)
390    P1=P1+XD(I)*YD(1,I)
400    P2=P2+XD(I)*YD(2,I)
410  NEXT I
```

85

```basic
420 D=N*X2-X1*X1
430 IF D<>0 THEN 460
440 PRINT "no solution"
450 STOP
460 B1=(N*P1-X1*Y1)/D:B2=(N*P2-X1*Y2)/D
470 A1=(Y1-B1*X1)/N:A2=(Y2-B2*X1)/N
480 PRINT:COR1=(N*P1-X1*Y1)/SQR((N*X2-X1*X1)*(N*YSQ1-Y1*Y1))
490 PRINT:COR2=(N*P2-X1*Y2)/SQR((N*X2-X1*X1)*(N*YSQ2-Y2*Y2))
500 PRINT
510 PRINT
520 PRINT "  1 . SCREEN "
530 PRINT "  2 . LPT1:   "
540 PRINT "  3 . ";DTA$+".OUT"
550 PRINT "  4 . Special"
560 INPUT "Enter output choice:",CHO
570 PRINT:PRINT
580 IF CHO > 4 OR CHO<1 THEN 520
590 ON CHO GOTO 600,610,620,630
600 OF$="SCRN:":GOTO 640
610 OF$="LPT1:":GOTO 640
620 OF$=DTA$+".OUT":GOTO 640
630 INPUT "Output file/device name";OF$
640 OPEN "O",#1,OF$
650 IF CHO > 1 THEN PRINT "Dumping Output to ";OF$
660 PRINT#1,"Sample name          = ";NA$
670 PRINT#1,"Propagation direction = ";DR$
680 PRINT#1,"Wave Type            = ";W$
690 PRINT#1,"Polarization direction= ";POL$
700 PRINT#1,"Sample dimension & p  = ";
710 PRINT#1,USING "##.#####";LS;:PRINT#1," cm ,  p = ";
720 PRINT#1,USING "#";P
730 PRINT#1,"Linear  fitting of the ";N;" measurement data
    pairs give:"
740 F$="##.#######^^^^":F2$="#.##########"
750 PRINT#1,"TL= ";
760 PRINT#1,USING F$;A1;
770 PRINT#1," + ";
780 PRINT#1,USING F$;B1;
790 PRINT#1,"*X    Cor.cof=";
800 PRINT#1,USING F2$;COR1
810 PRINT#1,"TH= ";
820 PRINT#1,USING F$;A2;
830 PRINT#1," + ";
840 PRINT#1,USING F$;B2;:PRINT#1,"*X    Cor.cof=";
850 PRINT#1,USING F2$;COR2
860 SG$=STRING$(62,45)
870 PRINT#1,SG$:FS0$="\   \":FS1$="\            \"
880 PRINT#1,USING FS0$;"  X";
890 PRINT#1,USING FS1$;"  TL","  E(TL)","  TH","  E(TH),"
    (TL-TH)"
900 PRINT#1,USING FS0$;"  No";
910 PRINT#1,USING FS1$;"  µs","  µs","  µs","  µs","  ns"
920 PRINT#1,SG$
```

```
930 ZXZ=INT((A2-A1)/(B1-B2))
940 FOR I=(ZXZ-4) TO (ZXZ+4)
950    ETL=0:ETH=0
960    TL=B1*I+A1:TH=B2*I+A2
970    IF I>0 AND I<=N THEN ETL=YD(1,I)-TL:ETH=YD(2,I)-TH
980    PRINT#1,USING "###   ";I;
990    PRINT#1,USING "###.#####   ";TL,ETL,TH,ETH,(TL-TH)*1000
1000 NEXT I
1010 PRINT#1,SG$
1020 IF CHO=1 THEN INPUT "Strike ENTER to continue...",NUL$
1030 FL=1/B1:FH=1/B2:FR=FH
1040 PRINT#1,"Estimated Low RF frequency = ";
1050 PRINT#1,USING "###.######   MHz";FL
1060 PRINT#1,"Estimated High RF frequency= ";
1070 PRINT#1,USING "###.######   MHz";FH;
1080 PRINT#1,USING "  LF/HF = #.##";FL/FH
1090 PRINT#1,"Bond material used         =   ";BM$
1100 PRINT#1,"Bond impedance             = ";
1110 PRINT#1,USING "##.####";ZB;:PRINT#1," x1e6 kg/m$^2$.s"
1120 PRINT#1,"Transducer impedance       = ";
1130 PRINT#1,USING"##.####";ZT;:PRINT#1," x1e6 kg/m$^2$.s"
1140 PRINT#1,"sample density in g/cc     = ";
1150 PRINT#1,USING "##.#####";RHO
1160 ZS=P*RHO*1000!*2*LS*.01/((B2*ZXZ+
     A2)*.000001):ZS=ZS/1000000!
1170 PRINT#1,"estimated sample impedance = ";
1180 PRINT #1,USING "###.####";ZS;:PRINT #1,"  x1e6 kg/m$^2$.s"
1190 PRINT#1,"Other information          = ";OTR$
1200 PRINT
1210 IF CHO=1 THEN INPUT "Strike enter to continue....",NUL$
1220 PI=3.141592654#:COLOR 31:LOCATE 25,55
1230 PRINT "COMPUTING"
1240 AL=0:X=AL:GOSUB 1650
1250 DTMIN=DT
1260 AH=60*PI/180:X=AH:GOSUB 1650:DTMIN2=DT
1270 X=(AL+AH)/2:GOSUB 1650 :DTMAX=DT:XMAX=X
1280 AIN=(AH-AL)/4
1290 FOR I=1 TO 20
1300    X=XMAX-AIN:GOSUB 1650
1310    IF DT>DTMAX THEN DTMAX=DT:XMAX=X:CRMAX=CR
1320    X=XMAX+AIN:GOSUB 1650
1330    IF DT>DTMAX THEN DTMAX=DT:XMAX=X:CRMAX=CR
1340    AIN=AIN/2
1350    IF AIN<.000001 THEN 1370
1360 NEXT I
1370 COLOR 15
1380 PRINT #1,STRING$(16,45);"CALCULATION OF CORRECT OVERLAP";
1390 PRINT #1,STRING$(16,45)
1400 F3$="####.###"
1410 PRINT #1,"estimated maximum value of  delta t     [ns] =
     ";
1420 PRINT #1,USING F3$;DTMAX
1430 PRINT #1,"bond angle corresponding to max delta t [deg]=
```

```
    ";
1440 PRINT #1,USING F3$;XMAX*180/PI
1450 PRINT #1,"correction corresponding to max delta t [ns]
     = ";
1460 PRINT #1,USING F3$;CRMAX*1000
1470 PRINT #1,"delta t for 0,60 deg bond angles [ns] = ";
1480 PRINT #1,USING F3$;DTMIN,DTMIN2
1490 FLG=0:XMIN2=60*PI/180
1500 FOR I= (ZXZ-7) TO (ZXZ+4)
1510  TL=B1*I+A1:TH=B2*I+A2
1520  DTE=(TL-TH)*1000
1530  IF DTE<DTMAX AND DTE>DTMIN THEN
     FLG=FLG+1:XL=0:XH=XMAX:GOSUB 1750
1540  IF DTE<DTMAX AND DTE>DTMIN2 THEN
     FLG=FLG+1:XL=XMAX:XH=XMIN2:GOSUB 1750
1550 NEXT I
1560 LOCATE 25,55:PRINT "                    "
1570 IF FLG=0 THEN PRINT "No possible case in allowed  range"
1580 IF FLG=0 THEN PRINT#1,SG$:PRINT#1, "No possible case in
     allowed range"
1590 IF FLG>2 THEN PRINT#1,"Multiple case found"
1600 IF FLG=0 THEN GOSUB 2040
1610 LOCATE 24,1
1620 CLOSE:PRINT
1630 IF CHO=1 THEN INPUT "Strike enter to continue....",NUL$
1640 GOTO 10
1650 BH=TAN(X) 'SUBR. DLT
1660 BL=TAN(X*FL/FR)
1670 R=ZB/ZT
1680 ZH=ZB*BH
1690 ZL=ZB*(R*BL+TAN(PI*FL/FR))/(R-BL*TAN(PI*FL/FR))
1700 GH=ATN(-2*ZH*ZS/(ZS*ZS-ZH*ZH))
1710 GL=ATN(-2*ZL*ZS/(ZS*ZS-ZL*ZL))
1720 DT=((GH/FH-GL/FL)*P/2/PI)*1000!
1730 CR=(GH/FH/2/PI)*P
1740 RETURN
1750 X=XL:GOSUB 1650
1760 F1=DTE-DT:IF F1=0 THEN 1890
1770 X=XH:GOSUB 1650
1780 F2=DTE-DT:IF F2=0 THEN 1890
1790 IF ABS(XL-XH)<.00001 THEN X=XH:GOTO 1880
1800 X0=(XL+XH)/2
1810 X=X0:GOSUB 1650
1820 F0=DTE-DT:IF F0=0 THEN 1890
1830 IF F1*F0<0 THEN 1860
1840 XL=X0:F1=F0
1850 GOTO 1790
1860 XH=X0:F2=F0
1870 GOTO 1790
1880 GOSUB 1650
1890 IF FLG>1 THEN GOTO 1940
1900 PRINT#1,SG$:FS2$="\              \"
1910 PRINT #1,USING FS2$;"  BOND","  DELTA t","  TH"," CR","
```

```basic
2400 RETURN
2410 PRINT
2420 CLEAR:LOCATE 17,1:PRINT SPACE$(50):PRINT SPACE$(50)
2430 PRINT SPACE$(50):PRINT:PRINT SPACE$(50):LOCATE 1,1
2440 PRINT "Files present are...":FILES "*.IN":PRINT
2450 INPUT "enter the data file name to be created:[    .IN]
     ",DAT$
2460 DAT$=DAT$+".IN"
2470 DEFDBL Y
2480 INPUT "Name of sample";NA$
2490 INPUT "bond material used";BM$
2500 INPUT "direction of propagation";DR$
2510 INPUT "length in cm";LS
2520 INPUT "wave type  L or T ";W$
2530 IF W$="L" OR W$="l" THEN W$="Longitudinal":POL$=DR$:GOTO
     2560
2540 IF W$="T" OR W$="t" THEN W$="Transverse":GOTO 2550  ELSE
     2520
2550 INPUT " Polarization direction ";POL$
2560 INPUT "number of data values";N
2570 INPUT "value of p";P:PRINT
2580 DIM YL(N),YH(N)
2590 PRINT "             yl is rep.rate in MHz x 100 for low
     rf"
2600 PRINT "             yh is rep.rate in MHz x 100 for high
     rf"
2610 PRINT "            m is a case of overlap"
2620 PRINT
2630 INPUT "Multiplication factor for yl&yh [1 for
     default]";MULF
2640 PRINT
2650 FOR I=1 TO N
2660   PRINT "FOR m=";I;
2670   INPUT ;"    yl=";YL
2680   INPUT "     yh=";YH
2690   YL(I)=YL*MULF:YH(I)=YH*MULF
2700 NEXT I
2710 INPUT "Bond impedance in  x1e6 kg/m²·s";ZB
2720 INPUT "Sample density in g/cc ";RHO
2730 INPUT "transducer impedance x1e6 kg/m²·s";ZT
2740 INPUT "any other information (nill for nothing)";OTR$
2750 PRINT "creating file ";DAT$
2760 OPEN "o",#1,DAT$
2770 WRITE #1,DAT$
2780 WRITE #1,NA$,BM$,DR$
2790 WRITE #1,W$,POL$
2800 WRITE #1,LS,N,P
2810 ON SGN(YH(1)-YH(N))+2 GOSUB 2890,2930,2950
2820 WRITE #1,ZB,RHO,ZT
2830 WRITE #1,OTR$
2840 CLOSE
2845 ERASE YL,YH
2850 PRINT " File ";DAT$;"  is created"
```

```
2860 INPUT "More data file   y/n ";SEL$
2870 IF SEL$="y" OR SEL$="Y" THEN 2450
2880 GOTO 10
2890 FOR I=N TO 1 STEP -1
2900   WRITE #1, YL(I),YH(I)
2910 NEXT I
2920 RETURN
2930 PRINT "data invalid"
2940 RETURN
2950 FOR I=1 TO N
2960   WRITE #1, YL(I),YH(I)
2970 NEXT I
2980 RETURN
```

References

2.1   H. J. Mc Skimin: J. Acoust. Soc. Am. $\underline{33}$, 12 (1961)

2.2   H. J. Mc Skimin, P. Andreatch: J. Acoust. Soc. Am. $\underline{34}$, 609 (1962)

2.3   T. J. Moran, B. Lüthi: Phys. Rev. $\underline{187}$, 710 (1969)

2.4   R. D. Holbrook: J. Acoust. Soc. Am. $\underline{20}$, 590 (1948)

2.5   N. P. Cedrone, D. R. Curram: J. Acoust. Soc. Am. $\underline{26}$, 963 (1954)

2.6   E. P. Papadakis: J. Appl. Phys. $\underline{35}$, 1474 (1964)

2.7   E. P. Papadakis: In *Physical Acoustics,* Vol.12, ed. by W. P. Mason, R. N. Thurston (Academic Press, New York 1976)

2.8   E. P. Papadakis: In *Physical Acoustics,* Vol.19, ed. by R. N. Thurston, Allan D. Pierce (Academic Press, New York 1990)

2.9   R. Turrel, C. Elbaum, B. B. Chick: *Ultrasonic Methods in Solid State Physics* (Academic Press, New York 1969)

2.10 E. R. Fuller, A. V. Granato, J. Holder, E. R. Naimon: In *Methods of Experimental Physics*, Vol.11, ed. by R. V. Coleman (Academic Press, New York 1974)

2.11 D. I. Bolef: In *Physical Acoustics*, Vol.IV, part A, ed. by W. P. Mason, R. N. Thurston (Academic Press, New York 1966)

2.12 D. I. Bolef, J. G. Miller: In *Physical Acoustics,*

Vol.VIII, ed. by W. P. Mason, R. N. Thurston (Academic Press, New York 1971)

2.13 T. A. Read, C. A. Wert, M. Metzger: In *Methods of Experimental Physics*, Vol.6A, ed. by K. Lark-Horovitz, V. A. Johnson (Academic Press, New York 1974)

2.14 W. P. Mason: *Piezoelectric Crystals and Their Application to Ultrasonics* (Van Nostrand, Princeton 1950)

2.15 G. Rupprecht, W. H. Winter: Phys. Rev. 155, 1019 (1967)

2.16 E. Schreiber, O. L. Anderson, N. Soga: *Elastic constants and their measurement* (McGraw-Hill, New York 1973)

2.17 B. Lüthi, W. Rehwald in *Topics in current physics: Structural Phase Transitions I,* eds. K. A. Müller, H. Thomas (Springer- Verlag, Heidelberg 1981)

2.18 J. E. May, Jr.: IRE Natl. Conv. Rec. 6, Pt.2, 134 (1958)

2.19 R. L. Roderic, R. Turrel: J. Appl. Phys. 23, 267 (1952)

2.20 B. B. Chick, G. Anderson, R. Turrel: J. Acoust. Soc. Am. 32, 186 (1960)

2.21 J. Williams, J. Lamb: J. Acoust. Soc. Am. 30, 308 (1958)

2.22 W. C. Johnson: *Transmission lines and networks* (McGraw-Hill, Singapore 1963)

2.23 A. A. Chernov: *Springer Series in Solid State Sciences 36: Modern Crystallography III -Crystal Growth* (Springer-Verlag, Berlin 1984)

2.24 J. C. Brice: *The Growth of Crystals from Liquids* (North-Holland, Amsterdam 1973)

2.25 B. R. Pamplin: *Crystal Growth* (Pergamon, Oxford 1975)

2.26 J. J. Gilman: *The Art and Science of Growing Crystals* (Wiley, New York 1963)

2.27 R. A. Laudise: *The Growth of Single Crystals* (Prentice Hall, Englewood Cliffs, NJ 1970)

2.28 H. E. Buckley: *Crystal Growth* (Wiley, New York 1951)

2.29 J. D. B. Featherstone, N. A. Dickinson: J. Phys. E: Sci. Instrum. 10, 334 (1977)

2.30 M. Grubic, R. Strey: J. Phys. E: Sci. Instrum. 10, 142 (1977)

2.31 M. A. Handschy: J. Phys. E: Sci. Instrum. 13, 998 (1980)

2.32 L. Godfrey, J. Philip: J. Phys. E: Sci. Instrum. 22, 516 (1989)

2.33 C. E. Davis, P. B. Coates: J. Phys. E: Sci. Instrum. 10, 613 (1977)

2.34 L. Godfrey, K. Viswanathan: Indian J. Pure & Appl. Phys. 22, 505 (1984)

2.35 J. Isaac, L. Godfrey, J. Philip: Indian J. Pure & Appl. Phys. 29, 195 (1991)

CHAPTER 3

ELASTIC CONSTANTS OF LITHIUM HYDRAZINIUM SULPHATE

3.1 Introduction

Lithium Hydrazinium Sulphate, $LiN_2H_5SO_4$ or LHS, has been the subject of extensive investigations due to its interesting electrical properties. It has been considered as a member of the ferroelectric sulphate family [3.1] because it exhibits what appear to be hysteresis loops in the c-axis dielectric constant, although no conclusive evidence for a ferroelectric phase transition has been found. It exhibits unusually large electrical conductivity along the c-axis [3.2]. It has been demonstrated that LHS is a protonic semiconductor whose conductivity along the c-axis is about 10^3 times as great as along the a or b axis at room temperature. Similar results have been obtained from electrical conductivity measurements on deuterated LHS^3. Hugo Schmidt *et al.*[3.3] have proposed a one dimensional partially blocked channel model for the unusual electrical properties of this material and the hysteresis loop is interpreted as arising from a saturation of the a.c.conductivity. Temperature dependence of the real part of the high frequency dielectric constant measured between -200 and $+200^\circ$C do not carry any signature of a ferroelectric phase transition [3.4].

LHS was first shown to be a protonic conductor by Vanderkooy *et al.* [3.2] and the conductivity was further investigated by Kreuer *et al.* [3.5]. The conductivity is largest along the c axis. The mechanism of protonic conductivity in LHS is not well understood and two models have been proposed to describe the dynamics of the proton transport. One is the Grotthuss mechanism, where the protons move along the extended hydrogen bonded network in the c direction by tunneling to an adjacent hydrazinium ion followed

by reorientation (rotation) of the $-NH_2$ portion of the hydrazinium ion [3.6,3.7]. More recently, the proton transport in LHS has been explained in terms of the Vehicle mechanism, in which a mobile species (in this case the hydrazinium ion, $N_2H_5^+$) is responsible for carrying the proton through the host lattice [3.5,3.6].

LHS is orthorhombic with space group $Pbn2_1$ (C_{2v}^9). The structure has been determined by X-ray [3.8-3.10] and neutron diffraction [3.11] techniques. The unit cell has dimensions a = 8.99 Å, b = 9.94 Å, c = 5.18 Å and contains four formula units. The choice of axes is different in different structure works and we have adopted the convention given in the first X-ray work [3.8]. The lattice parameters a and b are exchanged when compared to the values given in ref.[3.8], [3.10] and [3.11]. The density of the crystal is 1.966 $g.cm^{-3}$ [3.1]. The lithium and sulphur atoms are at the center of the tetrahedra of oxygen atoms. The tetrahedra share corner oxygen atoms to form a three-dimensional framework containing channels running parallel to the c-axis. The hydrazinium ions ($NH_2-NH_3^+$) lie in these channels with their N-N bond axis perpendicular to c and are linked to infinite chains by hydrogen bonding between their $-NH_2$ groups. This chain is illustrated in Figure 3.1. The electrical properties are related to the movement of protons within this chain. One proton from each $-NH_2$ group contributes a link to the chain of N-H---N bonds while the other proton in the $-NH_2$ group and the protons of the $-NH_3^+$ groups form N-H---O bonds to the oxygens of the SO_4^{2-} tetrahedra.

The investigations by Cuthbert and Petch [3.12] on the proton and Li^7 spectra and second moments in LAS indicated that the NH_2 and NH_3 groups undergo hindered rotation. In a subsequent study, MacClement *et al.* [3.13] found evidence for hydrazinium ion ($N_2H_5^+$) tumbling and diffusion at high temperature. Knispel and Petch [3.14] measured proton spin-lattice relaxation time in the rotating frame ($T_{1\rho}$) and
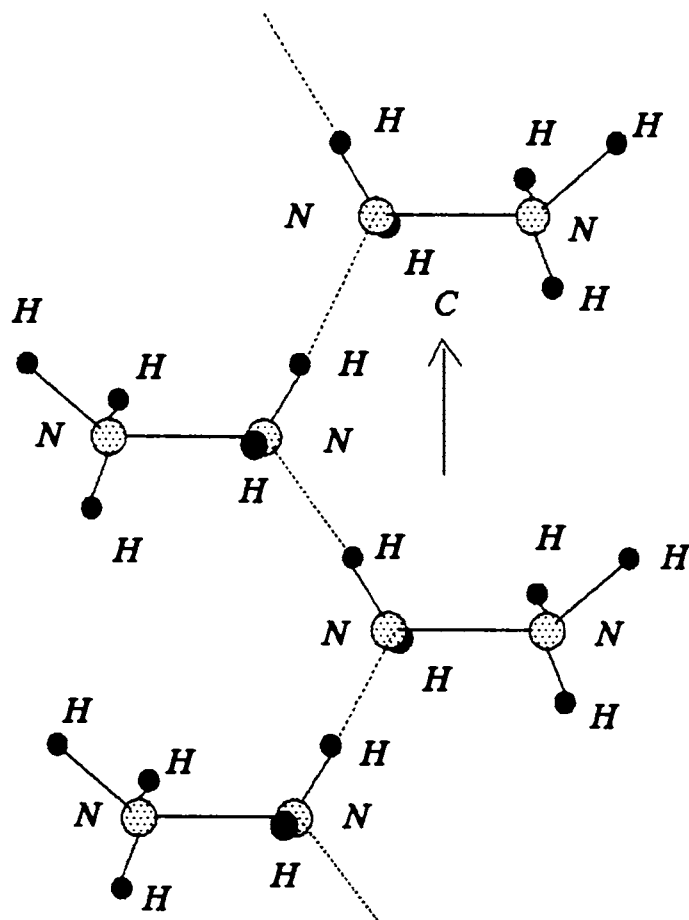
Figure 3.1
Arrangement of Hydrazinium ions in channels running
along the c-axis

from the results determined the activation energies for NH_3^+ rotation, NH_2 rotation and $N_2H_5^+$ ion tumbling. Hastings and Oja [3.15] performed Nuclear Quadrapole Resonance studies on LHS at low temperatures. More recent investigations on LHS include an electrical conductivity and dielectric study by Badarinath [3.16] and polarized Raman scattering studies by Brown and Frech [3.17,3.18].

Eventhough electrical conductivity, dielectric properties and molecular orientation and vibrations in LHS have been understood well, no report on the elastic properties of this crystal has yet appeared in literature. This and the fact that LHS can be grown as large crystal for ultrasonic work , has prompted us to investigate the elastic properties of LHS using ultrasonic technique. We have determined all the nine elastic constants of LHS for the first time. This was made possible by measuring the velocity of ultrasonic waves of different polarizations propagating along different symmetry directions in the sample. To check for the presence of elastic anomalies, which would indicate phase transitions in the crystal, we have also measured the temperature variation of the elastic constants of LHS both above and below room temperature. The results of the present measurements have been published [3.19] and it is the first paper in the literature on the elastic properties of LHS.

In this chapter the experimental details and results of the measurements of room temperature elastic constants of LHS are presented. Further, a novel numerical technique for misorientation correction and a computer program developed for the same are also described in detail. The velocity surfaces in the three symmetry planes of LHS have been computed using the measured set of elastic constants and the plots of the velocity surfaces are also presented in this chapter. The results of temperature variation studies are presented in next chapter.

3.2 Sample preparation

Large single crystals, up to 5 cm size, of LHS have been grown from aqueous solution by slow evaporation at a constant temperature of 313 K over a period of several weeks. The solution has been prepared by dissolving equimolar fractions of Li_2CO_3 and $(NH_2)_2.H_2SO_4$ in distilled water. The details of the apparatus used for crystal growth were described in section 2.4. Large single crystals of LHS usually have well developed natural faces in the [100], [110] and [101] directions. The crystals are elongated along the c-axis. A drawing of the morphology of the crystal is shown in Figure. 3.2. The natural faces of the sample are identified by measuring the interfacial angles of the crystal and comparing it with the calculated angles. The angles have been calculated using the lattice parameters and the usual crystallographic formulae [3.20] for interplanar angles. For the orthorhombic lattice it is given by

$$\cos(\theta) = \frac{h_1 h_2 \frac{bc}{a} + k_1 k_2 \frac{ca}{b} + l_1 l_2 \frac{ab}{c}}{\sqrt{h_1^2 \frac{bc}{a} + k_1^2 \frac{ca}{b} + l_1^2 \frac{ab}{c}} \sqrt{h_2^2 \frac{bc}{a} + k_2^2 \frac{ca}{b} + l_2^2 \frac{ab}{c}}}$$

(3.01)

where θ is the angle between the normals to two faces whose indices are $h_1 k_1 l_1$ and $h_2 k_2 l_2$, and a, b, c, are the latticeparameters. The measured angles were well in agreement with the calculated values when the faces of the crystal were correctly identified.

Bulk samples have been cut using a slow speed diamond wheel saw (Model 650, South Bay Technology, USA). The diamond saw blade consists of a thin metal disc with micron sized diamond powder embedded on the outer edge. The blade is fixed
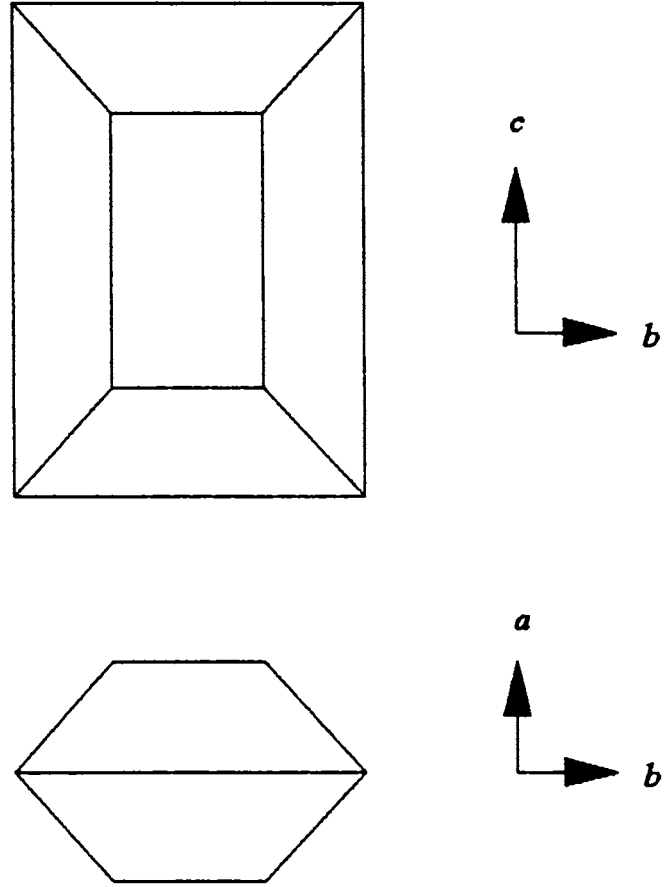
Figure 3.2
The Lithium Hydrazinium Sulphate crystal

to a rotation mechanism driven by a speed controlled motor. The crystal to be cut is glued to a precision movable arm with a goniometer and a counterweight. Once the directions are carefully adjusted with respect to the blade, the arm can be lowered so that the crystal rests on the rotating blade edge. The blade is continuously cooled and cleaned by a coolant which is kept below in a tray. Water based coolants cannot be used for cutting water soluble crystals and it was found that liquid paraffin can be effectively used for this. One advantage of this diamond saw is that samples can be cut easily to have parallel faces. This is very important for ultrasonic work because the nonparallelsm will bring in a nonexponintally decaying echo pattern and additional errors in velocity measurements. Once a face is cut then the arm can be given a linear translation (which decides the thickness of the cut sample) using a micrometer screw without disturbing the glued crystal and the goniometer. The next cutting is done in this position to get a face parallel to the first face.

The samples have been cut so as to have propagation directions along a, b and c axes, [101] and [110] directions and along a direction which makes an angle $\theta = 43°$ with the b-axis in the b-c plane. It may be noted that while this crystal is having natural faces in a-b and a-c planes it does not have a natural face in the b-c plane. In all cutting operation the reference for the directions in the crystal were taken from the natural faces or edges of the crystal. Extreme planing is needed while deciding where to cut a crystal to ensure maximum number of pieces of different directions from a given crystal. The sample lengths along the measurement directions are in the range of 0.9–1.3 cm. The sample ends have been polished carefully using cerium oxide to optical reflection level so as to ensure proper bonding of the transducer to the sample surface.

3.3 Misorientation measurements

Due to the inaccuracy in fixing and aligning the crystal in the crystal cutter, the actual cut faces were misoriented by few degrees with respect to the required directions. This can cause an error in the measurement of elastic constants. In order to apply a correction to the measured elastic constants on account of misorientation the the direction cosines of the misorientated direction in the crystal should be known. One way to find the misorientated direction is to use a highly specialized X-ray set up to take back reflection Laue photograph of each cut face. By studying the Laue spots the misorientation can be deducted with considerable amount of labor. One difficulty in this method is that there must be some precision arrangement (possibly by using optical ray) by which it must be ensured that the X-ray strikes the crystal exactly normal to the cut face. An error in this makes the misorientation measurement meaningless.

Another method, which was used in present work is to deduct the direction cosines of these misorientations in each case by measuring the angle between the cut face and the natural faces of the crystal. The necessary mathematical relations were presently derived using the equations of spherical triangles [3.21]. The method of deducting the misorientation from interfacial angle measurements is described below.

Consider the rectangular co-ordinate system with orthogonal directions x, y, and z. The crystal may be assumed to be at the centre with crystallographic directions a, b, and c aligned in parallel with x, y, and z directions respectively. This also means that the normals drawn from the a, b, and c faces are along x, y, and z respectively. Consider also a unit sphere whose centre coincide with the centre of the co-ordinate system. A normal of a crystal face drawn from the centre will intersect the sphere at a point on the

surface. Three such points on the surface corresponding to three different directions can form a spherical triangle on the sphere surface. Such a triangle has three sides expressed in angles which corresponds to the angle between the respective normals, and three included angles defined on the surface of the sphere. An interesting feature of a spherical triangle is that all parameters of the triangle are expressed in degrees and the sum of the included angles can be greater than 180 degrees.

If a, b, and c are the three sides of the triangle (not the lattice parameters which use the same notation) and A, B, and C are the included angles such that A, B, and C faces the sides a, b, and c respectively then the equation of spherical triangle can be written as

$$\cos c = \cos a \cos b + \sin a \sin b \cos C \qquad (3.02)$$

with $C = 90°$ this reduces to

$$\cos c = \cos a \cos b \qquad (3.03)$$

Now, coming to the problem of misorientation, consider the situation at a face of the crystal. The cut face in this direction can have a tilt towards c direction or it can have a tilt towards the b direction or in general it can have tilt towards both c and b directions. This tilt can be calculated from the interfacial angle measurements of the cut face with the the natural faces of the crystal. The angular tilts of the normal of the cut face towards c and b directions from the a direction may be denoted as a_c and a_b respectively.

If α_a, β_a, and γ_a are the angles made by the normal of the cut face with the directions a, b, and c respectively, then by using equation (3.03) the cosine of angles α_a, β_a and γ_a can be expressed in terms of a_c and a_b. The cosine of the α_a, β_a and γ_a are in fact the direction cosines of the misoriented direction, and denoted as l_{a1}, l_{a2} and l_{a3}. The following relations results

$$l_{a1} = \cos \alpha_a = \cos a_c \cos a_b$$

$$l_{a2} = \cos \beta_a = \cos a_c \sin a_b \qquad (3.04)$$

$$l_{a3} = \cos \gamma_a = \sin a_c \cos a_b$$

A similar analysis can be carried out for a misoriented direction near the b direction of the crystal and the following expressions result.

$$l_{b1} = \cos \alpha_b = \sin b_a \cos b_c$$

$$l_{b2} = \cos \beta_b = \cos b_a \cos b_c \qquad (3.05)$$

$$l_{b3} = \cos \gamma_b = \cos b_a \sin b_c$$

Similarly in the c direction the following relations are obtained

$$l_{c1} = \cos \alpha_c = \sin c_a \cos c_b$$

$$l_{c2} = \cos \beta_c = \cos c_a \sin c_b \qquad (3.06)$$

$$l_{c3} = \cos \gamma_c = \cos c_a \cos c_b$$

While working with directions it is more convenient to have spherical polar co-ordinates θ and ϕ. The direction cosines can be converted to θ and ϕ by using the relations

$$\theta = \tan^{-1}\left(\frac{\sqrt{1 - l_3^2}}{l_3}\right) \qquad (3.07)$$

$$\phi = \tan^{-1}\left(\frac{l_2}{l_1}\right) \qquad (3.08)$$

The misorientations in the cut faces of the sample have been found using the method discussed above. The interfacial angle measurements have been performed using an accurate Contact Goniometer (Carl Zeiss Jena make, 5 arc minute resolution). The maximum deviation from the specified directions are found to be less than 3.2 degrees. The overall accuracy in the determination of the misorientation is better than ± 0.5 degree. The results of the measurements are tabulated in Table 3.1. With the knowledge of the misorientation direction we have been able to apply misorientation correction for the elastic constants numerically, the details of which are discussed in section 3.5.

3.4 Ultrasonic velocity measurements in LHS

3.4.1 Velocity measurements

In Section 1.2.3 the details of measuring the elastic constants of orthorhombic crystal were discussed. The necessary expressions for the same, which relate the measured velocities with the elastic constants, were obtained and tabulated in Table 1.2. The ultrasonic velocities were measured using the Pulse Echo Overlap technique and the details of this technique were explained in Section 2.1.2. The basic experimental setup used for the measurements appears in Section 2.2.1. In all the velocity measurements, the correct overlap identification and bond correction have been performed using the computer program developed for the same and the details of the methodology and the program were presented in section 2.3.3. Specific experimental details of the velocity measurements and results in orthorhombic LHS are given in this section.

X and Y cut quartz transducers with resonance frequency 10 MHz, excited at their fundamental mode of operation, have

Table 3.1

Measured values of misorientations in cut samples of LHS

Crystal face	Measured tilt angles	Direction cosines of misorientation	Spherical polar co-ordinates	Required Symmetry direction
a	$a_c = 2.1°$	$l_{a1} = 0.99879$	$\phi = 358°$	$\phi = 0°$
	$a_b = -2°$	$l_{a2} = -0.03487$	$\theta = 87.9°$	$\theta = 90°$
	$(\alpha_a = 2.90°)$	$l_{a3} = 0.03662$		
b	$b_a = 2.2°$	$l_{b1} = 0.03836$	$\phi = 87.8°$	$\phi = 90°$
	$b_c = 2.3°$	$l_{b2} = 0.99846$	$\theta = 87.7°$	$\theta = 90°$
	$(\beta_b = 3.18°)$	$l_{b3} = 0.04010$		
c	$c_a = -1.3°$	$l_{c1} = -0.02267$	$\phi = 242.5°$	$\phi = 0°$
	$c_b = -2.5°$	$l_{c2} = -0.04361$	$\theta = 2.82°$	$\theta = 0°$
	$(\gamma_c = 2.82°)$	$l_{c3} = 0.99879$		

been used to generate longitudinal and transverse ultrasonic waves respectively. The transducers are gold plated with annular type of geometry so that the bottom electrode reaches the top surface through the edges and appears as an outer ring. Thus both connections can be given from the top and makes it unnecessary to have a metal foil between the transducer and the sample. Neglecting the thickness of the gold plating there is only a thin layer of the bond material between the transducer and the sample and this makes the bond correction technique effective. Bond correction and overlap identification technique is not very effective in the presence of a metal foil.

Silicone grease and Salol (Phenyl Salicylate) have been used, at room temperature, as the bonding media between the transducer and sample for longitudinal and transverse waves respectively. Polishing of the sample surface and the cleaning of the transducer and the sample surface are very important for successful bonding. Salol makes a good transverse wave bond when the bonding takes place but making a bond with Salol is a difficult operation especially when the bonding is required on a crystal surface. When heated, Salol melts at about 40°C and while it is in the liquid form in between the sample and transducer it is allowed to cool. To make the bond thin the transducer has to be held pressed to the sample under spring action. On cooling below the melting point Salol goes to a supercooled state and do not solidify immediately. At this stage if a tiny seed crystal of Salol is allowed to get in contact with the liquid from the edge of the transducer then full solidification takes place to form a successful single crystal Salol bond.

One problem in this process while making a Salol bond to a crystal sample is the heating, because if it is not done properly it can crack the crystal sample which is usually very sensitive to thermal gradients. We have found that by using a small jet of hot air the heating can be done quite safely. A

simple apparatus for this , in fact, have been fabricated by us.

Of the 18 propagation modes listed in Table 1.2, measurements have been performed for 12 different modes. Using these 12 measurements all the 9 elastic constants of LHS can be determined with cross checking possible on some of the values. Of the 12 measurements 9 measurements were in the near symmetry direction (considering the misorientation) and 3 were in the symmetry planes, a-b, a-c and b-c. In all cases the correct overlap identification and bond correction have been done using computer program described in Section 2.3.3. In Appendix 3.1, a typical experimental data and the program output are given. It may be noted that the program output for a measurement is a complete record of the experiment as it contains all the necessary information.

As observed in Section 3.3 the sample used for the present measurements do have some misorientation from the exact symmetry directions. These deviations from the pure mode directions will bring in contributions from other constants in velocity measurements. So the elastic constants calculated with the measured velocities are to be corrected for misorientation errors. This is the topic of Section 3.5. In Table 3.2 the results of the velocity measurements in Lithium Hydrazinium Sulphate are presented. The uncorrected values of the elastic constants are also tabulated in the same table along with the relevant formulae.

3.4.2 Precision and accuracy

Papadakis [3.22] has analysed the question of precision and accuracy of the Pulse Echo Overlap method in measuring the travel time in the sample. In PEO method the overlap can be accomplished to within a small fraction of the period τ of the radio frequency f in the burst. The precision of the method is good to $\tau/100$ or better. In our measurements using 10 MHz RF

Table 3.2

Measured ultrasonic velocities and the uncorrected elastic constants of Lithium Hydrazinium Sulphate at 300 K

No.	Mode	Direction of particle motion	Velocity measured (v) km/s	Uncorrected[*] elastic constant (ρv^2) GPa	Involved elastic constant
Propagation along a-axis					
1	L	a	4.7528	44.41	$C_{11} = \rho v^2$
2	T	b	3.3558	22.14	$C_{66} = \rho v^2$
3	T	c	3.3217	21.69	$C_{55} = \rho v^2$
Propagation along b-axis					
4	L	b	5.8063	66.28	$C_{22} = \rho v^2$
5	T	a	3.3625	22.23	$C_{66} = \rho v^2$
6	T	c	2.3737	11.08	$C_{44} = \rho v^2$
Propagation along c-axis					
7	L	c	5.6185	62.06	$C_{33} = \rho v^2$
8	T	a	3.3331	21.84	$C_{55} = \rho v^2$
9	T	b	2.3705	11.05	$C_{44} = \rho v^2$
Propagation in a-b plane, [110] direction, angle $\theta = 42.14°$					
10	QL	$\perp$ to c	5.5481	60.52 $C_{12} = 22.06$[†]	$C_{12} = f_{ab}$
Propagation in b-c plane, cut direction, angle $\theta = 43°$					
11	QL	$\perp$ to a	5.4323	58.02 $C_{23} = 29.30$[†]	$C_{23} = f_{bc}$
Propagation in a-c plane, [101] direction, angle $\theta = 30°$					
12	QL	$\perp$ to b	5.6248	62.20 $C_{13} = 21.90$[†]	$C_{13} = f_{ac}$

Table 3.2 continued

The abbreviations used have the following meanings:

L - Longitudinal, T - Transverse, QL - Quasi-longitudinal, QT - Quasi-transverse, ρ = density (1.966 g.cm^{-3} for LHS) , v = velocity of propagation of respective mode. a, b, c -Crystallographic axis.

†Calculated values using respective formulae given below

$$f_{ab} = \left[\frac{\left(c^2 C_{11} + s^2 C_{66} - \rho v^2 \right)\left(c^2 C_{66} + s^2 C_{22} - \rho v^2 \right)}{c^2 s^2} \right]^{\frac{1}{2}} - C_{66} \; ,$$

$$f_{bc} = \left[\frac{\left(c^2 C_{22} + s^2 C_{44} - \rho v^2 \right)\left(c^2 C_{44} + s^2 C_{33} - \rho v^2 \right)}{c^2 s^2} \right]^{\frac{1}{2}} - C_{44} \; ,$$

$$f_{ac} = \left[\frac{\left(s^2 C_{11} + c^2 C_{55} - \rho v^2 \right)\left(s^2 C_{55} + c^2 C_{33} - \rho v^2 \right)}{c^2 s^2} \right]^{\frac{1}{2}} - C_{55} \; .$$

where s = sine and c = cosine of respective angle θ. (See Figure 1.1 for definition of θ)

and a travel time in the sample to be about 10 μs the precision is about 0.01% .

Accuracy is however different from precision. Precision is vital for monitoring small changes when only one parameter extrinsic to the measurement itself is varied, such as for a temperature variation study of elastic constants. Accuracy is needed when many parameters, including some intrinsic to the measurement, are changed, or when the actual value of a physical constant such as an elastic modulus is desired. Thus to estimate the accuracy, one should consider all sources of error in the travel time. The main sources of error in PEO method are, e_1 the error in overlapping, e_2 the error in the bond angle determination (after bond correction) and e_3 the error due to the diffraction effects (after diffraction phase correction). Papadakis estimated the total error to be less than 0.015τ. In a case where RF frequency is 10 MHz and travel time 100 μs this corresponds to an error of 15 ppm .

For the present work the diffraction phase correction have not been applied which brings in an additional error of about 0.05τ which makes the total to be about 0.065τ. For our experiments small crystal samples have been used where the travel time is of the order of 10 μs. With 10 MHz RF used, the error in our measurements works out to be 650 ppm or 0.065%. In some cases the travel time have been down to 5 μs and there the error can be double the value quoted above (i.e. 0.13%). Taking into account the uncertainties in measuring the length and various other experimental limitations we have an absolute accuracy better than 0.3% in our velocity measurements.

3.5 Accurate determination of elastic constants with misorientation correction

In Section 3.3 the measured values of misorientations of the samples used have been presented, and the measured velocities along with the uncorrected elastic constants have

111

been tabulated in Section 3.4. In this Section the correction procedure is explained and a computer program for the same are also described. Finally the corrected elastic constants are tabulated.

3.5.1 The misorientation correction procedure

The aim of misorientation correction is to find a set of corrected elastic constants so that the velocities calcualted using the corrected set of constants along the misoriented directions do agree with the corresponding measured values of velocities in those directions.

When the waves propagate in a direction not exactly along a symmetry direction of the crystal then pure transverse or pure compressional waves are not possible and the amount of deviation from pure modes depends on the extend of deviation from a principal or pure mode axis. A description of the perturbed or quasi-pure modes resulting from small misorientations of the propagation direction with respect to the principal axis of a crystal has been developed by Waterman [3.23]. This was again discussed by Truell et al. [3.24] in line with Waterman. We have found these analytical techiniques to be difficult to use in practical measurements.

Every [3.25], while discussing the applications of his general closed-form expressions for acoustic waves in anisotropic solids, has given the following iteration equation for extracting the elastic constants from measured sound velocities associated with arbitrary nonsymmetric crystallographic directions. The equation with some change in notation reads as

$$v_n + (C_{n+1} - C_n) \frac{\partial v_n}{\partial C} = v_m \qquad (3.09)$$

where v_m is the measured value of velocity, C_n and C_{n+1} are the (n)th and (n+1)th value of the elastic constant in

iteration cycle. v_n (in measured direction) and its derivative are computed using the value of C_n and the closed form analytical expressions of Every.

For the purpose of dealing with the misorientation correction, we have modified the above equation and approached the problem more numerically. The velocity was computed by numerically solving the Christoffel matrix Γ (see Section 1.1.2) for its eigen values which corresponds to the three velocities. James [3.26] has used this method in a velocity computing program. For computing the derivative we have used the Difference Formula in numerical differentiation. The difference is defined in the small interval between the pure mode and the misorientated direction. The modified equation is derived below.

Equation (3.09) can be rewritten as,

$$C_{n+1} = (v_m - v_n) \frac{\Delta C}{\Delta v_n} + C_n \qquad (3.10)$$

In a near pure mode direction $C \approx \rho v^2$, and converting Eq. (3.10) to difference equation form, one gets

$$C_{n+1} = (v_m - v_n) \rho \frac{(v_n^2 - v_{n0}^2)}{(v_n - v_{n0})} + C_n \qquad (3.11)$$

Factoring the numerator of above equation and cancelling the common terms in numerator and denominator we get the final equation in the form,

$$C_{n+1} = \rho (v_m - v_n) (v_n + v_{n0}) + C_n \qquad (3.12)$$

In this equation v_m is the measured velocity, v_n is the computed velocity in the direction of misorientation using the constant C_n and the other constants in the full elastic constant matrix. The other constants do not change during the iteration cycle. The velocity v_{n0} is the computed velocity in

113

the symmetry direction. It was found that for small misorientations from the pure mode direction Equation (3.12) converges very fast and in a few iteration cycles the difference between v_m and v_n becomes very small which makes the correction term to approach zero.

For getting the full corrected set of elastic constants of the crystal, the following procedure has to be followed. First, all the constants which have been measured in misoriented directions should be corrected one by one using the iteration Equation (3.12). The constants appearing in combinations should then be recalculated using refined pure mode constants. This procedure gives the first corrected set of constants. The first process should again be repeated to get a second corrected set of constants. Further repetition of the process is necessary only if the first corrected and the second corrected set of constants show differences which cannot be negelected.

3.5.2 Computer program for misorientation correction

In this Section a description of the computer program developed presently for the misorientation correction of the elastic constants is described. This program is written in FORTRAN language and could be run easily in an IBM compatible PC having compilers like WATFOR 77. The program is self contained and do not require any external library subroutines. The source code listing of the program is given in Appendix 3.2.

Examination of the iteration equation (3.12) shows that the main computational overhead is the calculation of velocity in the misoriented as well as in the actual symmetry direction. Therefore a major portion of the program is for velocity computation. The program can also be used simply as a velocity computation program to calculate the velocity in any arbitrary direction in any crystal class. The program branches

to the misorientation correction subroutine only when that option is selected. The velocity is computed by SUBROUTINE VELOCT. This subroutine first assembles the Christoffel matrix through a summation DO loop. The eigen values (the three velocities) and corresponding eigen vectors (the particle displacement vectors) are then obtained using Jacobi's method. This numerical process is done by another subroutine called SUBROUTINE JACOBI. The eigen values are sorted by SUBROUTINE EIGSRT in the order of magnitude. The polar co-ordinates of the particle displacement are calculated from the eigen vectors by SUBROUTINE DIRECT. The program reads the elastic constant and density from a data file. This data file is created by the SUBROUTINE CINPU when the create data file option is selected.

The program is not fully automatic and do not cycle through different elastic constants one by one. Each constant and its corresponding velocity number are to be manually selected. Once a constant is selected then the corresponding corrected constant is calculated by the program using SUBROUTINE CORRECT. The velocity value in a selected direction is from 1 to 3, where 1 is for longitudinal mode, 2 for fast transverse and 3 for slow transverse. The polar co-ordinates θ and ϕ of the misoriented as well as of the corresponding symmetry direction are to be supplied. As one goes from one constant to another for the correction the constants are updated in memory and not automatically written to the disc and it is a better idea to store (using the create data option) the updated constants before going to the next constant. If this is not done, then after a power failure the whole process will have to be started from the first constant.

Using the above program all the measured elastic constants of Lithium Hydrazinium Sulphate have been corrected. The results of which are presented in the next section.

3.5.3 The corrected elastic constants of LHS

The misorientation measurements are presented in Section 3.3 and the measured velocities are tabulated in Table 3.2 of section 3.4. In this section the corrected set of elastic constants of LHS are presented.

The results of the correction process is fully tabulated in Table 3.3. The first corrected set of constants were obtained as a result of correcting all the constants one by one, starting with the uncorrected constants. Starting with the first corrected constants and correcting all the constants one by one the second corrected set was obtained. As it can be noted from the table the difference between first corrected and second corrected constants is negligibly small.Thus another correction cycle was found to be unnecessary. The final set of constants with error limits are given in the last column of the table.

To verify the correctness of the elastic constants we have computed the velocities in the misoriented directions in which measurements were taken. The second corrected set of elastic constants were used for the computation. The comparison of calculated and the measured values are shown in Table 3.4. We have made 12 measurements in LHS of which only 9 have been used for the determination of the 9 elastic constants of LHS. The other three cases were left for cross checking. In Table 3.4 these three cases are no. 5, 6 and 8. For these cases the calculated velocity is only less than 0.2% different from the measured values. For the other 9 cases there is no difference between the calculated and measured values.

3.6 Computed velocity surfaces of LHS

In section 1.2.1, we have derived the expressions for the velocities of acoustic waves in the symmetry planes of the

Table 3.3

Results of the misorientation correction applied to elastic constants (in GPa) of Lithium Hydrazinium Sulphate at 300 K

C_{ij}	Constants before correction	First corrected set	Second corrected set	Final set of constants	
C_{11}	44.4090	44.2470	44.2468	44.25	± 0.18
C_{22}	66.2800	66.3214	66.3217	66.32	± 0.27
C_{33}	62.0610	62.0935	62.0939	62.09	± 0.25
C_{44}	11.0470	10.9966	10.9968	11.00	± 0.04
C_{55}	21.6920	21.7723	21.7712	21.77	± 0.09
C_{66}	22.1400	22.2019	22.2004	22.20	± 0.09
C_{12}	22.0620	21.9880	21.9910	21.99	± 0.35
C_{13}	21.9030	21.7152	21.7167	21.72	± 0.35
C_{23}	29.2990	29.3609	29.3601	29.36	± 0.45

Table 3.4

The measured and calculated values of velocities in Lithium Hydrazinium Sulphate

No.	Mode	Direction of particle motion	Velocity measured km/s	Velocity calculated km/s	Variation %
Propagation along misoriented a-axis: $\theta = 87.9°$, $\phi = 358°$					
1	L	a	4.7528	4.7528	0.00
2	T	b	3.3558	3.3558	0.00
3	T	c	3.3217	3.3217	0.00
Propagation along misoriented b-axis: $\theta = 87.7°$, $\phi = 87.8°$					
4	L	b	5.8063	5.8063	0.00
5	T	a	3.3625	3.3579	0.14
6	T	c	2.3737	2.3705	0.13
Propagation along misoriented c-axis: $\theta = 2.82°$, $\phi = 242.5°$					
7	L	c	5.6185	5.6185	0.00
8	T	a	3.3331	3.3268	0.19
9	T	b	2.3705	2.3705	0.00
Propagation in a-b plane, in direction: $\theta = 90°$, $\phi = 42.14°$					
10	QL	⊥ to c	5.5481	5.5481	0.00
Propagation in b-c plane, in direction: $\theta = 47°$, $\phi = 90°$					
11	QL	⊥ to a	5.4323	5.4322	0.00
Propagation in a-c plane, in direction: $\theta = 30°$, $\phi = 0.0°$					
12	QL	⊥ to b	5.6248	5.6248	0.00

orthorhombic lattice. Since LHS belongs to the orthorhombic system, those expressions can be used to compute the velocity of acoustic waves in the symmetry planes of LHS. If the velocities are calculated using the corresponding elastic constants for different values of angle θ (defined in Figure 1.1) in the range from 0 to 360 degrees with some small step like 2°, then the resulting velocities can be plotted to get a phase velocity surface for the corresponding plane.

For the purpose of plotting the curve on an x-y plane of the paper, we have to convert the calculated velocity v and the angle θ to the x and y co-ordinates. If θ is measured from the x-axis of the graph, then x and y co-ordinates are given by

$$x = v \cos \theta$$

$$(3.13)$$

$$y = v \sin \theta$$

and if θ is measured from y-axis of the graph then

$$x = v \sin \theta$$

$$(3.14)$$

$$y = v \cos \theta$$

For plotting the velocity surface in the a-b plane of LHS, the Equations from (1.25) to (1.27) can be used. Here the velocity v_0 is a pure shear (S) mode with polarization perpendicular to a-b plane, v_1 is a quasi longitudinal (QL) mode and v_2 is a quasi shear (QS) mode except along symmetry directions a and b where they are pure modes. The plotted velocity surfaces are shown in Figure 3.3.

The velocity surface in the a-c plane can be computed using Equations from (1.34) to (1.36). Here v_0 is a pure S mode with polarization perpendicular to the a-c plane, v_1 and v_2 are QL and QS modes except along symmetry directions a and c. The plotted velocity surfaces are shown in Figure 3.4.

The velocity surface in the b-c plane can be computed using Equations from (1.42) to (1.44). Here v_0 is a pure S
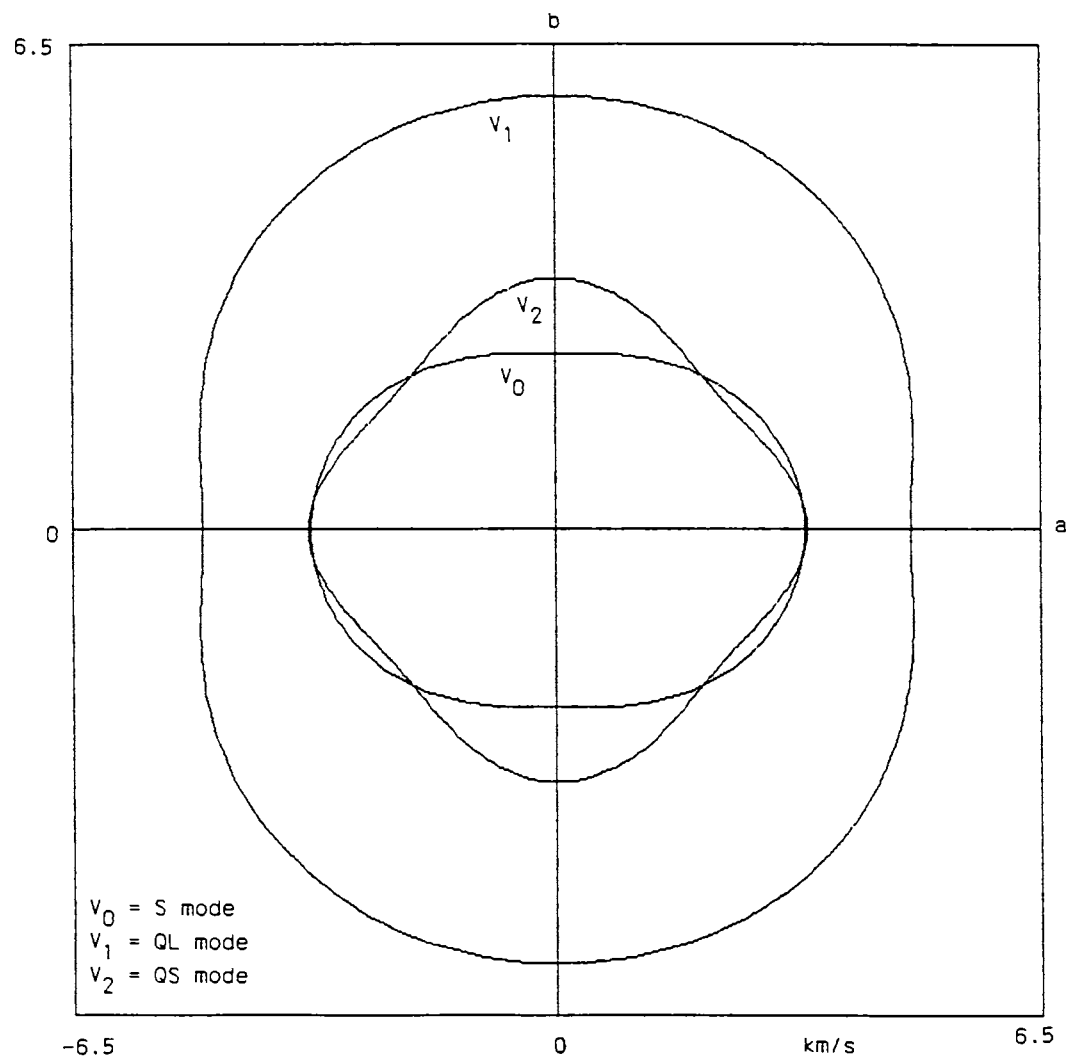
Figure 3.3

The velocity surfaces of LHS in a-b plane

120
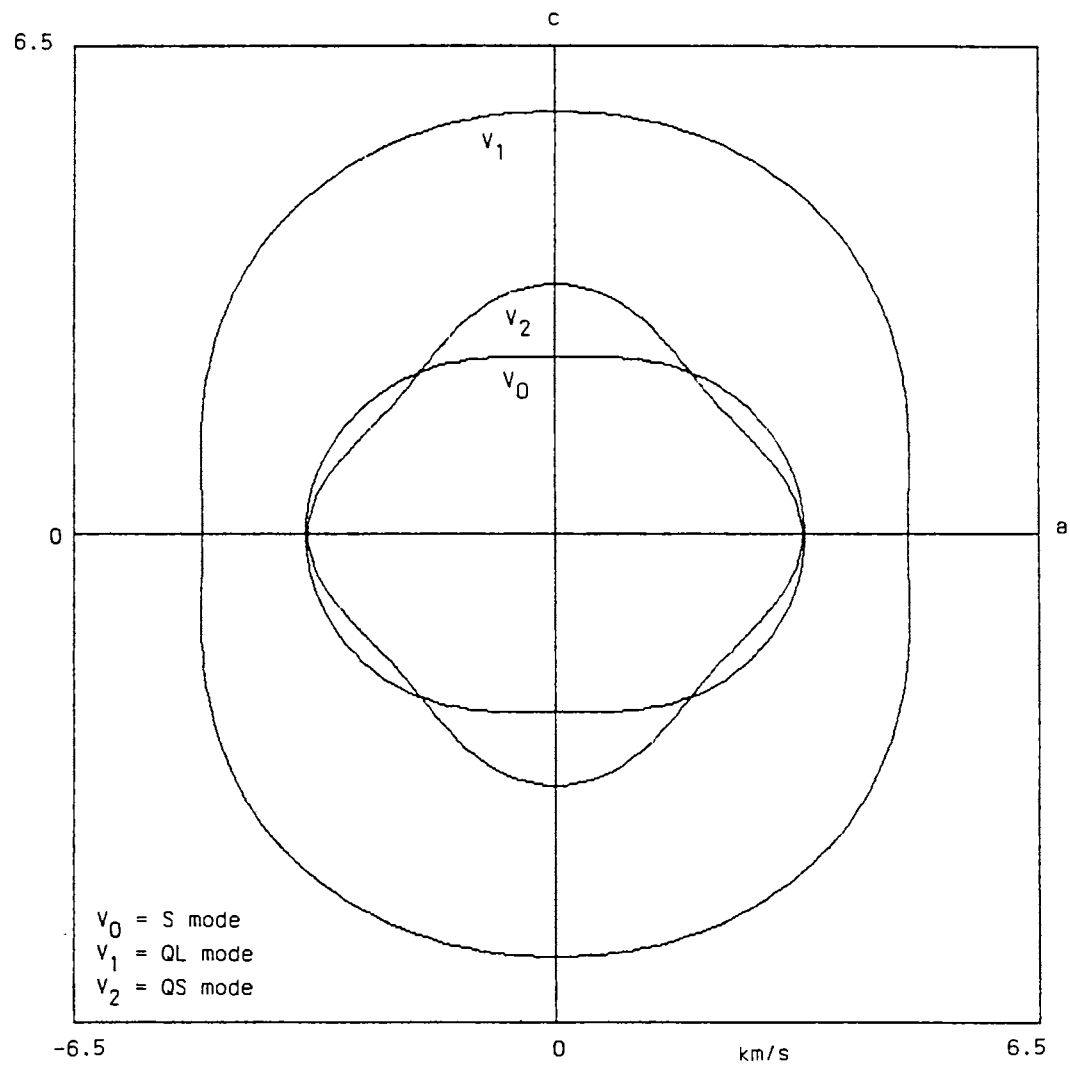
Figure 3.4

The velocity surfaces of LHS in a-c plane

121

mode with polarization perpendicular to the b-c plane, v_1 and v_2 are QL and QS modes except along symmetry directions b and c. The plotted velocity surfaces are shown in Figure 3.5.

From the above plots, the three velocities in any direction in any of the symmetry planes can be easily found by measuring the length of the straight line drawn from the centre to the curve at the required angle from the symmetry axis. The graph have been plotted with a scale of 1 cm for 1 km/s of velocity.

3.7 Discussion and conclusions

In this Chapter the results of elastic constant measurement in the orthorhombic crystal, Lithium Hydrazinium Sulphate are presented. The elastic constants of this crystal have not been measured by any other workers earlier and hence this is the first report. The ultrasonic velocity measurements for the determination of elastic constants have been performed accurately using PEO method with correct overlap identification and bond correction. For this a specially developed computer program has been used. The accuracy and precision of the measurements are analysed and a 0.3% accuracy is claimed in the velocity measurements.

The problem of misorientation in the cut samples have been analysed in detail. The misorientations in the sample have been measuerd with respect to the natural faces of the crystal. The necessary equations for the determination of the direction cosines of misorientation have been derived and presented.

A highly useful numerical technique for misorientation correction have been developed. A computer program in FORTRAN language have been developed for the misorientation correction process. The measured elastic constants are corrected for misorientation using the computer program.

The corrected elastic constants are tabulated along

122
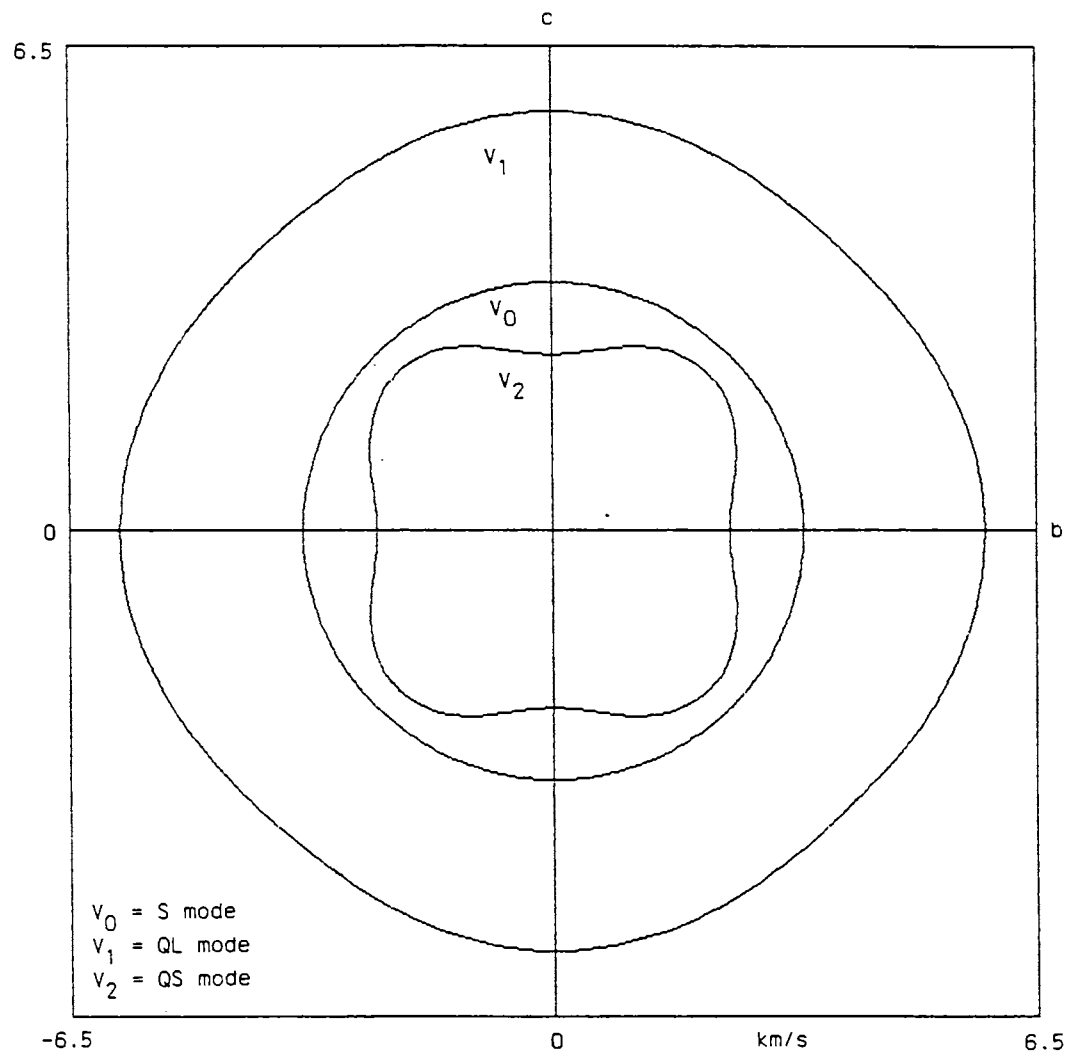
Figure 3.5

The velocity surfaces of LHS in b-c plane

123

with the uncorrected constants to reveal the magnitude of the correction. It is observed that, for small misorintations of the order of a few degrees, the elastic constants of this crystal do not undergo drastic variations. The difference between the corrected and uncorrected constants are found to be less than 0.4%.

Using the corrected elastic constants the velocities are calculated in the measured directions and the complete agreement of the calculated values with measured values demonstrate the accuracy of the correction procedure developed.

The velocity surfaces of LHS have been computed in three different symmetry planes and plotted on a scaled graph.

Appendix 3.1

A typical experimental data and the output of the program for
correct overlap identification and bond correction.

  Given below is a typical input data file, called
LHS_CTA.IN,   created by the program PEO.BAS (see
Appendix 2.1). This input file contains all the experimental
data from the measurement of transverse velocity in the c
direction with polarization in the a direction in LHS.

```
"LHS_CTA.IN"
"Lithium Hydrazinium Sulphate","silcon grease ","c"
"Transverse","a"
.9915,6,1
17.51277,17.37426
17.16656,17.08965
16.85067,16.80695
16.54374,16.53529
16.24984,16.27468
15.96846,16.01859
1.2,1.966,10.4
"Temperature = 300 K "
```

  The 1st line of the file is the name of the file
itself. The 2nd line contains the name of the sample, name of
bond used, and the direction of propagation. The 3rd line
contains the type of wave, and the direction of polarization.
The 4th line contains the length of the sample, no. of
overlaps measured, and the no. of round trips p. Lines 5 to 10
contains   repetition rates corresponding to f_L and f_H for
different overlap cases. Line 11 has bond impedance, sample
density, and transducer impedance. Line 12 is other
informations.

  After processing the above data file, the program
produces an output file called LHS_CTA.OUT. The contents of
the output file is shown on next page.

Contents of the output file LHS_CTA.OUT, produced by the program PEO.BAS.

```
Sample name              = Lithium Hydrazinium Sulphate
Propagation direction = c
Wave Type                = Transverse
Polarization direction= a
Sample dimension & p  =  0.99150 cm ,  p = 1
Linear  fitting of the  6  measurement data pairs give:
TL= 56.0274108E-01 + 11.0203206E-02*X    Cor.cof=0.99995884141
TH= 56.5743069E-01 + 97.4953927E-03*X    Cor.cof=0.99999486147
------------------------------------------------------------------
```

X	TL	E(TL)	TH	E(TH)	(TL-TH)
No	μs	μs	μs	μs	ns
0	5.60274	0.00000	5.65743	0.00000	-54.68961
1	5.71294	-0.00283	5.75493	0.00071	-41.98180
2	5.82315	0.00213	5.85242	-0.00093	-29.27398
3	5.93335	0.00113	5.94992	0.00000	-16.56617
4	6.04355	0.00103	6.04741	0.00026	-3.85836
5	6.15376	0.00015	6.14491	-0.00039	8.84946
6	6.26396	-0.00162	6.24240	0.00034	21.55727
7	6.37416	0.00000	6.33990	0.00000	34.26509
8	6.48437	0.00000	6.43739	0.00000	46.97290

```
------------------------------------------------------------------
Estimated Low RF frequency =   9.074146   MHz
Estimated High RF frequency= 10.256895   MHz   LF/HF = 0.88
Bond material used       =  silcon grease
Bond impedance           =  1.2000 x1e6 kg/m².s
Transducer impedance     = 10.4000 x1e6 kg/m².s
sample density in g/cc   =  1.96600
estimated sample impedance =   6.4467  x1e6 kg/m².s
Other information        = Temperature = 300 K
----------------CALCULATION OF CORRECT OVERLAP----------------
estimated maximum value of  delta t     [ns] =   -9.811
bond angle corresponding to max delta t [deg]=   38.769
correction corresponding to max delta t [ns] =   -4.605
delta t for 0,60 deg bond angles [ns] =  -19.250 -12.050
------------------------------------------------------------------
```

BOND	DELTA t	TH	CR	CR+TH
deg	ns	μs	ns	μs
4.113152	-16.566169	5.949917	-0.415386	5.949501

```
..................................................................
Computed velocity           =  3333.0524 m/s
Computed elastic constant   =   2.1840762 x1e10 kg/m.s²
------------------------------------------------------------------
```

The Computer program developed for velocity calculation and
misorientation correction

(See section 3.5.2 for a description of the program)

USVC.FOR

```
      PROGRAM ULTRASONIC VELOCITY AND CORRECTION
      LOGICAL RESP
      REAL LL,LD
      CHARACTER FN*12,FI*12,TITLE*50,OUT*12,QUS*50
      DIMENSION C(6,6),LL(3),V(3),A(3,3),
     *D(3),G(3,3),SS(3,3),LD(3)
      PI=3.141592654
      Z=PI/180.0
      DO I=1,25
        PRINT *,' '
      ENDDO
      WRITE(*,400)
      PRINT *,' '
      PRINT *,' '
      PRINT *,'THE VELOCITY OF ',
     *'ULTRASONIC WAVES IN ANY DIRECTION'
      PRINT *,'IN A CRYSTAL IS CALCULATED BY THIS PROGRAM'
      PRINT *,'THE DIRECTION IS SPECIFIED BY'
      PRINT *,'POLAR COORDINATES THETA AND PHI'
      PRINT *,'MISORIENTATION ',
     *'CORRECTION POSSIBLE THROUGH OPTION'
      PRINT *,' '
      ITIMES=0
   23 PRINT *,' '
      PRINT *,'Enter control integer - 3, 2,1, or 0'
      PRINT *,'2= new title ,  1=new direction,  0=quit'
      PRINT *,'3= create new elastic constant data file'
      PRINT *,' '
      READ(*,104)IC
      IF (ITIMES.EQ.0.AND.IC.EQ.1) GOTO 23
      IF (IC.EQ.3)THEN
        PRINT *,'NAME OF DATA FILE TO BE CREATED  ? '
        READ(*,100)FI
        CALL CINPU(FI)
      ENDIF
      IF (IC-1) 1000,33,1
    1 PRINT *,'Data file name TO PROCESS ?'
      READ(*,100)FN
```

```fortran
      PRINT *,' '
      PRINT *,'Specify output device'
      PRINT *,'0=console,1=lpt1,2=file'
      PRINT *,' '
      READ *,IO
      OUT='CON '
      IF (IO.EQ.0) OUT='CON '
      IF (IO.EQ.1) OUT='LPT1 '
      IF (IO.EQ.2)THEN
        PRINT *,'Enter  output file name    ? '
        READ(*,100)OUT
      ENDIF
      IF (ITIMES.EQ.1) CLOSE (UNIT=2)
      OPEN (UNIT=2,FILE=OUT)
      OPEN (UNIT=1,FILE=FN)
      READ(1,50)TITLE
      WRITE(2,50)TITLE
      WRITE(2,208)
      DO I=1,6
          READ(1,22)(C(I,J),J=1,6)
          WRITE(2,22)(C(I,J),J=1,6)
      ENDDO
      READ(1,101)RHO
      WRITE(2,201)RHO
   22 FORMAT (1X,6F10.4)
   50 FORMAT ( A50)
      CLOSE(UNIT=1)
   33 CONTINUE
      QUS='Want correction sub.program '
      IF (RESP(QUS)) THEN
      CALL CORRECT(RHO,C)
      GOTO 23
      ELSE
      CONTINUE
      ENDIF
      PRINT *,'Enter  value of theta'
      READ *,TL
      PRINT *,'Enter  value of phi'
      READ *,PL
      IF (IC.EQ.1.AND.ITIMES.EQ.1)WRITE(2,50)TITLE
      WRITE(2,206)
  100 FORMAT(1A12)
  101 FORMAT(  F10.5)
  102 FORMAT(2F3.3,I3)
  104 FORMAT(1I2)
  201 FORMAT(/ ' DENSITY = ',F10.4,' *1000 KGM-3'/)
  202 FORMAT('CIJ MATRIX   ',6F10.4)
  205 FORMAT(/,'MODE VELOCITY ',F10.4,' KM/S')
  206 FORMAT(///,32X,
     *'THETA        PHI        L1        L2        L3',/)
  207 FORMAT(/,
     *'ONE EIGEN VALUE NEEDS MORE THAN 30 ITERATIONS',/)
```

```fortran
208 FORMAT('ELASTIC CONSTANTS GNM-2')
400 FORMAT('Program by L.Godfrey')
    T=TL*Z
    P=PL*Z
    IFAIL=1
    CALL VELOCT(RHO,T,P,C,V,LL,A,IFAIL)
    THETA=T/Z
    PHI=P/Z
    WRITE(2,209)THETA,PHI,LL(1),LL(2),LL(3)
    IF (IFAIL.GT. 30) THEN
      WRITE(6,207)
      GOTO 4
    ELSE
      CONTINUE
    ENDIF
209 FORMAT(//,'PROPAGATION DIRECTION       ',5F10.4)
    DO NR=1,3
        WRITE(2,205)V(NR)
        CALL DIRECT(A,NR,LD,THETA,PHI)
        WRITE(2,210)THETA,PHI,LD(1),LD(2),LD(3)
    ENDDO
210 FORMAT('PARTICLE MOTION',T28,5F10.4)
  4 CONTINUE
    ITIMES=1
    GOTO 23
1000 CONTINUE
    CLOSE(UNIT=2)
    STOP
    END
C   ------------------------------------------
    SUBROUTINE VELOCT(RHO,T,P,C,V,LL,A,IFAIL)
C   ------------------------------------------
    REAL LL
    DIMENSION C(6,6),G(3,3),A(3,3),LL(3),V(3),D(3),E(3)
    LL(1)=SIN(T)*COS(P)
    LL(2)=SIN(T)*SIN(P)
    LL(3)=COS(T)
    DO  JS=1,3,1
        DO KS=1,3,1
        SUMS=0.0
         DO  IS=1,3,1
            DO  LS=1,3,1
            MS=NOT(IS,JS)
            NS=NOT(KS,LS)
            SUMS=SUMS+LL(IS)*LL(LS)*C(MS,NS)
            ENDDO
         ENDDO
        G(JS,KS)=SUMS
        IF(JS.NE.KS) G(KS,JS)=G(JS,KS)
        ENDDO
    ENDDO
    CALL JACOBI(G,3,3,D,A,IFAIL)
```

```fortran
      IF (IFAIL.GT. 30) RETURN
      CALL EIGSRT(D,A,3,3)
       DO  JS =1,3
         V(JS)=SQRT(D(JS)/RHO)
       ENDDO
      RETURN
      END
C     ------------------------------------
      SUBROUTINE DIRECT(A,NR,L,THETA,PHI)
C     ------------------------------------
      REAL L
      DIMENSION L(3),A(3,3)
      PI=3.141592654
      Z=PI/180.0
      S=0.0
      DO ID=1,3
       IF (ABS(A(ID,NR)).GT.S) S=ABS(A(ID,NR))
      ENDDO
      DO ID=1,3
       L(ID)=A(ID,NR)/S
      ENDDO
      S=0.0
      DO ID=1,3
       S=S+L(ID)**2
      ENDDO
      S=SQRT(S)
      DO ID=1,3
       L(ID)=L(ID)/S
      ENDDO
         IF (L(1).EQ.0.0.AND.L(2).EQ.0.0)THEN
            PHI=0.0
            THETA=0.0
         ELSE
            THETA=ATAN2(SQRT(1-L(3)*L(3)),L(3))
            PHI= ATAN2(L(2),L(1))
            IF(PHI.LT.0.0)PHI=PHI+2*PI
            IF(THETA.EQ.0.0)PHI=0.0
         ENDIF
      THETA=THETA/Z
      PHI=PHI/Z
      RETURN
      END
C     ---------------------------------------
      SUBROUTINE JACOBI(A,N,NP,D,V,NROT)
C     ---------------------------------------
      PARAMETER (NMAX=100)
      DIMENSION A(NP,NP),D(NP),V(NP,NP),B(NMAX),Z(NMAX)
      DO IP=1,N
      DO IQ=1,N
      V(IP,IQ)=0.
      ENDDO
      V(IP,IP)=1.
```

```
      ENDDO
      DO IP=1,N
      B(IP)=A(IP,IP)
      D(IP)=B(IP)
      Z(IP)=0.
      ENDDO
      NROT=0
      DO I=1,50
      SM=0.
      DO IP=1,N-1
      DO IQ=IP+1,N
      SM=SM+ABS(A(IP,IQ))
      ENDDO
      ENDDO
      IF(SM.EQ.0.)RETURN
      IF(I.LT.4)THEN
      TRESH=0.2*SM/N**2
      ELSE
      TRESH=0.
      ENDIF
      DO IP=1,N-1
      DO IQ=IP+1,N
      G=100.*ABS(A(IP,IQ))
      IF((I.GT.4).AND.(ABS(D(IP))+G.EQ.ABS(D(IP)))
     *  .AND.(ABS(D(IQ))+G.EQ.ABS(D(IQ))))THEN
      A(IP,IQ)=0.
      ELSE IF(ABS(A(IP,IQ)).GT.TRESH)THEN
      H=D(IQ)-D(IP)
      IF(ABS(H)+G.EQ.ABS(H))THEN
      T=A(IP,IQ)/H
      ELSE
      THETA=0.5*H/A(IP,IQ)
      T=1./(ABS(THETA)+SQRT(1.+THETA**2))
      IF(THETA.LT.0.)T=-T
      ENDIF
      C=1./SQRT(1+T**2)
      S=T*C
      TAU=S/(1.+C)
      H=T*A(IP,IQ)
      Z(IP)=Z(IP)-H
      Z(IQ)=Z(IQ)+H
      D(IP)=D(IP)-H
      D(IQ)=D(IQ)+H
      A(IP,IQ)=0.
      DO J=1,IP-1
      G=A(J,IP)
      H=A(J,IQ)
      A(J,IP)=G-S*(H+G*TAU)
      A(J,IQ)=H+S*(G-H*TAU)
      ENDDO
      DO J=IP+1,IQ-1
      G=A(IP,J)
```

```
H=A(J,IQ)
A(IP,J)=G-S*(H+G*TAU)
A(J,IQ)=H+S*(G-H*TAU)
ENDDO
DO J=IQ+1,N
G=A(IP,J)
H=A(IQ,J)
A(IP,J)=G-S*(H+G*TAU)
A(IQ,J)=H+S*(G-H*TAU)
ENDDO
DO J=1,N
G=V(J,IP)
H=V(J,IQ)
V(J,IP)=G-S*(H+G*TAU)
V(J,IQ)=H+S*(G-H*TAU)
ENDDO
NROT=NROT+1
ENDIF
ENDDO
ENDDO
DO IP=1,N
B(IP)=B(IP)+Z(IP)
D(IP)=B(IP)
Z(IP)=0.
ENDDO
ENDDO
PAUSE '50 iterations should never happen'
RETURN
END
-----------------------------
SUBROUTINE EIGSRT(D,V,N,NP)
-----------------------------
DIMENSION D(NP),V(NP,NP)
DO I=1,N-1
        K=I
        P=D(I)
        DO J=I+1,N
                IF(D(J).GE.P)THEN
                        K=J
                        P=D(J)
                ENDIF
        ENDDO
        IF(K.NE.I)THEN
                D(K)=D(I)
                D(I)=P
                DO J=1,N
                        P=V(J,I)
                        V(J,I)=V(J,K)
                        V(J,K)=P
                ENDDO
        ENDIF
ENDDO
```

```fortran
      RETURN
      END
C     --------------------
      SUBROUTINE CINPU(FN)
C     --------------------
      CHARACTER FN*12,TITLE*50
      DIMENSION C(6,6)
      OPEN(UNIT=1,FILE=FN)
      PRINT *,'Enter the identification title'
      READ (*,50)TITLE
      WRITE(1,50)TITLE
      PRINT *,'Enter elastic constant matrix '
      DO I=1,6
        DO J=I,6
          WRITE(*,22)I,J
          READ *,C(I,J)
          C(J,I)=C(I,J)
        ENDDO
      ENDDO
      PRINT *,'Enter density in    *1000 KGM-3'
      READ *,RHO
      DO I=1,6
        WRITE(1,30)(C(I,J),J=1,6)
        WRITE(*,30)(C(I,J),J=1,6)
      ENDDO
      WRITE(1,40)RHO
      CLOSE(UNIT=1)
   22 FORMAT ( 'C(',I1,',',I1,')=?')
   50 FORMAT ( A50)
   30 FORMAT (1X,6F10.4)
   40 FORMAT (1X,F10.4)
      RETURN
      END
C     ------------------
      FUNCTION  NOT(I,J)
C     ------------------
      NOT=9 -(I+J)
      IF (I.EQ.J) NOT=I
      RETURN
      END


C     ----------------------------------
      SUBROUTINE CORRECT(RHO,C)
C     ----------------------------------
      LOGICAL RESP
      CHARACTER  QUS*50
      REAL LL
      DIMENSION C(6,6),V(3),A(3,3),LL(3)
      PI=3.141592654
      Z=PI/180
  100 PRINT *,'Enter desired direction  theta'
      READ *,T0
```

133

```fortran
          T0=T0*Z
          PRINT *,'Enter desired direction phi'
          READ *,P0
          P0=P0*Z
          PRINT *,'Measured direction theta'
          READ *,TM
          TM=TM*Z
          PRINT *,'Measured direction phi'
          READ *,PM
          PRINT *,'Enter measured value of velocity'
          READ *,VM
          PM=PM*Z
          PRINT *,'Enter elastic constant subscripts i&j '
          READ (*,10)IC,JC
10        FORMAT(2I1)
          PRINT *,'Enter corresponding velocity no. 1,2,or 3'
          PRINT *,'1=longt.,2=fast transv.,3=slow transv.'
          READ *,IV
          WRITE (2,20)IC,JC,C(IC,JC)
20        FORMAT(1X,'initial value of C(',I1,I1,')  =',F10.4)
          DO I=1,500
          CALL VELOCT (RHO,T0,P0,C,V,LL,A,IFAIL)
          V0=V(IV)
          CALL VELOCT (RHO,TM,PM,C,V,LL,A,IFAIL)
          VMO=V(IV)
          C(IC,JC)= RHO*(VM - VMO)*(VMO + V0) + C(IC,JC)
          IF (ABS(VM - VMO).LT.0.00001) GOTO 25
          END DO
25        WRITE(2,30)I,C(IC,JC)
30        FORMAT (1X,'no. of iterations ',I4,/,
     *    1X,'final value ',12X,'=',F10.4)
          QUS='Want to try for another constant'
          IF (RESP(QUS)) GOTO 100
          RETURN
          END
C         ----------------------------------
          LOGICAL FUNCTION  RESP(QUS)
C         ----------------------------------
          CHARACTER QUS*50,ANS*1
          PRINT *,QUS
          PRINT *,'y/n  ?'
          READ (*,14)ANS
14        FORMAT (A1)
          IF (ANS.EQ.'Y'.OR.ANS.EQ.'y') THEN
          RESP=.TRUE.
          ELSE
          RESP=.FALSE.
          ENDIF
          RETURN
          END
```

References

3.1 R. Pepinsky, K. Vedam, Y. Okaya, S. Hoshino: Phys. Rev. 111, 1467 (1958).

3.2 H. Vanderkooy, J. D. Cuthbert, H. E. Petch: Can. J. Phys. 42, 1871 (1964)

3.3 F. L. Howell, R. R. Knispel, V. H. Schmidt: Bull. Amer. Phys. Soc. 12, 924 (1967)

3.4 V. Hugo Schmidt, J. E. Drumheller, F. L. Howell: Phys. Rev. B4, 4582 (1971)

3.5 K. D. Kreur, W. Weppner, A. Rabenau: Solid State Ionics 3/4, 353 (1981)

3.6 K. D. Kreuer, A. Rabenau, W. Weppner: Angew. Chem. Int. Ed. Engl. 21, 208 (1982)

3.7 J. Lundgren, R. Liminga, I. Olovsson: Arkiv Kemi 30, 81 (1968)

3.8 I. D. Brown: Acta Cryst. 17, 654 (1964)

3.9 J. H. Van den Hende, H. Boutin: Acta Cryst. 17, 660 (1964).

3.10 M. R. Anderson, I. D. Brown: Acta Cryst. B 30, 831 (1974)

3.11 V. M. Padmanabhan, R. Balasubramanian: Acta Cryst. 22, 532 (1967)

3.12 J. D. Cuthbert, H. E. Petch: Can. J. Phys. 41, 1629 (1963)

3.13 W. D. Mac Clement, M. M. Pintar, H. E. Petch: Can. J. Phys. 45, 3257 (1967)

3.14 R. R. Knispel, H. E. Petch: Can. J. Phys. 49, 870 (1971)

3.15 R. N. Hastings, T. Oja: J. Chem. Phys., 57, 2139 (1972)

3.16 K. V. S. Badarinath: J. Mater. Sci. Lett. 6, 609 (1987)

3.17 S. H. Brown, R. Frech: Spectrochim. Acta 44A, 1 (1988)

3.18 R. Frech, S. H. Brown: Solid State Ionics 35, 127 (1989)

3.19 L. Godfrey, J. Philip, M. T. Sebastian: J. Appl. Phys. 75, 2393 (1994)

3.20 A. R. Verma, O. N. Srivastava: *Crystallography for Solid State Physics* (Wiley Eastern, New Delhi 1962)

3.21 F. C. Phillips: *An Introduction to crystallography-4th Ed.* (Longman, England 1971)

3.22 E. P. Papadakis: In *Physical Acoustics,* Vol.12, ed. by W. P. Mason, R. N. Thurston (Academic Press, New York 1976)

3.23 P. C. Waterman: Phys. Rev. 113, 1240 (1959)

3.24 R. Truell, C. Elbaum, B. B. Chick: *Ultrasonic Methods in Solid State Physics* (Academic Press, New York 1969)

3.25 A.G. Every: Phys. Rev. B 22 1746 (1980)

3.26 B. W. James: In *Physics Programs*, ed. by A. D. Boardman (John Wiley, New York 1980)

CHAPTER 4

TEMPERATURE VARIATION OF ELASTIC CONSTANTS AND
PHASE TRANSITION IN LITHIUM HYDRAZINIUM SULPHATE

4.1 Introduction

There have been several temperature dependent studies on LHS or $Li(N_2H_5)SO_4$, which are connected with different physical properties of this crystal. Most of the interest on this crystal is related to its unusual electrical properties, such as ferroelectric like hysteresis loop, temperature dependent one-dimensional proton conductivity, frequency and temperature dependence of dielectric constant etc. There are no well established and strong phase transitions in LHS but certain weak phase transitions have been proposed in some of the investigation reports. An overview of the previous investigations is given below.

The compound LHS was first prepared by Sommer and Weise [4.1] and its dielectric properties were first investigated by Pepinsky et al. [4.2], who observed ferroelectric behavior at room temperature. They also observed good ferroelectric hysteresis loop from about $-15°C$ (258 K) to $80°C$ (353 K). Below $-15°C$ the loops become unsymmetric and difficult to saturate and above $80°C$ the conductivity interfered with the hysteresis test. They observed no dielectric peak between $-196°C$ (469 K) and $140°C$ (413 K). Their specific heat measurement in the region from $-120°C$ (153 K) to $205°C$ (478 K) could not reveal any anomaly. They concluded that the crystal is ferroelectric, with its ferroelectric axis along c, with no observed ferroelectric phase transition.

The proton and Li^7 nuclear magnetic resonance signals were investigated in LHS by Cuthbert and Petch [4.3]. They examined the quadrupolar splitting of the Li^7 resonance over a temperature range from $-70°C$ (203 K) to $205°C$ (478 K) and found

that it undergoes a rapid but continuous change between $80°C$ (353 K) and $160°C$ (433 K), which they considered as an indication of a phase transition in the crystal from a low to a high temperature polymorph. The results of their investigation of the second moment of the proton in the same temperature range also supported the phase transition picture. According to them the transition to the high temperature phase is complete at $164°C$ (437 K) and that it is a second order reversible phase transition.

Vanderkooy, Cuthbert and Petch [4.4] investigated the electrical conductivity of LHS and found that, at room temperature, the c-axis dc conductivity was over 200 times as great as along a or b axis. Through a coulometer experiment they established the protonic nature of the c-axis conductivity. The proton conductivity was related to the chains of hydrogen bonded hydrazinium ions in channels running along c-axis (see figure 3.1). They found an exponential increase in the c-axis conductivity with temperatures up to $160°C$ (433 K) and an unexpected decrease in the conductivity above this temperature. Above $200°C$ (473 K) the conductivity was found to be virtually isotropic. Decomposition of the crystal surface and the breaking up of the chain of hydrazinium ions were considered as two possible mechanisms responsible for the decrease in the c-axis conductivity near $160°C$.

Devanarayanan and Easwaran [4.5] investigated the thermal expansion of LHS in the temperature range $-170°C$ (103 K) to $220°C$ (493 K). They found the expansion coefficients to vary nonlinearly, and in particular, along the c-axis the thermal expansion showed an anomalous behaviour between $-160°C$ (113 K) and $-60°C$ (213 K) and also in the neighbourhood of $130°C$ (403 K). They have explained these anomalies as due to phase transitions involving reorientation of NH_3 group or NH_2 group about the N-N axis.

MacClement, Pintar and Petch [4.6] investigated the

temperature dependence of the spin-lattice relaxation time T_1 and of the second moment of the magnetic-resonance absorption signal in LHS, over the range 80-480 K. These measurements indicated that the hydrazinium ion is rigid only at very low temperatures. As the temperature is raised the $-NH_3$ group was found to undergo hindered rotation about the N-N axis. Above 435 K the hydrazinium ion appeared to tumble about several axes and at 480 K diffuses through the structure.

It is interesting to note that, the picture of $-NH_3$ group rotating around the N-N axis [4.3,4.6], was however contradictory to the findings of Padmanabhan and Balasubramanian [4.7], who in a single-crystal neutron diffraction investigation on LHS has located all the hydrogen atom positions and concluded that the hydrogen atoms of the $-NH_3$ group are static. Padmanabhan's argument was also supported by inelastic neutron scattering spectra of LHS.

Knispel and Petch [4.8] investigated the temperature dependence of the rotating frame relaxation time $T_{1\rho}$ for protons in LHS, in the range 140 to 495 K. Their measurements indicated that the $-NH_2$ group executes $180°$ flips about the bisectrix of the H-N-H angle. Evidence for the motion of the entire $N_2H_5^+$ ion was found. They have also obtained the activation energy for these motions.

Hastings and Oja [4.9] performed Nitrogen-14 nuclear quadrupolar resonance study of LHS and found that, between 40 and 320 K the NH_2 group undergoes small oscillations about the N-N axis whose amplitude increases linearly with temperature. Above 320 K the amplitude was found to increases more rapidly than a linear function. They also found that above 150 K, proton exchange in the H-N-H plane of the NH_2 group takes place rather than rigid rotation of the protons about the bisector of the H-N-H angle.

Hugo Schmidt, Drumheller and Howell [4.10] investigated the electrical dc conductivity and ac dielectric susceptibility of LHS over a wide temperature range (73 K to

473 K). They found the real and imaginary parts of susceptibility to be unusually large. They showed that this unusual behaviour is the result of the nearly one-dimensional protonic conductivity and its extreme sensitivity to barriers caused by local structural defects. They have conducted etching studies on LHS crystals and concluded that the crystal is not ferroelectric. The apparent hysteresis loops were explained to be the result of saturation of ac conduction. They also proposed a new model called partially blocked channel model for LHS to explain the dielectric properties. The ferroelectricity of LHS was also questioned earlier by Niizeki and Koizumi [4.11] on the basis of structural considerations.

Anderson and Brown [4.12] studied the effect of anomalous scattering of neutrons from ^{6}Li on the structure factors of Bijvot pairs both before and after the supposed ferroelectric domain switching in LHS. Their results were also against ferroelectricity in LHS. Klapper and Wardani [4.13] also could not observe any ferroelectric domains in LHS by X-ray topography, piezoelectric and pyroelectric examination and by etching. In another investigation, Sebastian, Becker and Klapper [4.14] obtained unusual X-ray topographic contrast in LHS, which they correlated with the proton conduction.

Temperature dependent thermal diffusivity measurements have been performed in LHS crystal by Krajewski and Stachowiak [4.15] in the range 20°C to 70°C. The highest diffusivity was found in the c direction and the lowest in the a direction.

Salman, Hilezer and Pawlaczyk [4.16] investigated the complex impedance of LHS from 290 K to 455 K. They supported the model of one dimensional protonic conduction with extrinsic barriers related with defects proposed by Schmidt et al. [4.10]. Further, they have noted that there is an indication of a structure change at about 433 K.

Reddy, Rao and Sastry [4.17] conducted electrical conductivity (from 320 to 475 K) and stimulated thermo-current

studies on VO^{2+} doped LHS crystals. They have estimated the activation energies and the variation of these energies with temperature was explained using the "one dimensional conductor model" [4.10]. They have made no mention about any phase transition in LHS.

Badarinath [4.18] investigated the dc electrical conductivity and dielectric properties of VO^{2+} doped LHS to study the effect of impurity-incorporated defects on the phase transition in LHS around $164\degree C$ (437 K) [4.3]. But no dielectric peaks were observed around $164\degree C$.

Frech and Brown [4.19] measured the polarized Raman scattering spectra over a temperature interval from 15 to 300 K in single crystal LHS. They observed no unusual temperature-dependent behaviour in any mode involving hydrazinium ion translatory motion, but all liberational modes and the internal torsional mode markedly decreased in intensity and frequency, while significantly broadening, when temperature was increased from 15 to 300 K. Some of the modes were found to show anomalous behaviour. These modes increase in intensity from 11 K until the temperature interval between 175 K and 200 K where the intensity abruptly decreases. They have noted that if these anomalies are due to a structure change then it must be a subtle one involving a small reorientation or displacement within the unit cell.

Given above is a fairly complete review of the previous temperature variation studies on lithium hydrazinium sulphate crystal.

We have, for the first time, investigated the temperature variation of elastic constants of LHS, both at high and low temperatures, using ultrasonics. Motivation for this investigation was to search for the suspected weak phase transitions in this crystal. Since ultrasonics is a very sensitive tool, it is ideally suited for studying weak phase transitions. Interesting results were obtained from the high temperature study. Observed elastic anomalies indicated a weak

phase transition near 425 K. The results of our high temperature investigation have been published already [4.20]. The details of the experiment and the results of both high and low temperature investigations are presented in this chapter.

4.2 High temperature investigations

In this section, the experimental details and results of the temperature variation study of the elastic constants of LHS crystal in the temperature range from 300 to 450 K are presented. The temperature variation of the attenuation of ultrasonic waves along certain directions in the crystal are also presented.

4.2.1 Experimental

The temperature variation of the velocity of longitudinal and shear waves propagating along the various directions in the crystal have been determined between 300 K and 450 K by keeping the sample, mounted on a suitable holder, in a temperature controlled chamber. The details of the experimental setup have been described in Section 2.2. The change in velocity with temperature with respect to the room temperature value has been measured by carefully adjusting the cw oscillator frequency keeping the selected rf echoes in the phase matched condition. The accuracy of this relative measurement of velocity is of the order of 10^{-5}. The rate of temperature change in all the measurements are in the range of 0.5 K to 1 K per minute.

Bonding of the transducer to the sample is a critical factor for successful temperature variation study. Bond formed with several materials works as very good bonds at room temperature but fail as the temperature is increased or decreased. The problem is more severe for phase transition study because the bond can break at phase transition points.

For the temperature variation measurement of the velocity of longitudinal waves at high temperatures, we have used silicon grease as a bond material.

Measurement of shear wave velocities at high temperatures cause problems with regard to bonding the transducer to the sample. We had to search for a suitable bond material for high temperature measurements with transverse waves. We have found a new bond material and have developed a method for making a bond with this material, details of which are given below.

We have found that an anaerobic adhesive [4.21] can be successfully used as a high-temperature transverse wave bond. This is a special type of adhesive used in industry for the purpose of preventing nut and bolt assembly from loosening and also for fixing the bearings in rotating parts. Adhesives of this type remain in the unreacted liquid state as long as it is in contact with oxygen in the air. But in oxygen free atmosphere these adhesives get polymerized into solid form. This polymerization proceeds rather slowly at room temperature but is accelerated at elevated temperatures. After application of this anaerobic adhesive bond between the cleaned surfaces of the sample and transducer, they are held together in a holder under spring loading. Exposure of the adhesive to air is prevented by sealing the edge of the transducer with silicon grease. The whole assembly is then kept in an oven at about 320 K for 12 hours for the complete curing of the bond. We have tested this bond up to a temperature of 480 K, and found to give good echo pattern even at this temperature. After the experiment, the detachment of transducer from the sample is done by soaking in chloroform for a few hours. This new bond and the bonding technique are also reported in our paper [4.20].

4.2.2 Results and discussion

We have measured the temperature variation of all the 6 diagonal constants (C_{11}, C_{22}, C_{33}, C_{44}, C_{55} and C_{66}) from pure mode measurements and the 3 offdiagonal constants (C_{12}, C_{13}, and C_{23}) in combination form, from quasilongitudinal wave measurements. The measured temperature variation of elastic constants are plotted in Figures 4.1 to 4.4.

As can be noted from the figures some of the elastic constants show anomalous changes around 425 K as the temperature is increased. The anomalies are rather small in magnitude and reveals themselves only under close examination of the curves. All the constants have a general parabolic decrease as the temperature is increased and the observed anomalies are deviations from this general trend. Measurements have been limited to 450 K because at still highertemperatures the crystal begins to decompose which is indicated by an irreversible cloudy appearance inside the crystal.

In the case of the constant C_{33}, there are dips near 415 K and 425 K . The constant C_{22} shows a small down ward deviation as 425 K is approached. For the constants C_{66} and C_{11} no significant variation from the normal variation is observed. For C_{55} there is a distinct jump at 425 K and for C_{44} a slope change occurs at 425 K. The combination constant in the [110] direction, which is connected with C_{12} do not show significant anomaly. Similarly in [101] direction, which is connected with C_{13}, also do not show any noticeable anomaly. But measurements in the b-c plane which involves C_{23}, C_{22}, C_{44}, and C_{33} there are clear anomalies near 425 K.

Generally an increase in Ultrasonic attenuation was observed as 425 K region is approached. Here we present two ultrasonic attenuation curves, one for wave propagation along a-axis (Figure 4.5) and the other for wave propagation along c-axis (Figure 4.6). Since the absolute accuracy in the
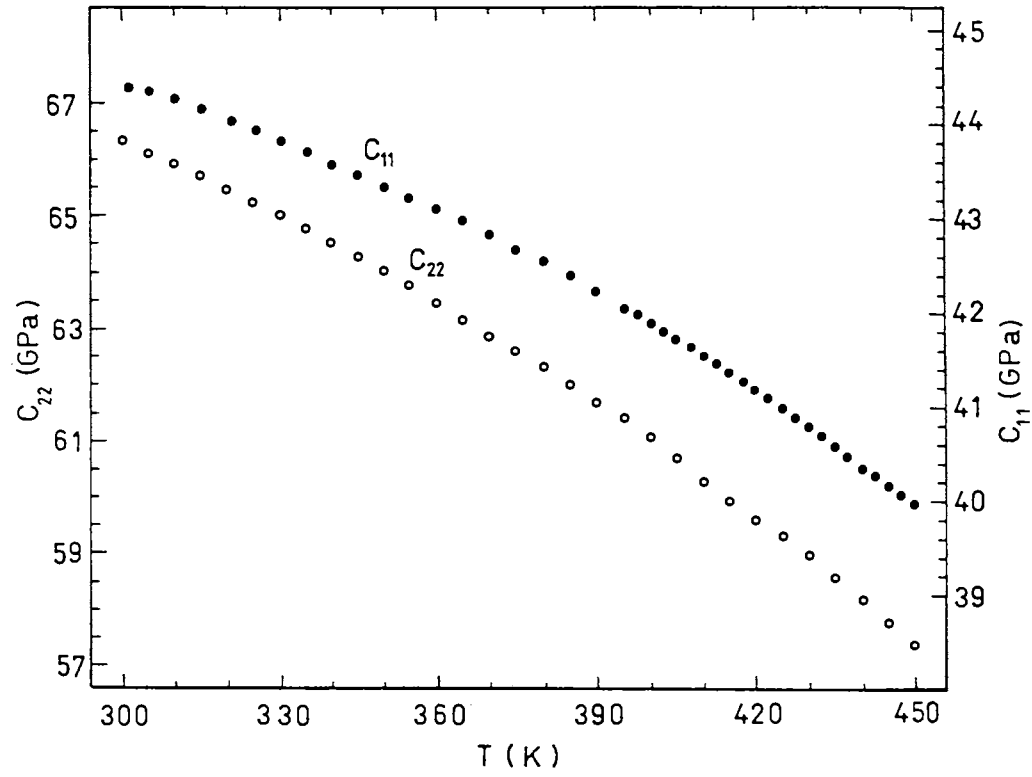
Figure 4.1

Temperature variation of elastic constants C_{11} and C_{22} of Lithium Hydrazinium Sulphate above room temperature.
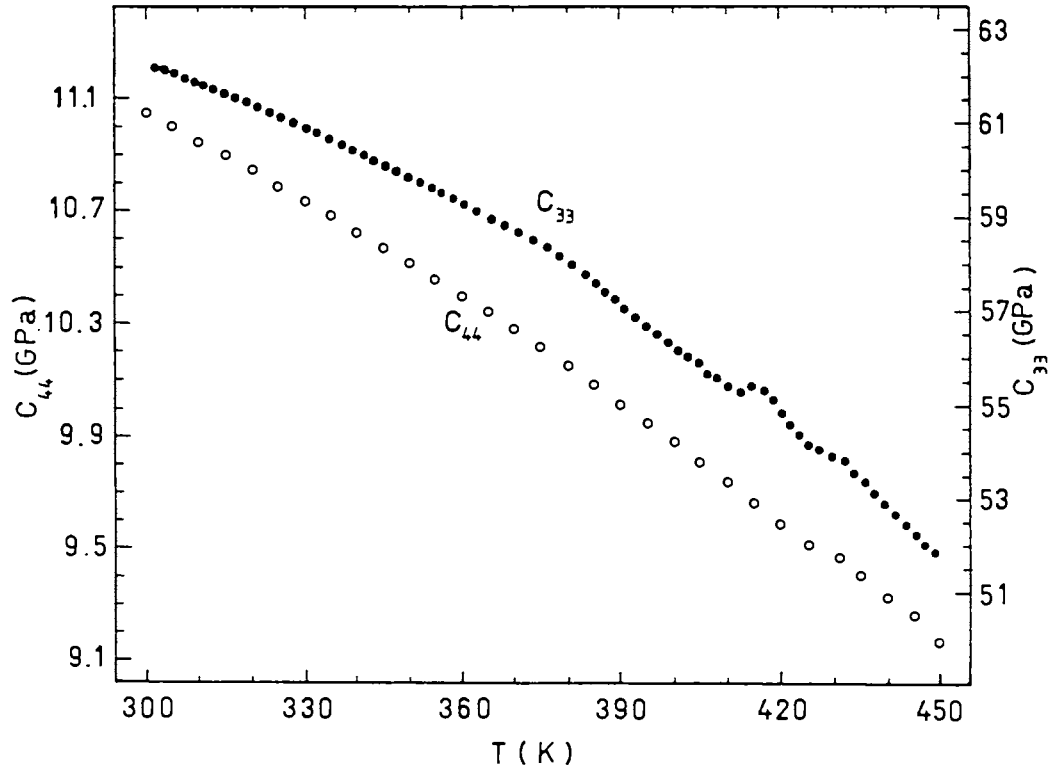
Figure 4.2

Temperature variation of elastic constants C_{33} and C_{44} of
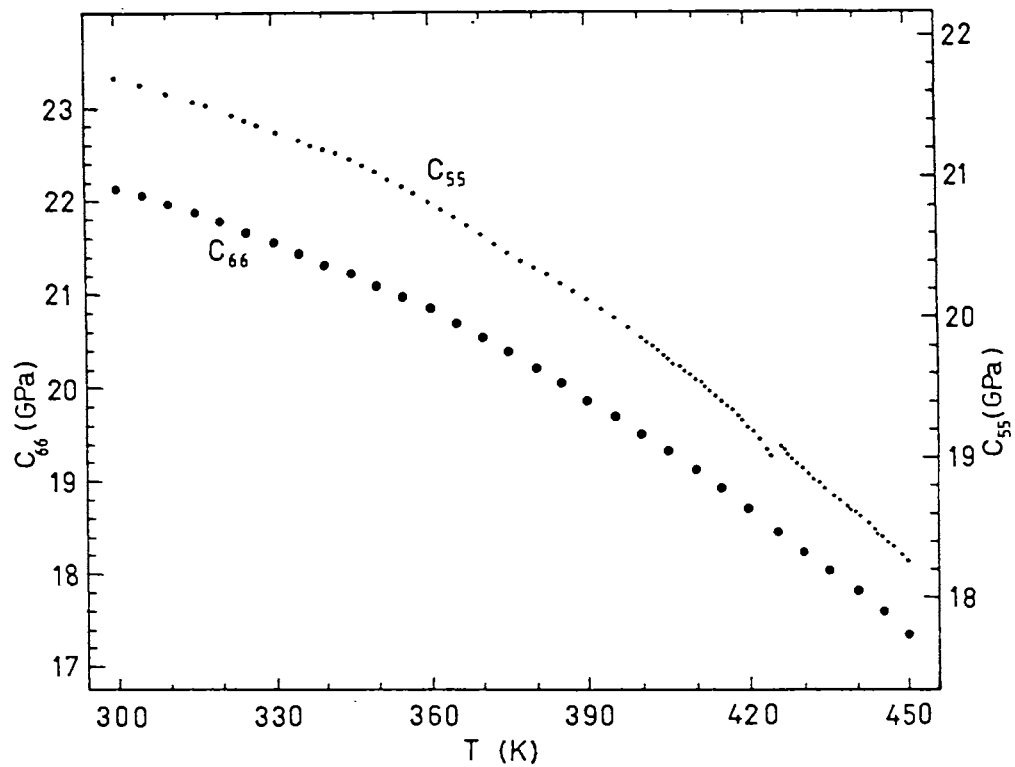Lithium Hydrazinium Sulphate above room temperature.

146

Figure 4.3

Temperature variation of elastic constants C_{55} and C_{66} of Lithium Hydrazinium Sulphate above room temperature.
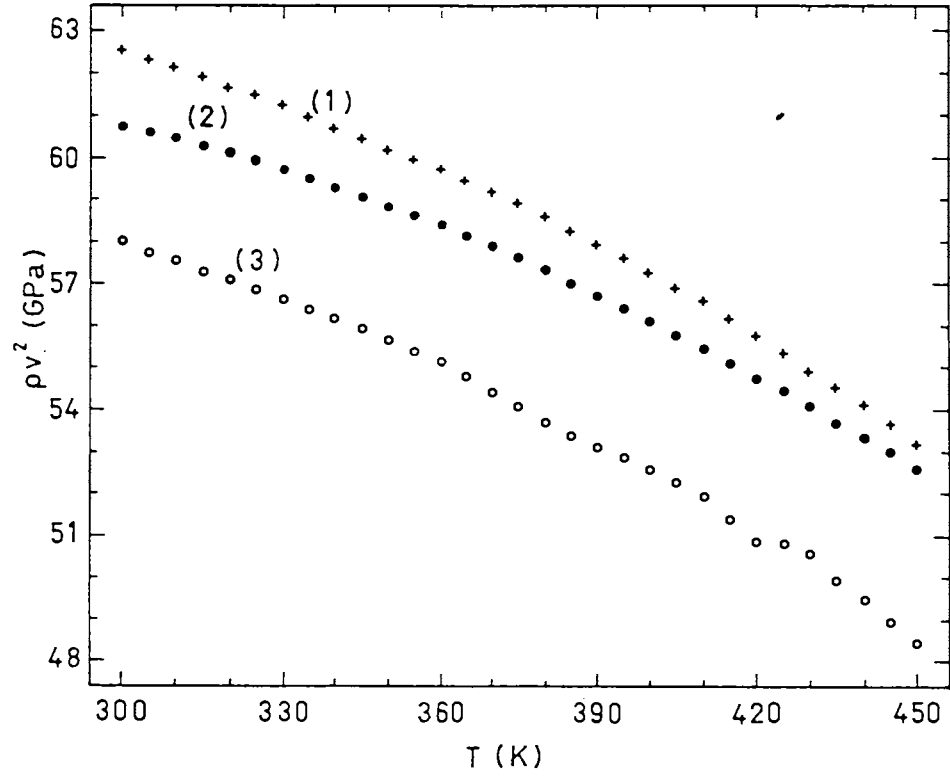
147

Figure 4.4

Temperature variation of the combination elastic constants of
LHS measured in three symmetry planes, above room temperature.
(1) combination constant in [101] direction in a-c plane,
(2) combination constant in [110] direction in a-b plane,
(3) combination constant in the cut direction in b-c plane.
(Refer Table 3.2 for relations to C_{13}, C_{12} and C_{23})
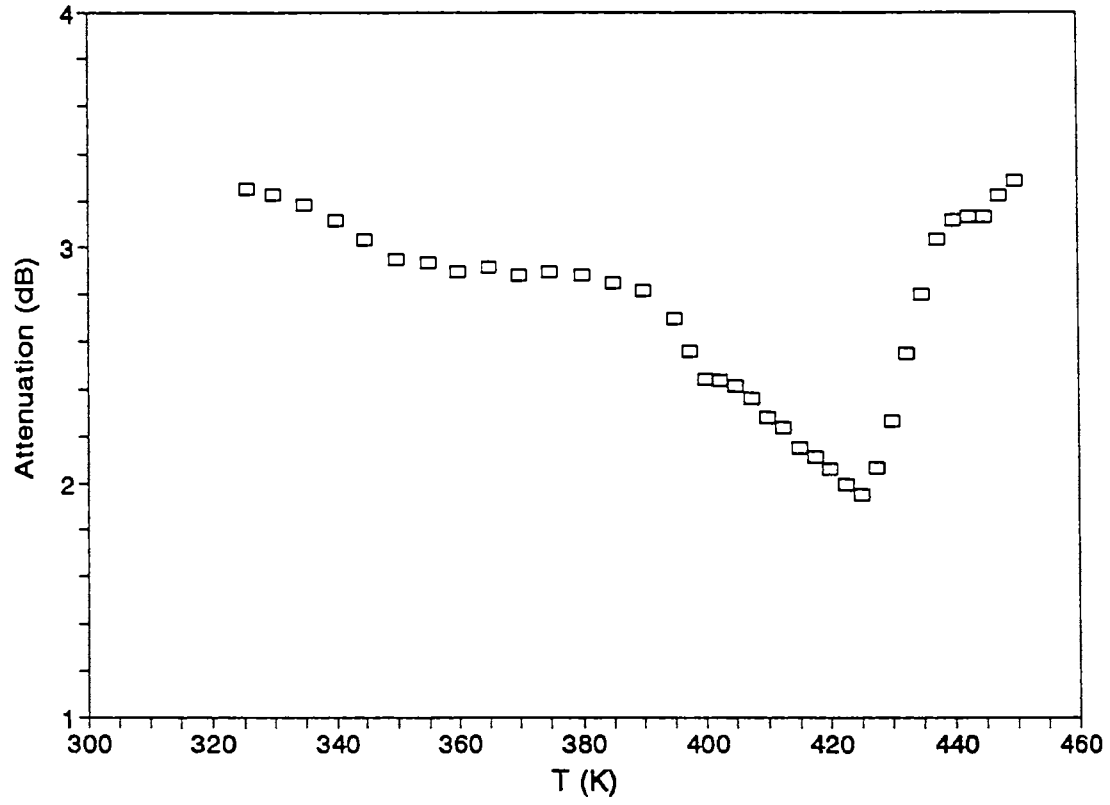
Figure 4.5

Temperature variation of the attenuation of ultrasonic waves propagating along the a-axis of Lithium Hydrazinium Sulphate, above room temperature.
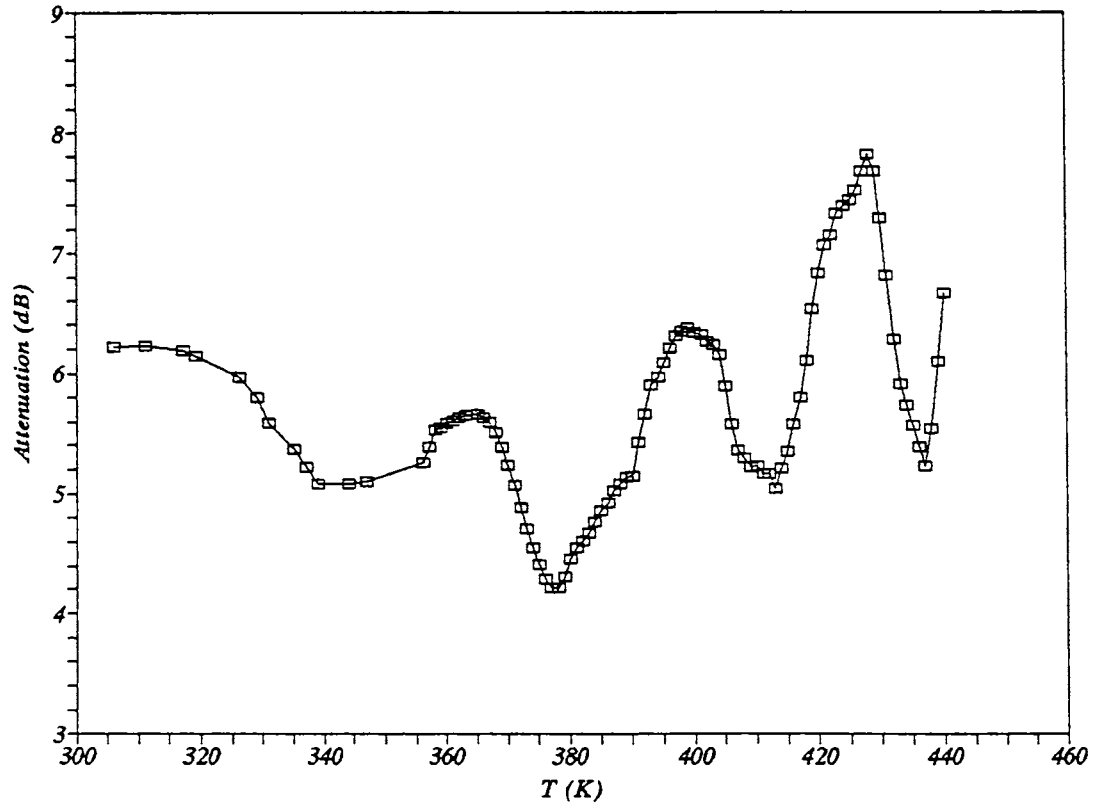
149

Figure 4.6

Temperature variation of the attenuation of ultrasonic waves propagating along the c-axis of Lithium Hydrazinium Sulphate, above room temperature.

150

measurement of attenuation is rather low, the given curves indicate only a relative measurement with respect to the room temperature. The attenuation is given in dB scale.

The attenuation of ultrasonic waves along a-axis shows an almost continuous decrease as the temperature is increased and at 425 K a sudden increase in attenuation can be found. Along the c-axis, the attenuation shows an anomalous oscillatory behaviour as the temperature is increased and near 425 K the attenuation has the highest peak. The exact reason for the unusual oscillatory behaviour of the attenuation is unknown but it may be related to the same mechanisms which are responsible for the proton transport and the unusual ferroelectric-like behaviour of this crystal along this axis.

From the observed anomalies in the elastic constants and the ultrasonic attenuation, we suspect a weak phase transition in the crystal near 425 K. We term this transition as weak because the observed anomalies are very small compared to what one expects in a usual structual phase transition in a crystal. To check for a possible specific heat anomaly at this temperature, we have measured the temperature variation of specific heat of LHS, in the range 300 to 450 K, using a differential scanning calorimeter (Perkin-Elmer model, Delta Series DSC7) and could not obtain any specific heat anomaly. Earlier, Pepinsky [4.2] also could not find any specific heat anomaly in this crystal. The absence of specific heat anomaly and the weak nature of this transition, points to the fact there are no major structural changes in the crystal during this transition. To undestand more about the possible mechanisms which are responsible for this phase transition, we have examined the previous investigations in this temperature range and the findings are given below.

It was Cuthbert and Petch [4.3] who first talked about observing phase transition in LHS. In their long 22 page paper, they have presented the results of their nuclear magnetic resonance (NMR) study of the proton and Li^7 in

powdered and single crystal samples of LHS. At the time of their investigation (1963), LHS was considered as a ferroelectric substance with an unknown transition temperature. According to them, in an NMR study, if a phase transition is taking place and if the crystal is properly oriented with respect to the magnetic field then certain lines will coalesce to form a reduced spectrum as the crystal transforms. In their Li^7 study, they could get five Li^7 lines in the NMR spectrum at room temperature. At $-70^{\circ}C$ (203 K) the spectrum was practically identical with that at room temperature. As the crystal was heated, the separation between the two satellites on the same side of the central line decreased gradually at first but, in the region of $70^{\circ}C$ (343 K), the separation started to decrease at an accelerating rate. According to them, at $164^{\circ}C$ (437 K) the separation reached zero and the crystal existed entirely in the high temperature phase. No further changes in the spectrum were detected as the temperature was increased to $205^{\circ}C$ (478 K). They found the above effects completely reversible upon cooling and heating.

In their study of second moment of the proton resonance in LHS, they found that, as they increased the crystal temperature from $-70^{\circ}C$ (203 K), the second moment remained constant over a wide temperature range. The second moment began to decrease continuously at $50^{\circ}C$ (323 K) and at $150^{\circ}C$ (423 K) they found a slight pause in the decrease. After this pause at $150^{\circ}C$ (423 K) the second moment again decreased rapidly to a low value at $210^{\circ}C$ (483 K) . According to their interpretation, the rapid decrease of the second moment between $50^{\circ}C$ (323 K) and $150^{\circ}C$ (423 K) is caused by the onset of rotation of the $-NH_2$ group about the N-N axis. They inferred that this rotation is triggering the transition observed in Li^7 study. They further inferred that this is a ferroelectric phase transition which Pepinsky *et al.* [4.2] could not observe in the hysteresis test because of excessive

electrical conductivity at high temperatures.

Further support for a phase transition in this temperature range came from the thermal expansion study of Devanarayanan and Easwaran [4.5]. They observed anomalies in the c-axis thermal expansion coefficient at 130°C (403 K). An examination of their data shows that, when the temperature is increased the increasing thermal expansion coefficient is taking a down ward trend near 130°C (403 K). As the temperature is further increased the trend changes to upward direction near 145°C (418 K). They have connected this anomaly to the phase transition reported by Cuthbert and Petch [4.3] and gave no further details on the mechanism of transition.

This transition is not observed in many dielectric and conductivity studies [4.2,4.4,4.10,4.17,4.18] except by Salman *et al* [4.16] who investigated the complex impedance of LHS, found some indication of a structure change at about 433 K.

From the above results of the previous works, and from the results of the present ultrasonic work, we find that there is sufficient reason to confirm a phase transition in LHS near 425 K. The exact mechanisms of this transition are not yet clear. So far no high temperature structure work have been conducted in this crystal to confirm the presence of a high temperature high symmetry phase.

4.3 Low temperature investigations

4.3.1 Experimental

We have investigated the temperature variation of some of the elastic constants of LHS below room temperature in the range 300 to 210 K. The low temperature measurements were performed in the fabricated cryostat described in Section 2.2.2. Liquid nitrogen was used as the cryogenic fluid. The experimental setup for the measurements were as

described in Section 2.2. As in the case of the high temperature study, 10 MHz ultrasonic waves excited by longitudinal and transverse mode quartz transducers were used for velocity measurements. We have used silicon grease as the bond material in these measurements. The change in velocity with temperature with respect to room temperature value has been measured by carefully adjusting the cw oscillator frequency keeping the selected rf echoes in the phase matched condition. The rate of temperature change in all these measurements are in the range of 0.5 K to 1 K per minute.

4.3.2 Results and discussion

The results of the temperature variation of elastic constants, C_{11}, C_{22}, C_{33}, and C_{44} of LHS below room temperature in the range 210 to 310 K are plotted in figures 4.7 to 4.10. As can be noted from the figures there are no elastic anomalies in this temperature range in LHS for the above constants. We have also found that attenuation of ultrasonic waves also do not show any anomalous changes in this temperature range. The results show that the temperature variation of the constants are more linear in the low temperature region than the the high temperature region. It may be noted that the results of the high temperature investigations indicated a general parabolic decrease in the elastic constants as the temperature was increased.

Anomalous behaviour in the low temperature range have been reported earlier. Thermal expansion anomalies have been reported by Devanarayanan and Easwaran [4.5] at low temperature range also. Their low temperature anomaly is in fact occurs in a range 113 K to 213 K with several kinks in between. Frech and Brown [4.19] from their polarized Raman scattering study found that in the range from 11 to 300 K some of the modes are increasing in intensity from 11 K until in
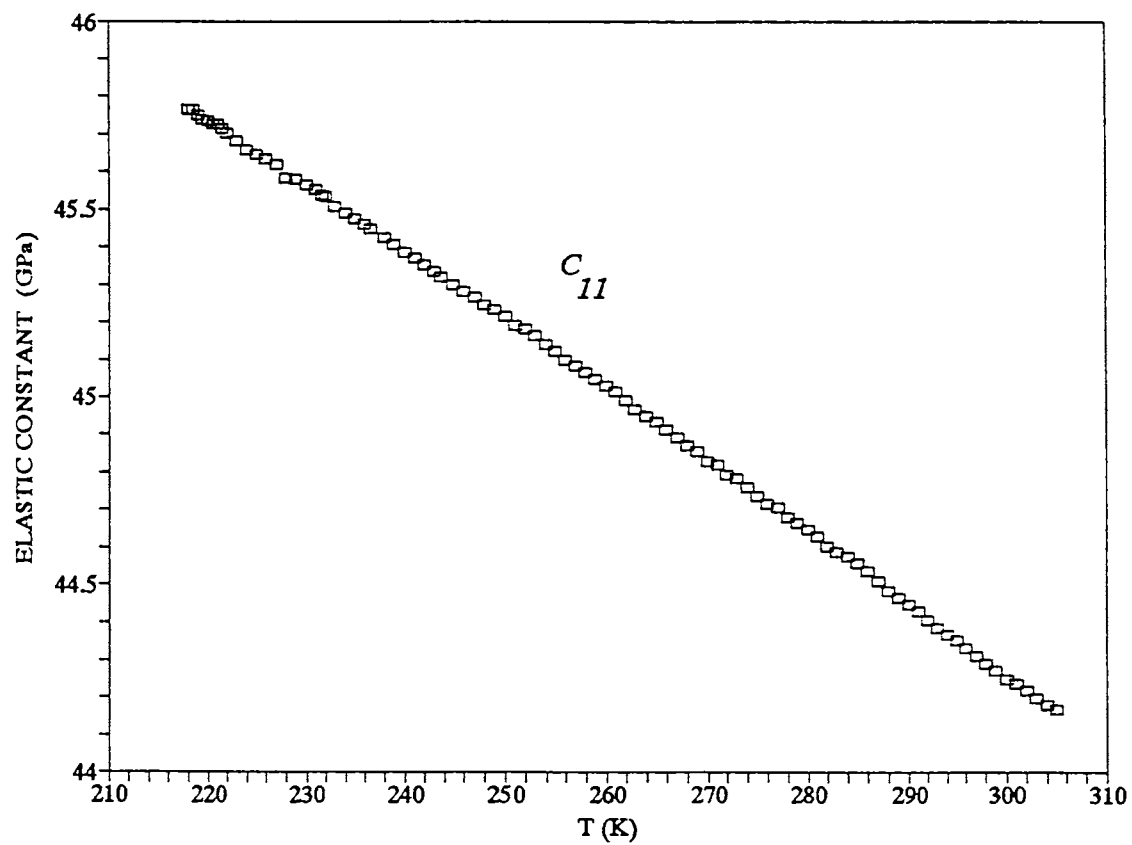
154

Figure 4.7

Temperature variation of elastic constant C_{11} of Lithium
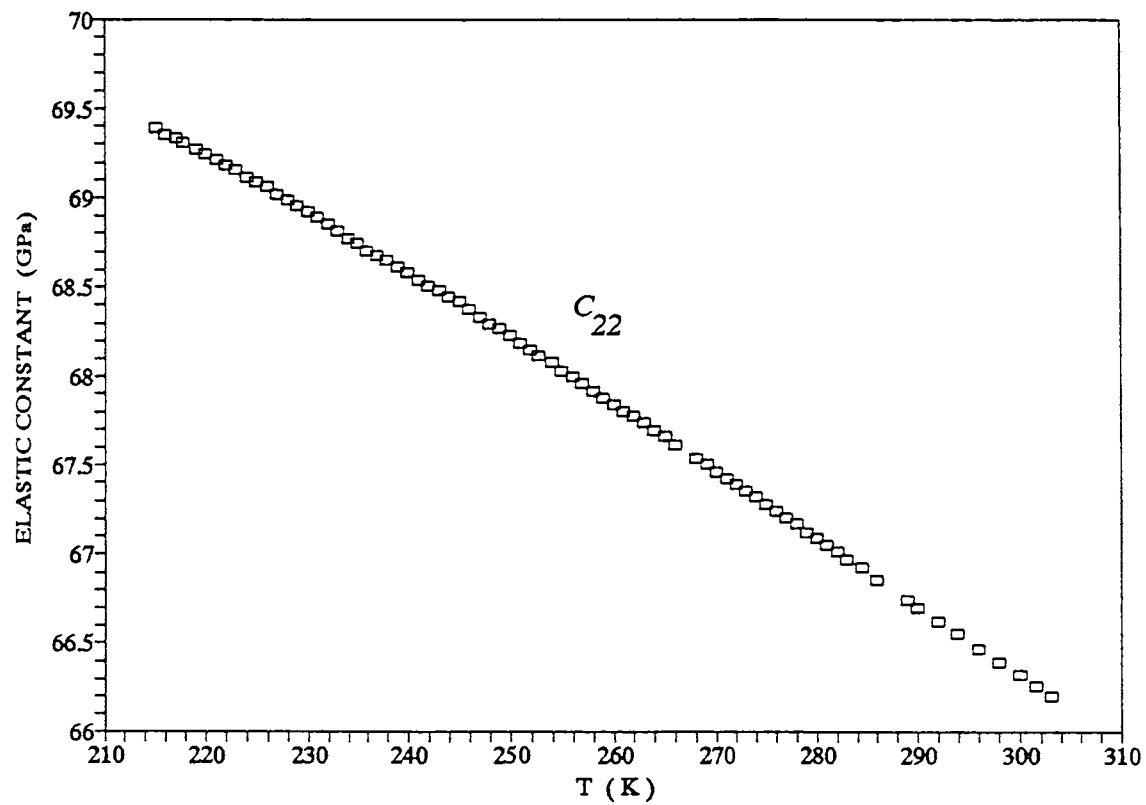Hydrazinium Sulphate below room temperature

Figure 4.8

Temperature variation of elastic constant C_{22} of Lithium
Hydrazinium Sulphate below room temperature

Figure 4.9

Temperature variation of elastic constant C_{33} of Lithium
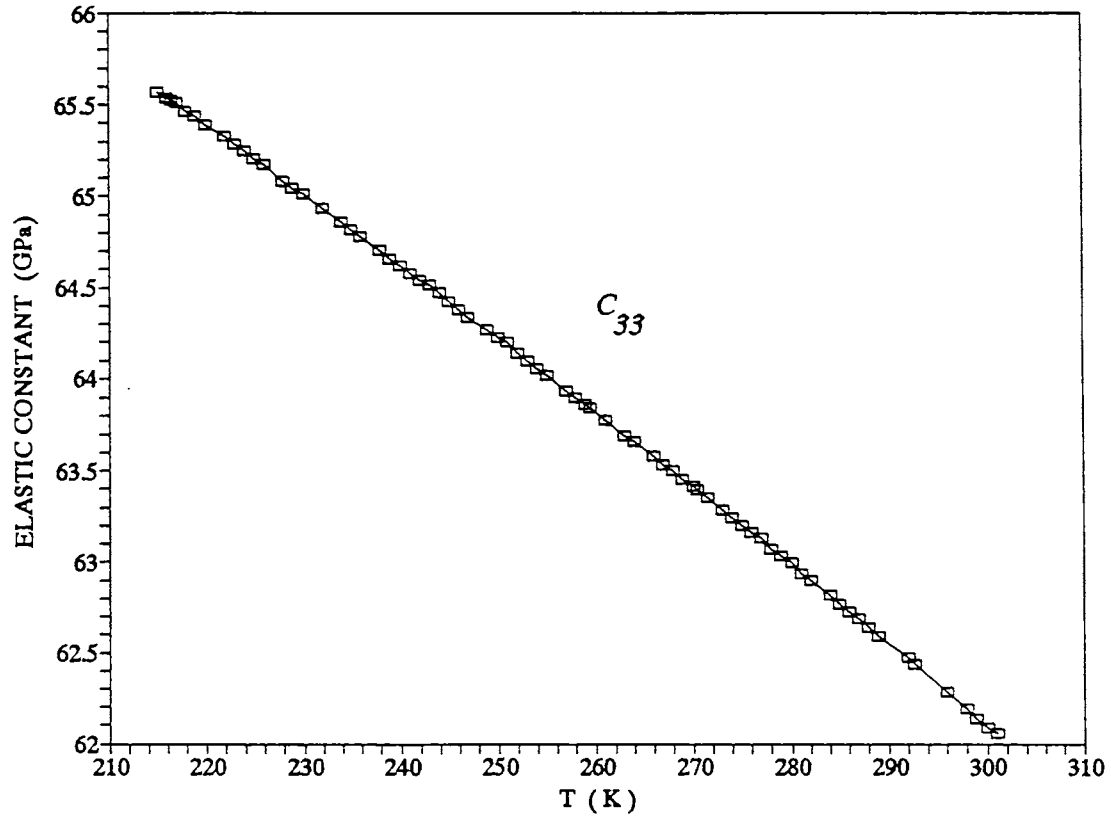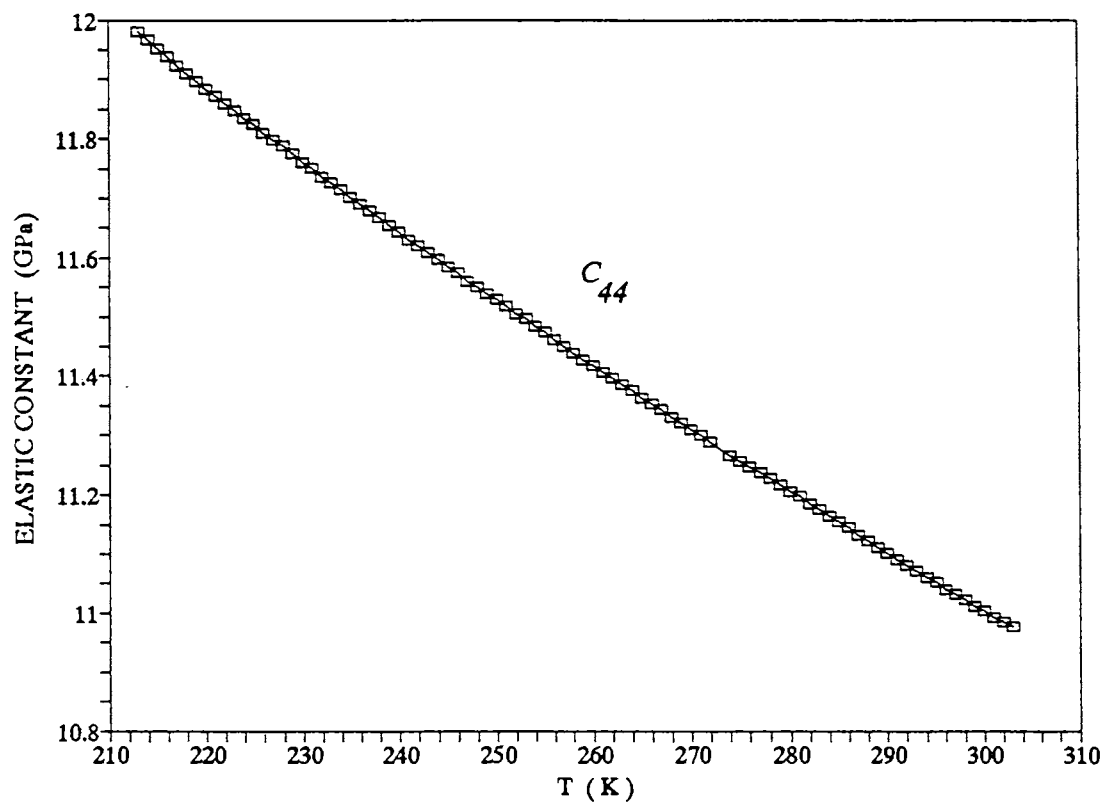Hydrazinium Sulphate below room temperature

157

Figure 4.10

Temperature variation of elastic constant C_{44} of Lithium
Hydrazinium Sulphate below room temperature

158

the temperature interval between 175 and 200 K the intensity abruptly decreases. They have observed that if this is due to a phase transition then the transition should be very weak since only a low percentage of the total number of vibrational modes are affected.

We have not been able to extent our low temperature ultrasonic measurements in LHS reliably below 210 K due to bonding problems. The bond was found to undergo breakdown below 210 K at different temperatures in different measurements. The bond breakdown results in complete loss of echo pattern and no measurements can be performed after a bond failure. In fact we have obtained some anomalous attenuation changes below 210 K which was initially correlated with phase transitions in the crystal. But the nature of these anomalies made us suspect that some other factors may be responsible for the anomalies. Further investigations conducted on a glass sample showed that these attenuation anomalies were actually due to physical changes in the bond like freezing. We have used silicon grease bond for the low temperature measurements and if the bond is freezing then it can become very brittle in the frozen state and is highly susceptible to breakdown. The measurements made by us below 210 K are not presented here due to its inconclusive nature.

4.4 Conclusions

In this chapter the results of the temperature variation study of elastic constants of lithium hydrazinium sulphate both above and below room temperature have been presented. Some of the attenuation measurements at high temperatures are also presented. A new bond material suitable for ultrasonic shear wave measurements at high temperatures have been identified and the details of the same are also presented.

Results of the measurements at high temperatures up to

159

450 K showed anomalies in the temperature variation of elastic constants and also in the temperature variation of ultrasonic attenuation. These anomalies are explained as due to a weak phase transition in the LHS crystal near 425 K. Previous investigation results in thermal expansion study and NMR study are found to be consistent with the present inference of such a phase transition at high temperature.

Low temperature measurements down to 210 K showed a more linear temperature variation of elastic constants. No anomalies are observed in the elastic constants indicating that there is no low temperature phase transitions in LHS down to this temperature.

References

4.1   F. Sommer, K. Weise: Z. anorg. allgem. Chem. $\underline{94}$, 51 (1916)

4.2   R. Pepinsky, K. Vedam, Y. Okaya, S. Hoshino: Phys. Rev. $\underline{111}$, 1467 (1958)   /Room temperature ferroelectricty in lithium hydrazinium sulfate, $Li(N_2H_5)SO_4$/

4.3   J. D. Cuthbert, H. E. Petch: Can. J. Phys. $\underline{41}$, 1629 (1963)   /Nuclear magnetic resonance study of ferroelectric lithium hydrazinium sulphate, $Li(N_2H_5)SO_4$/

4.4   H. Vanderkooy, J. D. Cuthbert, H. E. Petch: Can. J. Phys. $\underline{42}$, 1871 (1964)   /Proton conduction in lithium hydrazinium sulphate, $Li(N_2H_5)SO_4$/

4.5   S. Devanarayanan, K. R. K. Easwaran: Proc. Indian Acad. Sci. $\underline{64A}$, 173 (1966)   /Thermal expansion of ferroelectrics. Part II. lithium hydrazinium sulphate $[Li(N_2H_5)SO_4]$/

4.6   W. D. Mac Clement, M. M. Pintar, H. E. Petch: Can. J. Phys. $\underline{45}$, 3257 (1967)   /Molecular reorientation in ferroelectric lithium hydrazinium sulphate/

4.7   V. M. Padmanabhan, R. Balasubramanian: Acta Cryst. $\underline{22}$, 532 (1967)   /A neutron diffraction study of the crystal structure of lithium hydrazinium sulphate/

4.8   R. R. Knispel, H. E. Petch: Can. J. Phys. $\underline{49}$, 870 (1971) /Proton rotating frame relaxation in lithium hydrazinium sulfate, $Li(N_2H_5)SO_4$/

4.9 R. N. Hastings, T. Oja: J. Chem. Phys., $\underline{57}$, 2139 (1972) /Nitrogen-14 nuclear quadrupole resonance study of lithium hydrazinium sulfate/

4.10 V. Hugo Schmidt, J. E. Drumheller, F. L. Howell: Phys. Rev. $\underline{B4}$, 4582 (1971) /Dielectric properties of lithium hydrazinium sulfate/

4.11 N. Niizeki, H. Koizumi: J. Phys. Soc. Japan $\underline{19}$, 132 (1964)

4.12 M. R. Anderson, I. D. Brown: Acta Cryst. $\underline{A28}$, 663 (1972) /Anomalous neutron scattering and the question of ferroelectricty in $^{6}Li(N_2H_5)SO_4$/

4.13 H. Klapper, A. M. Wardani: Acta Cryst. $\underline{A34}$, S243 (1978) /Dislocation arrangements and mechanical properties of NH_4LiSO_4 and $N_2H_5LiSO_4$/

4.14 M. T. Sebastian, R. A. Becker, H. Klapper: J. Appl. Cryst. $\underline{24}$, 1015 (1991) /X-ray diffraction study of lithium hydrazinium sulphate and lithium ammonium sulfate crystals under a static electric field/

4.15 T. Krajewski, M. Stachowiak: Acta Phys. Pol. $\underline{A53}$, 841 (1978) /Thermal diffusivity of lithium hydrazinium sulfate (LHzS) crystals/

4.16 F. E. Salman, B. Hilezer, C. Pawlaczyk: Jpn. J. Appl. Phys. Suppl. $\underline{24-2}$, 668 (1985) /Protonic conductivity in $Li(N_2H_5)SO_4$ single crystals/

4.17 A. D. Reddy, S. D. M. Rao, G. S. Sastry: Phys. Stat. solidi A $\underline{70}$, 269 (1982) /Electrical conductivity and stimulated thermo-current studies on VO^{2+} doped

Li(N$_2$H$_5$)SO$_4$ single crystals/

4.18 K. V. S. Badarinath: J. Mater. Sci. Lett. <u>6</u>, 609 (1987) /D.c. electrical conductivity and dielectric properties of Li(N$_2$H$_5$)SO$_4$ single crystals/

4.19 R. Frech, S. H. Brown: Solid State Ionics <u>35</u>, 127 (1989) /Hydrazinium ion vibrational motion and proton transport in lithium hydrazinium sulfate/

4.20 L. Godfrey, J. Philip, M. T. Sebastian: J. Appl. Phys. <u>75</u>, 2393 (1994) /Elastic constants and high-temperature elastic anomalies near 425 K in lithium hydrazinium sulfate/

4.21 A. J. Kinloch, *Durability of structural adhesives,* (Applied science publishers, London), p.198-200 (1983)

CHAPTER 5

ELASTIC PROPERTIES AND PHASE TRANSITIONS IN
LITHIUM AMMONIUM SULPHATE

5.1 Introduction

Lithium ammonium sulphate, $LiNH_4SO_4$ or LAS is a more extensively studied crystal than lithium hydrazinium sulphate. LAS shows an interesting sequence of phase transitions and the phase transitions around 460 K and 284 K are well known. LAS is ferroelectric from 460 K to 284 K, below which it is ferroelastic. Further a number of phase transitions have been reported in LAS at low temperatures, some of which have not been confirmed.

A variety of experiments carried out on this material by different workers [5.1-5.4] have established the sequence of Phase transitions depicted in Figure 5.1. At room temperature the structure of LAS crystals belongs to a $P2_1cn$ (C_{2v}^9) (orthorhombic) space group, with four molecules per unit cell. Both the ferroelectric transition at 460 K and the ferroelastic transition at 285 K are of first order. X-ray results show that there are four molecules per unit cell in phases I and II, eight in phase III and sixteen in phase IV. Hildmann *et al* [5.5] have shown that phase III is ferroelastic making LAS the first example for a ferroelastic crystal which is not simultaneously ferroelectric. X-ray results of Simonson et.al. [5.6], infrared absorption curves of Gerbaux et.al. [5.7] and dielectric constant and Raman spectroscopic measurements of Martins et.al. [5.8] have established a second order Phase transition occurring at 28 K taking LAS to a C_s^4 space group (Phase IV) with a doubling of the unit cell volume.

The elastic constants of LAS at room temperature have

$$D_{2h}^{16} \quad (v)$$

PHASE I

PARAELECTRIC

460 K

ORTHORHOMBIC

$$C_{2v}^{9} \quad (v)$$

PHASE II

FERROELECTRIC

285 K

MONOCLINIC

$$C_{2h}^{5} \quad (2v)$$

PHASE III

FERROELASTIC

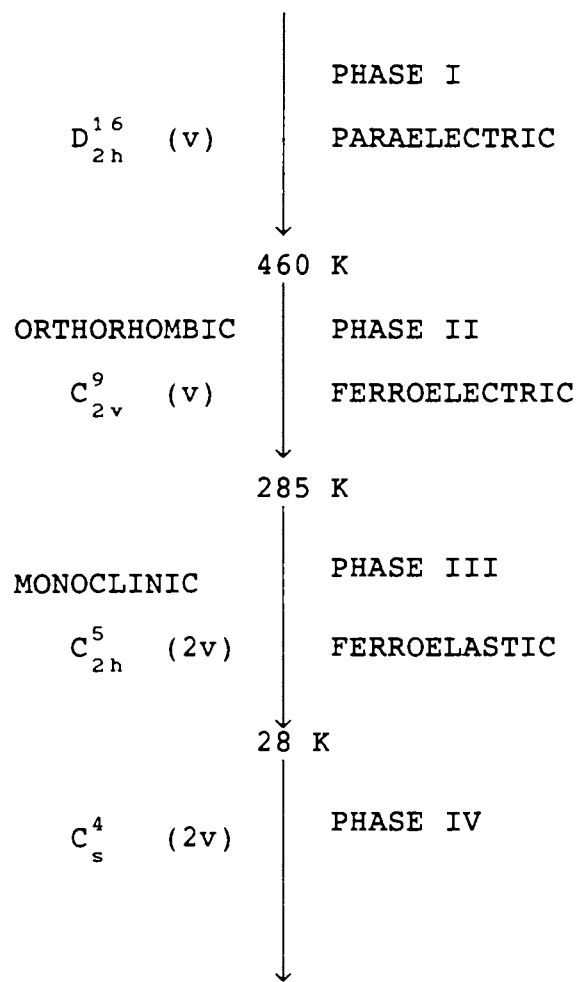28 K

$$C_{s}^{4} \quad (2v)$$

PHASE IV

Figure 5.1

Sequence of phase transitions in LAS

165

been measured by earlier workers using ultrasonic [5.3] and Brillouin scattering [5.9-5.11] techniques. The temperature variation of selected elastic constants near the 460K ferroelectric Phase transition has been determined by ultrasonic [5.12] and Brillouin scattering [5.13,5.14] techniques. Also, clear evidence for the ferroelastic transition at 285 K has been obtained in the experimental results on the temperature variation of the elastic constants using Brillouin scattering technique [5.11]. These experimental results and the Landau type theoretical models proposed by Torgashev et.al. [5.15], Luspin et.al. [5.16,5.17] have made it possible to get a clear understanding of the ferroelectric and ferroelastic phase transitions occurring in LAS.

Several questions have been raised about the polar nature of Phase III. Kruglik et.al [5.4] claimed that this Phase is nonpolar with a monoclinic structure belonging to the $P2_1c$ (C_{2h}^5) space group. the nonpolar nature of LAS in Phase III was rejected by Poulet and Mathieu [5.18] who used Raman scattering to study the Phase II $\longrightarrow$ Phase III transition. Their results showed that some Raman bands appearing below the transition point at 285 K where an indication of cell doubling, carrying modes from the boundary to the centre of the Brillouin zone. They have described this transition as a first order ferroelastic one but phase III was considered polar, belonging to a $P2_1$ (C_2^2) space group. They also proposed that phase III could be a modulated phase with a long modulation period. The polar nature of phase III was supported by Gerbaux et al [5.7] who found a weak anomaly in the dielectric constant and pyroelectric response on both sides of the transition point. Based on their Raman studies, Torgashev et al agreed with Poulet and Mathieu on the doubling of the unit cell but argued that phase III belongs to the $P2_1c$ (C_{2h}^5) space group, in accordance with Kruglik et.al [5.4] and

Simonson et.al [5.6]. Then this phase would be monoclinic and nonpolar with eight molecules per unit cell. The ambiguity is raised by a mode with frequency 24 cm^{-1} in Raman spectra at 183 K that behaves as a soft mode when the temperature approaches the transition point at 285 K. However, if Phase III has a centre of inversion, then polar modes would only be infrared active. This led Poulet and Mathieu to propose that Phase III is polar, with a structure belonging to a noncentrosymmetric space group, probably C_2^2.

Some of these discrepancies have been addressed by Martins et.al [5.8] who undertook dielectric constant and polarized Raman scattering measurements on LAS below room temperature. They detected a new Phase transition taking place at 256 K which was probably overlooked by earlier workers. Infrared absorption and dielectric measurements by Gerbaux et.al [5.7] also have indicated a transition taking place at this temperature. Specific heat measurements [5.20] also have shown an anomaly at 256 K. Martins et.al. [5.8] have, by analysing various experimental data, suggested that the transition at 256K is second order, order-disorder type and reversible. Their results were not sufficient to decide whether LAS goes from C_{2h}^5 to a new space group at 256 K.

In order to throw more light on the nature of the transitions at 285 K and 256 K, we have carried out a detailed ultrasonic study of the temperature dependence of the elastic constants of LAS at low temperatures in the range 310 to 220 K. This is the first ultrasonic study in LAS in this low temperature range. The absolute values of all the 9 elastic constants of LAS have been determined and are tabulated and compared with the previous measurements. The details of the experimental technique used and the results obtained are described in the following sections.

5.2 Elastic constants of LAS

5.2.1 Introduction

The elastic constants of LAS was first measured by Aleksandrov et al [5.3] by using ultrasonic technique. They have measured and tabulated all the 9 elastic constants and their temperature variation in a small range from 285 K to 305 K. Using Brillouin scattering technique, Hirotsu et al [5.13] investigated the temperature variation of C_{11}, C_{22}, and C_{33} of LAS in the high temperature range from 293 to 523 K which included the high temperature transition at 460 K. Luspin *et al* [5.10] investigated the transverse modes using Brillouin scattering and measured C_{44}, C_{55} and C_{66}. Wyslouzil *et al* [5.12] have measured all the 9 elastic constants and their temperature variation in the range 290 K to 540 K, by using the ultrasonic pulse echo overlap method. But they have not given a tabulated data of elastic constants at room temperature. All the 9 elastic constants of LAS were again measured by Mróz et al [5.11] by using Brillouin scattering technique and they have provided a tabulated data of elastic constants and have compared their data with the previous measurements of elastic constants of LAS. They have, for the first time investigated the temperature variation of elastic constants of LAS at the low temperature transition near 285 K. Their measurements were limited to the temperature range from 273 K to 293 K.

On examination of the previous measurements, it can be found that there are wide disagreements between the values of elastic constants reported by various workers. We have resolved these disagreements to some extent by identifying the fact that different workers have taken different choice of axes for this orthorhombic crystal. Mróz et al [5.11], who have recently compared their values with the previous

measurements, have failed to identify this point.

Using the tensor notation of the elastic constants, all the elastic constants can be transformed from one choice of axes to another and it can be seen that there are 6 possible choices for selecting the 3 lattice parameters a, b and c. The conversion scheme for all the elastic constants of LAS under different choice of axes are presently derived and are tabulated in Table 5.1. The lattice parameters given in the table are from the very recent refined X-ray structure work on LAS by Mashiyama and Kasano [5.21].

We have compared the previous measurements after rearranging the elastic constants according to Table 5.1 and this showed much better agreement between the constants reported by previous workers. But even this agreement was not satisfactory because some of the measured elastic constants were showing more than 10% variation between different workers. These variations were clearly the result of inaccurate measurements and an accurate determination of all the elastic constants of LAS was found to be necessary.

We have accurately determined all the 9 elastic constants of LAS and the results are presented in Section 5.2.3. In section 5.2.2, the details of sample preparation are given and in Section 5.2.4 the velocity surface plots of LAS are given.

5.2.2 Sample preparation

Single crystals of LAS were grown by evaporation of an equimolar solution of $Li_2SO_4.H_2O$ and $(NH_4)_2SO_4$ at a constant temperature of 311 K. The details of the apparatus used for the crystal growth have been discussed in Section 2.4. During the growth the crystal was continuously rotated in opposite directions using the crystal rotation mechanism. Large single crystal of LAS, measuring about 5 cm in the c-axis direction

Table 5.1

Conversion table for elastic constants of orthorhombic LAS
under different choice of crystallographic axes

Lattice parameters	Axes choice					
	(1)[†]	(2)[*]	(3)	(4)	(5)	(6)
5.282 Å =	a	c	b	c	b	a
9.131 Å =	b	b	a	a	c	c
8.780 Å =	c	a	c	b	a	b
C_{11}	C_{11}	C_{33}	C_{22}	C_{33}	C_{22}	C_{11}
C_{22}	C_{22}	C_{22}	C_{11}	C_{11}	C_{33}	C_{33}
C_{33}	C_{33}	C_{11}	C_{33}	C_{22}	C_{11}	C_{22}
C_{44}	C_{44}	C_{66}	C_{55}	C_{66}	C_{55}	C_{44}
C_{55}	C_{55}	C_{55}	C_{44}	C_{44}	C_{66}	C_{66}
C_{66}	C_{66}	C_{44}	C_{66}	C_{55}	C_{44}	C_{55}
C_{12}	C_{12}	C_{23}	C_{12}	C_{13}	C_{23}	C_{13}
C_{13}	C_{13}	C_{13}	C_{23}	C_{23}	C_{12}	C_{12}
C_{23}	C_{23}	C_{12}	C_{13}	C_{12}	C_{13}	C_{23}

[*] This choice of axes were adopted for the present work and this choice was also taken by Aleksandrov *et al* [5.3] and Luspin *et al* [5.10]

[†] Choice by Mashiyama and Kasano [5.21]

was obtained after a period of 60 days. LAS usually grows in two different forms, one is the prismatic form and the other is the pseudohexagonal form. The pseudohexagonal form is a twined crystal and is usually obtained from spontaneously nucleated seeds at room temperature. We have grown the untwined prismatic form of LAS for our studies. A drawing of the morphology of the prismatic form of LAS is shown in Figure 5.2.

The crystallographic directions of the grown crystal were determined from interfacial angle measurements. The identification of the correct directions in LAS have been more difficult than in LHS. This is due to the presence of comparatively large number of natural faces in LAS and also due to the confusion existing in literature regarding the choice of axes. Using the lattice parameters, a = 8.78, b = 9.131 and c = 5.282 [5.21], the interfacial angles of LAS were calculated using the crystallographic formula, Eq. (3.01) for orthorhombic lattice. The good agreement between the calculated and measured values of the interfacial angles proved that our direction identification is correct. In Table 5.2 the calculated and measured values of interfacial angles of LAS are given.

The grown crystal of LAS have been cut using the slow speed diamond wheel saw as discussed in Section 3.2 for LHS. The samples have been cut so as to have propagation directions along a, b and c axes, [101], [110] and [011] directions. The cut samples in different directions had thickness in the range 0.8 to 1.2 cm. The cut samples were polished carefully using cerium oxide to optical reflection level. The misorientations of the cut samples were less than 1°.

5.2.3 Velocity measurements and elastic constants

In Section 1.2.3 the details of measuring the elastic
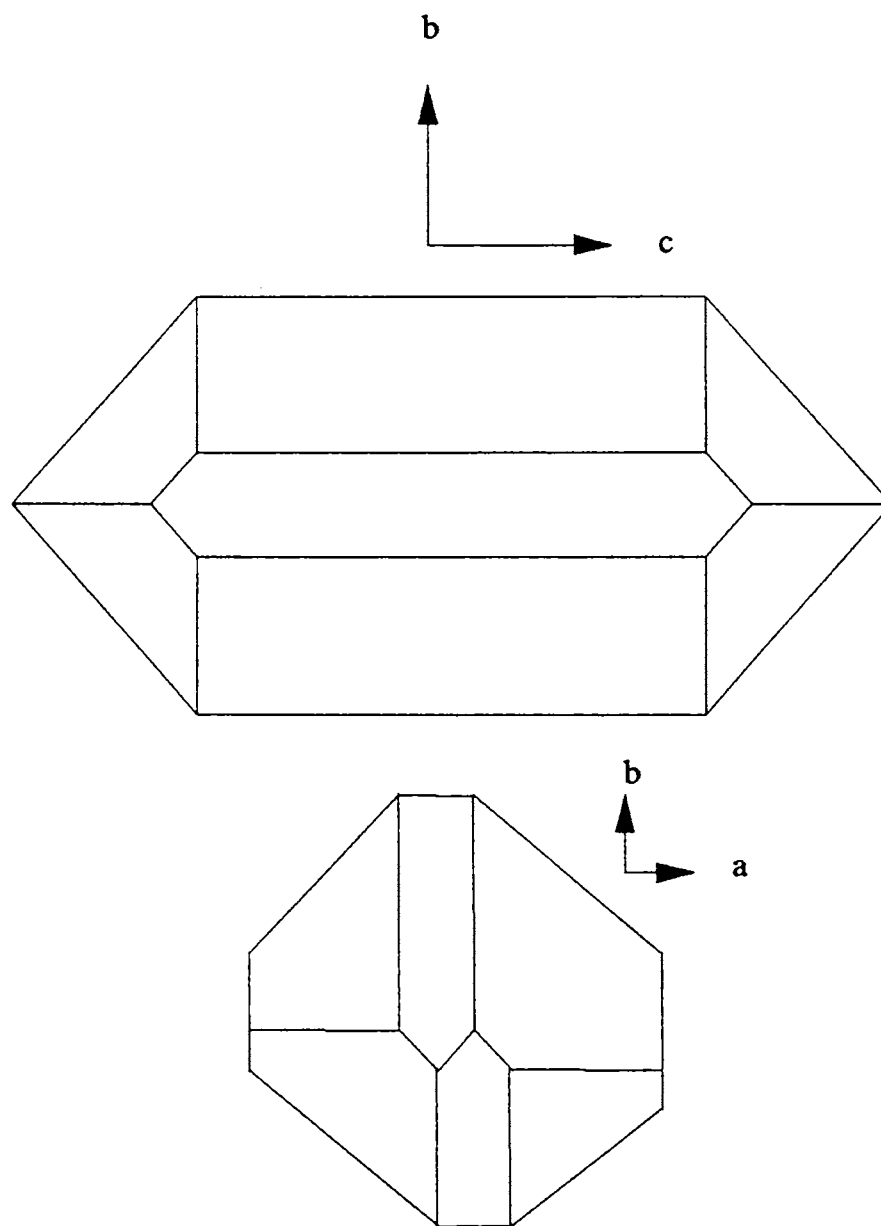
Figure 5.2

Schematic representation of the morphology of
prismatic form of LAS

Table 5.2

Calculated and measured values of interfacial angles of LAS
(the angles are given in degrees)

Face 1 h_1 k_1 l_1			Face 2 h_2 k_2 l_2			Calculated angles	Measured angles	Difference angles
1	0	0	1	1	0	136.12	135.5	0.62
1	0	0	1	2	0	117.47	117.5	−0.03
1	0	0	1	1	1	117.51	117.4	0.11
1	0	0	1	1	0	136.12	135.5	0.62
0	1	0	0	1	1	120.05	120.0	0.05
1	1	0	1	1	1	129.85	128.6	1.25
1	1	1	1	2	0	127.38	127.3	0.08
1	1	0	−1	1	0	87.75	88.6	−0.85
1	1	1	0	1	1	152.49	153.7	−1.21
1	1	1	1	1	0	129.85	129.6	0.25
1	1	1	0	1	0	116.37	116.4	−0.03
1	1	1	−1	1	0	88.56	88.8	−0.19

173

constants of orthorhombic crystal have been discussed. The necessary expressions for the same, which relate the measured velocities with the elastic constants, have been obtained and tabulated in Table 1.2. The ultrasonic velocities have been measured using the Pulse Echo Overlap technique and the details of this technique are explained in Section 2.1.2. The basic experimental setup used for the measurements appears in Section 2.2.1. In all the velocity measurements, the correct overlap identification and bond correction have been performed using a computer program developed for the same and the details of the methodology and the program are presented in section 2.3.3. X and Y cut quartz transducers with resonance frequency 10 MHz, excited at their fundamental mode of operation, have been used to generate longitudinal and transverse ultrasonic waves. Specific experimental details regarding the bonding of the transducer to the sample have been discussed in Section 3.4.1 in connection with the measurements in LHS.

Of the 18 propagation modes listed in Table 1.2, measurements have been performed for 12 different modes. Using these 12 measurements all the 9 elastic constants of LAS can be determined with cross checking possible on some of the values. Of the 12 measurements 9 measurements are along the symmetry directions and 3 are in the symmetry planes, a-b, a-c and b-c, in the [110], [101] and [011] directions respectively.

Results of the velocity measurements in LAS are presented in Table 5.3 along with the corresponding elastic constants. In Table 5.4, we compare the results of our measurement of elastic constants of LAS with the previously reported values by different workers. As has been discussed in Section 5.1, there is no general agreement on the choice of axes for this orthorhombic crystal. Hence we have rearranged the elastic constants reported by previous workers using the

174

Table 5.3

Measured ultrasonic velocities and the elastic constants of Lithium Ammonium Sulphate at 300 K

No.	Mode	Direction of particle motion	Velocity measured (v) km/s	Elastic constant (ρv^2) GPa	Involved elastic constant
Propagation along a-axis					
1	L	a	4.7863	43.57	$C_{11} = \rho v^2$
2	T	b	2.9876	16.98	$C_{66} = \rho v^2$
3	T	c	2.3554	10.55	$C_{55} = \rho v^2$
Propagation along b-axis					
4	L	b	4.9531	46.66	$C_{22} = \rho v^2$
5	T	a	2.9837	16.93	$C_{66} = \rho v^2$
6	T	c	2.9343	16.38	$C_{44} = \rho v^2$
Propagation along c-axis					
7	L	c	5.3827	55.11	$C_{33} = \rho v^2$
8	T	a	2.3229	10.26	$C_{55} = \rho v^2$
9	T	b	2.9179	16.19	$C_{44} = \rho v^2$
Propagation in a-b plane, [110] direction, angle θ = 43.88°					
10	QL	$\perp$ to c	5.0914	49.30 $C_{12} = 19.67^\dagger$	$C_{12} = f_{ab}$
Propagation in b-c plane, [011] direction, angle θ = 59.95°					
11	QL	$\perp$ to a	5.4251	55.98 $C_{23} = 26.26^\dagger$	$C_{23} = f_{bc}$
Propagation in a-c plane, [101] direction, angle θ = 31.03°					
12	QL	$\perp$ to b	5.2455	52.33 $C_{13} = 28.88^\dagger$	$C_{13} = f_{ac}$

Table 5.3 continued

The abbreviations used have the following meanings:

L - Longitudinal, T - Transverse, QL - Quasi-longitudinal, QT - Quasi-transverse, ρ = density (1.902 g.cm^{-3} for LAS) , v = velocity of propagation of respective mode. a, b, c -Crystallographic axis.

[†]Calculated values using respective formula given below

$$f_{ab} = \left[\frac{\left(c^2 C_{11} + s^2 C_{66} - \rho v^2 \right)\left(c^2 C_{66} + s^2 C_{22} - \rho v^2 \right)}{c^2 s^2} \right]^{\frac{1}{2}} - C_{66} \; ,$$

$$f_{bc} = \left[\frac{\left(c^2 C_{22} + s^2 C_{44} - \rho v^2 \right)\left(c^2 C_{44} + s^2 C_{33} - \rho v^2 \right)}{c^2 s^2} \right]^{\frac{1}{2}} - C_{44} \; ,$$

$$f_{ac} = \left[\frac{\left(s^2 C_{11} + c^2 C_{55} - \rho v^2 \right)\left(s^2 C_{55} + c^2 C_{33} - \rho v^2 \right)}{c^2 s^2} \right]^{\frac{1}{2}} - C_{55} \; .$$

where s = sine and c = cosine of respective angle θ. (See Figure 1.1 for definition of θ)

Table 5.4

Elastic constants* of LAS in comparison with previously measured values (after rearrangement according to Table 5.1).

Elastic constant	Different investigations					
	$[1]^{U,T}$	$[2]^{B,C}$	$[3]^{B,C}$	$[4]^{U,C}$	$[5]^{B,T}$	$[6]^{U}$
C_{11}	41.59	44.5	–	39.3	43.8	43.57 ± 0.6
C_{22}	44.10	46.2	–	40.3	52.2	46.66 ± 0.6
C_{33}	49.73	54.5	–	50.2	55.2	55.11 ± 0.6
C_{44}	15.40	–	16.1	15.7	13.1	16.29 ± 0.2
C_{55}	9.88	–	10.6	10.0	10.8	10.41 ± 0.2
C_{66}	15.73	–	16.4	15.5	15.1	16.96 ± 0.2
C_{12}	19.7	–		21.5	23.6	19.67 ± 1.5
C_{13}	26.1	–		24.7	27.7	28.88 ± 1.5
C_{23}	22.8	–		21.0	34.1	26.26 ± 1.5

*Piezoelectric couplings neglected

[U]Ultrasonic measurements

[B]Brillouin scattering measurements

[T]Values from tabulated data

[C]Values from the temperature variation curves

[1] Aleksandrov *et al* [5.3] (1975) at 300 K, axes chosen = (2)

[2] Hirotsu *et al* [5.13] (1981), at 300 K, axes chosen = (1)

[3] Luspin *et al* [5.10] (1985), at 300 K, axes chosen = (2)

[4] Wyslouzil *et al* [5.12] (1986), at 300 K, axes chosen = (3)

[5] Mróz *et al* [5.11] (1989), at 293 K, axes chosen = (1)

[6] Present work (1994), at 300 K, axes chosen = (2)

(See Table 5.1 for details of axes choice)

conversion scheme given in Table 5.1. It may be noted that the conversion process does not actually change the numerical values but only change the subscript of the notation for elastic constants. Some workers have not indicated their choice of axes and in these cases the choice used by them could be deducted by examining their elastic data. Only Aleksandrov *et al* [5.3] and Mróz *et al* [5.11] have given tabulated data of elastic constants and in other cases the values have been obtained from their temperature variation curves which starts from room temperature and goes to high temperatures. There have been only two previous ultrasonic measurements on LAS , one by Aleksandrov *et al* [5.3] and the other by Wyslouzil *et al* [5.12].

On comparing the previous results with the present measured values the following observations could be made. The values reported by Aleksandrov *et al* [5.3] appears to be about 0.95 times smaller than our values. The origin of this difference can possibly be related to a difference in the value of sample density used by them for the calculation of elastic constant from the ultrasonic velocity. We have used the value $\rho = 1.902$ [5.10,5.11] and Aleksandrov *et al* [5.3] have not indicated the value used by them but could be $\rho = 1.8$. The Brillouin scattering measurements of Hirotsu *et al* [5.13] and Luspin *et al* [5.10] are in agreement with present values. The ultrasonic measurements of Wyslouzil *et al* [5.12] (no tabulated data given) appears to be inaccurate especially for the longitudinal mode constants. This inaccuracy can be traced to the small sample size (0.5 cm) used by them. With this size of sample the travel time for longitudinal waves in the sample will be less than 2 μs and an error in overlap identification can considerably affect the velocity measurement. However their interest was mainly the investigation of elastic anomalies near the high temperature phase transition in LAS. The Brillouin scattering measurements

178

of Mróz *et al* [5.11] show that the value of C_{44} measured by them is too small when compared to others and this has affected their estimation of C_{23} also.

5.2.4 Velocity surface plots of LAS

In section 1.2.1, we have derived the expressions for the velocities of acoustic waves in the symmetry planes of the orthorhombic lattice. Since LAS belongs to the orthorhombic system, those expressions can be used to compute the velocity of acoustic waves in the symmetry planes of LAS as has been done for LHS in Section 3.6. If the velocities are calculated using the corresponding elastic constants for different values of angle θ (defined in Figure 1.1) in the range from 0 to 360 degrees with some small step like $2°$, then the resulting velocities can be plotted to get a phase velocity surface diagram for the corresponding plane.

For the purpose of plotting the curve on an x-y plane of the paper, we have to convert the calculated velocity v and the angle θ to the x and y co-ordinates. These conversions can be performed using Equations (3.13) and (3.14).

For plotting the velocity surface in the a-b plane of LAS, the Equations from (1.25) to (1.27) can be used. Here the velocity v_0 is a pure shear (S) mode with polarization perpendicular to a-b plane, v_1 is a quasilongitudinal (QL) mode and v_2 is a quasishear (QS) mode except along symmetry directions a and b where they are pure modes. The plotted velocity surfaces are shown in Figure 5.3.

The velocity surface in the a-c plane can be computed using Equations from (1.34) to (1.36). Here v_0 is a pure S mode with polarization perpendicular to the a-c plane, v_1 and v_2 are QL and QS modes except along symmetry directions a and c. The plotted velocity surfaces are shown in Figure 5.4.

The velocity surface in the b-c plane can be computed

using Equations from (1.42) to (1.44). Here v_0 is a pure S mode with polarization perpendicular to the b-c plane, v_1 and v_2 are QL and QS modes except along symmetry directions b and c. The plotted velocity surfaces are shown in Figure 5.5.

From the above plots, the three velocities in any direction in any of the symmetry planes can be easily found by measuring the length of the straight line drawn from the centre to the curve at the required angle from the symmetry axis. The graphs have been plotted with a scale of 1 cm for 1 km/s of velocity.

5.3 Study of low temperature phase transitions in LAS

5.3.1 Low temperature ultrasonic measurements

We have investigated the temperature variation of all the diagonal elastic constants of LAS in orthorhombic pure mode directions below room temperature in the range 310 to 220 K. This range include the well known phase transition near 285 K and the recently proposed [5.8] phase transition near 256 K. The low temperature measurements are performed in the fabricated cryostat described in Section 2.2.2. Liquid nitrogen is used as the cryogenic fluid. The experimental setup for the measurements are as described in Section 2.2. 10 MHz ultrasonic waves excited by longitudinal and transverse mode quartz transducers are used for velocity measurements. We have used silicon grease as the bond material in these measurements. The change in velocity with temperature with respect to the room temperature value has been measured by carefully adjusting the cw oscillator frequency keeping the selected rf echoes in the phase matched condition. Temperature variation measurements are carried out in temperature intervals of about 1 K and in intervals of about 0.1 K near the transition points. The rate of temperature change in all
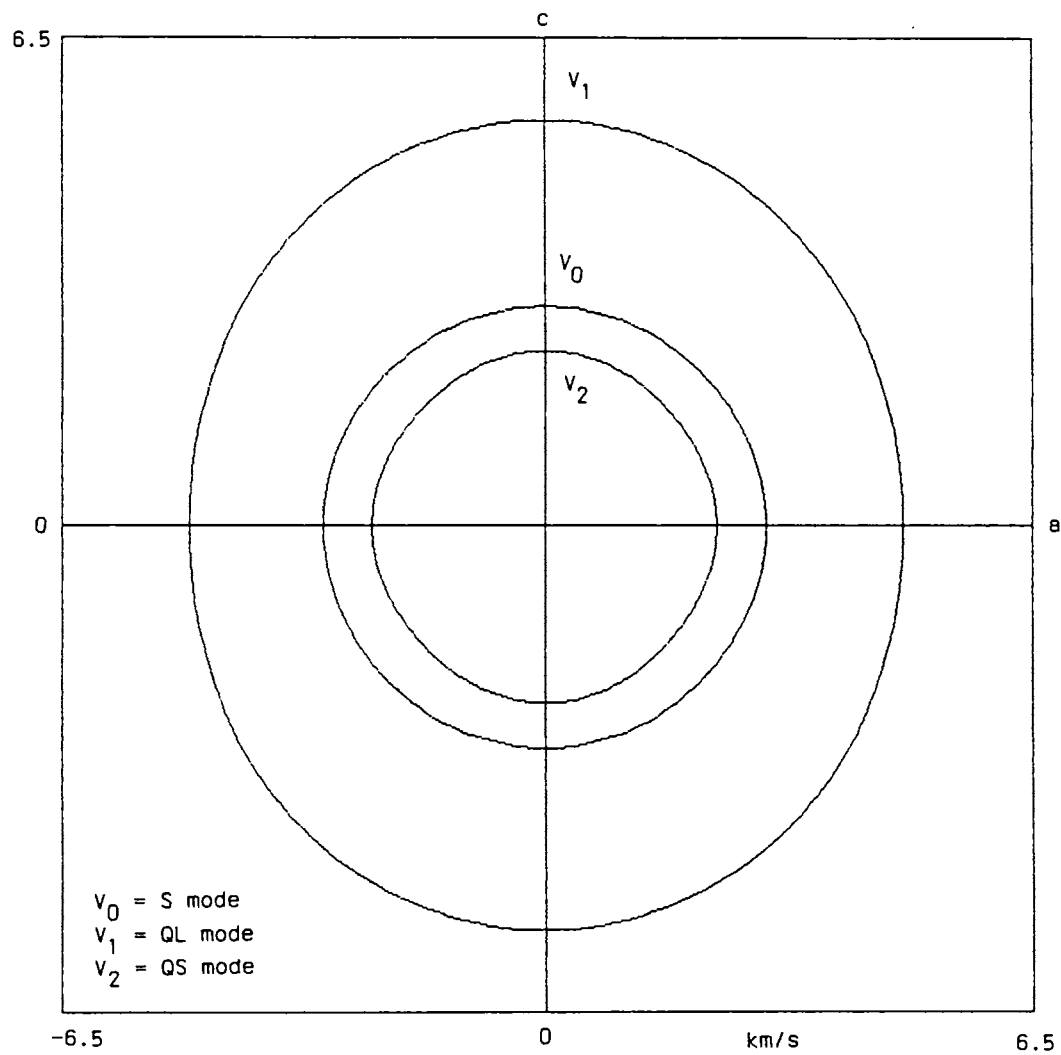
Figure 5.3

The velocity surfaces of LAS in a-b plane

181

Figure 5.4

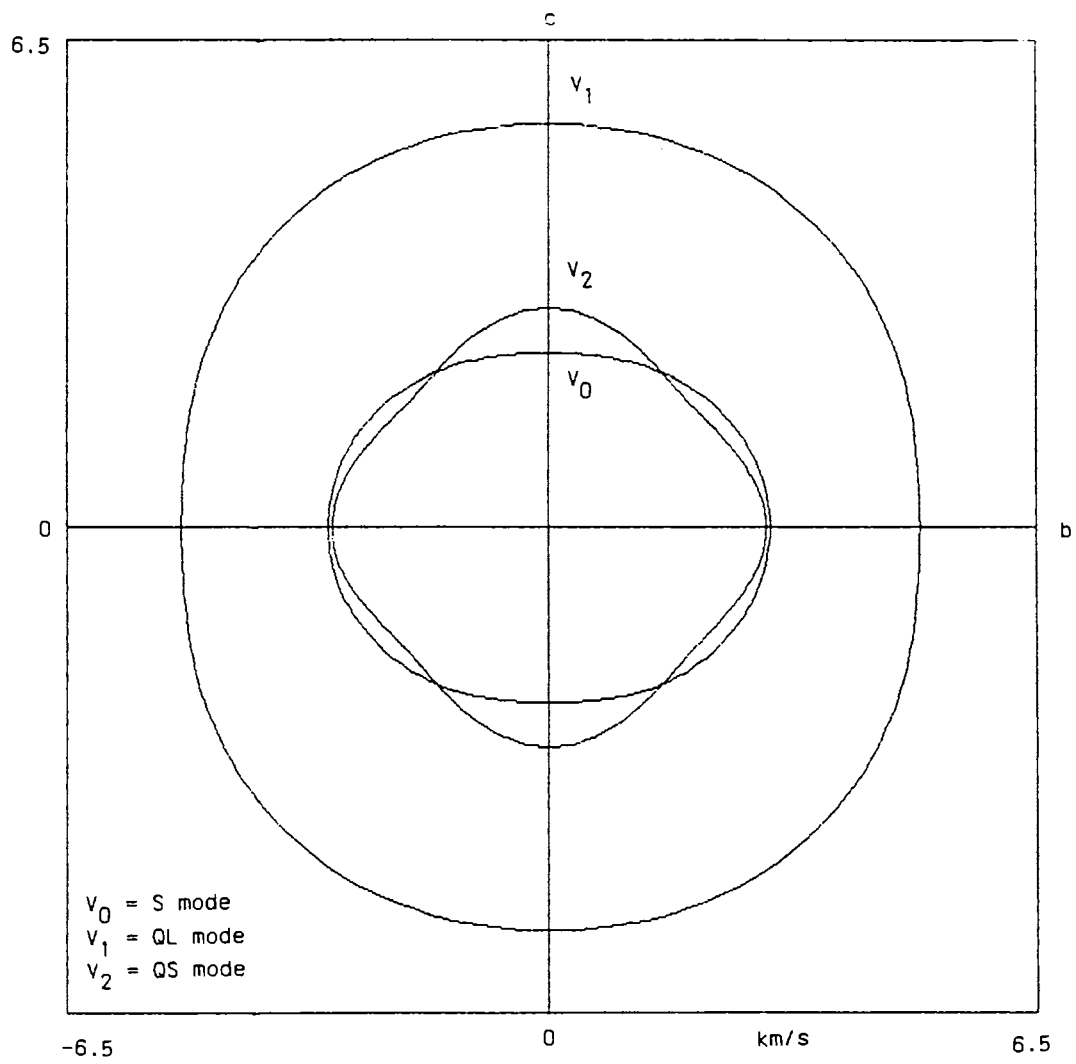The velocity surfaces of LAS in a-c plane

182

Figure 5.5

The velocity surfaces of LAS in b-c plane

183

these measurements are in the range of 0.1 K to 0.5 K per minute. Measurements are carried out both for cooling and heating cycles. This is to reveal the thermal hysteresis effects of the phase transitions.

One major difficulty for low temperature ultrasonic measurements in LAS is the cracking of the crystal at the 285 K phase transition. Aleksandrov et al [5.3] have also noted this point and they have not been able to make ultrasonic measurements below the transition temperature. Large crystals are required for ultrasonic study and these crystals always develop cracks at the transition temperature even under extremely slow cooling rates. We have found that ultrasonic measurements are still possible below the transition temperature with considerably reduced echo amplitudes. This is achieved by careful tuning and sensitive adjustments of our measuring system. Attenuation measurements could not be performed due to the poor quality of the echo pattern.

The phase transition at 285 K changes the symmetry of the crystal. The crystal goes from the room temperature (phase II) orthorhombic mm2 (C_{2v}) point group to monoclinic 2/m (C_{2h}) point group below the phase transition temperature (phase III). Many of the pure modes in orthorhombic phase are no longer pure modes in the monoclinic phase and combination constants of monoclinic symmetry are only applicable in phase III. With our choice of axes (see choice (2) in Table 5.1) the c-axis coincide with the two fold y-axis in the monoclinic phase. Cell doubling upon transition takes place along orthorhombic a-axis [5.4] which is also made to correspond with monoclinic x-axis. The orthorhombic b-axis is made to correspond with monoclinic z-axis. For the choice of axes in both orthorhombic and monoclinic phases we have followed the convention adopted by IRE standards Committee [5.22] which have been listed by Neighbours and Schacher

[5.23].

The involved constants in both phases for different propagation modes are tabulated in Table 5.5 with our choice of axes. We indicate different modes with a three letter notation; the first letter (a, b or c) indicates the direction of wave propagation, the second letter (l or t) indicates whether the waves are longitudinal or transverse, the third letter (a, b or c) indicates the direction of polarization.

We would like to point out that Mróz *et al* [5.11] who have provided a table of relations for propagation modes in orthorhombic and monoclinic phases have not clearly defined their choice of axes and we find their table inconsistent with their choice of axes. Further, the relations given by them for monoclinic phase shows some mistakes.

5.3.2 Results and discussion

The temperature variation of the elastic constants C_{11}, C_{22}, C_{33}, C_{44}, C_{55} and C_{66}, corresponding to the modes indicated in Table 5.5, below room temperature during cooling and heating cycles are shown in Figures 5.6 to 5.16. The phase transition occurring at 285 K is clearly visible in all the figures. There is a clear step like change in the elastic constant values and there is a clear thermal hysteresis of 2.5 K between the cooling and heating cycles for this transition. On cooling the transition takes place at 285.5 K and on heating the transition takes place at 288 K. This has not been reported by previous workers [5.11] who undertook the study of elastic properties near this transition in LAS using Brillouin scattering technique.

It can also be seen that the C_{22} constant in monoclinic phase which correspond with the clc mode (Figures 5.10 and 5.11) shows an anomaly at 242 K on cooling and at 258 K on heating. Similarly a clear anomaly is observed for the

Table 5.5

The involved elastic constants in orthorhombic mm2 and monoclinic 2/m phase of LAS for different modes of propagation

Modes	mm2 phase	2/m phase
ala[*]	C_{11}	$\frac{1}{2}\left(C_{11} + C_{55} + \sqrt{(C_{11} - C_{55})^2 + 4C_{15}^2} \right)$
atc	C_{55}	C_{66}
atb[*]	C_{66}	$\frac{1}{2}\left(C_{11} + C_{55} - \sqrt{(C_{11} - C_{55})^2 + 4C_{15}^2} \right)$
clc[*]	C_{33}	C_{22}
ctb[*]	C_{44}	$\frac{1}{2}\left(C_{44} + C_{66} + \sqrt{(C_{44} - C_{66})^2 + 4C_{46}^2} \right)$
cta[*]	C_{55}	$\frac{1}{2}\left(C_{44} + C_{66} - \sqrt{(C_{44} - C_{66})^2 + 4C_{46}^2} \right)$
blb[*]	C_{22}	$\frac{1}{2}\left(C_{33} + C_{55} + \sqrt{(C_{33} - C_{55})^2 + 4C_{35}^2} \right)$
bta	C_{66}	$\frac{1}{2}\left(C_{33} + C_{55} - \sqrt{(C_{33} - C_{55})^2 + 4C_{35}^2} \right)$
btc	C_{44}	C_{44}

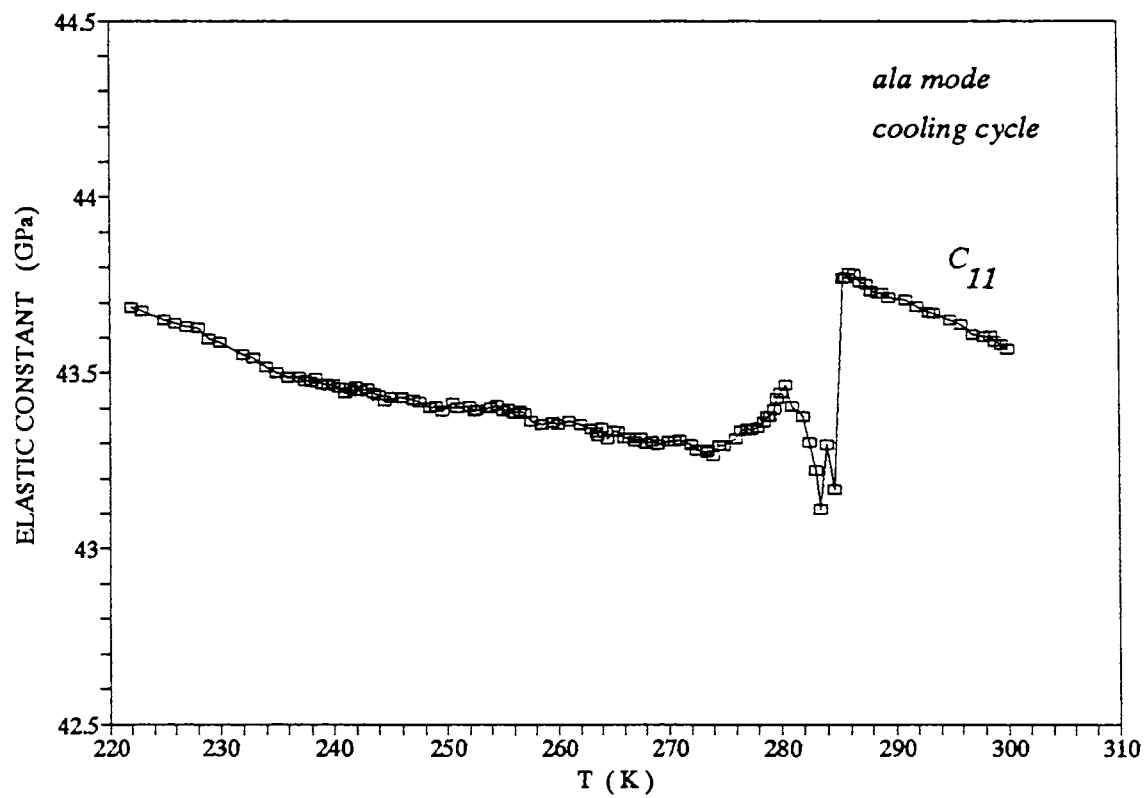[*] Modes which have been investigated presently

Figure 5.6

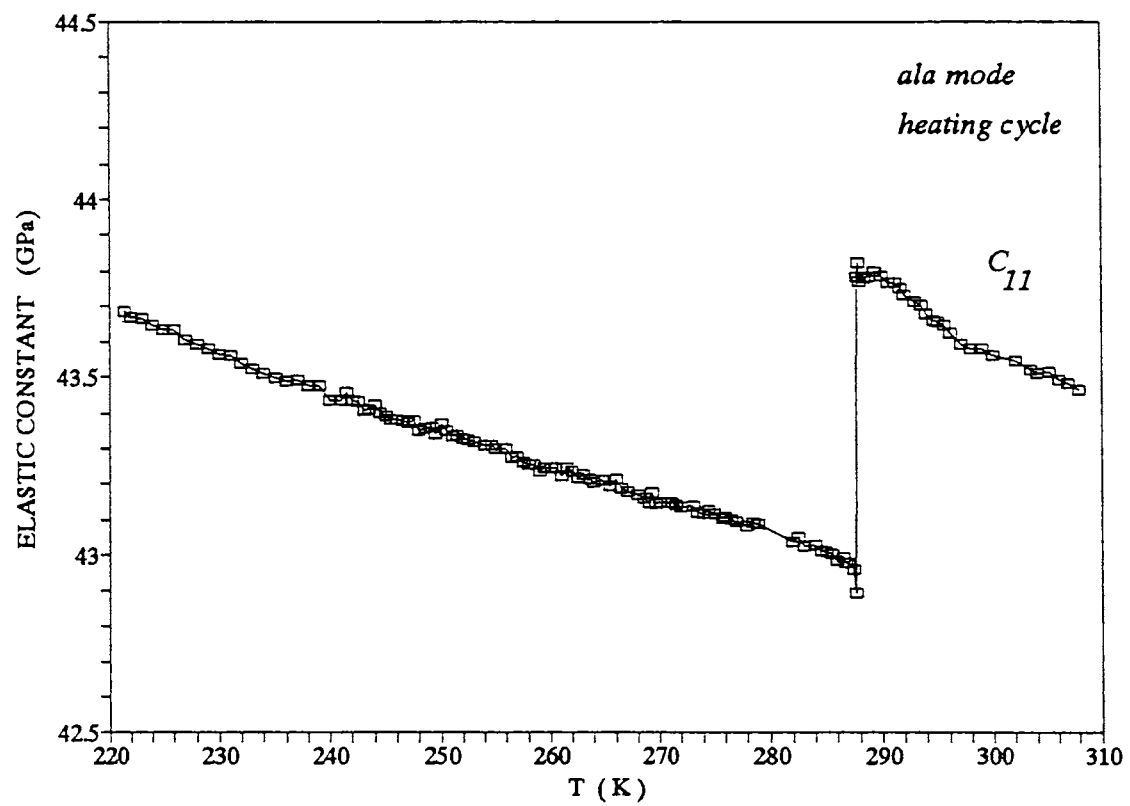Temperature variation of elastic constant of LAS for the
cooling cycle of ala mode

187

Figure 5.7

Temperature variation of elastic constant of LAS for
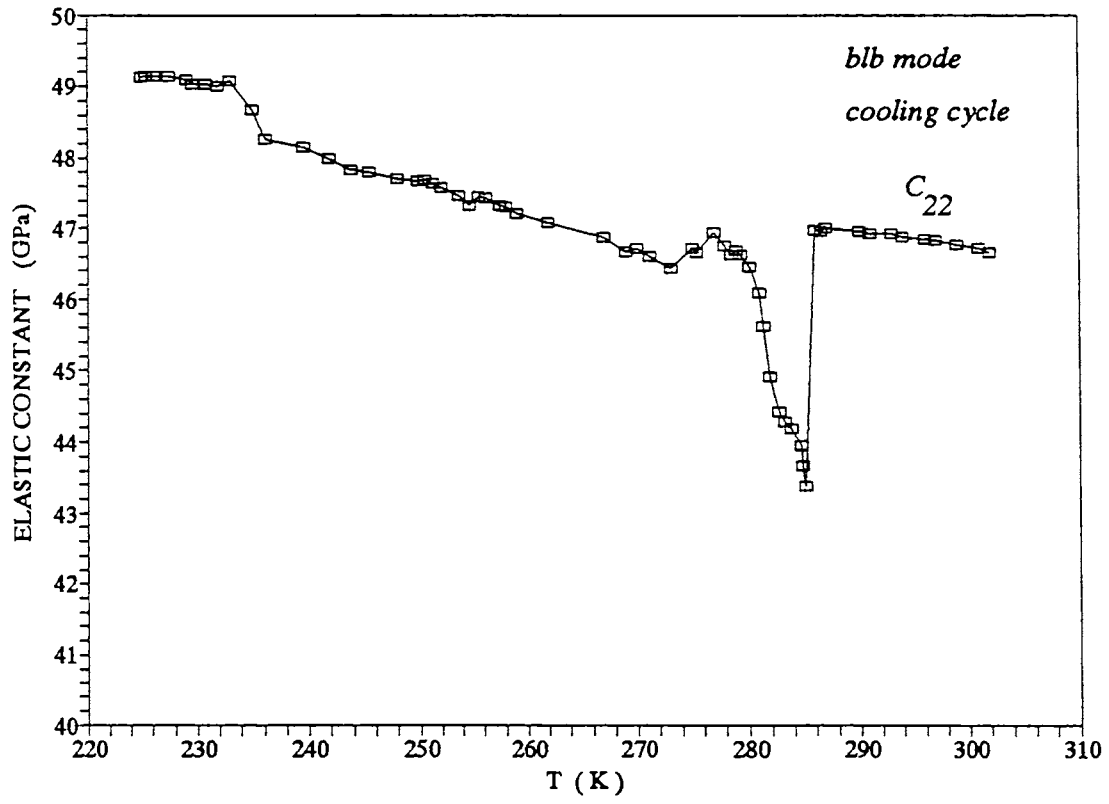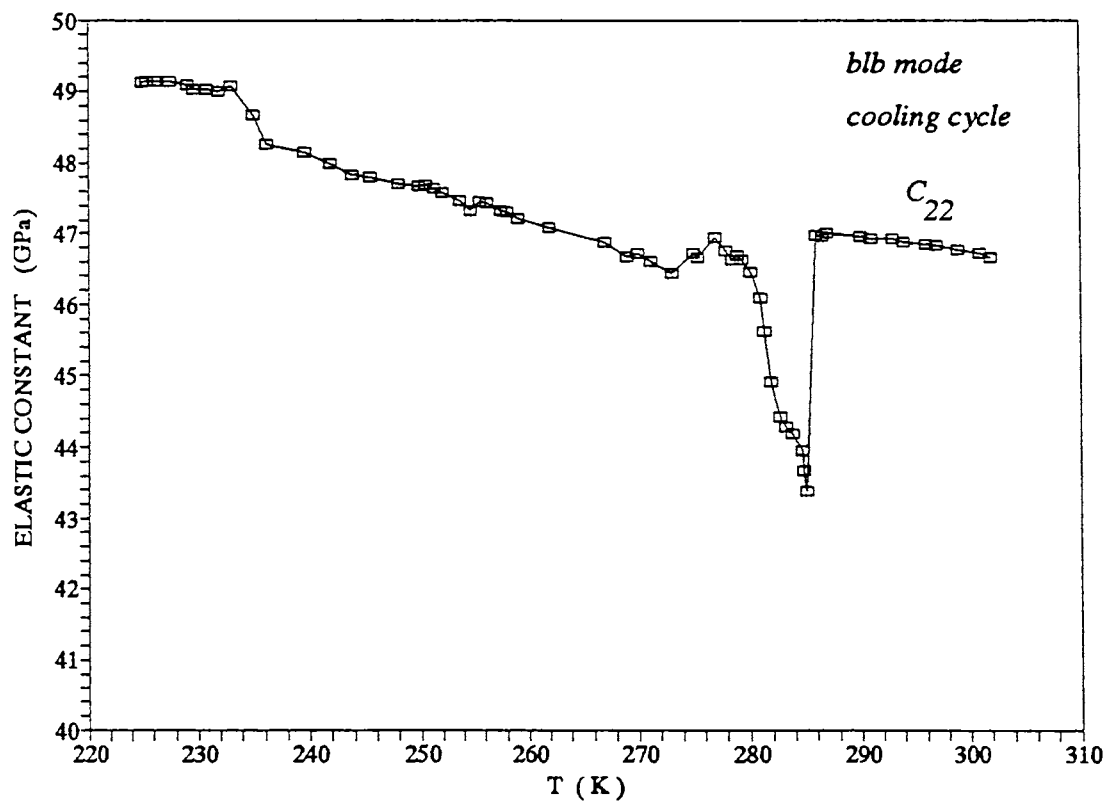the heating cycle of ala mode

188

Figure 5.8

Temperature variation of elastic constant of LAS for
the cooling cycle of blb mode

Figure 5.8

Temperature variation of elastic constant of LAS for
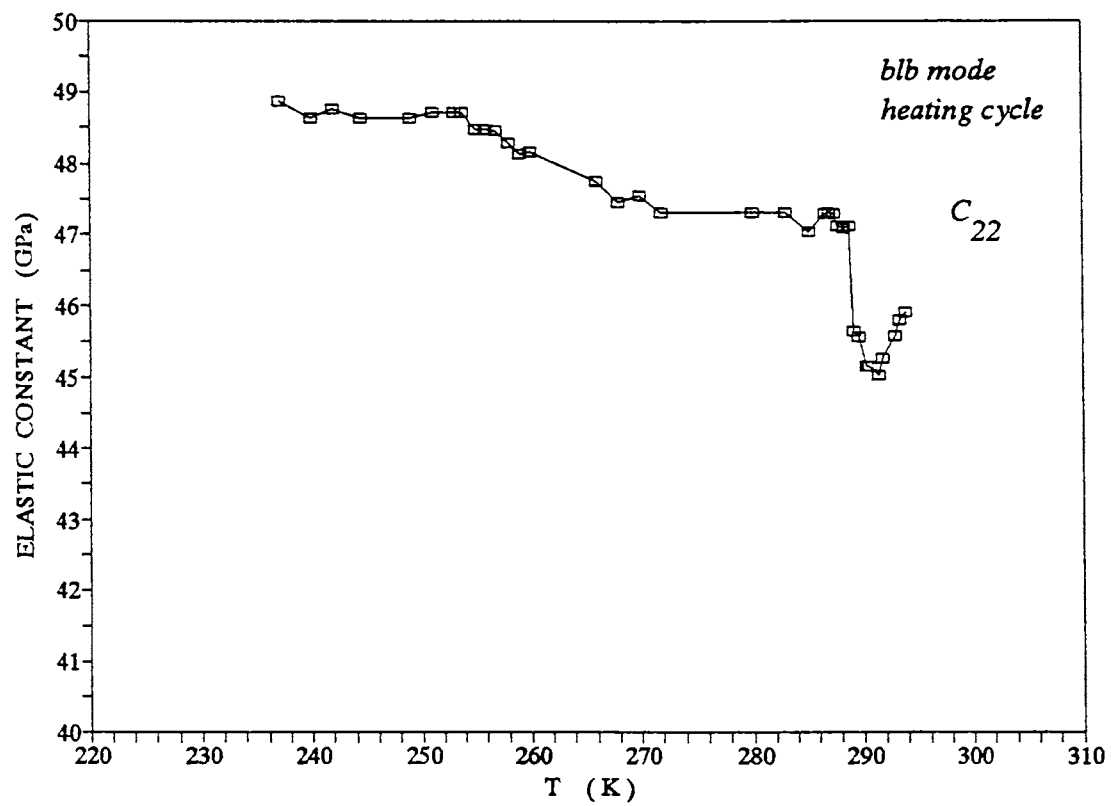the cooling cycle of blb mode

Figure 5.9

Temperature variation of elastic constant of LAS for
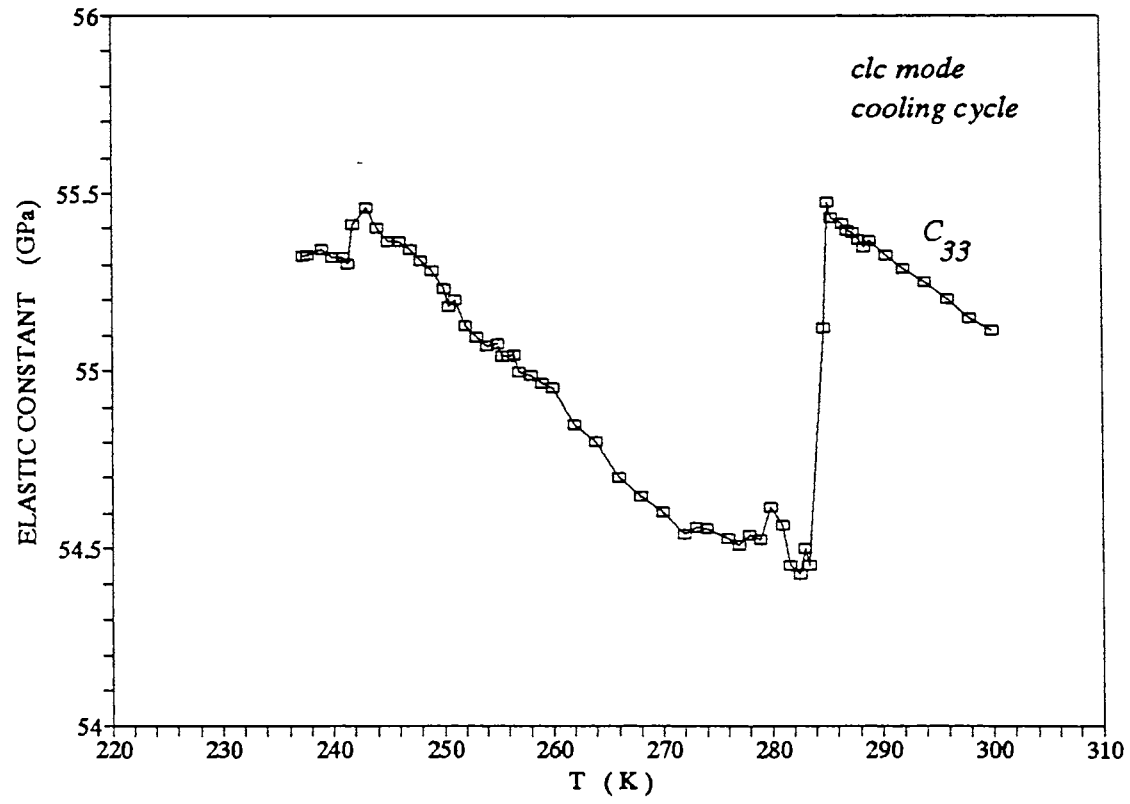the heating cycle of blb mode

Figure 5.10

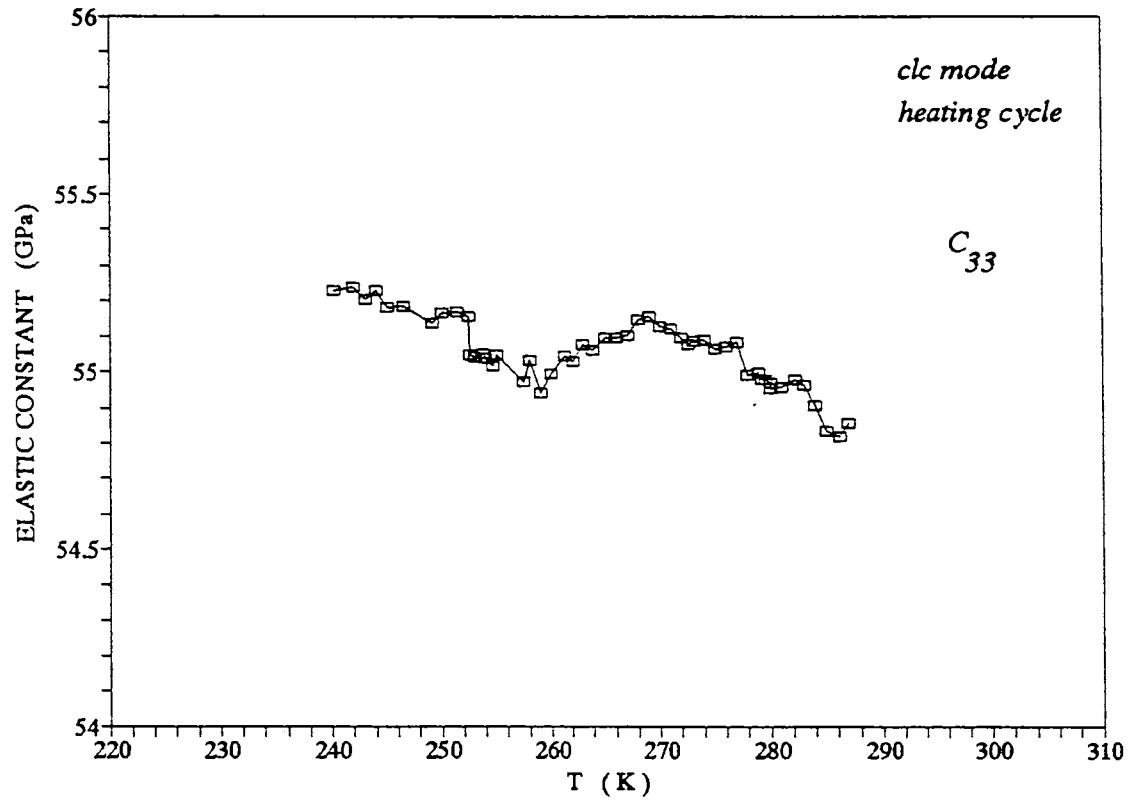Temperature variation of elastic constant of LAS for
the cooling cycle of clc mode

191

Figure 5.11

Temperature variation of elastic constant of LAS for
the heating cycle of clc mode

192

Figure 5.12

Temperature variation of elastic constant of LAS for
the cooling cycle of ctb mode

193

Figure 5.13

Temperature variation of elastic constant of LAS for the
heating cycle of ctb mode

194

Figure 5.14

Temperature variation of elastic constant of LAS for
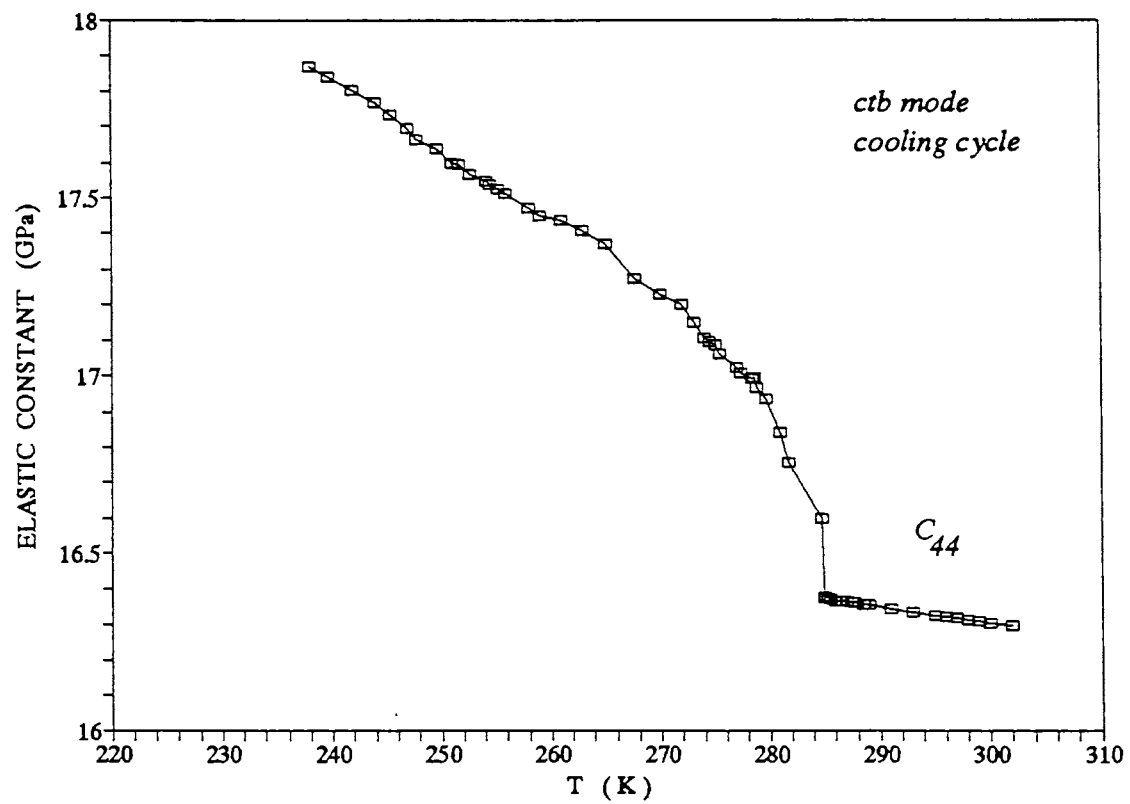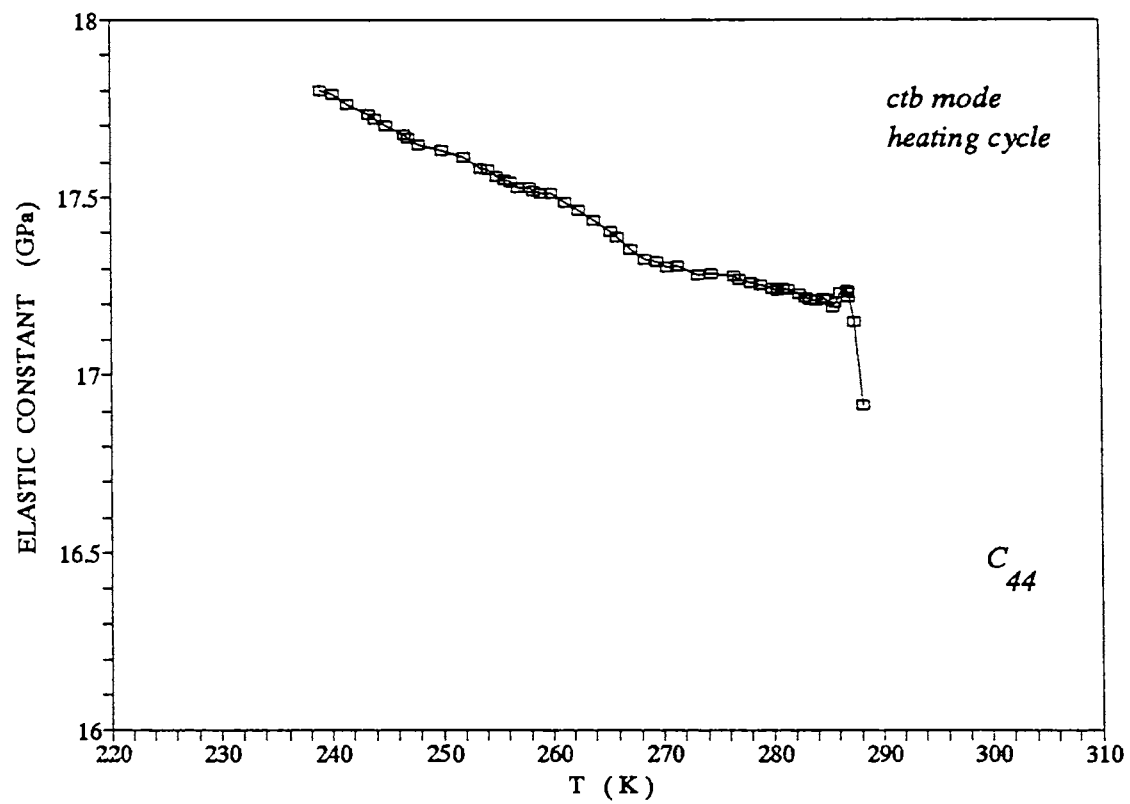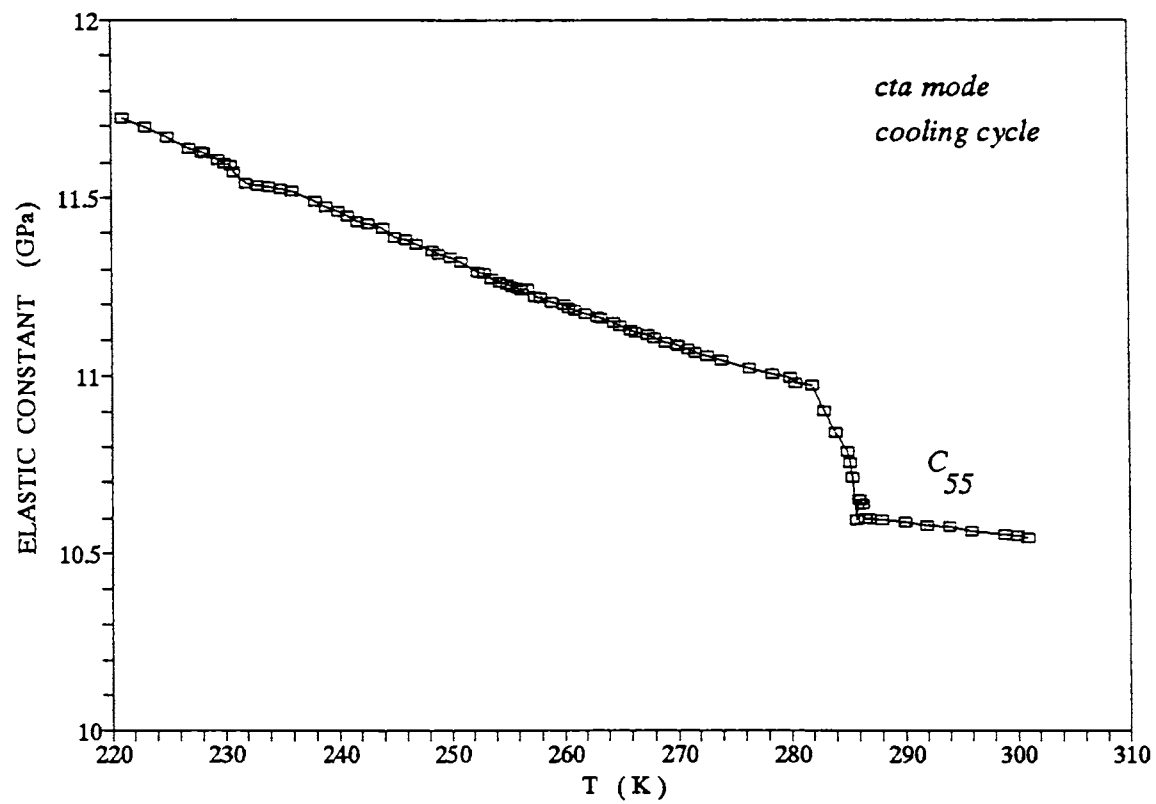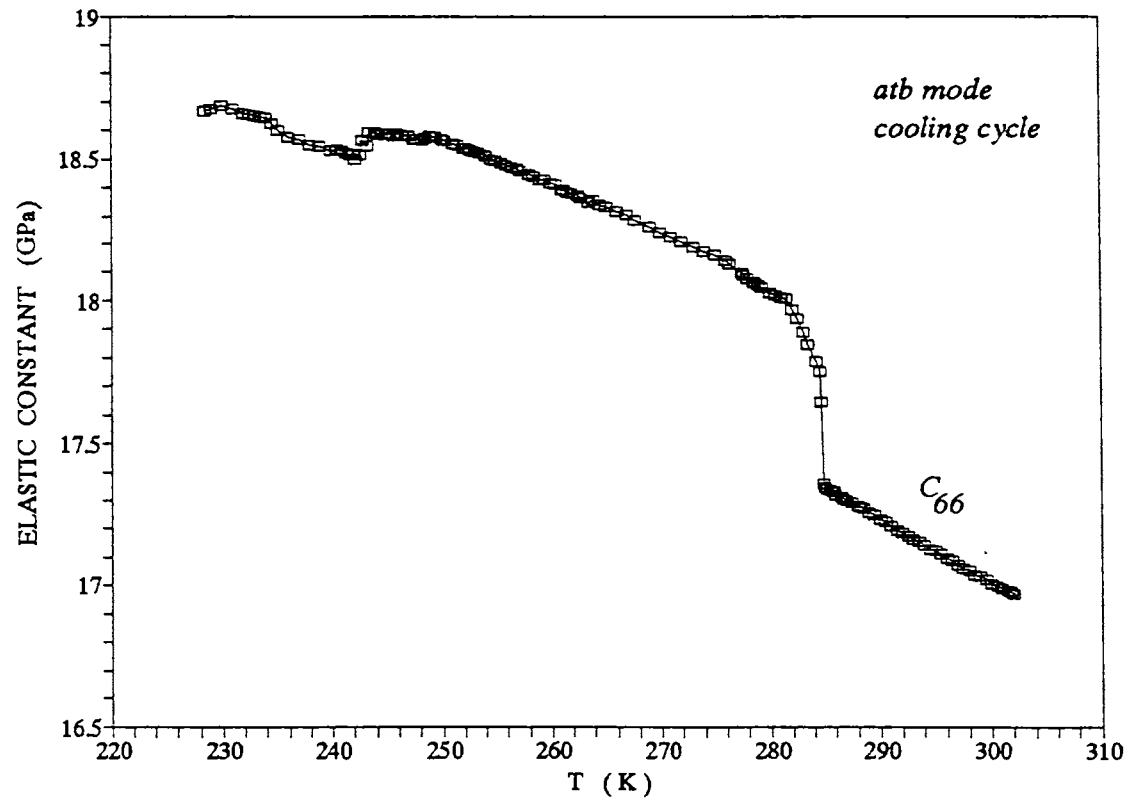the cooling cycle of cta mode

195

Figure 5.15

Temperature variation of elastic constant of LAS for the
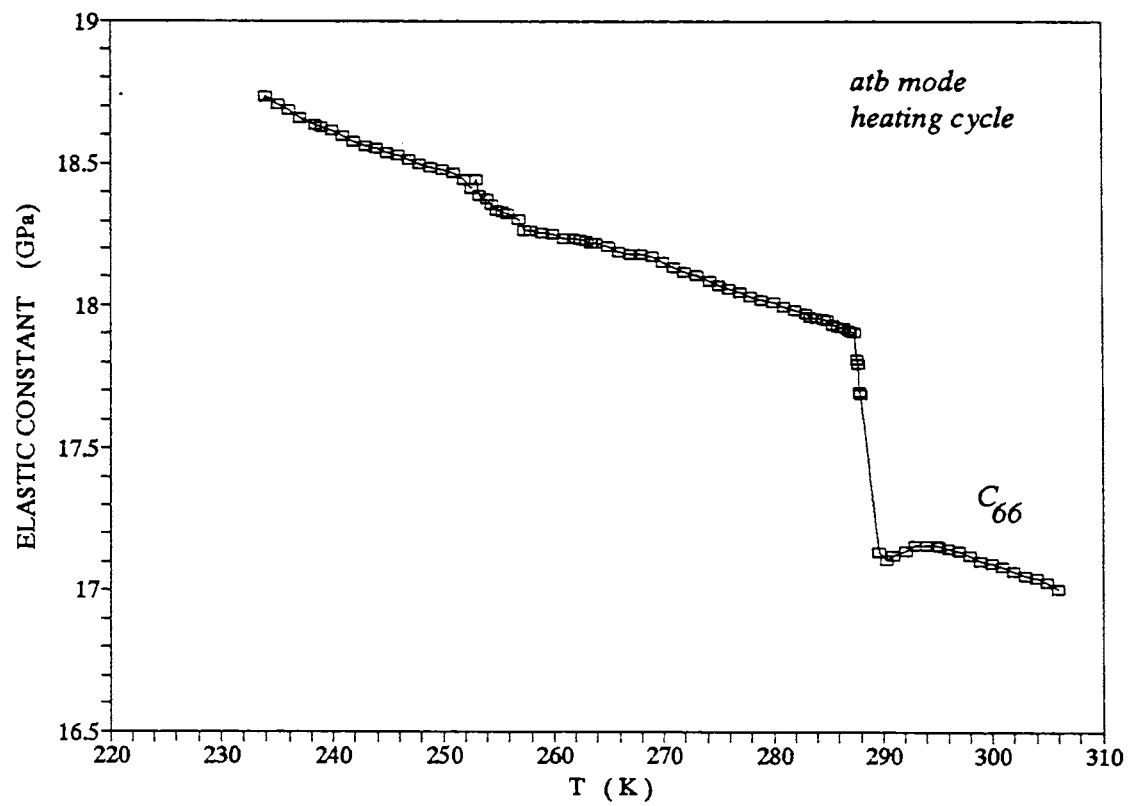cooling cycle of atb mode

196

Figure 5.16

Temperature variation of elastic constant of LAS for the
heating cycle of atb mode

197

combination constant in atb mode which appears as sudden dip at 242 K on cooling and a distinct slope change at 256 K on heating (Figures 5.15 and 5.16). Further a small slope change is also observed at 255 K in the heating cycle for the combination constant of blb mode (Figure 5.9). These anomalies are indicative of a phase transition occurring in LAS with a thermal hysteresis of about 14 K between the cooling and heating cycles.

Another weak anomaly can be noticed near 272 K for several modes during heating and cooling. For the ala mode a dip can be seen at 272 K during cooling cycle. For the blb mode an anomaly can be found at 272 K for both cooling and heating cycles. For clc mode there is a slope change on cooling and peak on heating can be found at this temperature. The ctb mode shows a slope change near this temperature on heating cycle. The atb mode shows a small slope change at 270 K on heating cycle. A characteristic of this anomaly is that it does not show any thermal hysteresis effect and is present during cooling and heating cycles. A phase transition at this temperature have not been reported or suspected previously by any workers. Examination of the experimental curves of previous workers reveals a correlation with the pyroelectric response curve of Gerbaux *et al* [5.7]. The pyroelectric signal observed in phase III is showing a continuous increase on heating and reaches a peak value near this temperature and thereafter it sharply falls to a zero value at 285 K transition and recovers after the transition. Thus the anomaly at 272 K can be connected with the temperature at which the pyroelectric response starts to fall on approaching the 285 K transition. It is tempting to argue that this anomaly is connected with the 285 K transition but the possibility of a new phase transition in LAS at 272 K cannot be ruled out.

a) Phase transition at 285 K

As has been reported by earlier workers, the phase transition at 285K is clearly a first order ferroelastic one. In the temperature dependence of elastic constants shown in Figures 5.6 to 5.16, one can notice a clear thermal hysteresis of $\approx$ 2.5K between the cooling and heating cycles. One expects this kind of a hysteresis in elastic constant values when a crystal undergoes a first order ferroelastic phase transition [5.24]. This small hysteresis can be attributed to the pinning of the ferroelastic domains when the sample is cycled through the transition. The elastic constant data obtained from Brillouin scattering experiments [5.11] do not show this hysteresis, probably because these authors did not make the measurements during cooling and heating cycles. This is the first time this hysteresis in elastic constant data is reported.

A Landau model describing the sequence of phase transitions occurring in LAS has been put forward by Torgashev *et al* [5.15]. Schranz *et al* [5.16,5.17] have theoretically analysed the possible couplings between strains and the order parameter involved. Mróz *et al* [5.11] have put forward a theoretical model for the ferroelastic phase transition in LAS focusing attention on the vicinity of the transition. After writing down the free energy expression and considering the strain e_5, one can show that the order parameter η is given by

$$\eta = [(C_{55}^0 + 2\ G_5\ P^2)/1\ ]\ e_5 \qquad\qquad (5.1)$$

where P is the polarization. The coupling between e_5 and P shifts the transition temperature by a constant value. With the transition to the ferroelastic phase (F), the polarization of the sample vanishes leading to a destabilization of the polarized phase. The effective second order elastic

coefficients experience a discontinuity at $T = T_c$ which is increased by the simultaneous disappearance of polarization. In the paraelastic phase (P), $e_5 \approx 0$ (not exactly zero due to coupling with polarization) and

$$C_{55}^P \cong 2(b_2 + \mu P_s^2) \tag{5.2}$$

whereas in the ferroelastic phase (F), the relevant combination constant is

$$C_{55}^F \cong 17b_2 \tag{5.3}$$

such that

$$\Delta C_{55} = C_{55}^F - C_{55}^P$$

$$\cong 15b_2 - 2\mu P_s^2 \tag{5.4}$$

The ferroelastic phase transition is driven by a two component soft mode which couples strongly to the spontaneous strains and to the polarization. Owing to the associated metastability of the phases, thermal hysteresis can be expected to occur. Similar theoretical formulations and arguments apply to the discontinuities exhibited by other strains. These discontinuities and thermal hysteresis are clearly seen in our elastic constant results shown in Figures 5.6 to 5.16. In our results, the thermal hysteresis is observed both for the transition temperature and for the elastic constants. The thermal hysteresis effect of elastic constants is more evident in longitudinal mode constants.

Above observation supports the presence of a metastable phase in LAS below 285 K. Evidence for the presence of a two phase system was also obtained by Smutny and Polomska [5.25] in their study on the effect of electric field on the phase

transition in LAS. A two phase system below the transition was also earlier reported by Aleksandrov *et al* [5.26]. Martins et al. [5.8], from their Raman scattering study, has recently concluded that the phase between 285 and 256 K is nonpolar but the pyroelectric signal obtained earlier by Gerbaux *et al* [5.7] in this temperature range shows that LAS is polar in this region. This discrepancy can be explained on the basis of a mixed phase system. The spontaneous deformation of ferroelastic Phase III may produce electric response via the hydrostatic piezoelectric effect along the two fold axis. Signals thus produced can be misinterpreted as pyroelectric response.

b) Phase transition at 256K

Both Gerbaux et.al. [5.7] and Martins et.al.[5.8] have proposed a phase transition taking place in LAS at 256K based on their infrared absorption, dielectric constant and Raman scattering measurements. Change in the slope of the dielectric constant curve [5.8] leads one to believe that the transition at 256K is second order and reversible. The anomalies seen in our elastic constant curves shown in Figures 5.9, 5.10, 5.11, 5.15 and 5.16 are indicative of a transition taking place between 240K and 260K. During the cooling cycle the anomaly is seen at 242K and during the heating cycle it appears at 256K indicating that there is a thermal hysteresis of $\approx$ 14K for this transition between the cooling and heating cycles. Gerbaux et.al. [5.7] and Martins et.al. [5.8] reported transition only at 256K, probably because these authors made their measurements only during the heating cycle. The thermal hysteresis of the temperature of this transition is evident in the differential scanning calorimetric curves reported by Chhor et al [5.20] but they have interpreted the transition temperature as 248 K which in fact is near the mean value of

242 and 256 K.

According to Martins et.al.[5.8], the transition at 256K (or 242K) is a diffuse order-disorder type one involving a reordering of the SO_4 ions. A similar type of mechanism has been proposed for the transition occurring in Lithium Potassium Sulfate crystal [5.27]. The oxygen atoms at the top of the SO_4 tetrahedra freeze in such a way that the symmetry of inversion of the phase is broken and the structure stabilizes with a symmetry belonging to the C_s^1 or C_s^2 space group. This transition is observed for the first time in elastic measurements in LAS and the thermal hysteresis of this transition is established for the first time

c) Modulated structure in LAS : A new model

The results of the previous investigations and our results suggest the need of a new model to resolve the controversies regarding the low temperature phase of LAS. In this model we propose the presence of a modulated structure below the 285 K transition. Earlier Poulet and Mathieu [5.18] on the basis of their Raman scattering experiment has proposed that the low temperature phase could be a modulated one. This idea did not receive much attention after that.

Present ultrasonic investigation shows some difference in elastic behaviour with Brillouin scattering investigation [5.11]. While the ultrasonic results show some anomalous variations near the 285 K transition the Brillouin results show temperature independent straight line curves with step like discontinuities at the transition temperature. While ultrasonic technique is a low frequency technique, Brillouin scattering technique is a very high frequency technique and this difference in behaviour can be interpreted as frequency dispersion of elastic constants. This frequency dispersion of elastic constant is a characteristic feature of an

incommensurate transition [5.28]. Therefore we propose that LAS is undergoing an incommensurate transition at T_I = 285 K or at 272 K where we find an anomaly in many modes. According to this picture the transition at 285 K can still be ferroelastic one and between 285 and 272 K LAS is nonpolar and at 272 K the incommensurate transition takes the crystal to an incommensurate ferroelastic state. If there is no transition at 272 K then the crystal must be entering the incommensurate ferroelastic state at 285 K itself and the elastic anomaly at 272 K may be related to the incommensurate ferroelastic transition at 285 K. In this phase a mixed phase like behaviour can be observed due to the ferroelastic modulation. This modulation can give rise to spatially periodic strain or polarization which can be influenced by external stress or electric fields. The modulation period and amplitude can change with temperature. The pyroelectric signals observed by Gerbaux *et al* [5.7] can be explained by this temperature dependent periodic polarization. The mixed phase model is no longer required to explain the polar-nonpolar controversy.

Next we propose that the transition at 256 K is the incommensurate to commensurate phase transition or lock in transition T_c which takes LAS to a cell doubled antiferroelastic phase. Thermal hysteresis of the commensurate transition temperature (T_c) is observed in a number of crystals which show incommensurate phase [5.29]. In LAS we have established that the transition is taking place at 242 K on cooling and at 256 K on heating which shows a clear thermal hysteresis of 14 K. Weak, higher order and diffuse behaviour of this transition further supports the view that this transition is an incommensurate to commensurate transition.

Evidence for an antiferro order below the 256 K transition can be first found in the work of Martins *et al* [5.8]. They have found that below 256 K transition there is a modification of the structure leading to two distinct sites

203

for the SO_4 unit. They proposed that the phase below 256 K can be a modulated phase going to a locked phase around 100 K. But no lock-in transition have been reported near 100 K. We propose that the two distinct site for SO_4 found by them is due to the antiferroelastic order.

Martins *et al* [5.8] have described phase below 256 K as polar belonging to C_s^1 or C_s^2 space group with no cell doubling. This was in discordance with the X-ray results (at 213 K) of Kruglik *et al* [5.4] who described this phase as nonpolar C_{2h}^5 space group with cell doubling. Recent X-ray structure refinement of LAS by Mashiyama and Kasano [5.21] confirms the low temperature (at 190 K) space group as C_{2h}^5 with cell doubling. Further they have found the low temperature phase as a periodically aligned micro-domain structure with alternating polarization. The modulated phase proposed by Martins *et al* [5.8] from 256 K to 100 K if present would have been found in the refined X-ray work at 190 K [5.21]. On the other hand the recent X-ray result [5.21] that the low temperature phase at 190 K is a periodically aligned micro-domain structure with alternating polarization, is consistent with our model which propose a commensurate antiferroelastic order below 256 K (or 242 K).

The new model discussed above have been mainly based on qualitative arguments and the correctness of it can be established only by further experiments and theoretical formulations.

5.4 Conclusions

In this chapter the measured values of the elastic constants of LAS and the results of low temperature phase transition study in LAS are presented. All the nine elastic constants of orthorhombic LAS are accurately determined and tabulated. Measured velocities in 12 modes of propagation are

also presented in a table. A conversion table is presented to clarify the problem of different choice of axes adopted by different workers. With the help of this table the previous measurements of elastic constants of LAS could be compared correctly with the present values. Using the measured elastic constants the velocity surfaces of LAS are computed in the three orthogonal symmetry planes and the plots are presented.

Temperature variation study of elastic constants are performed for 6 different modes of propagation during cooling and heating cycles.

Our measurements establish a soft mode driven ferroelastic phase transition at 285.5 K which is characterized by a thermal hysteresis of 2.5 K. The observed hysteresis in elastic constants is in accordance with the predictions of the Landau theory. Our experimental results establish an order-disorder type phase transition occurring in LAS at 242 K during the cooling cycle and at 256 K during the heating cycle which is detected for the first time in elastic constant measurements. The 14 K thermal hysteresis of this transition is established for the first time. Based on our results and the earlier workers, the successive phase transitions exhibited by LAS can be redrawn as shown in Figure 5.17. These results indicate that LAS is another interesting member of the sulfate family exhibiting a sequence of phase transitions as the temperature is varied.

Finally, we have proposed a new model for the presently observed low temperature phase transitions in LAS. According to this model an incommensurate ferroelastic phase is proposed below the 285 K transition and the transition at 256 K is considered as a lock in transition to an antiferroelastic order. The new model could resolve some controversies but it was concluded that further research is required to establish the incommensurate phase.

Cooling cycle   Heating cycle

Phase I   Phase I

460 K ↓ Ferroelectric

Phase II

285.5 K ↓ Ferroelastic   288 K

Phase III

242 K ↓ Order-disorder   256 K
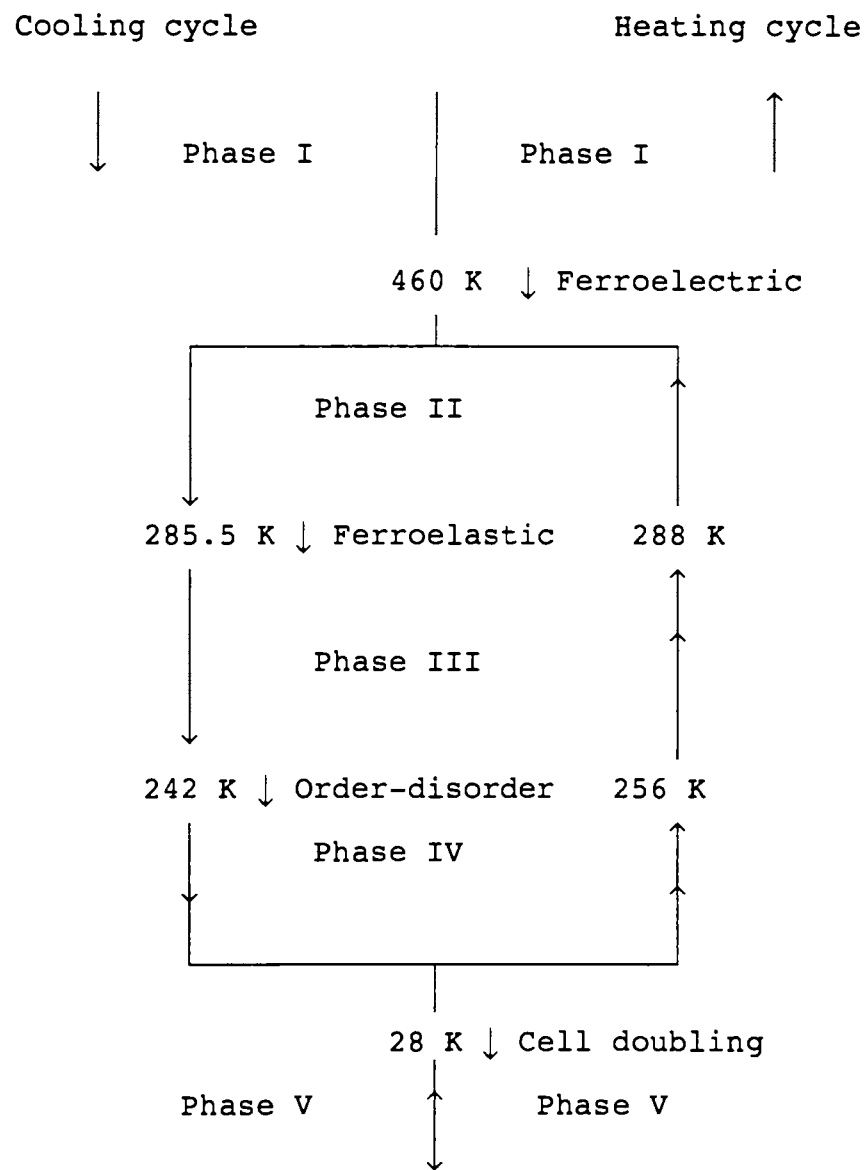
Phase IV

28 K ↓ Cell doubling

Phase V   Phase V

Figure 5.17

Modified sequence of phase transitions in LAS

References

5.1 R. Pepinsky, K. Vedam, Y. Okaya and S. Hoshino, Phys. Rev. B $\underline{111}$, 1467 (1958)

5.2 W. A. Dollase, Acta Cryst. B $\underline{25}$, 2298 (1969)

5.3 K. S. Aleksandrov, I. P. Aleksandrova, L. I. Zherebtsova, A. I. Kruglik, A. I. Krupnyi, S. V. Melnikova, V. E. Shneider, and L. A. Shuvalov, Akad. Nauk SSR $\underline{39}$, 943 (1975) [Bull. Acad. Sci. USSR, Phys. Ser. $\underline{39}$, 44 (1975)] /Lithium ammonium sulfate: the first pyroelectric ferroelastic/

5.4 A. I. Kruglik, M. A. Simonov, and K. S. Aleksandrov, Kristallografia $\underline{23}$, 494 (1978) [Sov. Phys. Crystallogr. $\underline{23}$, 274 (1978)] /Crystal structure of the low temperature III phase of lithium ammonium sulfate/

5.5 B. O. Hildmann, Th. Hahn, L. E. Cross, and R. E. Newnham, Appl. Phys. Lett. $\underline{27}$, 103 (1975)

5.6 T. Simonson, F. Denoyer, and R. Moret, J. Physique $\underline{45}$, 1257 (1984)

5.7 X. Gerbaux, J. Mangin, A. Hadni, D. Perrin, and C. D. Tran, Ferroelectrics $\underline{40}$, 53 (1982) /Electrical properties and infrared spectra of $LiNH_4SO_4$ between 4 and 300 K/

5.8 A. R. M. Martins, F. A. Germano, J. Mendes Filho, F. E. A. Melo, and J. E. Moreira, Phys. Rev. B $\underline{44}$, 6723 (1991) /Phase transitions in $LiNH_4SO_4$ below room temperature/

5.9 I. Yamamoto, A. Hiroe, and S. Hirotsu, J. Phys. Soc. Japan $\underline{52}$, 920 (1983) /Anomalous temperature dependence of the intensity of Brillouin scattering near the ferroelectric phase transition point of NH_4LiSO_4/

5.10 Y. Luspin, G. Hauret, and A. M. Gillet, Ferroelectrics $\underline{65}$, 1 (1985)

5.11 B. Mróz, J. A. Tuszynski, H. Kiefte, and M. J. Clouters, J. Phys. Condens. Matter $\underline{1}$, 783 (1989) /On the ferroelastic phase transition of $LiNH_4SO_4$: a Brillouin scattering study and theoretical modelling/

5.12 R. Wyslouzil, W. T. Schranz, A. H. Fuith, and H. Warhanek, Z. Phys. B - Condensed Matter $\underline{64}$, 473 (1986) /The elastic stiffness constants of $\beta-NH_4LiSO_4$ around its phase transition at 460 K/

5.13 S. Hirotsu, Y. Kunii, I. Yamamoto, M. Miyamoto, and T. Mitsui, J. Phys. Soc. Japan $\underline{50}$, 3392 (1981) /Brillouin scattering study of the ferroelectric phase transition in NH_4LiSO_4/

5.14 S. Hirotsu, Ferroelectrics $\underline{52}$, 25 (1983) /Brillouin scattering study of ferroelectric NH_4LiSO_4: relaxation time and anomalous temperature dependence of elastic constants/

5.15 V. I. Torgashev, V. Dvorák, and F. Smutny, Phys. Status Solidi b $\underline{126}$, 459 (1984) /On Phase Transitions in $LiNH_4SO_4$/

5.16 W. T. Schranz, A. Fuith, H. Kabella, and H. Warhanek, Ferroelectrics Lett. $\underline{7}$, 37 (1987)

5.17 W. T. Schranz, K. Parlinski, H. Warhanek, and K. Zabinska, J. Phys. C: Solid State Phys. $\underline{20}$, 5045 (1987) /Elastic Constant behaviour of $LiNH_4SO_4$ above 460 K/

5.18 H. Poulet and J. P. Mathieu, Solid State Commum. $\underline{21}$, 421 (1977) /Polarized Raman study of lattice modes and the $10°C$ phase transition of β-lithium ammonium sulphate/

5.19 V. I. Torgashev, Yu. I. Yuziuk, F. Smutny, and M. Polomska, Kristallografiya $\underline{31}$, 951 (1986) [Sov. Phys. Crystallogr. $\underline{31}$, 565 (1986)]

5.20 K. Chhor, L. Abello, and C. Pommier, J. Phys. Chem. Solids $\underline{50}$, 423 (1989) /Low temperature calorimetric and Raman spectrometric studies on lithium ammonium sulphate, $LiNH_4SO_4$/

5.21 H. Mashiyama, H. Kasano: J. Phys. Soc. Japan $\underline{62}$, 155 (1993) /Refined crystal structure of $LiNH_4SO_4$ including hydrogen atoms in phase II and III/

5.22 Standards committee, Proc. IRE $\underline{37}$, 1378 (1949)

5.23 J. R. Neighbours, G. E. Schacher: J. Appl. Phys. $\underline{38}$, 5366 (1967)

5.24 P. Toledano, M. M. Fejer, B. A. Auld: Phys. Rev. B $\underline{27}$, 5717 (1983) /Nonlinear elasticity in proper ferroelastics/

5.25 F. Smutny and M. Polomska, Phys. Stat. Sol. a $\underline{82}$, k33
(1984)
/Effects of electric field on the II-III phase transition
in lithium ammonium sulphate and its deuterated analog/

5.26 I. P. Aleksandrova, I. S. Kabanov, S. V. Mel'nikova, T.
I. Chekmasova, and V. I. Yuzvak, Kristallografiya $\underline{22}$, 321
(1977) [Sov. Phys. Crystallogr. $\underline{22}$, 182 (1977)
/Nature of phase transitions in lithium ammonium sulfate/

5.27 A. J. Oliveira, F. A. Germano, J. Mendes Filho, F. E. A.
Melo, and J. E. Moreira, Phys. Rev. B $\underline{38}$, 12633 (1988)
/Phase transitions in $LiKSO_4$ below room temperature/

5.28 R.Blinc, P. Prelovsek, V. Rutar, J. Seliger, S. Zumer: in
Incommensurate phases in dielectrics I, ed. by R. Blinc
and A. P. Levanyuk (North Holland, Amsterdam 1986) p.143
/Experimental observations of incommensurate phases/

5.29 V. V. Lemanov, S. K. Esayan: Ferroelectrics $\underline{73}$, 125
(1987)   /Ultrasonic study of incommensurate phase
transitions in ferroelectrics/

CHAPTER 6

ELASTIC PROPERTIES AND PHASE TRANSITION IN
LITHIUM POTASSIUM SULPHATE

6.1 Introduction

Lithium potassium sulphate (LPS), $LiKSO_4$, is a very extensively studied crystal. It exhibits a sequence of very interesting phase transitions as the temperature is varied from 20 K to 998 K (melt) [6.1,6.2]. A variety of experimental techniques such as thermal expansion [6.3], Raman scattering [6.1,6.4,6.5,6.6], dielectric constant [6.1,6.7,6.8], ferroelectricity [6.9], piezoelectricity [6.10], X-ray diffraction [6.11,6.12], ESR [6.13,6.14,6.15], thermal analysis [6.16], Neutron scattering [6.17], Brillouin scattering [6.18-6.21], Ultrasonics [6.2,6.22] etc. have been used to investigate the properties and behaviour of this crystal as the temperature is varied. The interest in this crystal is because of its pyroelectric and ferroelectric behaviour, electro-optic effect [6.23], the large number of phase transitions, and observation of incommensurate lattice phase in certain temperature regions. The series of phase transitions observed in LPS is said to be very peculiar [6.24]. There are phase transitions at high temperature at first from paraphase towards a state with commensurate, and then with incommensurate modulation [6.25,6.26]. In this state LPS is simultaneously ferroelastic [6.27,6.28] and superionic [6.21,6.29]. Up to the present, the crystal symmetry and structure of the modulated phase as well as the phase transition temperatures are not well established [6.22,6.30].

In the range from room temperature to 708 K , LPS has hexagonal symmetry and belongs to the space group C_6^6 ($P6_3$) with two molecules per unit cell. Below room temperature, LPS

undergoes a number of phase transitions. In spite of the many investigations done on LPS there are still inconsistent results concerning the low temperature phase transitions [6.2]. The sequence of phases [6.1,6.2] starting from melt is shown in Figure 6.1. The phase transitions in LPS shows large thermal hysteresis and the transition temperatures shown in the Figure 6.1 are not well established.

The elastic properties of LPS have been studied before using Brillouin scattering [6.18-6.21,6.31] and acoustic techniques [6.2,6.22,6.32]. Elastic properties have also been investigated earlier by resonance antiresonance technique [6.10,6.15] and torsion pendulum method [6.33].

Drozdowski et al [6.18] have reported the room temperature value of elastic constants C_{11}, C_{33}, and C_{66} of LPS at room temperature measured by Brillouin scattering technique. The numerical value they found for C_{66} was unusually high. Later Pimenta et al [6.19] measured the elastic constants C_{11}, C_{33}, C_{44}, C_{66} and deducted the value of C_{12} using the relation $C_{12} = C_{11} - 2C_{66}$ of LPS at room temperature. They found that C_{66} is not as high as reported by Drozdowski et al [6.18]. Kabelka and Kuchler [6.2] made the first ultrasonic determination of the elastic constants of LPS along with their low temperature study. They have measured all the constants reported by Pimenta et al [6.19] and compared their values with that of Pimenta et al [6.19]. We find that in all the above measurements the independent elastic constant C_{13} of LPS have not been measured. Thus, surprisingly the complete set of 5 independent elastic constants of this widely investigated crystal is not available in literature.

Drozdowski et al [6.18] have reported a phase transition occurring in this crystal around 333 K (60°C) from their Brillouin scattering measurements. They have reported that the elastic constants C_{22}, C_{33} and C_{66} undergo anomalous changes at this temperature indicative of a phase transition.

melt

998 K ↓ ↑

hexagonal

948 K ↓ ↑

orthorhombic, ferroelastic

743 K ↓ ↑

incommensurate ?

709 K ↓ ↑

Hexagonal, $P6_3$ (C_6^6)

pyroelectric

207 K ↓ , 245 K ↑

Hexagonal $P6_3mc$ (C_{6v}^4)

or trigonal $P31c$ (C_{3v}^4)

ferroelectric

185 K ↓ , 190 K ↑

orthorhombic $Cmc2_1$ (C_{2v}^{12})

or monoclinic Cc (C_5^4)

or triclinic

ferroelastic

20 K ↓ , 30 K ↑

(?)

Figure 6.1

Sequence of phase transitions in $LiKSO_4$

213

Later Brillouin scattering study of Pimenta *et al* [6.19] could not detect any anomaly in elastic constants at this temperature. But Wan Ji-fang *et al* [6.32], from their ultrasonic studies, reported that there is an abrupt change of C_{33} near 333 K with large temperature hysteresis and that the peak of C_{33} reduces with successive heating and cooling. On examining early investigations, we find that there is a dip at 333 K in the thermal expansion coefficient curve of LPS in the a-axis direction which was reported by Sharma [6.3].

The purpose of the present investigation is twofold:

(i) To determine all the 5 independent elastic constants of LiKSO$_4$ at room temperature.

(ii) To determine whether there is a phase transition in LiKSO$_4$ at 333 K by measuring the temperature variation of all the 5 independent elastic constants of LPS and ultrasonic attenuation in the temperature interval from 300 K to 370 K.

Ultrasonic velocity and attenuation measurements are more sensitive than Brillouin scattering in detecting phase transitions. We have measured all the 5 independent elastic constants of LPS at room temperature and performed temperature variation study of the elastic constants and attenuation in the range 300 to 370 K. The experimental details and the results obtained are outlined in the following sections.

6.2 Elastic constants of LPS

6.2.1 Sample preparation

LiKSO$_4$ single crystals were grown from equimolar mixture of Li_2CO_3 and $KHSO_4$ dissolved in distilled water. On mixing, the following reaction takes place

$$2KHSO_4 + Li_2CO_3 \longrightarrow 2LiKSO_4 + H_2O + CO_2$$
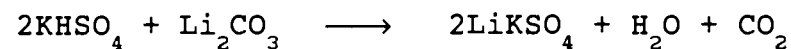
Crystals obtained from the solution prepared in the above

method was found to be of good quality than from the method of making LiKSO$_4$ by mixing equimolar mixture of Li$_2$SO$_4$ and K$_2$SO$_4$. The crystals were grown at 311 K from a seed crystal by constant temperature solvent evaporation method. The apparatus used for this have been described in Section 2.4. The solution was stirred in opposite directions while the growth was in progress. Large single crystals of good optical quality with typical sizes of about 3 cm in a and c directions were obtained over a period of 45 days. The grown crystals were having well developed faces perpendicular to [100], [001] and [101] directions, as shown in Figure 6.2.

The grown crystals were accurately cut using a slow speed diamond wheel saw so as to have propagation direction along [100], [001] and [101] directions. The cut crystals were carefully polished to optical reflection level. The cut samples were having thickness in the range 1 to 2 cm in the propagation direction.

The following choice of axes have been taken for the ultrasonic study: the [001] axis is the hexagonal one, [100] axis is in the basal plane and perpendicular to a natural face of the crystal and [010] axis is in the basal plane and perpendicular to both others. The X-ray parameters are a = 5.147 Å and c = 8.633 Å [6.34]. The density of the crystal was measured by Kabelka and Kuchler [6.2] as 2.396 gm/cm^3. This value of the density was used in the present experiments.

6.2.2 Velocity measurements and elastic constants of LPS

The velocity of longitudinal and transverse ultrasonic waves of frequency 10 MHz propagating along the symmetry directions have been measured accurately by ultrasonic pulse echo overlap method. The details of the experimental setup were discussed in Section 2.2. and specific details of velocity measurement and bonding of transducer etc. were
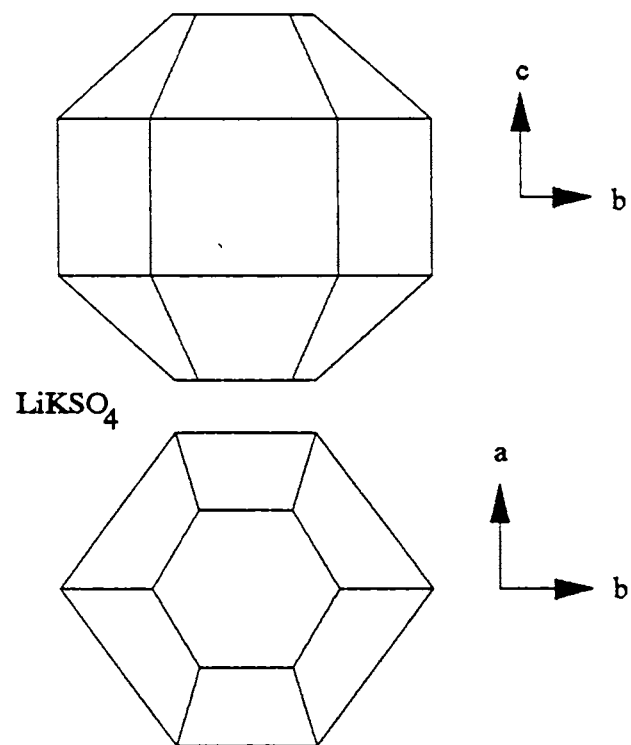
LiKSO$_4$

Figure 6.2

Morphology of LiKSO$_4$ crystal

216

discussed in Section 3.4 in connection with measurement in LHS. Bond correction and correct overlap identification have been done using the computer program discussed in Section 2.3. The general method for determining all the 5 independent elastic constants of an Hexagonal crystal was discussed in Section 1.3.3. The number of nonzero elastic constants of orthorhombic and hexagonal crystals are the same. But for orthorhombic all the 9 elastic constants are independent while for hexagonal only 5 are independent.

We have carried out measurements on a total of 6 modes in LPS from which all the 5 independent elastic constants have been deduced. Misorientations in the cut directions were less than $1°$. The absolute accuracy of the measurement is better than 1%. The results of the velocity measurements and the computed values of elastic constants for various modes of propagation are presented in Table 6.1.

In Table 6.2, we compare the values of elastic constants measured by previous investigators [6.2,6.18,6.19] with the presently measured values. Our values are in good agreement with previous reports [6.2,6.19] except with the measurements of Drozdowski *et al* [6.18] whose accuracy have been questioned earlier by Pimenta *et al* [6.19].

The numerical value of constant C_{13} is reported for the first time. This elastic constant of LPS was deduced from the quasilongitudinal mode velocity in the [101] direction as indicated in Table 6.1. The elastic constant C_{12} of hexagonal symmetry is not an independent elastic constant since it can be calculated from the value of C_{11} and C_{66} using the relation $C_{12} = C_{11} - 2C_{66}$. Present measurements provide the complete set of elastic constants of LPS.

6.2.3 Velocity surfaces of LPS

The phase velocity surfaces of LPS can be plotted by

Table 6.1

Measured ultrasonic velocities and the elastic constants
of Lithium potassium Sulphate at 300 K

No.	Mode	Direction of particle motion	Velocity measured (v) km/s	Elastic constant GPa (ρv^2)	Involved elastic constant

Propagation along a-axis

No.	Mode	Direction	Velocity	Elastic constant	Involved elastic constant
1	L	a	4.8878	57.24	$C_{11} = C_{22} = \rho v^2$
2	T	b	2.4418	14.29	$C_{66} = \rho v^2$
3	T	c	2.9961	21.51	$C_{44} = C_{55} = \rho v^2$

Propagation along c-axis

No.	Mode	Direction	Velocity	Elastic constant	Involved elastic constant
4	L	c	5.3019	67.35	$C_{33} = \rho v^2$
5	T	a	2.9962	21.51	$C_{44} = C_{55} = \rho v^2$

Propagation in a-c plane, [101] direction, angle $\theta = 59.20°$

No.	Mode	Direction	Velocity	Elastic constant	Involved elastic constant
6	QL	⊥ to b	5.0577	61.29	$C_{13} = C_{23} = f_{ac}$
				$C_{13} = C_{23} = 22.37^†$	

†Calculated value using formula given below

$$f_{ac} = \left[\frac{\left(s^2 C_{11} + c^2 C_{44} - \rho v^2 \right) \left(s^2 C_{44} + c^2 C_{33} - \rho v^2 \right)}{c^2 s^2} \right]^{\frac{1}{2}} - C_{44}$$

$s = \sin \theta$, $c = \cos \theta$

$C_{12} = C_{11} - 2C_{66} = 28.66$ GPa

$\rho = 2.396$ gm/cm^3 for LPS [6.2]

Table 6.2

Elastic constants (in GPa) of $LiKSO_4$ in comparison with previous measurements.

C_{ij}	Present study[*] (1994)	Kabelka & Kuchler [6.2] (1988)	Pimenta *et al* [6.19] (1986)	Drozdowski *et al* [6.18] (1983)
C_{11}	57.24	55.0	57.4	51.6
C_{12}	28.66	26.4	29.2	–
C_{13}	22.37	–	–	–
C_{33}	67.35	67.3	67.3	59.3
C_{44}	21.51	20.5	21.1	–
C_{66}	14.29	14.3	14.2	57.0

[*] Absolute accuracy better than 1%

similar computation and plotting operations as has been done for LHS and LAS. The details of the method and required equations were presented in Section 3.6. The required expressions for velocities in hexagonal symmetry were derived and presented in Section 1.2.2. For hexagonal system the acoustic wave propagation has circular symmetry for directions that rotate about the c-axis. Thus the velocity surfaces in a-b plane will be concentric circles. Similarly there will be no difference between the velocity surfaces in the a-c and b-c planes. Further, all the modes in the a-b plane are pure modes.

The velocity surfaces in the a-b plane for LPS is shown in Figure 6.3. V_0 is a pure shear mode polarized parallel to c-axis. V_2 is a pure shear mode polarized normal to c-axis and V_1 is a pure longitudinal mode.

The velocity surfaces in the a-c plane is shown in Figure 6.4. Here, V_0 is a pure shear mode polarized normal to the a-c plane. V_1 is a quasilongitudinal mode and V_2 is a quasishear mode. It may be noted that these surfaces are rotationally invariant for rotations about the c-axis and hence the three dimensional surface generated by the rotation of these curves about the c-axis gives the full three dimensional velocity surface of LPS.

The three velocities in any direction in the crystal can be found from the velocity surfaces plotted in Figure 6.4. The graphs have been plotted with a scale of 1 cm for 1 km/s of velocity.

6.3 Investigation of suspected phase transition in LPS

6.3.1 Ultrasonic measurements

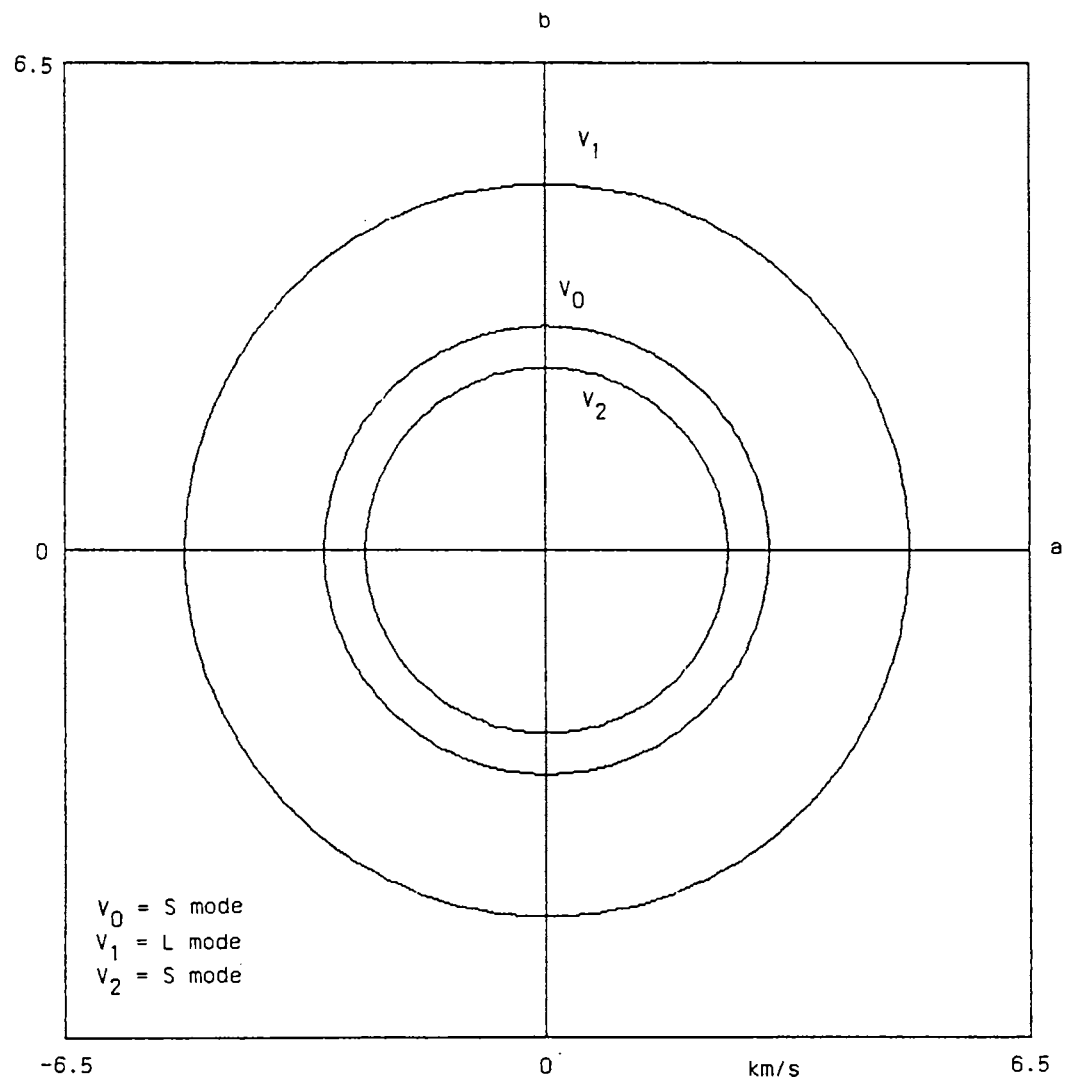The temperature variation of all the elastic constants have been measured from room temperature to 370 K by keeping

Figure 6.3

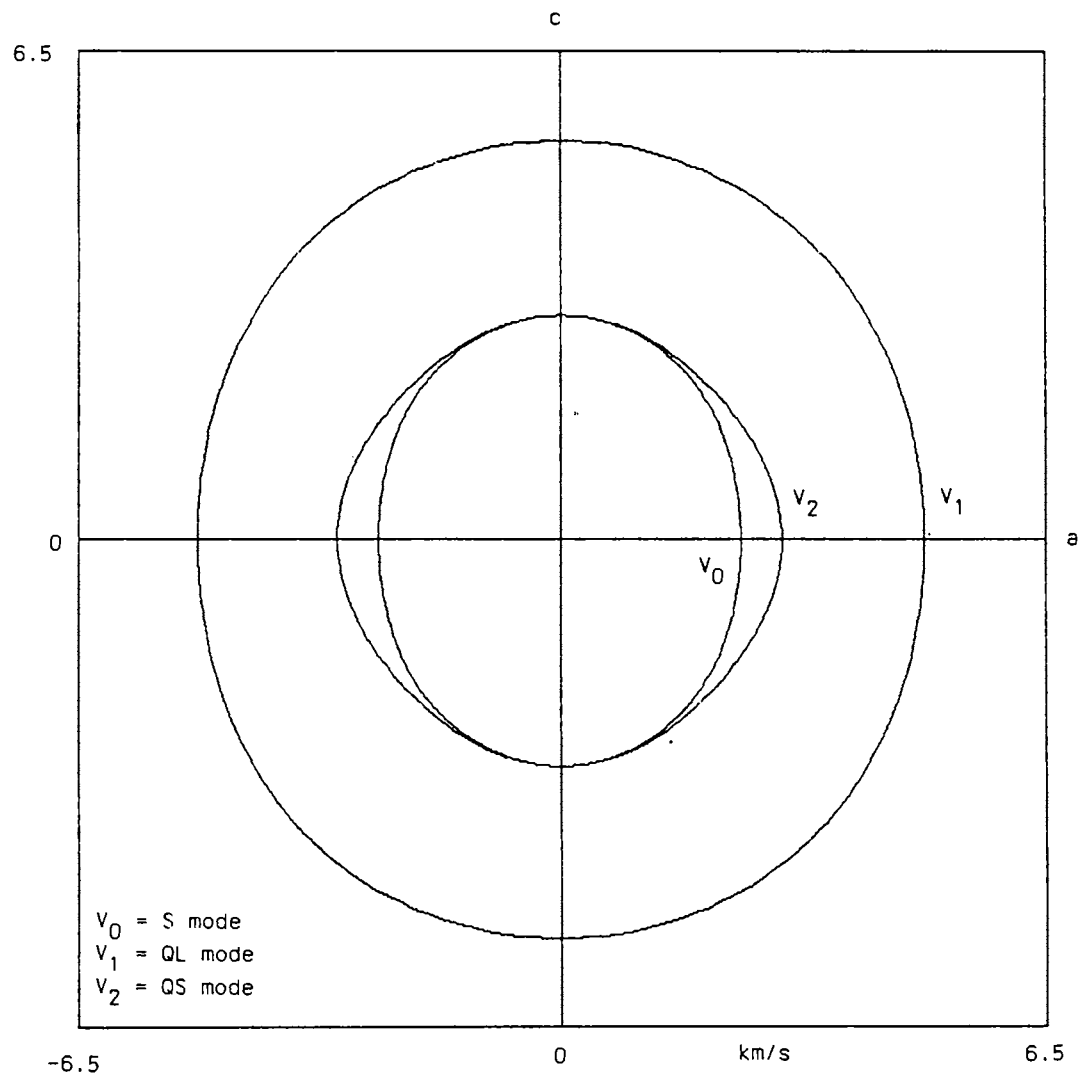The phase velocity surfaces of LPS in a-b plane

221

Figure 6.4

The phase velocity surfaces of LPS in a-c plane

222

the sample in a temperature controlled high temperature cell. The details of the experimental technique have been discussed in Section 4.2 in connection with the high temperature measurements in LHS. Special attention has been paid to temperatures around 333 K where Drozdowski *et al* [6.18] and Wang Ji-fang *et al* [6.32] have found anomaly in Brillouin scattering and ultrasonic measurements respectively. The experimental curves of Drozdowski *et al* [6.18] shows anomaly of the order of 0.5 GPa variation and an anomaly of this magnitude, if present, can be easily detected in the present ultrasonic measurements which has a precision of 0.01%. The ultrasonic attenuation measurements have also been performed relative to the room temperature value along with the velocity measurements. Ultrasonic attenuation anomaly is a very sensitive indicator of phase transitions.

6.3.2 Results and discussion

The results of our temperature variation measurements of elastic constants of LPS in the range from 300 K to 370 K are displayed in Figures 6.5 to 6.9. As is evident from these figures, none of the elastic constants undergo any anomaly at 333 K. The ultrasonic attenuation shows a linear variation with respect to the temperature and do not show any anomaly near 333 K and are not plotted here because they are nonabsolute relative measurements showing no anomaly.

Our results are in agreement with Pimenta *et al* [6.19] who could not detect any anomaly at 333 K in the temperature variation of C_{11}, C_{33} or C_{66} in their Brillouin scattering results. Since ultrasonics is a very sensitive technique than Brillouin scattering , we can conclude that LPS does not undergo any phase transition at 333 K. All the elastic constants decrease slightly with increasing temperature which is the general behaviour exhibited by most solids.
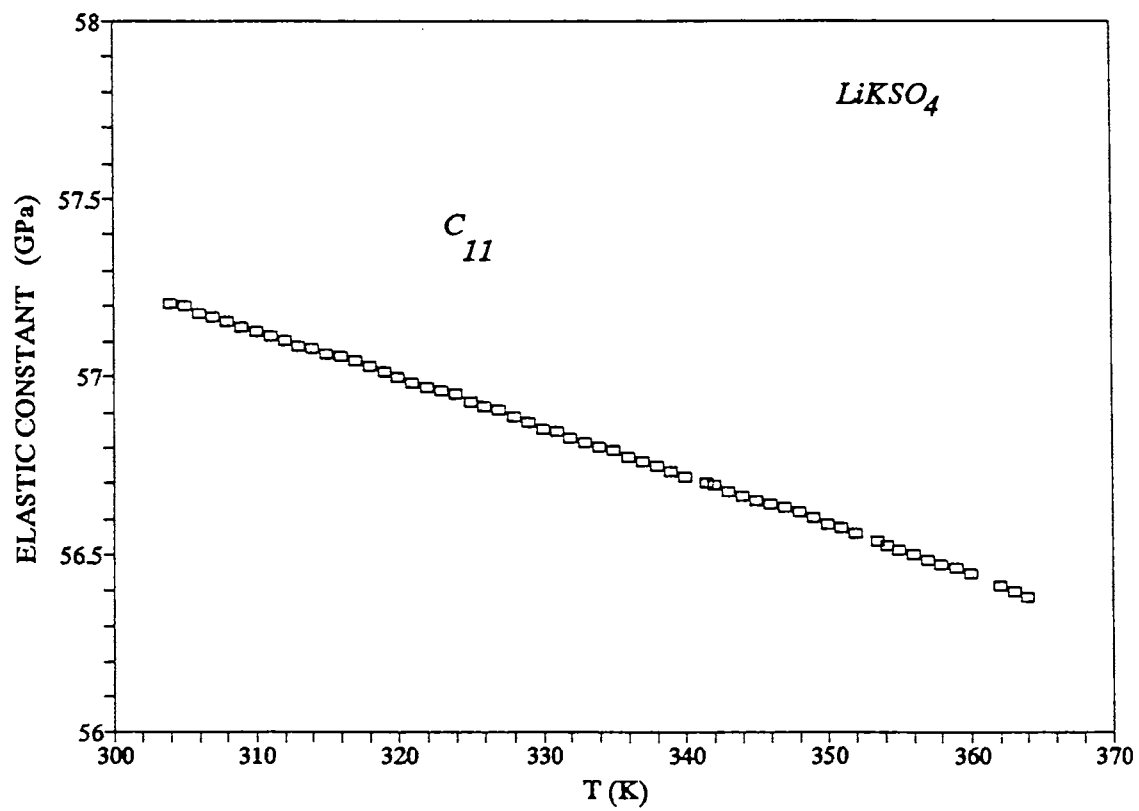
Figure 6.5

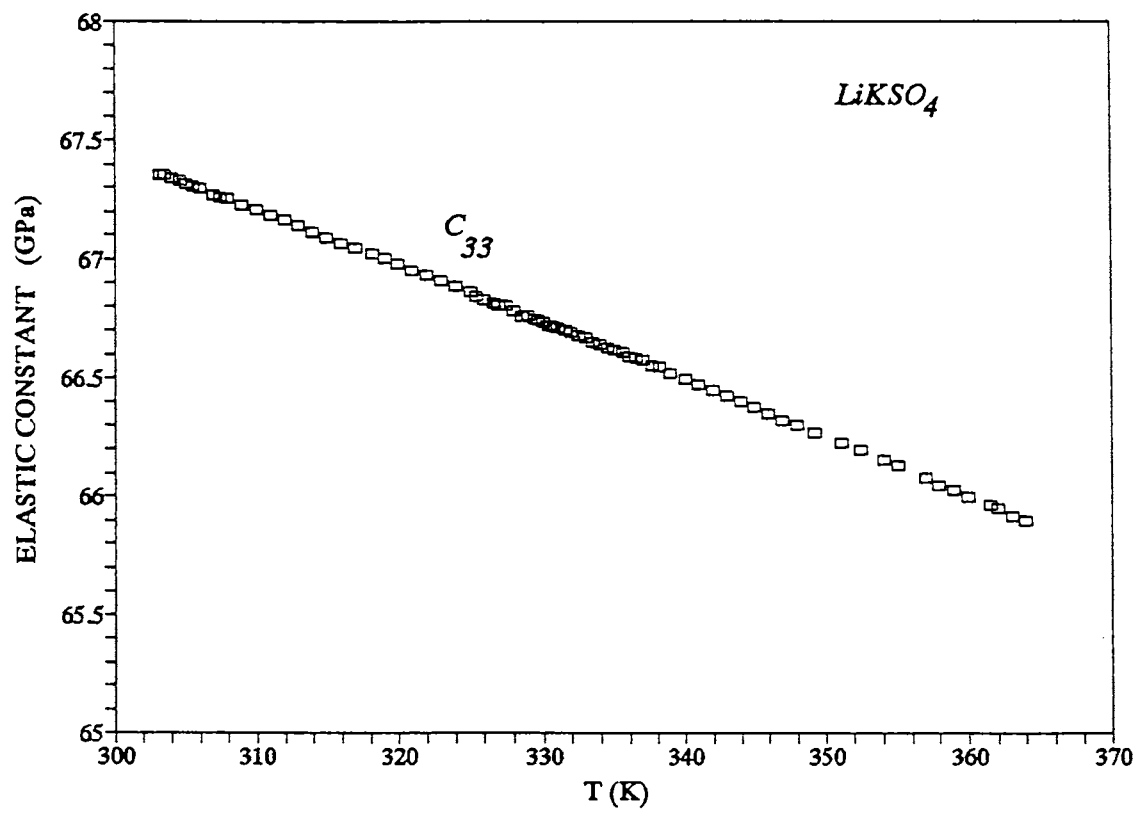Temperature variation of the elastic constant C_{11} of LPS

Figure 6.6

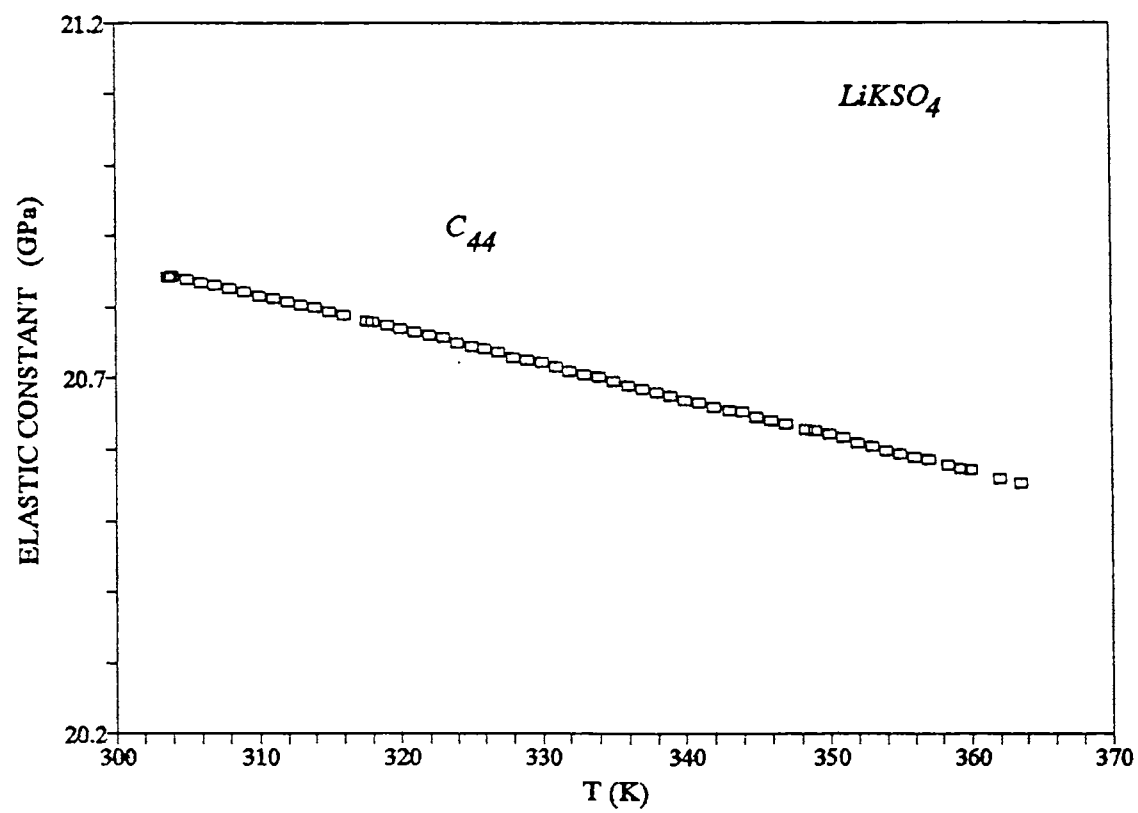Temperature variation of the elastic constant C_{33} of LPS

Figure 6.7

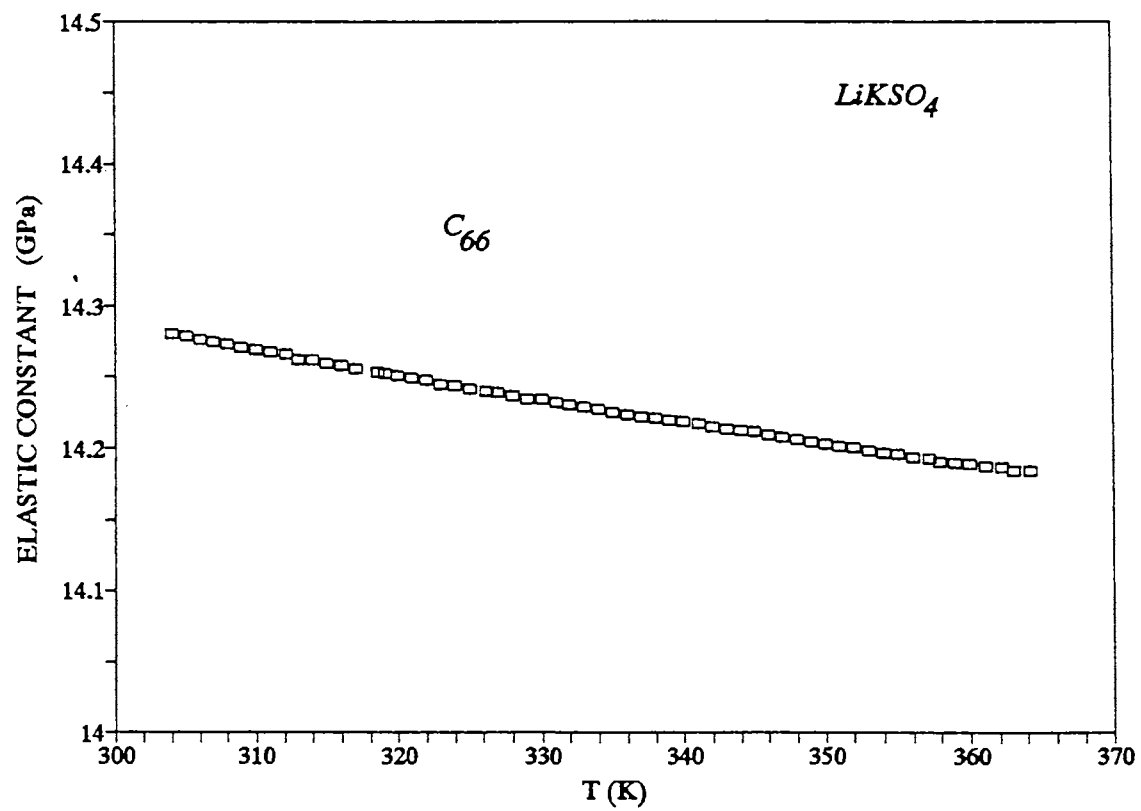Temperature variation of the elastic constant C_{44} of LPS

Figure 6.8

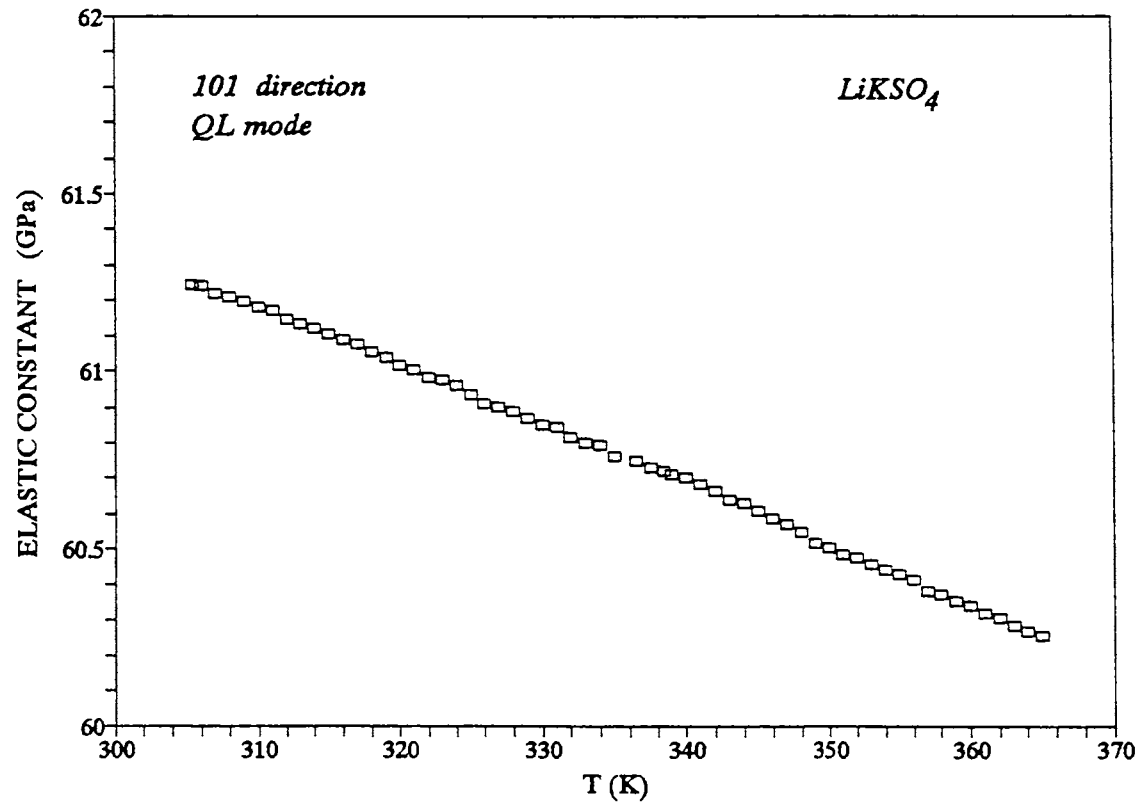Temperature variation of the elastic constant C_{66} of LPS

227

Figure 6.9

Temperature variation of the combination elastic
constant of LPS in the QL mode in [101] direction

228

However the difference in observation by different workers about the anomaly at 333 K requires some explanation. Pimenta *et al* [6.19] has suggested that a possible explanation of this discrepancy would be the existence of two stable different structures of LPS near room temperature. We find that a similar idea has also been proposed by Tomaszewski and Lukaszewicz [6.11,6.12], to explain the difference in the thermal hysteresis of the low temperature phase transition temperature in LPS. They have suggested that there are two types of crystals, type A and type B which are characterised with the thermal hysteresis of the low temperature transition.

We feel that the possibility of two types of LPS at room temperature may be a correct explanation for the inconsistent experimental results of LPS found in the literature. During crystal growth experiments on LPS we have found two types of seed formation. In the first type of crystal a natural face in the a-axis direction is absent and appeared like a twinned crystal and the natural faces present is only in c and [101] directions. In the second type the natural faces are developed in a, c and [101] directions and exhibited good hexagonal morphology. We have grown the crystals from the second type of seeds only. An experiment conducted on the crystals grown from both type of seeds can reveal whether these are the A and B type crystals. However an experiment of this sort is not undertaken in this work.

6.4 Conclusions

Investigations on LPS has been carried out with two main objectives. First, to determine all the 5 independent elastic constants of LPS crystal because it is found that the numerical value of the elastic constant C_{13} is not available in literature. Second, to find out whether a phase transition occurs in LPS near 333 K where an anomaly in the temperature

variation of elastic constants has been reported by some workers but where no anomaly has been reported by some other workers.

The present velocity measurements in LPS provide all the 5 independent elastic constants of this crystal which includes the constant C_{13}. The measured constants are compared with previous measurements and show good agreement.The complete set of elastic constants of LPS enable one to calculate the velocity in any direction in the crystal and the phase velocity surfaces are computed and plotted for the symmetry planes a-b and a-c. It is shown that the plot in the b-c plane is same as that in the a-c plane. The specialties of the plots for the hexagonal symmetry are discussed.

Results of the temperature variation studies of elastic constants and ultrasonic attenuation indicate no anomaly near 333 K from which it is concluded that LPS crystal does not undergo a phase transition near this temperature. However, the observation of the workers who have reported an anomaly at this temperature has been critically analysed. Possible existence of two types of LPS at room temperature is considered as an explanation for the discrepancies in the experimental results.

References

6.1   A. J. Oliveira, F. A. Germano, J. Mendes Filho, F. E. A. Melo, J. E. Moreira: Phys. Rev. B$\underline{38}$, 12633 (1988) /Phase transitions in $LiKSO_4$ below room temperature/

6.2   H. Kabelka, G. Kuchler: Ferroelectrics $\underline{88}$, 93 (1988) /Elastic Stiffness constants and Elastic relaxation around the first low temperature phase transition in $LiKSO_4$./

6.3   D. P. Sharma: Pramana $\underline{13}$, 223 (1979) /Thermal expansion and a new phase transition in pyroelectric $LiKSO_4$/

6.4   M. L. Bansal, A. P. Roy: Phys. Rev. B $\underline{30}$, 7307 (1984) /Orientational phase transition in $LiKSO_4$/

6.5   M. L. Bansal, S. K. Deb, A. P. Roy, V. C. Sahni: Solid State Commun. $\underline{36}$, 1047 (1980)

6.6   M. L. Bansal, S. K. Deb, A. P. Roy, V. C. Sahni: Pramana $\underline{20}$, 183 (1983)

6.7   R. Cach, P. E. Tomaszewski, J. Bornarel: J. Phys. C: Solid State Phys. $\underline{18}$, 915 (1985) / Dielectric measurements and domain structure in $LiKSO_4$ at low temperatures /

6.8   S. Fujimoto, N. Yasuda, H. Hibino: J. Phys. D: Appl. Phys. $\underline{18}$, 1871 (1985) /Pressure and temperature dependence of dielectric properties of lithium potassium sulphate/

6.9   S. Fujimoto, N. Yasuda, H. Hibino, P. S. Narayanan: J. Phys. D: Appl. Phys. $\underline{17}$, L35 (1984)
/ Ferroelectricity in lithium potassium sulphate /

6.10 B. Mróz, T. Krajewski, T. Breczewsci, W. Chomka, D. Sematowicz: Ferroelectrics $\underline{42}$, 71 (1982)
/Anomalous changes in the piezoelectric and elastic properties of $LiKSO_4$ crystals/

6.11 P. E. Tomaszewskii, K. Lukaszewicz: Phys. Status Solidi A $\underline{71}$, K53 (1982)

6.12 P. E. Tomaszewskii, K. Lukaszewicz: Phase Trans. $\underline{4}$, 37 (1983)

6.13 F. Holuji, M. Drozdowski: Ferroelectrics $\underline{36}$, 379 (1981)

6.14 C. H. A. Fonseca, G. M. Ribeiro, R. Gazzenelli, A. S. Chaves: Solid State Commun. $\underline{46}$, 221 (1983)

6.15 K. Maezawa, H. Takeuchi, K. Ohi: J. Phys. Soc. Japan $\underline{54}$, 3106 (1985)
/ESR study of low temperature phase transitions in Se doped $LiKSO_4$/

6.16 L. Abello, K. Chhor, C. Pommier: J. Chem. Thermodynamics $\underline{17}$, 1023 (1985)
/Thermodynamic studies on the successive phase transitions in $LiKSO_4$ crystals at low temperatures/

6.17 S. Bhakay-Tamhane, A. Sequeira, R. Chidambaram: Solid State Commun. $\underline{53}$, 197 (1985)
/Low temperature phase transition in $LiKSO_4$: a neutron

study/

6.18 M. Drozdowski, F. Holuj, M. Czajkowski: Solid State
Commun. <u>45</u>, 1005 (1983)
/Brillouin light scattering in LiKSO$_4$/

6.19 M. A. Pimenta, Y. Luspin, G. Hauret: Solid State Commun.
<u>59</u>, 481 (1986)
/Brillouin light scattering in LiKSO$_4$ between 20 and
80°C/

6.20 Tu An, Liu Jing-qing, Gu Ben-yuan, Mo Yu-jun, Yang
Hua-guang, Wang Yan-yun: Solid state Commun. <u>61</u>, 1 (1987)
/Brillouin study of the phase transition in LiKSO$_4$ in the
low temperature range/

6.21 M. A. Pimenta, P. Echegut, Y. Luspin, G. Hauret, F.
Gervais, P. Alberd: Phys. Rev. B <u>39</u>, 3361 (1989)

6.22 E. V. Charnaya, B. F. Borisov, T. Krajewski, A. K.
Radjabov: Solid State Commun. <u>85</u>, 443 (1993)   /Sound
velocity   hysteresis   in   the   high   temperature
incommensurate phase range of LiKSO$_4$ crystal/

6.23 S. Fujimoto, N. Yasuda, H. Hibino: J. Phys. D: Appl.
Phys. <u>18</u>, L135 (1985)   /Temperature dependence of the
electro-optic coefficient in LiKSO$_4$/

6.24 Narayani Choudhury, S. L. Chaplot, K. R. Rao: Phys. Rev.
B <u>33</u>, 8607 (1986)
/Phonon density of states, free energy, and anharmonicity
of LiKSO$_4$/

6.25 Y. Y. Li, Solid State Commun. <u>51</u>, 355 (1984)

6.26 M. S. Zhang, R. S. Katiyar, J. F. Scott: Ferroelectrics $\underline{74}$, 305 (1987)

6.27 T. Breczewski, T. Krajewski, B. Mroz: Ferroelectrics $\underline{33}$, 9 (1981)

6.28 T. Krajewski, T. Breczewski, P. Piskunowicz, B. Mroz: Ferroelectrics Lett. $\underline{4}$, 95 (1985)

6.29 M. A. Pimenta, P. Echegut, F. Gervais, P. Abelard: Solid State ionics $\underline{28}$ - $\underline{30}$, 224 (1988)

6.30 B. Mroz, J. A. Tuczynski, H. Kiefte, M. J. Clouter: J. Phys. Condens. Matter $\underline{1}$, 5965 (1989)

6.31 F. Ganot, B. Kihal, R. Farhi, P. Moch: Jap. J. Appl. Phys. $\underline{24}$, 491 (1985)

6.32 Wang Ji-fang, Zhang Dao-fan, Wang Ru-ju, Zang Liang-kun: Chin. Phys. Lett. $\underline{2}$, 201 (1985). /The characteristics of abrupt change on elastic constant C_{33} of $LiKSO_4$ crystal at $60°C$/

6.33 M. E. M. Kassem, B. Mroz: Acta Phys. Polonica $\underline{63A}$, 449 (1983)

6.34 H. Schulz, U. Zucker, R. Frech: Acta Cryst. B$\underline{41}$, 21 (1985)

CHAPTER 7

SUMMARY AND CONCLUSIONS

The present work is an attempt to probe the elastic properties and phase transitions in some of the mixed sulphate crystals by using ultrasonic pulse echo overlap technique. Three mixed sulphate crystals are investigated in this work which are Lithium Hydrazinium Sulphate (LHS) or $LiN_2H_5SO_4$, Lithium Ammonium Sulphate (LAS) or $LiNH_4SO_4$, and Lithium Potassium Sulphate (LPS) or $LiKSO_4$.

Large single crystals of these mixed sulphates necessary for ultrasonic investigation are not readily available and hence they are grown in the laboratory as a part of the present work. Crystal growth apparatus like constant temperature bath with battery back up, bath temperature controller, crystal rotation controller etc. are newly designed and fabricated. A cryostat is also specially designed and fabricated presently for the low temperature measurements.

Computer oriented techniques are extensively used in the present work for improving the basic measuring technique and also for the processing and presentation of the measured data. Two major numerical techniques and the corresponding computer programs developed as part of present work are presented in this thesis. The computer program developed for bond correction and correct overlap identification replaces the conventional laborious and error prone graphical technique for the same. The program and numerical procedure developed for misorientation correction replaces the analytical techniques which are difficult to use in practical measurements.

All the 9 elastic constants of LHS are determined accurately from ultrasonic measurements and the constants are refined by applying misorientation correction. This is the

first report of the elastic constants of LHS in literature. The phase velocity surface in the three symmetry planes of LHS are computed and plotted in the thesis.

Temperature variation of the elastic constants of LHS is investigated for the first time. A new bond material for high temperature shear wave measurements is identified during the course of investigation. Results of the measurements at high temperatures up to 450 K show anomalies in the temperature variation of elastic constants and attenuation. These anomalies are explained as due to a weak phase transition in LHS crystal near 425 K. Previous investigation results in thermal expansion study and NMR study are found to be consistent with the present inference of such a phase transition at high temperature. Low temperature measurements down to 210 K show no anomalous variations. It is inferred that there is no phase transition in LHS down to this temperature.

Ultrasonic measurements are performed in LAS to determine the elastic constants and to study the low temperature phase transitions. All the 9 elastic constants of LAS are accurately determined. A conversion table is presented to clarify the problem of different choice of axes adopted by different workers. Measured elastic constants are compared in a table with previous reports. The computed phase velocity surfaces of LAS are plotted and presented for three different symmetry planes.

Temperature variation study of elastic constants of LAS are performed for 6 different modes of propagation for heating and cooling at low temperatures. Results establish the thermal hysteresis of the temperature of the ferroelastic transition at 285 K. During cooling the transition occurs at 285.5 K and during heating the transition occurs at 288 K. This is the first time that the 285 K transition is studied using ultrasonics. The observed anomalies in elastic constants at

the transition temperature like step variation and thermal hystersis are found to be consistent with the predictions of a Landau theory model of this ferroelastic transition formulated recently in connection with a Brillouin scattering study of this transition.

Present investigation of the 256 K phase transition establish for the first time a large thermal hysteresis of about 14 K for this transition. On cooling the transition takes place at 242 K and during heating the transition occurs at 256 K. With the present findings a new phase sequence diagram is presented for LAS.

A new model is also presently proposed to explain the low temperature properties of LAS. According to this model an incommensurate ferroelastic phase is proposed below the 285 K transition and the transition at 256 K is considered as a lock-in transition to an antiferroelastic order. This new model could resolve some controversies but it is concluded that further research is required to establish the incommensurate phase.

All the 5 independent elastic constants of LPS is determined using ultrasonic measurements. Of these constants the constant C_{13} is reported for the first time. The phase velocity surface for the two symmetry planes of LPS are plotted and presented. Results of the temperature variation studies of elastic constants and ultrasonic attenuation indicate no anomaly near 333 K from which it is concluded that LPS crystal does not undergo a phase transition near this temperature. However, the observation of the workers who have reported an anomaly at this temperature has been critically analysed. Possible existence of two types of LPS at room temperature is considered as an explanation for the discrepancies in the experimental results.

A comparison of the three crystals studied shows that LPS has maximum number of phase transitions and LHS has the

least number. It is interesting to note that LPS has the simplest formula unit among the three. Despite the large number of investigations on these crystals in various fields a definite picture of the phase transition phenomena in these materials is not available. There is considerable scope for future work on these crystals and others belonging to the sulphate family.